Volume 25 March 2024

Journal of Food Bioactives

An Official Scientific Publication of the International Society for Nutraceuticals and Functional Foods (ISNFF)

An Official Journal of the International Union of Food Science and Technology (IUFoST)

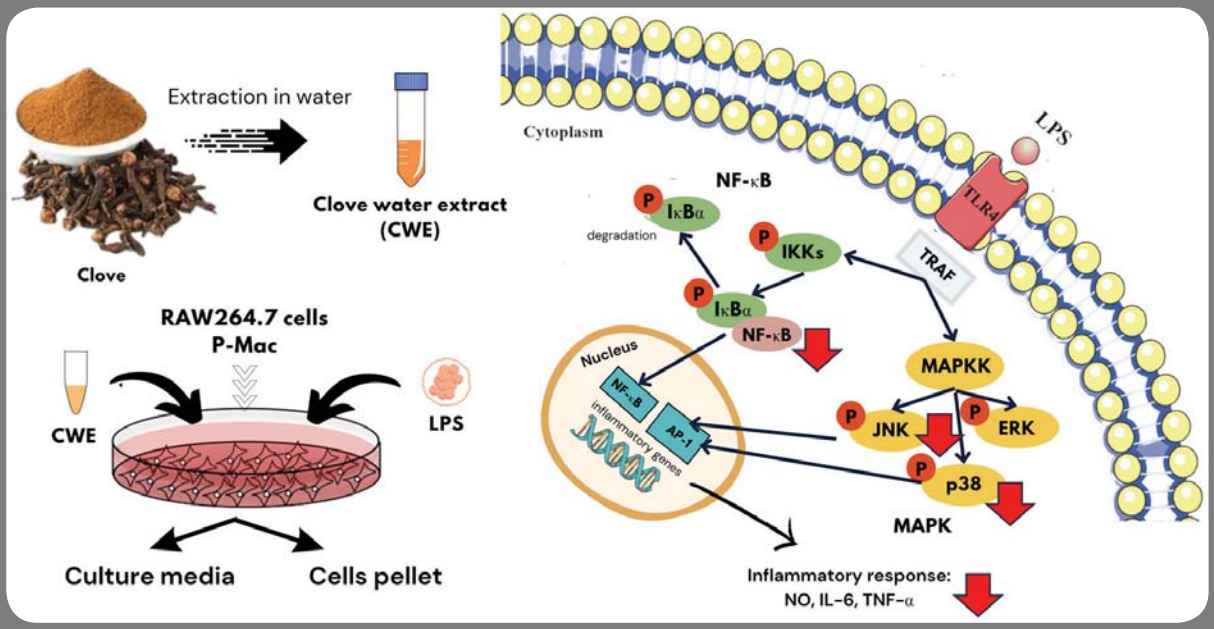

ISNFF & ASSOCIATES Publishing Company, Inc.

Journal of Food Bioactives

Bring together the results of fundamental and applied research on food bioactives, functional food ingredients, nutraceuticals and natural health products that are known to possess or perceived to have health-promoting properties

www.isnff-jfb.com

Editorial Board

Instructions for Authors

Journal of Food Bioactives with open access option is an official scientific publication of the International Society for Functional Foods and Nutraceuticals (ISNFF), a not-for-profit Disciplinary Interest Group of the International Union of Food Science and Technology (IUFoST) that was founded in 2007. It publishes original research articles, short communications/research notes, opinion pieces and review articles.

ISSN 2637-8752 Print
ISSN 2637-8779 Online

ISNFF & ASSOCIATES Publishing Company, Inc.
Connecticut, USA

Preface

Celebration of the lifetime achievements of Professor Chi-Tang Ho on the occasion of his 80th birthday

Professor Chi-Tang Ho has been the cornerstone of many innovative developments and contributions to the Food Chemistry, starting with his pioneering work in food flavors and antioxidants such as those of rosemary and then many other natural antioxidants and phenolic compounds from different sources that unraveled many mechanistic pathways previously unknown to the field. In addition, he has trained many graduate students and highly cited scientists that serve in key positions in academia, industry and government institutes.

Dr. Ho graduated with a B.S. from National Taiwan University in 1968 and then an M.A. and a Ph.D. degree in organic chemistry in 1971 and 1974, respectively, from Washington University in St. Louis. He then joined the Department of Food Science at Rutgers in 1978 as an assistant professor and moved through the ranks to professor in 1993, where he is now a Distinguished Professor. Dr. Ho was a main proponent of many initiatives and served as the associate editor of the Journal of Agricultural and Food Chemistry for many years as well as all other activities in the Agricultural and Food Chemistry Division.

In recognition of his scientific groundbreaking achievements, it is our great honor and privilege to dedicate this issue to recognize him on the occasion of his 80th birthday.

The following is an excerpt by Professor Min-Hsiung Pan, a Distinguished Professor at the National Taiwan University who serves as the Guest Editor for this issue. Dr. Pan was a Visiting Professor in Dr. Ho's lab while serving as a professor at National Kaohsiung Marine University.

"Prof. Chi-Tang Ho was an illuminating thread, woven with unparalleled brilliance through the realms of food science and more. I recount the transformative experience under his guidance and a distinguished mentor."

He continues to say "Our academic camaraderie blossomed through scholarly discussions, unveiling numerous research avenues, and fostering intellectual curiosity. At every turning point, as new information or research direction surfaced, Prof. Ho promptly shared and discussed with me potential developments of each new project. Our collaboration persisted in my tenure at Taiwan, transcending the challenges of a 12-hour time difference. Prof. Ho remained my trusted confidant, and the first to consult on intriguing research and cutting-edge technologies." He then adds "To date, the countless individuals who have collaborated with Prof. Ho attest to his continuous willingness to mentor and contribute to the flourishing development of the field of food science. Prof. Ho's distinguished outstanding in the academic community is underscored by numerous honours, including election as a Fellow of the American Chemical Society in 2010, the Royal Society of Chemistry in the UK in 2014, the International Academy of Food Science & Technology in 2006, the Institute of Food Technologists in 2003, and the International Society for Nutraceuticals & Functional Foods in 2018."

This preface/foreword not only serves as an expression of profound admiration we all have for Prof. Ho but also stands as a testament to the transformative influence he has wielded upon the academic journey for many of us. Perhaps, in the grand design of academic encounters, our connection with Prof. Ho was orchestrated by a higher force, adding an extra layer of significance to our scholarly journey and to the rest of the scientific community in the global arena.

Fereidoon Shahidi and Min-Hsiung Pan

Journal of Food Bioactives
International Society for Nutraceuticals and Functional Foods
Review
J. Food Bioact. 2024;25:2–12

Bioactive peptides as antioxidants and antimicrobials: fundamentals and applications

Sarika Kumari and Fereidoon Shahidi*

Department of Biochemistry, Memorial University of Newfoundland, St. John's, NL A1C 5S7, Canada
*Corresponding author: Fereidoon Shahidi, Department of Biochemistry, Memorial University of Newfoundland, St. John's, NL A1C 5S7, Canada. E-mail: fshahidi@mun.ca
DOI: 10.31665/JFB.2024.18367
Received: March 14, 2024; **Revised received & accepted:** March 19, 2024
Citation: Kumari, S., and Shahidi, F. (2024). Bioactive peptides as antioxidants and antimicrobials: fundamentals and applications. J. Food Bioact. 25: 2–12.

Abstract

Bioactive peptides are well-known for their remarkable tissue affinity, specificity, and effectiveness in promoting health. Extracted from food proteins, these bioactive peptides have displayed significant potential as functional foods and nutraceuticals. Throughout the years, numerous potential bioactive peptides derived from food sources have been documented. These bioactive peptides offer a wide range of crucial functions within the human body, including acting as antioxidants, antimicrobial agents, anti-inflammatory compounds, anti-hypertensive substances, and immunomodulators. More recently, extensive research has been conducted to investigate the origins, bioavailability, potential physiological effects and functionality, as well as the mechanisms of action of bioactive peptides in rendering health benefits. Researchers have also delved into various technological methods for preparing, purifying, and characterizing these peptides. This contribution primarily centers on exploring the antioxidant and antimicrobial aspects of bioactive peptides.

Keywords: Bioactive peptides; Antioxidant activity; Antimicrobial activity and mechanism.

1. Introduction

Bioactive peptides (BP) are composed of specific amino acid sequences that positively impact bodily functions or conditions that may influence health (Akbarian et al., 2022). BP commonly are made up of 2–20 amino acids, whereas proteins are polypeptides with higher molecular weights (MW) (Zaky et al., 2022). The sequence and composition of BP define their bioactivity characteristics. These peptides can be released from their precursor proteins by digestive enzymes during gastrointestinal digestion or by *in vitro* proteolytic processes with exogenous proteases (Shahidi and Zhong, 2015; Udenigwe and Aluko, 2012).

Bioactive peptides are isolated and generally produced from animal and plant proteins or other sources (Daliri et al., 2017, Awuchi et al., 2022). Animal proteins have traditionally been investigated for their high protein content and balanced essential amino acids (Qin et al., 2022). Milk and dairy products have been identified as potential sources of bioactive peptides (Punia et al., 2020). In addition, they can be produced from eggs and meat (Madhu et al., 2022). Various marine species, such as tuna, sardine, herring, and salmon, are an important source of BP (Mirzapour-Kouhdasht and Garcia-Vaquero, 2022). BP, derived from crustaceans, regulate various physiological processes such as cardiac function, pigmentation shifts, exoskeleton and internal muscle movements, metabolic activities, growth, transformation stages, and reproductive functions, some of these are also observed for those generated from other sources (Daliri et al., 2017).

Since plant sources have greater sustainability, low cost, and serve as an essential component in diet, the search for acquiring peptides from plant sources has increased (Rizzello et al., 2017). For example, Val-Tyr (VY), a multifunctional dipeptide, may be released from a protein source such as brewed sake or milk (Jakubczyk et al., 2020). The vegetable protein sources have also yielded favorable results using rice, soy, peanuts, peas, corn, algae, pseudo cereals, garlic, turmeric, spinach, and cocoa (Chalamaiah et al., 2019; Esfandi et al., 2019; Fernández-Tomé and Hernández-

Ledesma, 2019; Montesano et al., 2020; Phongthai et al., 2018; Rizzello et al., 2017; Shi et al., 2016; Wang et al., 2019).

Bioactive peptides generated from food possessing provide excellent potential for creating functional foods and/or nutraceuticals to prevent or treat certain chronic diseases. The production and characterization of bioactive peptides with antimicrobial, anti-inflammatory, antihypertensive, anti-obesity, and antioxidant attributes have been extensively published. These are classified into two types of endogenous and exogenous peptides (Abril et al., 2022; Zambrowicz et al., 2013). Endogenous peptides are produced in different cells, such as neural cells (analgesic/opioid application), immune cells (role in inflammation and antimicrobial), or various glands, such as the pituitary and adrenal glands (Froehlich, 1997). Exogenous peptides enter the body from various sources, such as food, dietary supplements, and medications (Akbarian et al., 2022; Chakrabarti et al., 2018; Geissler et al., 2010; Satake et al., 2002). BP have received much attention due to their application for enhancing health and reducing the risk of diseases by producing healthy foods, drugs, and other products (Akbarian et al., 2022).

2. Action mechanism of bioactive peptides

2.1. Food processing

Bioactive peptides derived from food proteins can be obtained either by enzymatic hydrolysis or by fermentation using starter cultures. Few studies have shown a combination of these two methods to produce peptides with enhanced biological activities. Additionally, bioactive peptides can be chemically synthesized due to their low presence in nature and the growing commercial interest in creating synthetic bioactive peptides. Here, we are primarily focusing on enzymatic hydrolysis and microbial fermentation.

2.2. Enzymatic hydrolysis

Enzymatic hydrolysis is a common method for procuring protein and hydrolysates/peptides from various food sources, especially by using digestive enzymes (Luna-Vital et al., 2015; Cruz-Casas et al., 2021). Enzymatic hydrolysis can be carried out in three different ways: i) using immobilized enzymes, ii) under traditional batch conditions, and iii) using ultrafiltration membranes.

The immobilized enzymes in a two-phase system, where one phase exclusively contains the enzyme and the other solely the product, as described by Rizzello et al. (2016), offer substantial benefits. The immobilization of enzymes is more economically advantageous and simplifies the separation of enzymes and products, thereby minimizing the risk of product contamination and enabling enzyme reuse, thus lowering the production cost (Michalak et al., 2017). The method conducted under traditional batch conditions is the least favored. This is due to the high enzyme costs, low yields and productivity, as well as the production of unwanted secondary metabolites resulting from enzymatic autolysis that contribute to its limited use (Cruz-Casas et al., 2021).

Ultrafiltration membranes have become the most known method for obtaining bioactive peptides. Ultrafiltration membranes, which hold back the enzyme and protein substrate while facilitating the separation of peptides through the application of hydraulic pressure, play a crucial role (Boukil et al., 2018). Throughout hydrolysis, proteins are continuously transformed into bioactive peptides, which are then released and separated from the reactor based on the membrane's molecular weight cut-off. By selecting a membrane with the appropriate pore size, typically recommended to be 3–6 times smaller than the molecular mass of the enzyme, the molecular weight of the final product can be precisely managed, ensuring the enzyme's retention (Ewert et al., 2022; Mora and Toldrá, 2023).

The final product of enzymatic hydrolysis depends on the type of enzyme used, the type of protein precursor, the degree of hydrolysis, and the separation method of the product. Even though crude and purified peptides are used for different applications to reduce the final production cost, the use of crude peptides is often preferred (Alavi and Ciftci, 2023).

2.3. Microbial fermentation

Microbial fermentation is a biotechnological method used to derive bioactive peptides. This technique employs microorganisms that produce proteolytic enzymes, aiming for these enzymes to break down proteins into smaller peptide fragments (Jia et al., 2021). The microorganisms typically utilized include bacteria, fungi, or yeasts, which might naturally occur in the substrate or be introduced as a starter culture (Najafian et al., 2021; Chakrabarti et al., 2018, Maghraby et al., 2023).

The microbial fermentation process encompasses various systems, with submerged fermentation and solid-state fermentation being the most prevalent. Submerged fermentation involves cultivating microorganisms in a liquid, nutrient-rich medium. This method is particularly effective for microorganisms that thrive in high-moisture environments, such as bacteria. It has the benefit of facilitating the purification of bioactive peptides produced during the process (Tolpeznikaite et al., 2023). On the other hand, solid-state fermentation consists of microbial growth on nutrient-rich solid substrates. It has the advantage of releasing nutrients and is suitable for fungi and microorganisms with minor moisture requirements (Subramaniyam and Vimala, 2012). During the microbial fermentation process, it is essential to handle the appropriate substrate, suitable microorganisms, and optimal environmental conditions, such as pH, temperature, and humidity, to generate peptides with better bioactivity (Melini et al., 2019). Table 1 shows the few industrial bioactive peptides and their antioxidant activity.

Within the bacterial group, lactic acid bacteria (LAB) are notably prominent and acclaimed as some of the most effective microorganisms for producing bioactive peptides. Their significance stems from their remarkable ability to adapt to various environments and substrates, both animal and plant-based (Cruz-Casas et al., 2021; Melini et al., 2019). Furthermore, LABs are distinguished by their potent proteolytic system, which is a key feature contributing to their efficiency in peptide production (Kieliszek et al., 2021) and is used to produce BP. Their role in producing fermented products is not only due to their physiological effect but also their technological importance in developing texture and taste (Akbarian et al., 2022).

3. Antioxidant activity

Antioxidant peptides typically the size of these peptides plays a crucial role in determining their effectiveness and behavior in the body, affecting both how they are transported to their target sites and how the gastrointestinal system processes them (Tadesse and Emire, 2020). These factors can enhance their antioxidant capacity within the body. The antioxidant activity of the two aromatic amino acids tryptophan (Trp) and phenylalanine (Phe) has been related

Table 1. Bioactive peptides with their antioxidant properties

Bioactive peptide	Source	Amino acid sequence	Method of production	Beneficial effects	References
Lacitum	Milk	YLGYLEQLLR	Enzymatic hydrolysis with Alcalase	Stress relief	Nagai et al., 2006
Evolus	Milk	VPP IPP	Fermentation with *L. helveticus* LBK-16H	Antihypertensive effect	Flynn et al., 2008
Calpis	Sour milk	VPP IPP	Fermentation with *L. helveticus* CP790 and *S. cerevisiae*	Antihypertensive effect	Siltari et al., 2012
Bonito peptide	Bonito fish	LKPNM	Enzymatic hydrolysis with thermolysin	Helps regulate angiotensin-converting enzyme	Guénard et al., 2019
Vasotensin	Bonito fish	LKPNM	Enzymatic hydrolysis with thermolysin	Antihypertensive effect	Fujita and Yoshikawa, 1999
Capolac	Milk	CPP	Isolation process	Calcium absorption	Chalamaiah et al., 2019
Cholesterol blocker	Soy	CSPHP	Enzymatic hydrolysis	Cholesterol reduction	Chalamaiah et al., 2019

to their capacity to act as radical scavengers, and the antioxidant activity of tyrosine is attributed to the special capability of phenolic group that acts as a hydrogen donor. Moreover, the presence of histidine (His) in peptides is directly associated with their ability to donate hydrogen and trap lipid peroxyl radicals, further enhancing their antioxidant effectiveness (Ajibola et al., 2011). Bioactive peptides with antioxidant properties are found in plant-based proteins from industrial food processing and by-products. These sources include soybean, wheat germ, hemp seeds, rice bran, sesame bran, wheat bran, and rapeseed, highlighting the potential of plant-derived substances to contribute to health benefits through their antioxidant activities (Flynn et al., 2008, Toldrá et al., 2018).

Many proteins, protein hydrolysates, and specific amino acids have demonstrated significant antioxidant activity. For example, it has been shown that a mixture of tryptophan and lysine inhibits the oxidation of butter's fat (Amarowicz and Shahidi, 1997). Some non-polar amino acids, such as proline and methionine, also render antioxidant activity in sardine and vegetable oils (Harnedy and FitzGerald, 2012). Taurine, hypotaurine, carnosine and anserine have been demonstrated to exert an antioxidant effect *in vitro* (Surai et al., 2021). Proteins from animal, plant and microbial origin, such as gluten, egg albumin, casein and yeast protein, have also been shown to render antioxidant activity (Czelej et al., 2022). In almost all cases, low-molecular-weight peptides exhibit higher antioxidant activity than intact proteins.

Protein digests have different antioxidant activities depending on the size of the peptides and their amino acid sequences as well as, the protein source and the hydrolysis condition (Shahidi and Zhong, 2015). Some bioactive peptides and their antioxidant activity, such as soy peptides obtained from soy protein using different enzymes (papain, pepsin, chymotrypsin, Alcalase, and Flavourzyme), have resulted in different degrees of hydrolysis that dictate the outcome (Knežević-Jugović et al., 2022). Whey protein hydrolysates are known for their radical scavenging activity and lipid oxidation inhibition (Kleekayai et al., 2020). A study by Mann et al. (2015) assessed the antioxidant activity of flavoured milk enriched with whey protein hydrolysates (WPH) treated with Flavouzyme, Alcalase, and Corolase PP. The WPH evaluated for their degree of hydrolysis and antioxidant activity, using the ABTS method, showed higher antioxidant activity (Flavouzyme, 0.81; Alcalase, 1.16; and Corolase, 1.42) compared to whey protein concentrate (WPC, 0.19). Corolase-treated WPH exhibited the highest antioxidant activity. LC-MS/MS identified 15 β-lactoglobulin, 1 α-lactalbumin, and 6 β-casein peptides in the WPH, contributing to the antioxidant effect. Meanwhile, strawberry and chocolate-flavoured milk with 2% WPH showed up to 42% increased antioxidant activity, suggesting WPH is an effective natural antioxidant for inclusion in food products (Mann et al., 2015).

Plants are excellent sources of natural biopeptides, even though plant proteins are found in smaller quantities in crops eaten by plant-eating animals or in the leftover materials from agricultural and industrial processes (César et al., 2024). Nonetheless, due to their benefits, such as high production rates, cost-effectiveness, short harvesting times, lack of conflict with regional religious or cultural practices, and remarkable biological effectiveness, plant-based proteins are increasingly being explored as ideal starting materials for the production of bioactive peptides (Hossain et al., 2022; Senadheera et al., 2023; Yeo and Shahidi, 2020). Many plants and their waste products, including legumes, grains, vegetables, fruits, seeds, husks, and leaves, have served as sources for discovering antioxidant peptides. Thus, oilseeds such as rapeseed/ canola and soybean as well as cereals, and legumes stand out globally for their protein content, making them primary sources of phytochemical- containing proteins (Lizárraga-Velázquez et al., 2020). This situation presents more chances for access, cost-efficiency, and a variety of bioactive peptides, such as those with antioxidant properties, further evidenced by the extensive comparison between animal peptides and their protein sources. However, research has particularly highlighted that proteins from cereals and legumes are richest in peptide fragments known for their antioxidant capabilities (Zhu et al., 2022). Notably, antioxidant peptides have been found in major grains like oats (Du et al., 2016), wheat (Heo et al., 2022), rye (Leung et al., 2018), buckwheat (Luo et al., 2020), corn (Jin et al., 2016), and millet (Agrawal et al., 2016).

Antioxidative peptides from marine species and the by-products from the aquaculture industry have also been extensively studied (Awuchi et al., 2022; Jimeno et al., 2004; Noyer et al., 2011; Ngo et al., 2011). Furthermore, Amarowicz and Shahidi (1997) showed synergistic effects of capelin protein hydrolysates with synthetic antioxidants butylated hydroxyanisole (BHA), butylated hydroxy-

Table 2. Bioactive peptides and their antioxidant activity

Bioactive Peptide	Antioxidant activity	References
Whey protein hydrolysate	Radical scavenging activity	Mann et al., 2015
Egg yolk protein hydrolysate	Radical scavenging activity	Marcet et al., 2023
Porcine skin collagen hydrolysate	Radical scavenging activity	Chi et al., 2014
Capelin protein hydrolysate	Inhibition of carotene-linoleate oxidation	Shahidi and Amarowicz, 1996; Amarowicz et al., 1999
Seal protein hydrolysate	Inhibition of carotene-linoleate oxidation	Shahidi and Amarowicz, 1996
Canola protein hydrolysate	Radical scavenging activity	Cumby et al., 2008
Soy peptides	Inhibition of thiobarbituric acid reactive substances (TBARS)	Knežević-Jugović et al., 2022
ß-Lactoglobulin-derived peptides	Radical scavenging activity	Hernandez-Ledesma et al., 2004
Caseinophosphopeptides	Radical scavenging activity	Kim et al., 2007

toluene (BHT), and tert-butylhydroquinone (TBHQ) were observed (Amarowicz and Shahidi, 1997, 1999). Table 2 shows the food derived bioactive peptides with their antioxidant activity.

Several *in vivo* studies have examined the biological effects of antioxidant peptides derived from various protein sources. A notable example is the research conducted by Chou et al. (2014), which investigated the antioxidant effects of peptides obtained from chicken liver through pepsin-assisted hydrolysis. This study focused on measuring the reduction of malondialdehyde (MDA) type compound accumulation, a known marker of secondary lipid oxidation, and the stimulation of antioxidant enzymes CAT, GPx, and SOD in mice subjected to chronic d-galactose intake, a condition known to increase the production of reactive species. The administration of chicken liver hydrolysate to mice at doses of 0.05 and 0.25 g/kg resulted in antioxidant status in their brain, heart, liver, and kidney of the mice that were equivalent to or better than those of the control or d-galactose-treated animals (Lorenzo et al., 2018).

4. Action mechanism of antioxidant peptides

Several studies have shown that the antioxidant activity of BP is due to their action as 1) radical scavenger inhibitors, 2) chelators of metal ions or 3) physical shielding (Rajapakse et al., 2005; Wu et al., 2003).

Antioxidant peptide molecules neutralize free radicals through two primary mechanisms: hydrogen atom transfer (HAT) and single electron transfer (SET). These processes enable the quenching of reactive oxygen and nitrogen species. Evaluation methods like the oxygen radical absorbance capacity (ORAC) and total radical-trapping antioxidant parameter (TRAP) assays utilize HAT principles to assess the capability of antioxidants to scavenge free radicals by donating a hydrogen atom (Zhu et al., 2022). The effectiveness of the HAT reaction depends on the bond dissociation energy and the ionization potential (IP) of the antioxidant's hydrogen-donating group. On the other hand, SET-based assessments, such as the DPPH radical scavenging capacity, ferric reducing antioxidant power (FRAP), and ABTS, measure an antioxidant's ability to reduce radicals, metals or carbonyls by electron donation (Prior et al., 2005; Lorenzo et al., 2018). This capacity is affected by the deprotonation of reactive groups and their IP. Nonetheless, it is recognized that both HAT and SET mechanisms often occur simultaneously in most instances, with the predominant mechanism influenced by the antioxidant's structure, which affects its solubility and partition coefficient in the system (Akbarian et al., 2022; Awuchi et al., 2022; Sharma et al., 2011).

As chelators of metal ions, BP inhibit the production of free radicals by removing metallic prooxidants metal ions (Wang et al., 2014) The peptide's carboxyl and amino groups participate in the chelating function (López-garcía et al., 2022). Studies have shown that chelating peptides are rich in histidine (Holeček, 2020). The copper-chelating peptides are abundant in histidine and inhibit copper's oxidative activity. The imidazole ring of the histidine primarily facilitates the binding of copper. Copper chelating peptides can prevent copper-assisted oxidation activity that can damage the luminal of stomach cells and oxidation of low-density lipoprotein (LDL) if it reaches the bloodstream (Timoshnikov et al., 2022).

In the physical shielding mechanism, peptides inhibit lipid peroxidation by acting as a barrier or membrane. They can work as a surfactant component and split at the oil-water interface, forming a thick membrane coating to avoid the direct interaction of lipids with radicals and other oxidizing agents (Nikoo and Benjakul, 2015).

5. Antimicrobial activity

Antimicrobial peptides (AMP) are a diverse group of molecules with thousands of AMP sequences identified so far (Huan et al., 2020). These are mostly short-chain peptides with 10–55 amino acids, with overall positive charge and structures containing both hydrophobic and hydrophilic regions (Li et al., 2021). AMP are categorized differently by structure, amino acid sequence, or biological function (Mishra et al., 2018).

The first AMP structures that were identified had an α-helical configuration, and these have been extensively studied. An example of such an α-helical AMP is magainins, derived from the African clawed frog *Xenopus laevis*, which is effective against many pathogens, including bacteria, fungi, yeast, and viruses (Brogden, 2005). However, magainin failed in clinical trials due to being less effective than the standard antimicrobial treatment (Dijksteel et al., 2021). In current clinical trials as a topical antimicrobial treatment for foot ulcers in diabetic patients, an analog of magainin 2 with an increased content of positively charged amino acids, which is the C-terminally modified MSI-78, referred to as a pexiganan peptide, is being used (Ting et al., 2020).

The second category of antimicrobial peptides have a secondary

structure characterized by β strands. Upon interacting with a lipid membrane, these AMPs adopt a β sheet structure. However, the β sheet peptides' flexibility is limited by disulfide bonds between the β-strands, imposing structural constraints (Pirtskhalava et al., 2021; Zasloff, 2002).

The third class of antimicrobial peptides do not adopt either α-helix or β-sheet secondary structures. One example is the cathelicidin family, which contains a significant amount of proline, an amino acid known for disrupting both α-helical and β-sheet structures (Xhindoli et al., 2016).

6. Action mechanism of antimicrobial peptides

The primary target of antimicrobial peptides is membrane permeabilization, and there are various models (see Figure 1) that describe how AMP primarily disrupt the cytoplasmic membrane. The action mechanisms of AMPs can be categorized into groups based on whether they target the cell membrane or non-membrane cellular components (Wimley, 2010; Espeche et al., 2024). In the case of AMP that specifically act on membranes, it is established that electrostatic interactions play a significant role, primarily facilitating the attraction between cationic AMP and negatively charged bacterial membrane components like lipopolysaccharide, peptidoglycan, and teichoic acid (Espeche et al., 2024). AMP that do not target the membrane act on intracellular targets (Matsuzaki, 2019).

The cellular membranes of both Gram-positive and Gram-negative bacteria contain high levels of phospholipids, phosphatidylglycerol, and cardiolipin. These components possess negatively charged principal groups that effectively draw in positively charged antimicrobial peptides. Among AMP, the cationic amphipathic α-helix represents one of the most prevalent forms. There are multiple theories detailing the mechanisms by which amphipathic α-helix peptides function. In the barrel-stave model (Figure 1a), AMP organizes into a barrel-like ring around an aqueous pore (Chen et al., 2019; Epand et al., 2016). Initially, the AMP are oriented parallel to the membrane; however, they ultimately become inserted perpendicularly into the lipid bilayer, as observed in studies by Epand et al. (2016). Only a few numbers of AMP have been demonstrated to adopt barrel-stave models, with alamethicin being one example (Laver, 1994), pardaxin (Rapaport and Shai, 1991), and protegrin (Brogden, 2005) as examples.

Another model, known as the toroidal pore model (Figure 1b), provides valuable insights into peptide-membrane interactions. In this model, AMP bind to the polar head groups of lipids, causing a separation of the headgroups and introducing a positive curvature strain (Kabelka and Vácha, 2021; Matsuzaki, 2019). AMP like Aurein 2.2 (Cheng et al., 2009), melittin (Raghuraman and Chattopadhyay, 2007), and several other AMP have been shown to form toroidal pores.

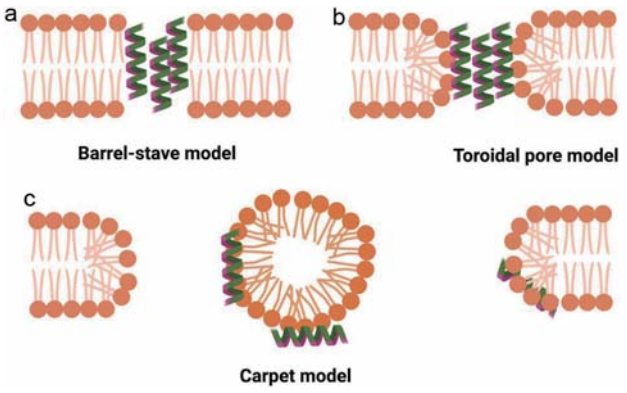

Figure 1. Models representing different mechanisms of action of antimicrobial peptides (AMP) in Barrel-stave model (a); Toroidal pore model (b); and Carpet model (c).

The third model, referred to as the carpet model (Figure 1c), is based on the concept that AMP can exert their action without forming specific pores in the membrane (Steiner et al., 1981; Shai, 2004). In this model, AMP accumulate parallel to the lipid bilayer, reaching a maximum concentration where they envelop the membrane surface, essentially creating a "carpet." This transformation results in unfavourable interactions on the membrane's surface, causing alterations in phospholipid interactions that increase membrane fluidity and ultimately lead to membrane disruption and loss of membrane integrity (Nakajima, 2003).

Several AMP have been shown to interact with bacteria without disrupting the membrane to cause substantial permeabilization. Such peptides usually cross the membrane and reach one or more intracellular targets (Kumari and Booth, 2022; Huang, 2000; Matsuzaki, 1998; Shai, 2004). These AMP first interact with the cytoplasmic membrane and then accumulate intracellularly to block cellular processes such as DNA and RNA replication and protein synthesis; this disruption could effectively kill bacteria (Singh et al., 2022).

Lactic acid bacteria (LAB) in fermented foods possess bioactive peptides with antimicrobial activity and many food component peptides and are good candidates as food additives. The rising incidence of infections caused by human pathogens like Mycobacterium tuberculosis and *Staphylococcus aureus* have demonstrated the consequences of growing resistance to traditional antibiotics (Prestinaci et al., 2015). In some cases, the pathogen could not be killed by any antibiotics. As a potential alternative to conventional antibiotics, antimicrobial peptides are good candidates to overcome this issue.

Antimicrobial peptides can be toxic to humans, and many efforts have been made to make them less toxic while improving their potency to eliminate bacteria. Some strategies, such as chemical strategies, enhance peptide specificity and stability. To improve the stability of AMP, researchers have tried to modify and optimize the cyclization of peptides linking C and N termini to improve serum stability and microbicidal activity (Etayash et al., 2020).

Another approach to improve the stability of AMP is to replace natural amino acids with non-natural amino acids or D-amino acids to protect AMP from proteolytic enzyme degradation since the host protease can identify and hydrolyze the natural L-amino acids (Lu et al., 2020). Zhao et al. (2016), isolated a lysine-rich AMP from the venom of social wasp MPI, which exhibited activity against Gram-positive and Gram-negative bacteria.

The researchers have developed two peptides: one composed entirely of D-amino acids, known as D-MPI, and the second peptide sequence in which only the lysine residues were replaced with D-amino acids, referred to as D-lys-MPI to test the proteolytic activity of trypsin. This is because trypsin cleaves positively charged amino acids like lysine. Results showed that both peptides, D-MPI and D-lys-MPI, were resistant to trypsin digestion. Interestingly, only D-MPI was equal in terms of activity compared to MPI. Meanwhile, D-Lys-MPI was inert because introducing of a single D-amino acids destabilized the secondary structure (Zhao et al., 2016).

Improving the function of AMPs may be achieved by conjugating peptides to other active molecules, such as incorporating peptides into non-biological molecules such as polyethylene glycol (PEG) or biological molecules like sugar, lipids and proteins,

hence taking advantage of both types of biological molecules to be combined and overcome their limitations (Chen and Lu, 2020; Erak et al., 2018; Wijesinghe et al., 2022; Zaman et al., 2019)

7. Limitations and challenges of the therapeutic use of bioactive peptides

In recent years, many bioactive peptides have been made to serve as antioxidants and antimicrobial peptides with limited success (Chalamaiah et al., 2019; Jakubczyk et al., 2020; Pei et al., 2022; Ulug et al., 2021). There are many reasons for this failure, but the main issue involves poor oral bioavailability and a short half-life in bloodstream stability observed for some bioactive peptides (Tan et al., 2018).

Bioactive or antimicrobial peptides, like dietary peptides, are susceptible to digestive enzymes in the gastrointestinal tract. Furthermore, even if peptides manage to pass through the stomach, their size often restricts their ability to permeate the intestines into the systemic circulation (Tan et al., 2018; Zhu et al., 2022, Fatoki et al., 2022).

The efficiency of the bioactive peptide depends on its ability to reach the organs where it would perform its function. Therefore, it is important to consider the *in vivo* differences between bioactive peptides. Peptides that are not broken down during gastrointestinal digestion, or their resulting fragments, must also navigate through additional breakdown by peptidases located at the brush border and/or on the cell membranes of the intestinal lining (Abeer et al., 2021). Before these peptides can enter the bloodstream through the cells of the intestinal wall, they face several barriers. There are four primary pathways for peptides to cross the intestinal barrier. These include the active transport via H^+-coupled peptide transporters PepT1 and PepT2, sodium-coupled oligopeptide transport mechanisms SOPT1 and SOPT2, passive movement through the tight junctions between cells, and trans-cellular movement via endocytosis, which is influenced by the molecular size and characteristics like the hydrophobicity of the peptides (Zhang et al., 2021).

For hydrolysates or peptides to effectively perform their biological functions, it is crucial to assess their digestibility and the subsequent liberation of bioactive peptides using appropriate *in vitro* intestinal models and in vivo studies within the gastrointestinal (GI) tract. Employing *in vitro* techniques, such as the use of human intestinal Caco-2 epithelial cell monolayers, alongside *in vivo* models that measure permeability, helps in predicting the oral bioavailability of these compounds (Mukker et al., 2014; Kellett et al., 2018). The ability of the intestinal barrier to selectively allow these candidate peptides through depends on a comprehensive understanding of the peptides' structural and chemical characteristics, their interactions within the GI tract, and a solid knowledge base regarding GI tract physiology (Vij et al., 2016). A few important properties of peptides, such as structural effects, hydrophobicity, size, and surface charge, affect the transport pathway.

As previously discussed, it is well-established that hydrolysates containing numerous short-chain peptides, particularly dipeptides and tripeptides, enhance absorption and are more effective than free amino acids or larger precursor peptides (Vij et al., 2016). When the molecular weight of a molecule exceeds 500 daltons (Da), its oral bioavailability declines. For instance, bioavailability was observed at 16.23% for casein-derived peptide fractions under 500 Da, whereas it dropped to 9.54% for those with a molecular weight between 500 and 1,000 Da (Singh et al., 2022). Additionally, the length of the peptide chain hints at the involvement of a transdermal transporter. Specifically, dipeptides and tripeptides are known as substrates for the PepT1 transporter, facilitating their transport across the cell membrane of enterocytes, utilizing an electrochemical protein gradient (Abeer et al., 2021). This transporter is located on the apical membrane of these intestinal cells. However, it was noticed that as the molecular weight of peptides increases, their ability to pass through the intestinal passage decreases (Wang and Li, 2017). Therefore, due to the incomplete bioavailability of a peptide after oral ingestion, a peptide with significant bioactivity observed *in vitro* may not necessarily translate to significant activity *in vivo* (Xue et al., 2021).

The process of gastrointestinal (GI) digestion has been studied merely for its capacity to transform food into nutrients, the energy source for our body. Only recently has the GI tract been considered a dynamic interface between the luminal environment and the internal environment. Interaction between nutrients and the intestinal barrier elicits the activation of multiple signalling pathways, including some involved in energy homeostasis regulation (Caron et al., 2017). With the exponential increase in the number of people affected by metabolic syndrome, alimentary proteins have become the subject of increasing interest since they reduce food intake, induce satiety by diseases, and increase energy expenditure. Yet, the underlying mechanisms are still not completely elucidated. The in vitro study of some mechanisms, notably the production and secretion of the GI hormones, highlighted the primary role of bioactive peptides originating from protein GI digestion (Sánchez-Velázquez et al., 2021).

Nonetheless, alternative delivery methods can enhance the likelihood of peptide absorption and decrease the problem (Erdmann et al., 2008). Vilcacundo et al. (2017) purified concentrate of quinoa protein that was digested under *in vitro* gastrointestinal conditions. Pepsin completely hydrolyzed quinoa proteins at pH 1.2, 2.0 and 3.2. At high pH, only partial hydrolysis was observed. No intact proteins were seen during the duodenal phase, indicating their susceptibility to simulate digestive conditions *in vitro* (Vilcacundo et al., 2017; Aluko and Monu, 2003).

8. Other bioactivities: antihypertensive, anti-inflammatory, and opioid effects

Bioactive peptides can modulate the renin-angiotensin system (RAS) because they decrease the activities of renin and angiotensin-converting enzyme (ACE). These two main enzymes regulate mammalian blood pressure (Balgir, 2016). Antihypertensive peptides, known as ACE inhibitors, have been extracted from fish protein, milk and corn (Xue et al., 2021). Although milk proteins are the main antihypertensive peptides, other dietary sources, including soy and cereals, have recently been studied as antihypertensive peptides (Xue et al., 2021).

Various antihypertensive constituents from food sources, such as soybean, fish, milk, cereal, egg, vegetables, and fruits, have been characterized. They provide cardiovascular health by inhibiting ACE inhibitory, reducing free radical formation, inducing vasorelaxation, and lowering blood pressure and lipid levels (Huang et al., 2013; Wu and Ding, 2002). Among cereals, wheat gliadin hydrolysates can act as ACE inhibitors. The peptide IAP (Ile-Ala-Pro) prepared with acid protease significantly decreased blood pressure in spontaneously hypertensive rats (SHRs) with intraperitoneal administration (Matsumura et al., 1993). Arginine-rich peptides from flaxseed protein isolate (FPI) obtained by enzymatic hydrolysis with trypsin and Pronase were observed to produce *in vivo* vasodilatory effects (Udenigwe et al., 2012). Cheonggukjang, an antihypertensive peptide, has been identified and characterized

in a Korean soy product and obtained by fermentation with *Bacillus subtilis* CH-1023 (Korhonen and Pihlanto, 2003; Kim et al., 2021).

It is also known that antihypertensive drugs cause negative side effects in patients and could reduce compliance with prescribed drug treatment for example, using Aliskiren, a recently approved renin-inhibitory antihypertensive drug, has been associated with gastrointestinal disorders (Iijima et al., 2022). Therefore, increased interest has been shown in developing natural compounds that are less likely to induce negative side effects (Aluko, 2015; Udenigwe and Aluko, 2012).

Inflammation is a biological response by which the immune system defends the body from harmful pathogens, cell injury, toxic substances, and irritation (Abril et al., 2022; Sánchez-Velázquez et al., 2021). Peptides from different food sources have been reported to have a neutralizing effect on the inflammatory process. Bioactive peptides extracted from fish and shellfish proteins have shown relevant anti-inflammatory effects. Gao et al. (2020) identified peptide sequences with potential anti-inflammatory activity derived from sturgeon muscle protein in the lipopolysaccharide (LPS)-induced RAW264.7 cell inflammatory model. LC-MS/MS identified fourteen novel peptides by mass spectrometry, and from that three peptides were synthesized (KIWHHTF, VHYAGTVDY, and HLDDALRGQE) for further studies. These synthetic peptides decreased the release of inflammatory mediators and inflammatory cytokines (NO, IL-6, and IL-1β), while significantly increasing superoxide dismutase (SOD) activity in the cell model. Salmon by-products have been reported to be important sources with anti-inflammatory properties. An enzymatic hydrolysate of salmon (*Salmo salar*) skin exhibited anti-inflammatory activity (Liu and Bo, 2022). Milk is another food source of bioactive peptides. Previous studies isolated the milk casein-derived peptide QEPVL (Gln-Glu-Pro-Val-Leu) from fermented milk. The results showed that QEPVL significantly activated lymphocytes *in vitro* and *in vivo* (Jiehui et al., 2014).

Opioid peptides derived from food proteins have affinities to bind to opiate receptors and express opiate activity, which in turn can be reversed by an opioid antagonist, such as naloxone (Froehlich, 1997; Kitts and Weiler, 2003). Naloxone crosses the blood-brain barrier and blocks opioid activity, thus being a helpful tool for determining the specific effects of agonist opioid peptides (Tyagi et al., 2020; Liu and Udenigwe, 2019). Food-derived opioid peptides resist further hydrolysis by intestinal brush border enzymes and directly affect specific gastrointestinal target receptors (Kostyra et al., 2004). Peptides with opioid activity have been generated by *in vitro* digestion of casein and separated using milk protein hydrolysates by solvent extraction and chromatography technique. Depending on the source of the β- or α-casein, they are classified as β- or α-casomorphins (Kostyra et al., 2004; Aslam et al., 2020). Bioactive peptides that have opioid activity have also been separated from plant protein hydrolysate, such as wheat gluten is a well-known source of opioid peptides among food proteins (Zaky et al., 2022).

9. Conclusions

The isolation and purification of bioactive peptides are very important for exploring their physicochemical properties and evaluating their *in vitro* and *in vivo* bioactivities. Bioactive peptides can be separated from a protein hydrolysate mixture by several approaches, mainly different chromatography and membrane-based separation techniques. For example, Enzymatic hydrolysis is a common method for procuring proteins and hydrolysates/peptides from various food sources, especially by using digestive enzymes. The microbial fermentation role in fermented products is not only due to their physiological effect but also their technological importance in developing texture and taste.

Bioactive peptides hold promise as potential food ingredients and pharmaceutical ingredients aimed at addressing or preventing certain medical conditions and lifestyle-related diseases like obesity, type II diabetes, and hypertension. Regardless of the significant progress in the isolation and purification of bioactive peptides from different natural sources and the characterization of their bioactivities, there are still several obstacles to overcome, particularly from the production prospect of large scale production without losing activity. Thus, this review article has made an attempt to shed light on a few factors that may contribute to the translational gap in bioactive peptide antioxidant and antimicrobial activities. While it is certain that bioactive peptides will hold an important place as food additives, in the fields of pharmaceuticals and healthcare, we are optimistic that future translational research will accelerate the integration of these advancements, incorporating these bioactive peptide therapeutics into general use as health promoting food ingredients.

Acknowledgments

We are grateful to the Natural Science and Engineering Research Council (NSERC) of Canada for financial support in the form of a Discovery Grant to FS (RGPIN-2016-04468).

References

Abeer, M.M., Trajkovic, S., and Brayden, D.J. (2021). Measuring the oral bioavailability of protein hydrolysates derived from food sources: A critical review of current bioassays. Biomed. Pharmacother. 144: 112275.

Abril, A.G., Pazos, M., Villa, T.G., Calo-Mata, P., Barros-Velázquez, J., and Carrera, M. (2022). Proteomics characterization of food-derived bioactive peptides with anti-allergic and anti-inflammatory properties. Nutrients 14(20): 4400.

Agrawal, H., Joshi, R., and Gupta, M. (2016). Isolation, purification and characterization of antioxidative peptide of Pearl Millet (Pennisetum glaucum) protein hydrolysate. Food Chem. 204: 365–372.

Ajibola, C.F., Fashakin, J.B., Fagbemi, T.N., and Aluko, R.E. (2011). Effect of peptide size on antioxidant properties of African Yam Bean seed (Sphenostylis stenocarpa) protein hydrolysate fractions. Int. J. Mol. Sci. 12(10): 6685–6702.

Akbarian, M., Ali, K., Sara, E., and Vladimir, N.U. (2022). Bioactive peptides: Synthesis, sources, applications, and proposed mechanisms of action. Int. J. Mol. Sci. 23(3): 1445.

Akbarian, M., Khani, A., Eghbalpour, S., and Uversky, V.N. (2022). Bioactive peptides: Synthesis, sources, applications, and proposed mechanisms of action. Int. J. Mol. Sci. 23(3): 1445.

Alavi, F., and Ciftci, O.N. (2023). Purification and fractionation of bioactive peptides through membrane filtration: A critical and application review. Trends Food Sci. Technol. 131: 118–128.

Aluko, R.E. (2015). Antihypertensive peptides from food proteins. Annu. Rev. Food Sci. Technol. 6: 235–262.

Aluko, R.E., and Monu, E. (2003). Functional and bioactive properties of quinoa seed protein hydrolysates. J. Food Sci. 68(4): 1254–1258.

Amarowicz, R., and Shahidi, F. (1997). Antioxidant activity of peptide fractions of capelin protein hydrolysates. Food Chem. 58(4): 355–359.

Amarowicz, R., Karamać, M., and Shahidi, F. (1999). Synergistic activity of capelin protein hydrolysates with synthetic antioxidants in a model system. J. Food Lipids 6(4): 271–275.

Aslam, H., Ruusunen, A., Berk, M., Loughman, A., Rivera, L., Pasco, J.A.,

and Jacka, F.N. (2020). Unravelled facets of milk derived opioid peptides: A focus on gut physiology, fractures and obesity. Int. J. Food Sci. Nutri. 71(1): 36–49.

Awuchi, C.G., Chukwu, C.N., Iyiola, A.O., Noreen, S., Morya, S., Adeleye, A.O., Twinomuhwezi, H., Leicht, K., Mitaki, N.B., and Okpala, C.O.R. (2022). Bioactive compounds and therapeutics from fish: Revisiting their suitability in functional foods to enhance human wellbeing. BioMed Res. Int. 2022: 3661866.

Balgir, P.P. (2016). Antihypertensive peptides derived from food sources. MOJ Food Proc. Tech. 2(1): 1–6.

Boukil, A., Suwal, S., Chamberland, J., Pouliot, Y., and Doyen, A. (2018). Ultrafiltration performance and recovery of bioactive peptides after fractionation of tryptic hydrolysate generated from pressure-treated β-lactoglobulin. J. Membr. Sci. 556: 42–53.

Brogden, K.A. (2005). Antimicrobial peptides: Pore formers or metabolic inhibitors in bacteria? Nat. Rev. Micro. 3: 238–250.

Caron, J., Domenger, D., Dhulster, P., Ravallec, R., and Cudennec, B. (2017). Protein Digestion-Derived Peptides and the Peripheral Regulation of Food Intake. Front. Endocrinol. 24: 8–85.

César, A.P.C., Lopes, F.E.S., Azevedo, F.F.N., Pinto, Y.O., Andrade, C.R., Mesquita, F.P., Silva, G.O., Freitas, C.D.T., and Souza, P.F.N. (2024). Antioxidant peptides from plants: A review. Phytochem. Rev. 23(1): 95–104.

Chakrabarti, S., Guha, S., and Majumder, K. (2018). Food-derived bioactive peptides in human health: Challenges and opportunities. Nutrients 10(11): 1–17.

Chalamaiah, M., Ulug, S.K., Hong, H., and Wu, J. (2019). Regulatory requirements of bioactive peptides (protein hydrolysates) from food proteins. J. Funct. Foods 58: 123–129.

Chen, C.H., and Lu, T.K. (2020). Development and challenges of antimicrobial peptides for therapeutic applications. Antibiotics 9(1): 24.

Chen, C.H., Starr, C.G., Troendle, E., Wiedman, G., Wimley, W.C., Ulmschneider, J.P., and Ulmschneider, M.B. (2019). Simulation-guided rational de novo design of a small pore-forming antimicrobial peptide. J. Am. Chem. Soc. 141(12): 4839–4848.

Cheng, J.T.J., Hale, J.D., Elliot, M., Hancock, R.E.W., and Straus, S.K. (2009). Effect of membrane composition on antimicrobial peptides aurein 2.2 and 2.3 from Australian southern bell frogs. Biophys. J. 96(2): 552–65.

Chi, C.F., Cao, G.H., Hu, F.Y., Li, Z.R., and Zhang, B. (2014). Antioxidant and Functional Properties of Collagen Hydrolysates from Spanish Mackerel Skin as Influenced by Average Molecular Weight. Molecules 19(8): 11211–11230.

Chou, C.H., Wang, S.Y., Lin, Y.T., and Chen, Y.C. (2014). Antioxidant activities of chicken liver hydrolysates by pepsin treatment. Int. J. Food Sci. Tech. 49(7): 1654–1662.

Cruz-Casas, D.E., Aguilar, C.N., Ascacio-Valdés, J.A., Rodríguez-Herrera, R., Chávez-González, M.L., and Flores-Gallegos, A.C. (2021). Enzymatic hydrolysis and microbial fermentation: The most favorable biotechnological methods for the release of bioactive peptides. Food Chem. 3: 100047.

Cumby, N., Zhong, Y., Naczk, M., and Shahidi, F. (2008). Antioxidant activity and water-holding capacity of canola protein hydrolysates. Food Chem. 109(1): 144–148.

Czelej, M., Garbacz, K., Czernecki, T., Wawrzykowski, J., and Waśko, A. (2022). Protein hydrolysates derived from animals and plants—A review of production methods and antioxidant activity. Foods 11(13): 1–28.

Daliri, E.B.M., Oh, D.H., and Lee, B.H. (2017). Bioactive peptides. Foods 6(5): 1–21.

Dijksteel, G.S., Ulrich, M.M., Middelkoop, E., and Boekema, B.K.H.L. (2021). Lessons learned from clinical trials using antimicrobial peptides (AMPs). Front. Microb. 12: 616979.

Du, XJ, Liu, XL, Zheng, XQ and Wang, XJ (2016). Preparation of antioxidative corn protein hydrolysates, purification and evaluation of three novel corn antioxidant peptides. Food Chem 204: 427–436.

Epand, R.M., Walker, C., Epand, R.F., and Magarvey, N.A. (2016). Molecular mechanisms of membrane targeting antibiotics. Biochim. Biophys. Acta, Biomembr. 1858(5): 980–987.

Erak, M., Bellmann-sickert, K., Els-heindl, S., and Beck-sickinger, A.G. (2018). Peptide chemistry toolbox – Transforming natural peptides into peptide therapeutics. Bioorg. Med. Chem. 26: 2759–2765.

Erdmann, K, Belinda, WYCheung and Henning, S (2008). The possible roles of food-derived bioactive peptides in reducing the risk of cardiovascular disease. J. Nutr. Biochem. 10: 643–654.

Esfandi, R., Walters, M.E., and Tsopmo, A. (2019). Antioxidant properties and potential mechanisms of hydrolyzed proteins and peptides from cereals. Heliyon 5(4): e01538.

Espeche, J.C., Varas, R., Maturana, P., Cutro, A.C., Maffía, P.C., and Hollmann, A. (2024). Membrane permeability and antimicrobial peptides: Much more than just making a hole. Pept. Sci. 116(1): e24305.

Etayash, H., Pletzer, D., Kumar, P., Straus, S.K., and Hancock, R.E.W. (2020). Cyclic derivative of host-defense peptide IDR-1018 improves proteolytic stability, suppresses inflammation, and enhances in vivo activity. J. Med. Chem. 63(17): 9228–9236.

Ewert, J., Eisele, T., and Stressler, T. (2022). Enzymatic production and analysis of antioxidative protein hydrolysates. Eur. Food Res. Technol. 248(8): 2167–2184.

Fatoki, T.H., Aluko, R.E., and Udenigwe, C.C. (2022). *In silico* investigation of molecular targets, pharmacokinetics, and biological activities of chicken egg ovalbumin protein hydrolysates. J. Food Bioact. 17: 34–48.

Fernández-Tomé, S., and Hernández-Ledesma, B. (2019). Current state of art after twenty years of the discovery of bioactive peptide lunasin. Food Res. Int. 116: 71–78.

Flynn, A., Korhonen, H., Marchelli, R., and Palou, A. (2008). Evolus® and reduce arterial stiffness - Scientific substantiation of a health claim related to Lactobacillus helveticus fermented Evolus® low-fat milk products and reduction of arterial stiffness pursuant to Article 14 of the Regulation (EC) No 1924/2006. EFSA J. 6(10): 824.

Froehlich, J.C. (1997). Opioid peptides. Alcohol Health Res. World 21(2): 132–136.

Fujita, H., and Yoshikawa, M. (1999). LKPNM: A prodrug-type ACE-inhibitory peptide derived from fish protein. Immunopharmacology 44(1-2): 123–127.

Gao, R., Shu, W., Shen, Y., Sun, Q., Bai, F., Wang, J., Li, D., Li, Y., Jin, W., and Yuan, L. (2020). Sturgeon protein-derived peptides exert anti-inflammatory effects in LPS-stimulated RAW264.7 macrophages via the MAPK pathway. J. Funct. Foods. 72: 104044.

Geissler, S., Zwarg, M., Knütter, I., Markwardt, F., and Brandsch, M. (2010). The bioactive dipeptide anserine is transported by human proton-coupled peptide transporters. FEBS J. 277(3): 790–795.

Guénard, F., Jacques, H., Gagnon, C., Marette, A., and Vohl, M.C. (2019). Acute effects of single doses of bonito fish peptides and vitamin D on whole blood gene expression levels: A randomized controlled trial. Int. J. Mol. Sci. 20(8): 1944.

Harnedy, P.A., and FitzGerald, R.J. (2012). Bioactive peptides from marine processing waste and shellfish: A review. J. Funct. Foods 4(1): 6–24.

Heo, H., Lee, H., Park, J., Kim, K.H., Jeong, H.S., and Lee, J. (2022). Antioxidant and cytoprotective capacities of various wheat (*Triticum aestivum* L.) cultivars in Korea. Foods 11(15): 2338.

Hernandez-Ledesma, B., Amigo, L., Ramos, M., and Recio, I. (2004). Angiotensin converting enzyme inhibitory activity in commercial fermented products. Formation of peptides under simulated gastrointestinal digestion. J. Agric. Food Chem. 52(6): 1504–1510.

Holeček, M. (2020). Histidine in health and disease: Metabolism, physiological importance, and use as a supplement. Nutrients 12(3): 848.

Hossain, A., Dave, D., and Shahidi, F. (2022). Antioxidant potential of sea cucumbers and their beneficial effects on human health. Mar. Drugs 20(8): 1–22.

Huan, Y., Kong, Q., Mou, H., and Yi, H. (2020). Antimicrobial peptides: Classification, design, application, and research progress in multiple fields. Front in Micro 11: 582779.

Huang, H.W. (2000). Action of antimicrobial peptides: Two-state model. Biochemistry 39(29): 8347–8352.

Huang, W.Y., Davidge, S.T., and Wu, J. (2013). Bioactive natural constituents from food sources-Potential use in hypertension prevention and treatment. Crit. Rev. Food Sci. Nutr. 53(6): 615–630.

Iijima, D., Sugama, H., Takahashi, Y., Hirai, M., Togashi, Y., Xie, J., Shen, J., Ke, Y., Akatsuka, H., and Kawaguchi, T. (2022). Discovery of SPH3127: A novel, highly potent, and orally active direct renin inhibitor. J. Medic. Chem. 65(16): 10882–1097.

Jakubczyk, A., Karas, M., Rybczynska-Tkaczyk, K., Zielinska, E., and Zielinski, D. (2020). Current trends of bioactive peptides - New sources and

therapeutic effect. Foods 9(7): 846.
Jia, L., Wang, L., Liu, C., Liang, Y., and Lin, Q. (2021). Bioactive peptides from foods: Production, function, and application. Food Funct. 12(16): 7108–7125.
Jiehui, Z., Liuliu, M., Haihong, X., Yang, G., Yingkai, J., Lun, Z., Li, D.X.A., Dongsheng, Z., and and Shaohui, Z. (2014). Immunomodulating effects of casein-derived peptides QEPVL and QEPV on lymphocytes in vitro and in vivo. Food and Funct. 5(9): 2061–2069.
Jimeno, J., Faircloth, G., Fernandez Sousa-Faro, J.M., Scheuer, P., and Rinehart, K. (2004). New marine derived anticancer therapeutics – A journey from the sea to clinical trials. Mar. Drugs 2(1): 14–29.
Jin, D.X., Liu, X.L., Zheng, X.Q., Wang, X.J., and He, J.F. (2016). Preparation of antioxidative corn protein hydrolysates, purification and evaluation of three novel corn antioxidant peptides. Food Chem. 204: 427–436.
Kabelka, I., and Vácha, R. (2021). Advances in molecular understanding of α-helical membrane-active peptides. Acc. Chem. Res. 54(9): 2196–2204.
Kellett, M.E., Greenspan, P., and Pegg, R.B. (2018). Modification of the cellular antioxidant activity (CAA) assay to study phenolic antioxidants in a Caco-2 cell line. Food Chem. 244: 359–363.
Kieliszek, M., Pobiega, K., Piwowarek, K., and Kot, A.M. (2021). Characteristics of the Proteolytic Enzymes Produced by Lactic Acid Bacteria. Molecules 26(7): 1858.
Kim, G.N., Jang, H.D., and Kim, C.I. (2007). Antioxidant capacity of caseinophosphopeptides prepared from sodium caseinate using alcalase. Food Chem. 104(4): 1359–1365.
Kim, I.S., Hwang, C.W., Yang, W.S., and Kim, C.H. (2021). Current perspectives on the physiological activities of fermented soybean-derived Cheonggukjang. Int. J. Mol. Sci. 22(11): 5746.
Kitts, D.D., and Weiler, K. (2003). Bioactive proteins and peptides from food sources. Applications of bioprocesses used in isolation and recovery. Curr. Pharm. Des. 9(16): 1309–1323.
Kleekayai, T., Le Gouic, A.V., Deracinois, B., Cudennec, B., and FitzGerald, R.J. (2020). In vitro characterisation of the antioxidative properties of whey protein hydrolysates generated under pH- and non pH-controlled conditions. Foods 9(5): 582.
Knežević-Jugović, Z., Culetu, A., Mijalković, J., Duta, D., Stefanović, A., Šekuljica, N., Đorđević, V., and Antov, M. (2022). Impact of different enzymatic processes on antioxidant, nutritional and functional properties of soy protein hydrolysates incorporated into novel cookies. Foods 12(1): 24.
Korhonen, H., and Pihlanto, A. (2003). Food-derived bioactive peptides - Opportunities for designing future foods. Curr. Pharm. Des. 9(16): 1297–1308.
Kostyra, E., Sienkiewicz-Szapka, E., Jarmoowska, B., Krawczuk, S., and Kostyra, H. (2004). Opioid peptides derived from milk proteins. Evolutionary aspect of the biological activity of peptides derived from food proteins.. Pol. J. Food Nutr. Sci. 13(1): 25–35.
Kumari, S., and Booth, V. (2022). Antimicrobial peptide mechanisms studied by whole-cell deuterium NMR. Int. J. Mol. Sci. 23(5): 2740.
Laver, D.R. (1994). The barrel-stave model as applied to alamethicin and its analogs reevaluated. Biophys. J. 66(2): 355–359.
Leung, R., Venus, C., Zeng, T., and Tsopmo, A. (2018). Structure-function relationships of hydroxyl radical scavenging and chromium-VI reducing cysteine-tripeptides derived from rye secalin. Food Chem. 254: 165–169.
Li, J., Hu, S., Jian, W., Xie, C., and Yang, X. (2021). Plant antimicrobial peptides: Structures, functions, and applications. Bot. Stud. 62(1): 5.
Liu, H., and Bo, L. (2022). Separation and identification of collagen peptides derived from enzymatic hydrolysate of Salmo salar skin and their anti-inflammatory activity in lipopolysaccharide (LPS)-induced RAW264.7 inflammatory model. J. Food Biochem. 46: 14122.
Liu, Z., and Udenigwe, C.C. (2019). Role of food-derived opioid peptides in the central nervous and gastrointestinal systems. J. Food Biochem. 43(1): e12629.
Lizárraga-Velázquez, C.E., Leyva-López, N., Hernández, C., Gutiérrez-Grijalva, E.P., Salazar-Leyva, J.A., Osuna-Ruíz, I., and Martínez-Montaño, E. (2020). Antioxidant molecules from plant waste. Processes 8(1566): 1–44.
López-garcía, G., Dublan-garcía, O., Arizmendi-cotero, D., and Gómez Oliván, L.M. (2022). Antioxidant and antimicrobial peptides derived from food proteins. Molecules 27(4): 1–32.
Lorenzo, J.M., Munekata, P.E.S., Gómez, B., Barba, F.J., Mora, L., Pérez-Santaescolástica, C., and Toldrá, F. (2018). Bioactive peptides as natural antioxidants in food products – A review. Trends Food Sci. Technol. 79: 136–147.
Lu, J., Xu, H., Xia, J., Ma, J., Xu, J., Li, Y., and Feng, J. (2020). D- and unnatural amino acid substituted antimicrobial peptides with improved proteolytic resistance and their proteolytic degradation characteristics. Front. Microbiol. 11: 563030.
Luna-Vital, D.A., Mojica, L., González de Mejía, E., Mendoza, S., and Loarca-Piña, G. (2015). Biological potential of protein hydrolysates and peptides from common bean (Phaseolus vulgaris L.): A review. Food Res. Int. 76: 39–50.
Luo, X., Fei, Y., Xu, Q., Lei, T., Mo, X., Wang, Z., Zhang, L., Mou, X., and Li, H. (2020). Isolation and identification of antioxidant peptides from Tartary buckwheat albumin (Fagopyrum tataricum Gaertn.) and their antioxidant activities. J. Food Sci. 85(3): 611–617.
Madhu, M., Kumar, D., Sirohi, R., Tarafdar, A., Dhewa, T., Aluko, R.E., Badgujar, P.C., and Awasthi, M.K. (2022). Bioactive peptides from meat: Current status on production, biological activity, safety, and regulatory framework. Chemosphere 307: 135650.
Maghraby, Y.R., El-Shabasy, R.M., Ibrahim, A.H., and Azzazy, H.M.E.S. (2023). Enzyme immobilization technologies and industrial applications. ACS Omega 8(6): 5184–5196.
Mann, B., Kumari, A., Kumar, R., Sharma, R., Prajapati, K., Mahboob, S., and Athira, S. (2015). Antioxidant activity of whey protein hydrolysates in milk beverage system. J. Food Sci. Technol. 52(6): 3235–3241.
Marcet, I., Carpintero, M., Rendueles, M., and Díaz, M. (2023). Antioxidant activity of egg yolk protein hydrolysates obtained by enzymatic and sub-critical water hydrolysis. Molecules 28(23): 7836.
Matsumura, N., Fujii, M., Takeda, Y., and Shimizu, T. (1993). Isolation and characterization of angiotensin I-converting enzyme inhibitory peptides derived from bonito bowels. Biosci., Biotechnol., Biochem. 57(10): 1743–1744.
Matsuzaki, K. (1998). Magainins as paradigm for the mode of action of pore-forming polypeptides. Biochim. Biophys. Acta, Rev. Biomembr. 1376(3): 391–400.
Matsuzaki, K. (2019). Membrane permeabilization mechanisms. Adv. Exp. Med. Biol. 1117: 9–16.
Melini, F., Melini, V., Luziatelli, F., Ficca, A.G., and Ruzzi, M. (2019). Health-promoting components in fermented foods: An up-to-date systematic review. Nutrients 11(5): 1–24.
Michalak, I., Dmytryk, A., Śmieszek, A., and Marycz, K. (2017). Chemical characterization of Enteromorpha prolifera extract obtained by enzyme-assisted extraction and its influence on the metabolic activity of Caco-2. Int. J. Mol. Sci. 18(3): 1–20.
Mirzapour-Kouhdasht, A., and Garcia-Vaquero, M. (2022). Cardioprotective peptides from milk processing and dairy products: From bioactivity to final products including commercialization and legislation. Foods 11(9): 1270.
Mishra, A.K., Choi, J., Moon, E., and Baek, K.H. (2018). Tryptophan-rich and proline-rich antimicrobial peptides. Molecules 23(4): 1–23.
Montesano, D., Gallo, M., Blasi, F., and Cossignani, L. (2020). Biopeptides from vegetable proteins: New scientific evidences. Curr. Opin. Food Sci. 31: 31–37.
Mora, L., and Toldrá, F. (2023). Advanced enzymatic hydrolysis of food proteins for the production of bioactive peptides. Curr. Opin. Food Sci. 49: 100973.
Mukker, J.K., Michel, D., Muir, A.D., Krol, E.S., and Alcorn, J. (2014). Permeability and conjugative metabolism of flaxseed lignans by Caco-2 human intestinal cells. J. Nat. Prod. 77(1): 29–34.
Nagai, T., Suzuki, N., and Nagashima, T. (2006). Antioxidative activities and angiotensin I-converting enzyme inhibitory activities of enzymatic hydrolysates from commercial kamaboko type samples. Food Sci. Technol. Int. 12(4): 335–346.
Najafian, L., Babji, A.S., Rodríguez-Herrera, R., and Cruz-Casas, D.E. (2021). Production of bioactive peptides using enzymatic hydrolysis and identification of antioxidative peptides from Patin (*Pangasius sutchi*) sarcoplasmic protein hydrolysate. Food Chem. 9: 280–289.
Nakajima, Y. (2003). Mode of action and resistance mechanisms of antimi-

crobial macrolides. In: Ōmura, S. (Ed.). Macrolide Antibiotics (Second Edition). Academic Press, San Diego, pp. 453–499.
Ngo, D.H., Wijesekara, I., Vo, T.S., Ta, Q.V., and Kim, S.K. (2011). Marine food-derived functional ingredients as potential antioxidants in the food industry: An overview. Food Res. Int. 44(2): 523–529.
Nikoo, M., and Benjakul, S. (2015). Potential application of seafood-derived peptides as bifunctional ingredients, antioxidant-cryoprotectant: A review. J. Funct. Foods 19: 753–764.
Noyer, C., Thomas, O.P., and Becerro, M.A. (2011). Patterns of chemical diversity in the Mediterranean sponge Spongia lamella. PLoS One 6(6): e20844.
Pei, J., Gao, X., Pan, D., Hua, Y., He, J., Liu, Z., and Dang, Y. (2022). Advances in the stability challenges of bioactive peptides and improvement strategies. Curr. Res. Food Sci. 5: 2162–2170.
Phongthai, S., D'Amico, S., Schoenlechner, R., Homthawornchoo, W., and Rawdkuen, S. (2018). Fractionation and antioxidant properties of rice bran protein hydrolysates stimulated by in vitro gastrointestinal digestion. Food Chem. 240: 156–164.
Pirtskhalava, M., Vishnepolsky, B., Grigolava, M., and Managadze, G. (2021). Physicochemical features and peculiarities of interaction of AMP with the membrane. Pharmaceuticals 14(5): 471.
Prestinaci, F., Pezzotti, P., and Pantosti, A. (2015). Antimicrobial resistance: A global multifaceted phenomenon. Pathog. Global Health 109(7): 309–318.
Prior, R.L., Wu, X., and Schaich, K. (2005). Standardized methods for the determination of antioxidant capacity and phenolics in foods and dietary supplements. J. Agric. Food Chem. 53(10): 4290–4302.
Punia, H., Tokas, J., Malik, A., Sangwan, S., and Baloda, S. (2020). Identification and detection of bioactive peptides in dairy products. Molecules 25(15): 3328.
Qin, P., Wang, T., and Luo, Y. (2022). A review on plant-based proteins from soybean: Health benefits and soy product development. J. Agric. Food Res. 7: 100265.
Raghuraman, H., and Chattopadhyay, A. (2007). Melittin: a membrane-active peptide with diverse functions. Biosci. Rep. 27(4-5): 189–223.
Rajapakse, N., Mendis, E., Jung, W.K., Je, J.Y., and Kim, S.K. (2005). Purification of a radical scavenging peptide from fermented mussel sauce and its antioxidant properties. Food Res. Int. 38(2): 175–182.
Rapaport, D., and Shai, Y. (1991). Interaction of fluorescently labeled pardaxin and its analogues with lipid bilayers. J. Bio. Chem. 266(35): 23769–23775.
Rizzello, C.G., Lorusso, A., Montemurro, M., and Gobbetti, M. (2016). Use of sourdough made with quinoa (Chenopodium quinoa) flour and autochthonous selected lactic acid bacteria for enhancing the nutritional, textural, and sensory features of white bread. Food Microbiol. 56: 1–13.
Rizzello, C.G., Lorusso, A., Russo, V., Pinto, D., Marzani, B., and Gobbetti, M. (2017). Improving the antioxidant properties of quinoa flour through fermentation with selected autochthonous lactic acid bacteria. Int. J. Food Microbio. 241: 252–261.
Rizzello, C.G., Tagliazucchi, D., Babini, E., Rutella, G.S., Taneyo Saa, D.L., and Gianotti, A. (2016). Bioactive peptides from vegetable food matrices: Research trends and novel biotechnologies for synthesis and recovery. J. Funct. Foods 27: 549–569.
Sánchez-Velázquez, O.A., Cuevas-Rodríguez, E.D., Mondor, M., Ribéreau, S., Arcand, Y., Mackie, A., and Hernández-Álvarez, A.J. (2021). Impact of *in vitro* gastrointestinal digestion on peptide profile and bioactivity of cooked and non-cooked oat protein concentrates. Curr. Res. Food Sci.. 4: 93–104.
Satake, M., Enjoh, M., Nakamura, Y., Takano, T., Kawamura, Y., Arai, S., and Shimizu, M. (2002). Transepithelial transport of the bioactive tripeptide, Val-Pro-Pro, in human intestinal Caco-2 cell monolayers. Biosci., Biotechnol., Biochem. 66(2): 378–384.
Senadheera, T.R.L., Hossain, A., and Shahidi, F. (2023). Marine bioactives and their application in the food industry: A review. Appl. Sci. 13(21): 12088.
Shahidi, F., and Amarowicz, R. (1996). Antioxidant activity of protein hydrolyzates from aquatic species. J. Am. Oil Chem. Soc. 73: 1197–1199.
Shahidi, F., and Zhong, Y. (2015). Measurement of antioxidant activity. J. Funct. Foods 18: 757–781.
Shai, Y. (2004). Mode of action of membrane active antimicrobial peptides. Pept. Sci. 66(4): 236–248.
Sharma, S., Singh, R., and Rana, S. (2011). Bioactive peptides: A review. Int. J. BIOautom. 15(4): 223–250.
Shi, F., Bai, B., Ma, S., Ji, S., and Liu, L. (2016). The inhibitory effects of γ-glutamylcysteine derivatives from fresh garlic on glycation radical formation. Food Chem. 194: 538–544.
Siltari, A., Kivimäki, A.S., Ehlers, P.I., Korpela, R., and Vapaatalo, H. (2012). Effects of milk casein-derived tripeptides on endothelial enzymes in vitro; A study with synthetic tripeptides. Arzneim.-Forsch./Drug Res. 62(10): 477–481.
Singh, T., Choudhary, P., and Singh, S. (2022). Antimicrobial peptides: Mechanism of action. Insights Antimicrob. Pept. 22: 1417.
Singh, U., Kaur, D., Mishra, V., and Krishania, M. (2022). Combinatorial approach to prepare antioxidative protein hydrolysate from corn gluten meal with dairy whey: Preparation, kinetics, nutritional study and cost analysis. LWT 153: 112437.
Steiner, H., Hultmark, D., Engström, A., Bennich, H., and Boman, H. (1981). Sequence and specificity of two antibacterial proteins involved in insect immunity. Nature 292(5820): 246–248.
Subramaniyam, R., and Vimala, R. (2012). Solid state and submerged fermentation for the production of bioactive substances. A comparative study.. Int. J. Sci. Nat. 3: 480–486.
Surai, P.F., Earle-Payne, K., and Kidd, M.T. (2021). Taurine as a natural antioxidant: From direct antioxidant effects to protective action in various toxicological models. Antioxidants 10(12): 1876.
Tadesse, S.A., and Emire, S.A. (2020). Production and processing of antioxidant bioactive peptides: A driving force for the functional food market. Heliyon 6(8): e04765.
Tan, H., Su, W., Zhang, W., Wang, P., Sattler, M., and Zou, P. (2018). Recent advances in half-life extension strategies for therapeutic peptides and proteins. Curr. Pharm. Des. 24: 4932–4946.
Timoshnikov, V.A., Selyutina, O.Y., Polyakov, N.E., Didichenko, V., and Kontoghiorghes, G.J. (2022). Mechanistic insights of chelator complexes with essential transition metals: Antioxidant/pro-oxidant activity and applications in medicine. Int. J. Mol. Sci. 23(3): 1247.
Ting, D.S.J., Beuerman, R.W., Dua, H.S., Lakshminarayanan, R., and Mohammed, I. (2020). Strategies in translating the therapeutic potentials of host defense peptides. Front. Immunol. 11: 983.
Toldrá, F., Reig, M., Aristoy, M.C., and Mora, L. (2018). Generation of bioactive peptides during food processing. Food Chem. 267: 395–404.
Tolpeznikaite, E., Bartkevics, V., Skrastina, A., Pavlenko, R., Ruzauskas, M., Starkute, V., and Zokaityte, E. (2023). Submerged and solid-state fermentation of Spirulina with lactic acid bacteria strains: Antimicrobial properties and the formation of bioactive compounds of protein origin. Biology 12(2): 248.
Tyagi, A., Daliri, E.B.M., Ofosu, F.K., Yeon, S.J., and Oh, D.H. (2020). Food-derived opioid peptides in human health: A review. Int. J. Mol. Sci. 21(22): 8825.
Udenigwe, C.C., and Aluko, R.E. (2012). Food protein-derived bioactive peptides: Production, processing, and potential health benefits. J. Food Sci. 77(1): R11–R24.
Udenigwe, C.C., Adebiyi, A.P., Doyen, A., Li, H., Bazinet, L., and Aluko, R.E. (2012). Low molecular weight flaxseed protein-derived arginine-containing peptides reduced blood pressure of spontaneously hypertensive rats faster than amino acid form of arginine and native flaxseed protein. Food Chem. 132(1): 468–475.
Ulug, S.K., Keskin, M., and Wu, J. (2021). Novel technologies for the production of bioactive peptides. Trends Food Sci. Technol. 108: 27–39.
Vij, R., Reddi, S., Kapila, S., and Kapila, R. (2016). Transepithelial transport of milk derived bioactive peptide VLPVPQK. Food Chem. 190: 681–688.
Vilcacundo, R., Barrio, D., Carpio, C., García-Ruiz, A., Rúales, J., Hernández-Ledesma, B., and Carrillo, W. (2017). Digestibility of quinoa (Chenopodium quinoa Willd.) protein concentrate and its potential to inhibit lipid peroxidation in the zebrafish larvae model. Plant Foods Hum. Nutr. 72(3): 294–300.
Wang, B., and Li, B. (2017). Effect of molecular weight on the transepithelial transport and peptidase degradation of casein-derived peptides by using Caco-2 cell model. Food Chem. 218: 1–8.
Wang, C., Li, B., and Li, H. (2014). Zn(II) chelating with peptides found in sesame protein hydrolysates: Identification of the binding sites of

complexes. Food Chem. 165: 594–602.
Wang, R., Zhao, H., Pan, X., Orfila, C., Lu, W., and Ma, Y. (2019). Preparation of bioactive peptides with antidiabetic, antihypertensive, and antioxidant activities and identification of α-glucosidase inhibitory peptides from soy protein. Food Sci. Nutr. 7(5): 1848–1856.
Wijesinghe, A., Kumari, S., and Booth, V. (2022). Conjugates for use in peptide therapeutics: A systematic review and meta-analysis. PLoS One 17(3): e0255753.
Wimley, W.C. (2010). Describing the mechanism of antimicrobial peptide action with the interfacial activity model. ACS Chem. Biol. 5(10): 905–917.
Wu, H.C., Chen, H.M., and Shiau, C.Y. (2003). Free amino acids and peptides as related to antioxidant properties in protein hydrolysates of mackerel (Scomber austriasicus). Food Res. Int. 36(9-10): 949–957.
Wu, J., and Ding, X. (2002). Characterization of inhibition and stability of soy-protein-derived angiotensin I-converting enzyme inhibitory peptides. Food Res. Int. 35(4): 367–375.
Xhindoli, D., Pacor, S., Benincasa, M., Scocchi, M., Gennaro, R., and Tossi, A. (2016). The human cathelicidin LL-37--A pore-forming antibacterial peptide and host-cell modulator. Biochim. Biophys. Acta 1858(3): 546–566.
Xue, L., Yin, R., Howell, K., and Zhang, P. (2021). Activity and bioavailability of food protein-derived angiotensin-I-converting enzyme-inhibitory peptides. Compr. Rev. Food Sci. Food Saf. 20(2): 1150–1187.
Yeo, J.D., and Shahidi, F. (2020). Identification and quantification of soluble and insoluble-bound phenolics in lentil hulls using HPLC-ESI-MS/MS and their antioxidant potential. Food Chem. 315: 126202.
Zaky, A.A., Simal-Gandara, J., Eun, J.B., Shim, J.H., and El-Aty, A.M.A. (2022). Bioactivities, applications, safety, and health benefits of bioactive peptides from food and by-products: A review. Front. Nutr. 8: 815640.
Zaman, R., Islam, R.A., Ibnat, N., Othman, I., and Zaini, A. (2019). Current strategies in extending half-lives of therapeutic proteins. J. Contr. Rel. 301: 176–189.
Zambrowicz, A., Timmer, M., Polanowski, A., Lubec, G., and Trziszka, T. (2013). Manufacturing of peptides exhibiting biological activity. Amino Acids 44(2): 315–320.
Zasloff, M. (2002). Antimicrobial peptides of multicellular organisms. Nature 415: 389–395.
Zhang, X., He, H., Xiang, J., Li, B., Zhao, M., and Hou, T. (2021). Selenium-containing soybean antioxidant peptides: Preparation and comprehensive comparison of different selenium supplements. Food Chem. 358: 129888.
Zhao, Y., Zhang, M., Qiu, S., Wang, J., Peng, J., Zhao, P., Zhu, R., Wang, H., Li, Y., Wang, K., Yan, W., and Wang, R. (2016). Antimicrobial activity and stability of the D-amino acid substituted derivatives of antimicrobial peptide polybia-MPI. AMB Expres 6: 122.
Zhu, Y., Lao, F., Pan, X., and Wu, J. (2022). Food protein-derived antioxidant peptides: Molecular mechanism, stability, and bioavailability. Biomolecules 12(11): 1622.

Journal of Food Bioactives
International Society for Nutraceuticals and Functional Foods
Original Research
J. Food Bioact. 2024;25:13–24

Exploring the phytochemical composition and pharmacological effects of fermented turmeric using the isolated strain *Lactobacillus rhamnosus* FN7

Kai-Jiun Lo[a,#], Sandeep Choudhary[a,#], Chi-Tang Ho[b] and Min-Hsiung Pan[a*]

[a]Institute of Food Science and Technology, National Taiwan University, Taipei 10617, Taiwan
[b]Department of Food Science, Rutgers University, New Brunswick, NJ, 08901, USA
[#]These authors contributed equally.
[*]**Corresponding author:** Min-Hsiung Pan, Institute of Food Science and Technology, National Taiwan University, No.1, Section 4, Roosevelt Road, Taipei 10617, Taiwan. Tel: +886-2-33664133; Fax: +886-2-33661771; E-mail: mhpan@ntu.edu.tw
DOI: 10.31665/JFB.2024.18368
Received: December 28, 2023; **Revised received & accepted:** January 26, 2024
Citation: Lo, K.-J., Choudhary, S., Ho, C.-T., and Pan, M.-H. (2024). Exploring the phytochemical composition and pharmacological effects of fermented turmeric using the isolated strain *Lactobacillus rhamnosus* FN7. J. Food Bioact. 25: 13–24.

Abstract

Turmeric (Curcuma longa), widely used in Asia as a spice, preservative, and colorant, contains curcuminoids known for diverse pharmacological benefits, including antimicrobial properties. However, their hydrophobic nature hampers bioavailability. Addressing this, we hypothesized that Lactic Acid Bacteria (LAB) fermentation could enhance curcuminoid content and bioactivity. This study isolated LAB strains to ferment turmeric and investigated the phytochemical and pharmacological outcomes. Twelve LAB strains from various sources were tested for fermenting 3% turmeric in MRS broth. L. *rhamnosus* FN7 emerged as a robust strain, tolerating turmeric's antibacterial properties and increasing curcuminoid content and anti-inflammatory effects. Fermented turmeric exhibited higher phenolic and flavonoid contents and improved radical scavenging activity than its non-fermented counterpart. Additionally, L. *rhamnosus* FN7 survived under simulated gastrointestinal conditions, indicating probiotic potential. Our findings suggest that L. *rhamnosus* FN7 fermentation significantly boosts turmeric's biochemical attributes, positioning it as a promising functional food.

Keywords: Fermented turmeric; Curcuminoids; Lactic acid bacteria; *L. rhamnosus*.

1. Introduction

Turmeric, a member of the *Zingiberaceae* family, is derived from the rhizome of *Curcuma longa* which is extensively cultivated in India, China, and various South Asian countries (Li et al., 2011). It has a rich history of traditional medicinal use, serving as both the natural coloring and flavoring agent in food (Prasad and Aggarwal, 2011). Previous research has highlighted the diverse health benefits of turmeric, encompassing anti-inflammatory, antineoplastic, hypolipidemic, and other pharmacological activities (Sharifi-Rad et al., 2020). In contemporary times, turmeric has gained widespread popularity as one of the most sought-after medicinal herbs, spices, and functional dietary supplements. The biological activity of turmeric is predominantly attributed to its abundant array of bioactive compounds, including curcuminoids, monoterpenes, sesquiterpenes, diterpenes, triterpenoids, alkaloids, and sterols (Li et al., 2011). Among these constituents, curcuminoids, which constitute 5% of the total weight in turmeric, have garnered significant global scientific attention for their pharmacological and therapeutic properties (Sharifi-Rad et al., 2020).

Within turmeric, curcuminoids exist three notable analogs including curcumin (diferuloylmethane), demethoxycurcumin (DMC), and bisdemethoxycurcumin (BDMC). These compounds manifest distinctions in their methoxy substitutions on the aromatic ring. Curcumin features two symmetric *o*-methoxy phenols

connected by the α, β-unsaturated β-diketone moiety. In contrast, BDMC, also symmetric, lacks two *o*-methoxy substitutions, and DMC displays an asymmetric structure with one phenyl ring incorporating *o*-methoxy substitution. Among these curcuminoids, curcumin predominates in turmeric, succeeded by DMC and BDMC (Jayaprakasha et al., 2002). A commercially available curcumin mixture comprises 77% curcumin, 17% DMC, and 3% BDMC (Anand et al., 2008). So far, extensive *in vitro* research indicates the antioxidant, cardioprotective, anti-inflammatory, anti-cancer, anti-Alzheimer, anti-diabetic, anti-microbial activities, and other medicinal properties of curcuminoids (Sharifi-Rad et al., 2020). However, despite their diverse bioactivities, the hydrophobic nature of dietary turmeric curcuminoids poses a limitation, rendering them practically insoluble in water. Additionally, the curcuminoid constituents of turmeric exhibit low absorption, rapid metabolism, and elimination in the body, thereby restricting their bioavailability when orally consumed as a supplement (Anand et al., 2007). To tackle these challenges, increasing the curcuminoid content in turmeric products or modifying curcuminoids to enhance their bioavailability presents a potential solution.

Fermentation has played a crucial role in human food production and consumption for an extended period. The process involves the breakdown of complex organic substances using microorganisms to enhance various aspects of food, including vitamins, essential amino acids, anti-nutrients, proteins, appearance, flavor, and aroma (Sharma et al., 2020). The United States Food and Drug Administration (USFDA) recognizes certain microorganisms as safe for producing fermented foods, such as *Aspergillus oryzae* and *Penicillium roqueforti* for koji and cheese, *Saccharomyces cerevisiae* for bread, and lactic acid bacteria (LAB) for yogurt and pickles. The market offers a variety of fermented food products based on the selection of microorganisms, raw materials, and manufacturing techniques (Anal, 2019). Recently, several reports have shown that the fermentation of turmeric by Generally Recognized as Safe (GRAS) microorganisms can enhance its efficacy. For instance, *Trichoderma* spp. fungus can boost the antioxidant and antibacterial activity of non-fermented turmeric, while fermented *Aspergillus oryzae* turmeric improves protective effects on CCl_4-induced liver damage in rats (Mohamed et al., 2016). The solid-state fermentation of turmeric using *Rhizopus oligosporus* increases major curcuminoids, total flavonoids, and antioxidant activity (Lim et al., 2022). Similarly, turmeric fermented with *L. fermentum* increases total curcumin content, exhibiting higher anti-inflammatory activity compared to unfermented turmeric (Sharma et al., 2022; Yong et al., 2019). Likewise, *L. johnsonii* IDCC 9203 fermented turmeric strongly inhibits pro-inflammatory cytokines, enhances water solubility of major curcuminoids, and improves consumer acceptance compared to non-fermented turmeric (Kim et al., 2011). These findings suggest that the fermentation of turmeric using microorganisms could serve as an alternative approach to enhance the overall efficacy of turmeric.

To date, a few specific strains of LAB that exhibit effectiveness on turmeric have been documented. However, the impact of a diverse array of LAB strains on turmeric remains unexplored. Furthermore, the identification of a potential strain within diverse LAB strains that can withstand the antimicrobial effects of turmeric is very crucial. In addition, there are still unanswered questions regarding the effects of LAB fermentation on the phytochemical changes in turmeric, particularly in terms of its anti-inflammatory properties. Thus, the study aimed to address these gaps through LAB isolation from different sources and comparing their ability to ferment turmeric. The results revealed that turmeric fermented with the *L. rhamnosus* FN7 strain displayed a notable capability to increase curcuminoid content and overall phytochemicals in turmeric, thereby enhancing its anti-inflammatory activity. Furthermore, *L. rhamnosus* FN7 exhibited potential probiotic properties. These findings suggest that the utilization of *Lactobacillus* fermentation in turmeric has the potential to elevate its curcuminoid content and phytochemical properties, positioning fermented turmeric as a promising functional food for addressing inflammation.

2. Material and Methods

2.1. Sample preparation and LABs isolation

The turmeric powder utilized in the study was supplied by ASAKUSA AGRICULTURE PROCESSING CO., located in Hualien City, Taiwan. The powder underwent a cool-air drying process and was vacuum-sealed for storage at −20°C. For LAB isolation, strains were isolated from distinct sources which included healthy human faeces, soil from turmeric cultivation (Hualien City, Taiwan), and a yogurt product from Uni-president in Taiwan. Briefly, each sample was mixed with 0.85% NaCl distilled water at a ratio of 1:10 and vortexed (Scientific Industries, USA) for 30 seconds. Subsequently, the mixture was suspended in sterilized 0.85% NaCl distilled water to prepare serial dilutions and 100 µL of each dilution were evenly spread on the surface of De Man-Rogosa-Sharpe (MRS) agar plates containing 3% turmeric powder (TMRS) using a sterilized L-shaped glass spreader. The plates were then anaerobically incubated with oxygen adsorbent packs (Mitsubishi Gas Chemical Co., Japan) for 48–72 hours at 37°C. Following incubation, an individual colony from each source on the MRS agar plate was selected, and a new series of dilutions was prepared. The colonies were streaked in a zig-zag pattern on TMRS agar. The isolation process was repeated until pure colonies were observed on an agar plate. Finally, the putative LAB colony from the agar plate was cultured in MRS broth at 37°C for 20 hours to determine through microscopic examination whether it was a single strain.

2.2. 16S rRNA gene sequencing for phylogenetic analysis of the isolated strains

The genomic DNA extraction was performed using the phenol/chloroform extraction method. After the centrifugation at 15,000×g for one minute, cells were collected, and 600 µL of phenol/chloroform/isopropanol (25:24:1) was added, and mixed well. Then the mixture was centrifuged at 15,000×g for 5 minutes and the upper aqueous phase was carefully transferred to a fresh tube. The step was repeated two times. Subsequently, an equal volume of chloroform was added to mix with the aqueous layer, and centrifugated at 15,000×g for 5 minutes. The resulting aqueous layer was again transferred to a fresh tube and four times the volume of absolute ethanol was added for DNA precipitation at −20°C for one hour. DNA pellets were obtained by centrifugation at 15,000×g for 15 minutes and washed twice with 70% ethanol at the same condition. DNA pellets were briefly air-dried and resuspended in TE buffer to obtain a DNA sample. The qualification was performed using the NANODROP 1000 spectrophotometer (Thermo Scientific, Taiwan) at 260 nm and 280 nm. The DNA samples prepared were used for PCR reactions and sequencing analysis.

The PCR reactions were done to amplify16S rRNA using uni-

versal primers, 27F (5′-AGAGTTTGATCCTGGCTCAG-3′) and 1492R (5′-GGTTACCTTGTTACGACTT-3′). The reactions were performed under the following conditions: 94°C for 2 minutes; 35 cycles of 30 seconds at 94°C, 30 seconds at 60°C, and 2 minutes at 72°C; a final extension at 72°C for 5 minutes. The PCR products were purified using a DNA Clean & Concentrator-5 kit (Zymo Research, USA) and sequenced by the Center for Biotechnology at National Taiwan University.

Individual 16S rRNA sequences were compared against the NCBI non-redundant nucleotide database using the Basic Local Alignment Search Tool (BLAST). For phylogenetic analysis, the sequences of type strains most similar to the isolates were downloaded from the NCBI database and aligned using BioEdit with the ClustalW multiple alignment program under default settings. The MEGA11 software was utilized to construct the topological tree of LAB strains using the maximum likelihood program with the general time-reversible model and gamma-distributed with the invariant model. One thousand resamplings were employed to evaluate the level of support for the internal branches.

2.3. Bacterial culture conditions and turmeric fermentation

The bacterial culture medium employed for turmeric fermentation was MRS powder (NEOGEN, Lansing, MI). A single activated bacterial colony was picked up and transferred to a glass tube containing 3 mL of MRS medium, then incubated at 37°C for 20 hours. Subsequently, 10% of the culture broth was transferred to fresh MRS broth and incubated at 37°C for another 20 hours. For turmeric fermentation, 1% of the bacterial cultures grown for 20 hours (adjusted OD_{600} value to 1.0) in the log phase were inoculated into the MRS medium containing 3% turmeric and incubated under static conditions at 37°C for 72 hours. Bacterial broth samples were collected at 12 hours intervals up to 72 hours. Colony-forming units were used to measure the growth of bacteria on the MRS agar plates. All experiments were performed with three biological replications.

2.4. Quantification of curcuminoids by High-performance Liquid Chromatography (HPLC) analysis

For HPLC analysis, curcuminoids were extracted from the freeze-dried fermented turmeric with little modifications from the previous study. Briefly, fermented turmeric was mixed with 1 mL of ethyl acetate containing 10 µg/mL methyl red (internal control) and vortexed vigorously. Next, the supernatant was collected by centrifugation at 15,000×g for 5 minutes, and the residual pellets were repeatedly extracted until became colorless. All of the supernatants were collected together and dried using nitrogen gas at 25°C. Finally, the residue was suspended in acetonitrile and filtered with a 0.22 µm syringe filter to obtain curcuminoid extract.

HPLC analysis was according to the previous study and performed by Jasco Pu-2080 plus an Intelligent HPLC pump system coupled with a UV-vis detector (set at 425 nm). The chromatographic separation was achieved using the C18 column (150 × 4.6 mm, 5 µm; Agilent Technologies, USA) at 30°C. The mobile phase was 0.1% formic acid in deionized water (A) and acetonitrile (B) at a flow rate of 1 mL/min. The elution gradient was used as follows: 60% A and 40% B in the beginning, decreased to 36% A at 7 minutes, maintained for 3 minutes, decreased to 10% A at 15 minutes, and returned to the original ratio at 17 minutes. The content of curcuminoids in sample extracts was calculated using the standard curve of pure curcumin, BDMC, and DMC.

2.5. Phytochemical properties of Isolated L. rhamnosus FN7 fermented turmeric

For sample preparation, 50 mg samples from both fermented and unfermented turmeric powders were taken and suspended in 1 mL of 70% aqueous ethanol, then stirred at 50°C for 2 hours to extract the bioactive compounds. Subsequently, the supernatant was collected using centrifugation at 3,000×g for 5 minutes and lyophilized. Finally, the residues were redissolved in methanol and filtered through a 0.22 µm filter membrane for further use. The total phenolic content was measured by the Folin-Ciocalteau (FC) method with slight modification. In short, 12.5 µL of the sample and 50 µL of distilled H_2O were mixed and added to a 96-well plate. Subsequently, 12.5 µL of FC reagent was added, and the mixture was allowed to mix for 5 minutes. Finally, 125 µL of 7% Na_2CO_3 was added and shaken for 90 minutes. The absorbance was measured at 750 nm against water blank (Synergy Instrument Inc., Vermont, USA). Gallic acid was served as the standard. For flavonoid content, an Aluminium chloride ($AlCl_3$) colorimetric assay with slight modification was used. Briefly, 15 µL of sample extracts and 45 µL of methanol were added to a 96-well plate, along with 3 µL of $AlCl_3$ and 3 µL of 0.1 M potassium acetate. Subsequently, 84 µL of distilled H_2O was added and incubated for 30 minutes. The absorbance of the acid-stable complex was measured at 415 nm against blank water (Synergy HT, BioTek Instrument Inc., Vermont, USA). Quercetin was applied as the standard. The DPPH, a stable radical was used to measure the total antioxidant potential of both fermented and unfermented turmeric samples. Briefly, 180 µL of 0.1 mM DPPH in methanol was added into a 96-well plate, followed by 20 µL of sample extracts. Further, the plate was incubated in the dark for 30 minutes and absorbance was measured at 517 nm. Ascorbic acid was used as standard.

2.6. Anti-inflammatory activity of fermented turmeric in vitro

To investigate the anti-inflammatory activity of fermented turmeric, RAW264.7 murine macrophages (derived from the American Type Culture Collection, Rockville, MD, USA) were selected in the study. RAW264.7 cells were seeded at a density of 1×10^6 cells/well in 24-well plates containing 1 mL of Dulbecco's modified Eagle medium (DMEM) supplemented with 10% (v/v) fetal bovine serum (FBS), 100 µg/mL streptomycin, and 100 µg/mL penicillin. The cells were cultured in a humidified atmosphere with 5% CO_2 at 37°C for 12 hours. Following, the medium was removed, and cells were gently washed twice with phosphate-buffered saline (PBS). Subsequently, the cells were incubated in FBS-phenol red-free DMEM containing four mM glutamic acid, then treated with various concentrations (final concentrations were 50, 100, 200, 250, 300, 350, and 400 µg/mL) of both unfermented and fermented turmeric powder for 24 hours with lipopolysaccharide (LPS) at a final concentration of 100 ng/mL. The cell viability was analyzed by using a classical MTT assay. The Griess assay was used to evaluate the nitrite production in RAW264.7 macrophages.

2.7. Probiotic characteristics of isolated L. rhamnosus FN7 strain

The simulation of gastric fluid tolerance in isolated strain through different pH values. Briefly, 2% (v/v) overnight cultured bacterial broth was incubated in an MRS medium with different pH values (2.0, 2.5, and 3.0) under anaerobic at 37°C. Bacterial broth

samples were collected at 3 hours intervals up to 6 hours. Colony-forming units were used to measure the growth of bacteria on MRS agar medium, while the samples taken at 0 hours were used as a control. To determine bile salt tolerance, 2% (v/v) overnight cultured *L. rhamnosus* FN7 isolate was added into 6 mL of fresh MRS medium containing 0.1, 0.2, 0.3, 0.4, 0.5, and 1% of bile salts (Sigma-Aldrich, New Zealand) under anaerobic conditions at 37°C. Bacterial broth samples were collected at 3 hours intervals up to 6 hours, and colony-forming units were used to measure the growth of bacteria on MRS agar medium. To analyze the milk fermentation capacity, one hundred milliliter aliquots of 10% (w/v) skim milk media (Millipore, Switzerland) was pasteurized at 85°C for 30 minutes and cooled down to 40°C. Subsequently, 2% (v/v) of *L. rhamnosus* FN7 strain was inoculated and incubated at 37°C for 24 hours under anaerobic conditions. After incubation, the pH of cultured milk was measured.

2.8. Statistical analysis

The results are expressed as the mean ± SD from three separate trials. Statistical distinctions among groups were assessed using one-way ANOVA followed by student's t-test analysis. A p-value <0.05 was considered indicative of a statistically significant difference between each group.

3. Result and discussion

3.1. 16S rRNA phylogeny of isolated strains

LAB strains are often associated with dairy products, human oral cavities and intestines, fecal matter, and compost. To isolate LAB strains suitable for the fermentation of turmeric, we selected soil from turmeric fields, commercial yogurt, and the gut microbiome of an Indian adult as potential sources for performing the isolation. Around 14 cultures were isolated from different sources that, include ten from human faeces (FN1, FN3, FN4, FN6, FN7, FN8, FN9, FN11, FN13, and FN14), three from yogurt (YN2, YN5, and YN10), and one from soil (SN12). As the morphological structure of microbes provides a better understanding of microbial physiology and allows us to identify them by species, we observed the morphology of all isolated strains. All the isolates were found to be rod-shaped except isolate FN6, which was cocci-shaped, consistent with the morphotype in a majority of LAB (Axelsson, 2004). Moreover, most of the isolates were Gram-positive bacteria except isolates FN6 and SN12. According to the previous reports, *Lactobacillales* are an order of gram-positive, thereby deducing that both strains (FN6 and SN12) may not belong to LAB. We further used 16S rRNA sequencing to identify these isolates. The result of the phylogenetic tree showed that the most of isolates from the human faeces have high identical similarities to the species *L. rhamnosus* (similarity >99%), including FN1, FN3, FN4, FN7, FN8, FN9, and FN11; they were grouped into the same clades (bootstrap support of 100%). The isolated strains from the yogurt were placed in the same group with *L. casei* ATCC393 (bootstrap support of 95%). However, two isolates (FN6 and SN12) from faeces and soil were grouped outside the *Lactobacillus* spp., and clustered to *Enterococcus faecalis* and *Klebsiella variicola* (Figure 1). Both *E. faecalis* and *K. variicola* are pathogens causing infection in humans and animals (Horsley et al., 2013; Martínez-Romero et al., 2018). Therefore, both these pathogenic strains were not introduced in turmeric fermentation.

3.2. Isolated strains present the potential ability to ferment turmeric

To investigate whether the isolates present a potential ability to ferment turmeric, isolated LAB strains were introduced in MRS medium containing 3% turmeric to check the growth. In our study, results demonstrated that most of isolated strains unexpectedly encountered growth inhibition after inoculation which might be attributed to the antimicrobial properties of curcuminoids found in turmeric. Nevertheless, despite encountering suppression in their growth during the initial phase, these bacterial strains exhibit a sustained, albeit gradual, and growth rate (Figure 2). Remarkably, some strains even demonstrated a capacity to proliferate to levels equivalent to the control group in the later stages of the fermentation process, such *as L. rhamnosus* FN1, *L. rhamnosus* FN7, and *L. rhamnosus* FN8 (Figure 2a, f, and g). The enhanced resilience can be linked to the strain's prior adaptation to external stress conditions within their specific sources, resulting in their ability to adapt more rapidly to the novel conditions presented by turmeric. Due to the fact that these strains still exhibit a certain level of growth ability during the fermentation of turmeric, all the isolated *Lactobacilli* strains were initially identified as potential strains capable of withstanding the curcuminoid effects of 3% turmeric.

It is noteworthy that two isolated strains, *L. crispatus* FN13 and *L. crispatus* FN14, exhibit a significant decrease in biomass after 24 hours of cultivation under MRS medium. However, the addition of turmeric appears to sustain their growth (Figure 2k and l). Intriguingly, both strains belong to the *L. crispatus* species. These findings suggest that *L. crispatus* may recognize components within turmeric as nutritional sources, thereby supporting their growth and metabolic activities. To elucidate whether the strain is a critical factor for the survival of strains during turmeric fermentation, we conducted additional experiments using various standard strains. Our experimental results revealed that the majority of strains were significantly inhibited in media containing turmeric. Only a limited number of strains were able to survive, including *B. longum* BCRC 11847, *L. gasseri* BCRC 14619, *L. reuteri* BCRC 14625, *L. rhamnosus* BCRC 10940, *L. rhamnosus* GG BCRC 16000, and *L. fermentum* BCRC 12190 (Figure S1). The behavior of these specific strains could be attributed to the presence of specific cell surface components and genes that enable bacteria to withstand the antimicrobial effects of curcuminoids found in turmeric (Marathe et al., 2010). These results may also explain why the variety of strains we selected is not extensive (Figure 1). Furthermore, it also indicates that, despite certain strains being evolutionarily closely related, there are still significant differences in their characteristics of turmeric fermentation.

3.3. Curcuminoid content of turmeric increases after fermentation using isolated LAB strains

Curcuminoids are the key bioactive compounds that contribute to the wide range of pharmacological activities of turmeric (Sharifi-Rad et al., 2020). Despite the numerous bioactivities, the use of curcuminoids has been limited due to their thermal degradation, photodegradation, oxidation, alkaline hydrolysis, and acid hydrolysis (Peram et al., 2017). Therefore, it was curious to investigate the effect of identified potential LAB strains on the curcuminoid content of fermented turmeric. The curcuminoid content of fermented samples were analyzed using HPLC. The results revealed that fermentation with *Lactobacillus* improved the curcuminoid content (Figure 3). After the fermentation of turmeric, the cur-

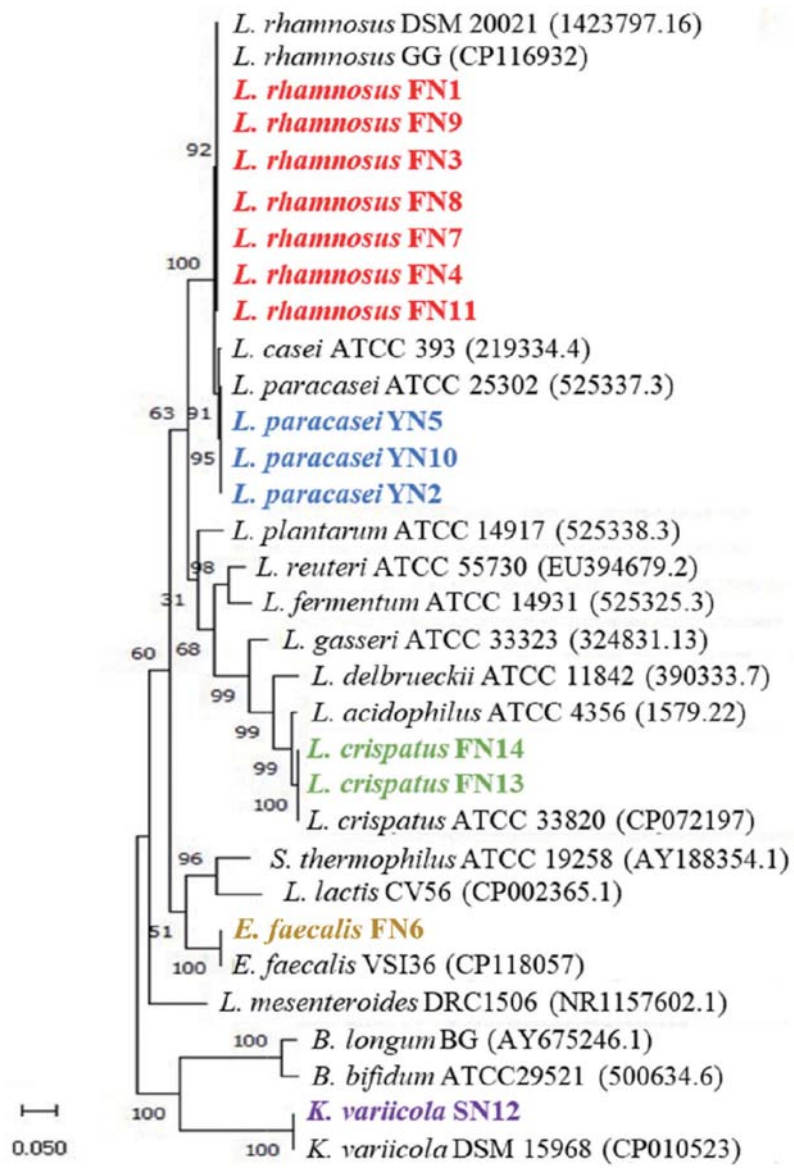

Figure 1. 16S rRNA gene-based phylogenetic tree of the isolated strains. The tree was constructed using the maximum likelihood method. The bootstrap value expressed as a percentage of 1,000 replicates is given at each node. Nucleotide sequence accession numbers are indicated in parentheses.

cuminoid content was significantly improved by *the L. rhamnosus* FN7 strain. Meanwhile, the curcuminoid content after fermentation by other isolated strains was insignificant except for FN8, FN9, FN10, and FN11 isolates. A possible explanation for the curcuminoid increase in turmeric after fermentation could be the utilization of enzymes by LAB strains. As reported in the earlier study, microorganisms use enzymes such as cellulases to aid in the extraction process by breaking or hydrolyzing plant tissues (Rosenthal et al., 1996). Similar results were observed by Yong, during the fermentation of turmeric using lactic acid bacteria (Yong et al., 2019). Unfortunately, our result revealed that none of the LAB strains displayed cellulase activity in isolates, as illustrated by *L. rhamnosus* FN7 (Figure S2). It is worth noting that we also assessed the curcuminoid concentration in fermented turmeric using six different types of strains with the potential for turmeric fermentation (Figure S1). The results indicated that there was no significant increase in curcumin content after fermentation (Figure S3). These results indicate that not all strains are capable of surviving the fermentation process possessing the ability to increase the curcuminoid content.

To explore the potential mechanism of *L. rhamnosus* FN7 improving curcuminoid content, we further examined the interaction between varying percentages of bacterial inoculation in an MRS medium containing various concentrations of pure curcumin to ascertain whether LAB either uptake or binds curcumin to the cell wall components. As illustrated in Figure S4, it was observed that the increase in curcumin was directly proportional to the biomass of bacteria. The observation suggests that the peptidoglycan within the bacterial cell wall can bind to curcumin, which may contribute to part of the mechanism leading to an increase in curcuminoids

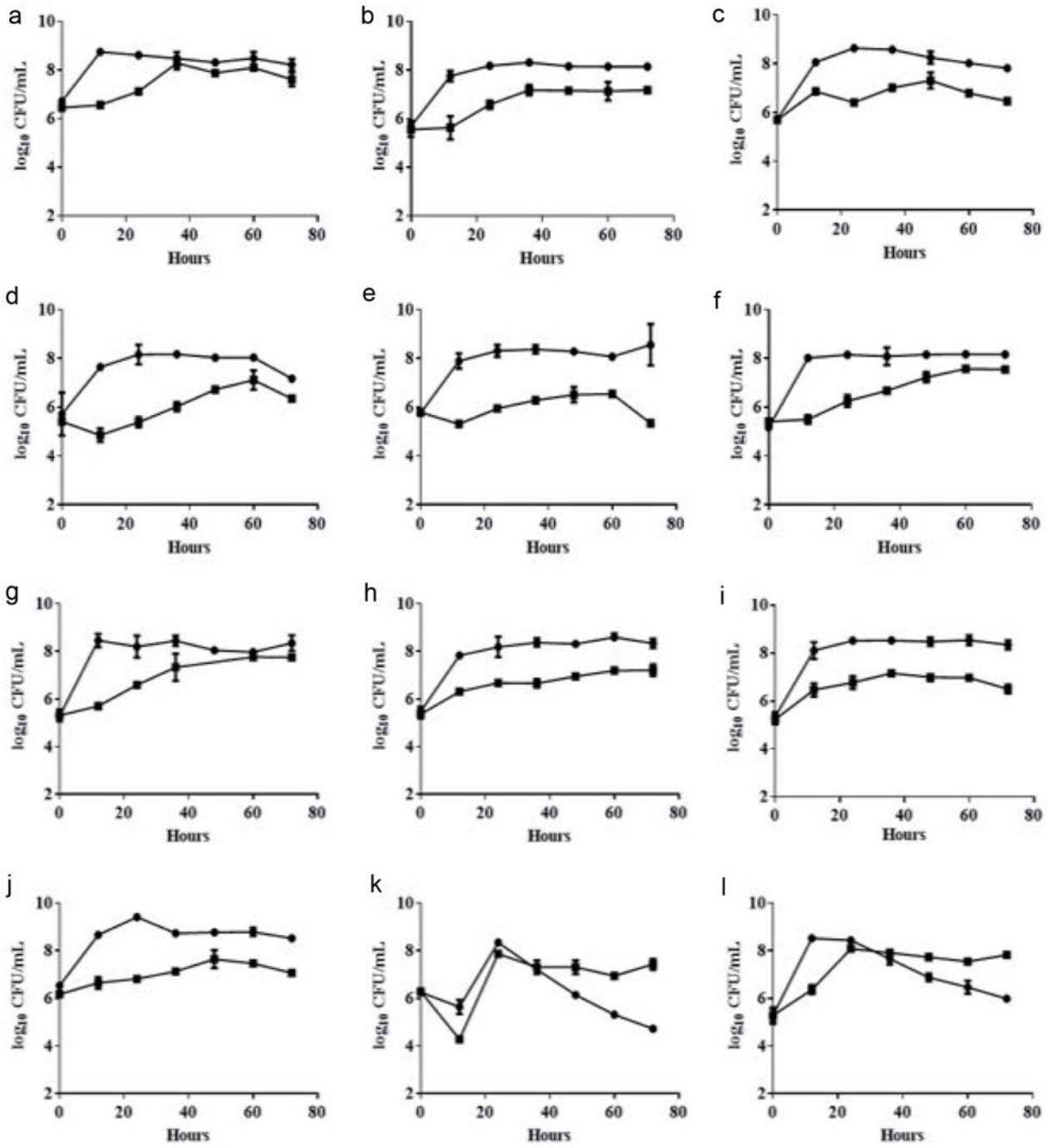

Figure 2. Growth curve of isolated LAB strains in 3% turmeric conditions. MRS medium (circle) and MRS medium containing 3% turmeric (square). (a) *L. rhamnosus* FN1 (b) *L. paracasei* YN2 (c) *L. rhamnosus* FN3 (d) *L. rhamnosus* FN4 (e) *L. paracasei* YN5 (f) *L. rhamnosus* FN7 (g) *L. rhamnosus* FN8 (h) *L. rhamnosus* FN9 (i) *L. paracasei* YN10 (j) *L. rhamnosus* FN11 (k) *L. crispatus* FN13 (l) *L. crispatus* FN14. The 1% of bacterial broth (OD_{600} = 1.0) was inoculated into the MRS medium containing 3% turmeric powder within the static culture under 37°C for 72 hours. The bacterial growth was evaluated using viable colonies forming unit (CFU). All experiments were carried out in triplicate, and bar values are expressed as the mean ± standard deviation.

during the fermentation of turmeric by *L. rhamnosus* FN7. Moreover, our findings are also consistent with previous studies (Mun et al., 2014).

On the other hand, it has been commonly seen that curcumin is present in higher concentrations than DMC and BDMC (Jayaprakasha et al., 2002). However, during HPLC quantification, an abnormal change in the ratio of curcuminoid content (especially Curcumin and DMC) of turmeric was observed (Figure 3). To fur-

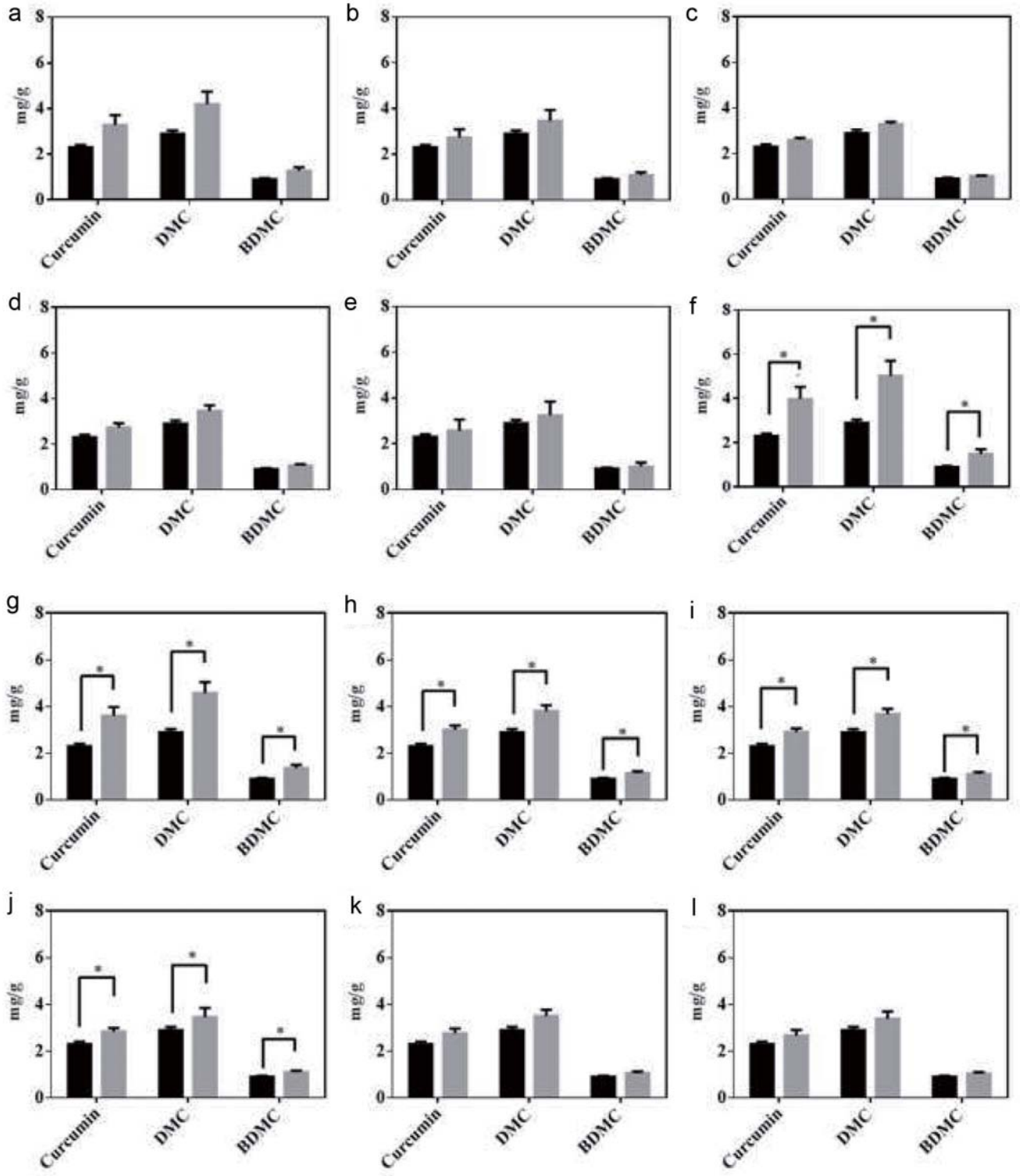

Figure 3. HPLC analysis of curcuminoids in unfermented (black bar) and fermented turmeric (grey bar). (a) *L. rhamnosus* FN1 (b) *L. paracasei* YN2 (c) *L. rhamnosus* FN3 (d) *L. rhamnosus* FN4 (e) I *L. paracasei* YN5 (f) *L. rhamnosus* FN7 (g) *L. rhamnosus* FN8 (h) *L. rhmanosus* FN9 (i) *L. paracasei* YN10 (j) *L. rhamnosus* FN11 (k) *L. crispatus* FN13 (l) *L. crispatus* FN14. After fermentation, curcuminoids were extracted from the freeze-dried fermented turmeric powders and analyzed using the HPLC system comprised of a C18 column with the UV-vis detector (set at 425 nm). All experiments were carried out in triplicate, and bar values are expressed as the mean ± standard deviation. Statistics were analyzed by unpaired t-test, $*p < 0.05$.

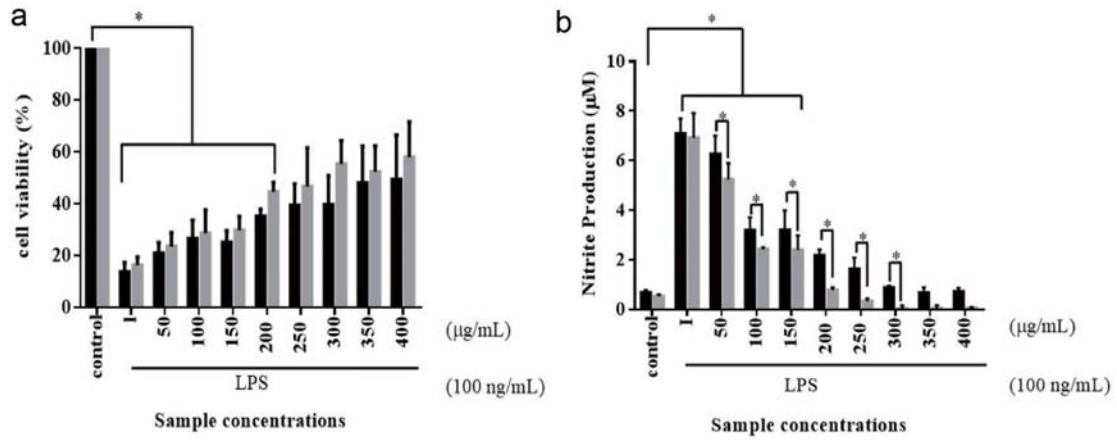

Figure 4. Cell viability (a) and nitrite production (b) of RAW264.7 murine macrophages were treated with various concentrations of unfermented turmeric (black bar) and fermented turmeric (grey bar) for 24 hours. RAW264.7 murine macrophages were cultured with lipopolysaccharide (LPS) and treated with various unfermented and fermented turmeric powder for 24 hours under a humidified atmosphere with 5% CO_2 at 37°C. The cell viability was analyzed using a classical MTT assay, and the Griess assay was used to evaluate the nitrite production. Results were statistically analyzed with the LSD method. Data are present as mean ± SD from at least triplicate wells and three independent experiments. Statistics were analyzed by unpaired t-test, $*p < 0.05$.

ther resolve this problem, an experiment was conducted to examine the impact of two different heating methods i.e. pasteurization and sterilization. The results, outlined in Figure S5, revealed that after the pasteurization, the concentration of curcumin and DMC was similar. Whereas, following the sterilization of turmeric, the concentration of the DMC was found to be higher than that of curcumin demonstrating its higher thermal stability than curcumin. There are two main possible reasons for curcumin decrease: (1) the thermal degradation of the β-diketone bond in its structure, which is quite vulnerable to break at temperatures higher than 100°C (Suresh et al., 2009). (2) The presence of additional functional methoxy groups in the curcumin structure lowers its stability (Heffernan et al., 2017).

3.4. L. rhamnosus FN7 fermentation enhances the anti-inflammatory activity of turmeric

LPS is an endotoxin derived from the outer cell wall of gram-negative bacteria, which plays a critical role in the regulation of inflammation (Yang et al., 2016). To assess the potential anti-inflammatory properties of unfermented and fermented turmeric, LPS-induced *in vitro* model was conducted. As turmeric fermented by *L. rhamnosus*, FN7 showed a higher curcuminoid than other groups. The turmeric sample derived from *L. rhamnosus* FN7 fermentation was selected as a target in our study. As shown in Figure 4a, it was found that the LPS reduced the cell viability of RAW264.7 cells more than 80% compared to the control group, while tested unfermented and fermented turmeric exhibited an influence on cell viability across all concentrations. The turmeric concentrations below 200 μg/mL had a significant difference in the cell viability compared to the control. As the concentration of the treatment increased, the cell proliferation gradually increased from the lower concentration to the higher concentration in fermented turmeric compared to unfermented turmeric. The result demonstrated the stimulatory effects of fermented and unfermented turmeric on the growth of RAW264.7 cells. However, there was no significant difference between unfermented and fermented turmeric treatment upon cell viability.

As mentioned in previous studies, a high level of NO could induce apoptosis directly or indirectly rendering many cells susceptible to apoptosis (Allione et al., 1999). In the current study, the accumulated nitrite in the cell culture supernatant was determined via Griess method as an index for NO produced by the LPS-induced RAW264.7 cells. To investigate the anti-inflammatory effect, we examined whether fermented turmeric could modulate nitrite (NO) synthesis in LPS-stimulated cultures of the RAW264.7 murine macrophages cells. As shown in the Figure 4b, it is evident that the production of NO in LPS-stimulated cells was significantly decreased when exposed to the fermented turmeric, starting from the concentrations of 50 μg/mL to 300 μg/mL, as compared to the unfermented turmeric, suggesting that the protective effect of fermented turmeric was attributed to the reduction of NO. While, concentrations beyond 300 μg/mL, there was no significant difference in the inhibitory effect on nitrite production between the two types of turmeric. Therefore, the analysis of our data strongly suggests that fermented turmeric showed more significant reductions in LPS-induced NO production in comparison to unfermented turmeric. The result is also consistent with a recent study, suggesting the suppression of the JNK signal pathway by fermented turmeric results in a profound protective effect on the LPS-induced RAW264.7 cells (Yong et al., 2019).

3.5. L. rhamnosus FN7 fermentation improves the phytochemical properties of turmeric

To date, around 235 compounds, primarily phenolic compounds and terpenoids, have been identified from the turmeric (Li et al., 2011). Due to their antioxidative properties of phenolic compounds, they are beneficial against diabetes, cardiovascular, mutagenesis, carcinogenesis, and neurogenerative disease. Thus, the content of phenolic compounds in fermented turmeric was disclosed before and after fermentation. As shown in Figure 5a, the results revealed a significant elevation in the phenolic compounds after fermentation. Numerically, the total phenolic compounds value of unfermented sample was 7.06 mg gallic acid/g which was significantly enhanced to 8.57 mg gallic acid/g after *L. rhamnosus* FN7 turmeric fermentation. The result was similar with previous research work in which phenolic compound content was investi-

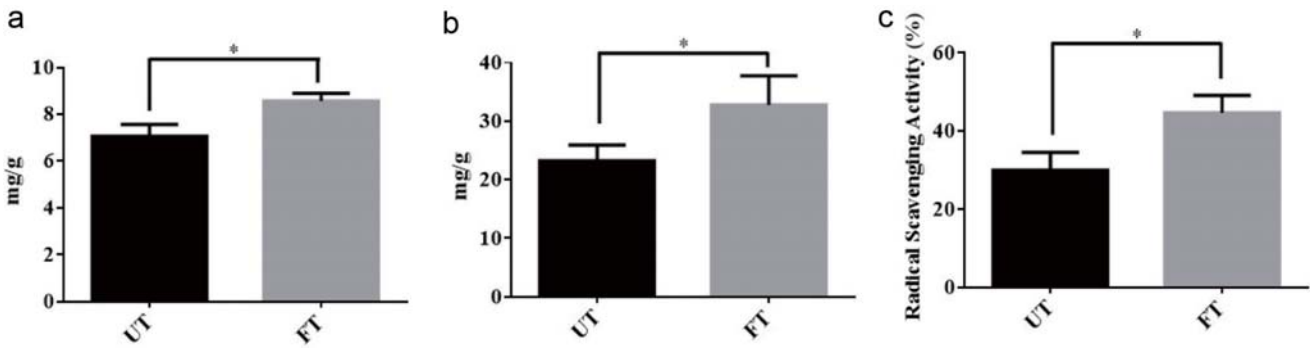

Figure 5. Phytochemical property of fermented turmeric by *L. rhamnosus* FN7. (a) Total Phenolic Content (b) Total Flavonoid Content (c) Radical Scavenging Activity of unfermented turmeric (UT) and fermented turmeric (FT). Freeze-drying fermented and unfermented turmeric powders were used to extract the total Phenolic and Flavonoid compounds and quantification was performed with a slightly modified Folin-Ciocalteau (FC) method and Aluminium chloride ($AlCl_3$) colorimetric assay, respectively. DPPH analysis was used to evaluate the Radical Scavenging Activity of fermented and unfermented turmeric. All experiments were carried out in triplicate, and bar values are expressed as the mean ± standard deviation. Statistics were analyzed by unpaired t-test, $*p < 0.05$.

gated during the fermentation of the blueberry-carrot blend and mulberry juice using *Lactobacillus* strains. These two fermented products possess more phenolic compounds after fermentation (Kwaw et al., 2018; Mauro et al., 2016). The possible reasons for the rise in phenolic levels in fermented turmeric can be associated with the breakdown of glycosylated phenolics present in the unfermented turmeric matrix, resulting in the release of bound and insoluble phenolics from the cellular structures of plant material during the fermentation process (Mauro et al., 2016). Moreover, the existing research supports the notion that microorganisms can break down phenolic complexes into simpler and more bioavailable phenolic compounds that can be easily absorbed (Adetuyi and Ibrahim, 2014). Therefore, the conversion and depolymerization of complex compounds by LAB during fermentation could be a possible explanation for the rise in phenolic content.

We further evaluated the total flavonoid content in the fermented turmeric and compared it with unfermented turmeric. The flavonoids are low molecular weight, secondary metabolites having a polyphenolic structure that not only play a role in determining the color and fragrance of flowers in fruits and vegetables but also have health-promoting effects (Panche et al., 2016). In turmeric, the flavonoids include not only curcuminoids but also other bioactive compounds such as luteolin-7-O-(6″-p-hydroxybenzoyl-β-D-glucopyranoside), luteolin 7-O-β-D-glucopyranoside, apigenin-7-O-β-D-glucopyranoside, luteolin, apigenin, apigenin 7-O-rhamnoside 4′-O-glucoside, 7-methoxyapigenin-6-C-glucoside (Shabana et al., 2015). As shown in Figure 5b, the total flavonoid contents of fermented turmeric showed a similar trend as total phenolic compounds. The total flavonoid content in fermented turmeric was determined significantly higher in comparison to unfermented turmeric. Before fermentation, the total flavonoid content value of the unfermented turmeric was 23.2 mg quercetin/g, which was significantly enhanced to 32.7 mg quercetin/g after *L. rhamnosus* FN7 fermentation. The increase in total flavonoid contents might be attributed to the enzymatic breakdown of complex polyphenols into simpler flavanol compounds during the fermentation process (Kwaw et al., 2018). Moreover, it may also be resulted from the higher curcuminoid content (Priyadarsini, 2013).

Reactive oxygen species (ROS) are molecules with unpaired electrons generated by various factors, including environmental pollutants, radiation, chemicals, toxins, physical stress, deep-fried and spicy foods. It has been reported that ROS significantly contributes to the onset of various physiological disorders, such as cellular damage, aging, cancer, and conditions affecting the liver, nervous system, heart, and kidneys (Madamanchi et al., 2005). To determine whether the scavenging ability of turmeric is enhanced after *L. rhamnosus* FN7 fermentation, the scavenging ability of DPPH radicals was investigated before and after fermentation. As shown in Figure 5c, the radical scavenging ability of fermented turmeric was significantly improved by *L. rhamnosus* FN7 fermentation. The radical scavenging ability of unfermented turmeric was 30.0 ± 2.6% which significantly increased to 44.6 ± 2.6% after fermentation of turmeric, indicating fermentation as the main cause of the enhancement in scavenging ability which may be due to the increase in total phenolic content (Ng et al., 2011). Moreover, it can also be attributed to the bacteria metabolization of the sugar attached to phenolic compounds and anthocyanins, leading to increased aglycone production, which enhances the radical scavenging capabilities of fermented turmeric (Sharma et al., 2023). In the past, it also has been reported that probiotic microorganisms chelate the metal ion and scavenge free radicals (Curiel et al., 2015). Overall, these findings suggested that turmeric fermented with *L. rhamnosus* FN7 helps in enhancing its phytochemical properties.

3.6. L. rhamnosus FN7 presents the potential ability to be applied as probiotics

LAB to become probiotic, need to exhibit specific attributes, including the ability to withstand gastrointestinal conditions (such as low pH and high bile salt concentrations) (Collins et al., 1998). In past, *Lactobacilli* strains are highly recognized as promising probiotics, and are extensively employed in both food and non-food applications. In order to be used as a probiotic, the *Lactobacilli* strain must survive in the low pH conditions of gastric juice in the stomach (Goldin and Gorbach, 1992). In this study, to investigate whether *L. rhamnosus* FN7 can be employed as a potential probiotic, we further utilized *in vitro* assays to simulate and analyze the survival rate of *L. rhamnosus* FN7 in GI conditions. As shown in Figure 6a, at pH 3, the results revealed that the strain CFU/mL remained constant even after 6 hours. When exposed to pH 2.5, the CFU/mL of the *L. rhamnosus* FN7 showed a slight decrease after 6 hours of incubation. However, when the strain was introduced to pH 2, it was not able to survive and succumbed within hours of incubation. In addition, it is important to note that in the presence of food, the pH level typically rises around pH 3 which usually takes 2 to 4 hours for the stomach to empty after food ingestion (Erkkilä and Petäjä, 2000). Therefore, such conditions can enhance

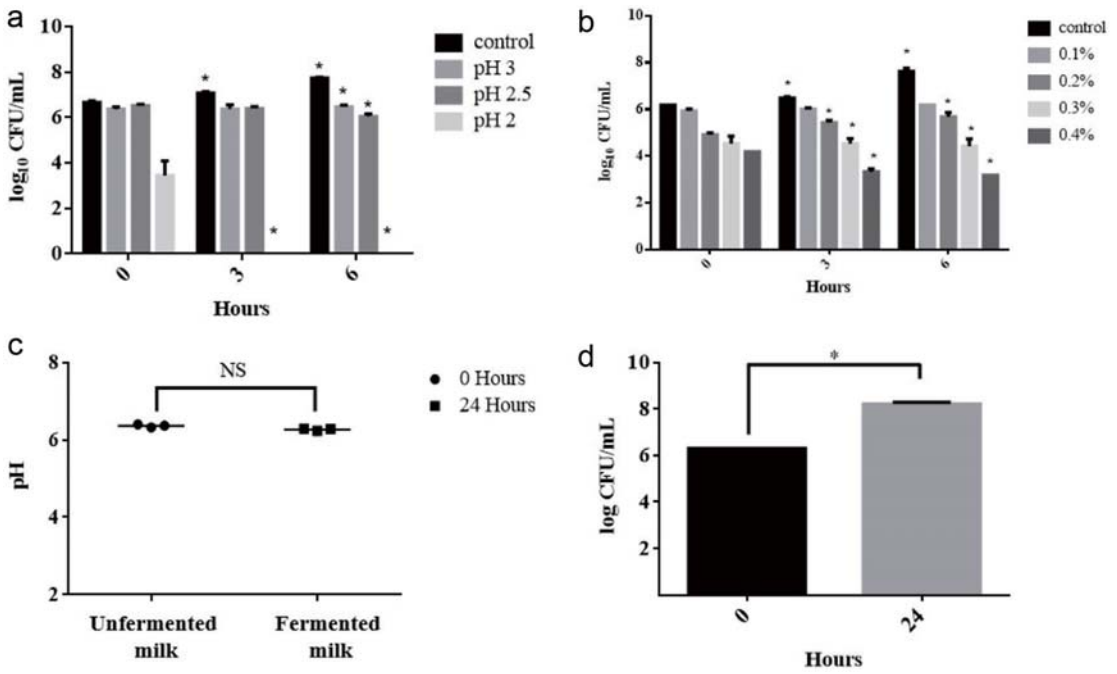

Figure 6. The probiotic property assay of fermented turmeric by *L. rhamnosus* FN7. (a) pH tolerance, (b) Bile tolerance, (c and d) Milk fermentation capacity. For pH and bile tolerance, the *L. rhamnosus* FN7 strain was cultured in the MRS medium with different conditions under anaerobic at 37°C for 6 hours. Milk fermentation capacity was performed by incubation of *L. rhamnosus* FN7 in 10% (w/v) skim milk. The viable colonies forming unit (CFU) was used to evaluate the growth of the *L. rhamnosus* FN7 strain in all experiments, and the pH of cultured milk was measured. Statistics were analyzed by unpaired t-test, $*p < 0.05$.

the survivability of *L. rhamnosus* FN7 strain within the low pH of the human gastrointestinal tract.

Bile salts synthesized in the liver from cholesterol are known to create critical conditions for *Lactobacillus* strains to survive in the gastrointestinal tract (Erkkilä and Petäjä, 2000). To address this, we investigated the bile tolerance ability of *L. rhamnosus* FN7 strain. Previous research has identified a concentration of 0.3% bile salts as a crucial threshold for screening bile-resistant strains (Gilliland et al., 1984). Similarly, Goldin and Gorbach suggested the same concentration level to select probiotics for human use (Goldin and Gorbach, 1992). In our test, the colony-forming units (CFU/mL) of *L. rhamnosus* FN7 were evaluated in bile salt concentrations of 0.1, 0.2, 0.3, 0.4, 0.5, and 1.0%. The results showed a gradual decrease in CFU/mL following inoculation, with successive colony counts at 3 hours intervals up to 6 hours (Figure 6b). Notably, no colony was observed at bile concentrations of 0.5% and 1%, respectively. Hence, the resistance of the *L. rhamnosus* FN7 strain to bile salts diminishes as the salt percentage increases. However, the strain can effectively survive at usual concentrations of bile salt in the gastrointestinal tract which typically encountered after food consumption (Erkkilä and Petäjä, 2000).

Milk fermentation generally involves the conversion of lactose into lactic acid by LAB, particularly *Lactobacilli* and *Lactococci*, which leads in the reduction of the pH of the fermented milk (Surono and Hosono, 2011). To assess the milk fermentation capability and the ability of *L. rhamnosus* FN7 strain to digest lactose, an experiment was conducted. Thus, it was observed that there was negligible change in pH after 24 hours of incubation at 37°C, while the strain CFU/mL increased from 6.3 to 8.2, suggesting that milk as a source of energy for the strain growth (Figure 6c and d). In addition, it is worth noting that various report indicates that *L. rhamnosus* GG strain cannot ferment lactose, which is consistent with our finding (Gorbach et al., 2017). However, a few strains of the same species have been reported to possess the capacity to ferment milk (Jeffrey et al., 2020). Hence, the probable reason for the *L. rhamnosus* FN7 inability to ferment the milk could be attributed to the frameshifts in the anti-terminator (*lacT*) and 6-phospho-β-galactosidase (*lacG*) genes, which affect the *Lactobacillus* strain ability to utilize D-lactose (Kankainen et al., 2009).

4. Conclusion

Recent research has increasingly focused on leveraging LAB fermentation to augment the bioactive functionality of foods. In this vein, our study has targeted the bioactivity enhancement of turmeric, a spice renowned for its health benefits but limited by the bioavailability of its active compounds, curcuminoids. Through meticulous strain selection, we have identified L. *rhamnosus* FN7 as a potent strain for turmeric fermentation, capable of augmenting its curcuminoid content. This process not only improves the phytochemical attributes of turmeric but also transforms it into a potent functional food with significant anti-inflammatory properties.

Our findings reveal that fermented turmeric, through the action of L. *rhamnosus* FN7, exhibits an increased concentration of curcuminoids and a broader spectrum of phytochemicals, thereby enhancing its efficacy in treating inflammatory conditions. Looking ahead, it is imperative to conduct thorough research to unravel the full spectrum of health benefits offered by L. *rhamnosus* FN7, particularly in its role as a probiotic for commercial application.

Moreover, our investigation has shed light on the mechanisms underlying the enhanced bioactivity post-fermentation. It has

been elucidated that the peptidoglycan layer in the cell walls of Gram-positive bacteria such as Lactobacillus forms a complex with curcuminoids, facilitating their bioavailability. This binding phenomenon positions the Lactobacillus-curcuminoid complex as a promising natural vehicle for disease prevention, offering a novel approach to utilizing turmeric and its derivatives in therapeutic applications. The potential of such a natural carrier holds immense promise, warranting further exploration into its role in disease management and prevention strategies

Acknowledgments

We would like to acknowledge the service provided by the DNA Sequencing Core of the Center for Biotechnology, National Taiwan University.

Funding

This work was supported by the Ministry of Science and Technology, Taiwan [109-2320-B-002 -012 -MY3 and 110-2320-B-002 -019 -MY3].

Conflict of interest

The authors declare no conflict of interest.

Supplementary Material

Suppl 1. Growth curve of different BCRC LAB strains in 3% turmeric conditions. MRS medium (circle) and MRS medium containing 3% turmeric (square). (a) *L. gasseri* BCRC 14619, (b) *L. rhamnosus* GG BCRC 16000, (c) *Lactobacillus* sp. MCL40.

Suppl 2. Cellulase activity test of *L. rhamnosus* FN7.

Suppl 3. Quantification of curcuminoids in unfermented (black bar) and fermented turmeric (grey bar) by different BCRC LAB strains. (a) *B. longum* BCRC 11847 (b) *L. rhamnosus* GG BCRC 16000 (c) *L. gasseri* BCRC 14619 (d) *L. reuteri* BCRC 14625 (e) *L. rhamnosus* BCRC 10940 (f) *L. fermentum* BCRC 12190.

Suppl 4. Effect of various percentage of *L. rhamnosus* FN7 biomass cell wall binding property in curcumin medium.

Suppl 5. Comparison of curcuminoids change in unfermented turmeric (UT) during Post-Heat retention time after autoclave.

References

Adetuyi, F., and Ibrahim, T. (2014). Effect of fermentation time on the phenolic, flavonoid, and vitamin C contents and antioxidant activities of okra (*Abelmoschus esculentus*) seeds. Niger. Food J. 32(2): 128–137.

Allione, A., Bernabei, P., Bosticardo, M., Ariotti, S., Forni, G., and Novelli, F. (1999). Nitric oxide suppresses human T lymphocyte proliferation through IFN-γ-dependent and IFN-γ-independent induction of apoptosis. J. Immunol. 163(8): 4182–4191.

Anal, A.K. (2019). Quality ingredients and safety concerns for traditional fermented foods and beverages from Asia: A Review. Fermentation. 5(1): 8.

Anand, P., Kunnumakkara, A.B., Newman, R.A., and Aggarwal, B.B. (2007). Bioavailability of curcumin: Problems and promises. Mol. Pharm. 4(6): 807–818.

Anand, P., Thomas, S.G., Kunnumakkara, A.B., Sundaram, C., Harikumar, K.B., Sung, B., Tharakan, S.T., Misra, K., Priyadarsini, I.K., Rajasekharan, K.N., and Aggarwal, B.B. (2008). Biological activities of curcumin and its analogs (congeners) made by man and mother nature. Biochem. Pharmacol. 76(11): 1590–1611.

Axelsson, L. Lactic Acid Bacteria: Classification and Physiology. In: Salminen, S., von Wright, A., and Ouwehand, A. (Ed.). Lactic Acid Bacteria: Microbiological and Functional Aspects, Third Edition. Marcel Dekker Publishers, New York, pp. 1–66.

Collins, J.K., Thornton, G., and Sullivan, G.O. (1998). Selection of probiotic strains for human applications. Int. Dairy J. 8(5-6): 487–490.

Curiel, J.A., Pinto, D., Marzani, B., Filannino, P., Farris, G.A., Gobbetti, M., and Rizzello, C.G. (2015). Lactic acid fermentation as a tool to enhance the antioxidant properties of Myrtus communis berries. Microb. Cell Fact. 14(1): 1–10.

Erkkilä, S., and Petäjä, E. (2000). Screening of commercial meat starter cultures at low pH and in the presence of bile salts for potential probiotic use. Meat Sci. 55(3): 297–300.

Goldin, B.R., and Gorbach, S.L. (1992). Probiotics for humans. In: Fuller, R. (Ed.). Probiotics. Springer Publishers, Dordrecht, pp. 355–376.

Gorbach, S., Doron, S., and Magro, F. (2017). *Lactobacillus rhamnosus* GG. In: Floch, M.H., Ringel, Y., and Allan Walker, W. (Ed.). The microbiota in gastrointestinal pathophysiology. Academic Press Publishers, Boston, pp. 79–88.

Heffernan, C., Ukrainczyk, M., Gamidi, R.K., Hodnett, B.K., and Rasmuson, A.C. (2017). Extraction and purification of curcuminoids from crude curcumin by a combination of crystallization and chromatography. Org. Process Res. Dev. 21(6): 821–826.

Horsley, H., Malone-Lee, J., Holland, D., Tuz, M., Hibbert, A., Kelsey, M., Kupelian, A., and Rohn, J.L. (2013). *Enterococcus faecalis* subverts and invades the host urothelium in patients with chronic urinary tract infection. PLoS One 8(12): 83637–83650.

Jayaprakasha, G.K., Rao, L.J.M., and Sakariah, K.K. (2002). Improved HPLC method for the determination of curcumin, demethoxycurcumin, and bisdemethoxycurcumin. J. Agric. Food Chem. 50(13): 3668–3672.

Jeffrey, M.P., Taggart, H.J., Strap, J.L., Edun, G., and Green-Johnson, J.M. (2020). Milk fermented with *Lactobacillus rhamnosus* R0011 induces a regulatory cytokine profile in LPS-challenged U937 and THP-1 macrophages. CRFS 3: 51–58.

Kankainen, M., Paulin, L., Tynkkynen, S., von Ossowski, I., Reunanen, J., Partanen, P., Satokari, R., Vesterlund, S., Hendrickx, A.P., and Lebeer, S. (2009). Comparative genomic analysis of *Lactobacillus rhamnosus* GG reveals pili containing a human-mucus binding protein. Proc. Natl. Acad. Sci. U.S.A. 106(40): 17193–17198.

Kim, S., Kang, B.-H., Kwon, H.-S., and Kang, J.-H. (2011). Anti-inflammatory and antiallergic activity of fermented turmeric by *Lactobacillus johnsonii* IDCC 9203. Microb. Biotechnol. Letter. 39(3): 266–273.

Kwaw, E., Ma, Y.K., Tchabo, W., Apaliya, M.T., Wu, M., Sackey, A.S., Xiao, L.L., and Tahir, H.E. (2018). Effect of lactobacillus strains on phenolic profile, color attributes and antioxidant activities of lactic-acid-fermented mulberry juice. Food Chem. 250: 148–154.

Li, S., Yuan, W., Deng, G.-R., Wang, P., Yang, P., and Aggarwal, B.B. (2011). Chemical composition and product quality control of turmeric (*Curcuma longa* L.). Pharm. Crop. 2: 28–54.

Lim, J., Nguyen, T.T.H., Pal, K., Kang, C.G., Park, C., Kim, S.W., and Kim, D. (2022). Phytochemical properties and functional characteristics of wild turmeric (*Curcuma aromatica*) fermented with *Rhizopus oligosporus*. Food Chem. 13: 100198.

Madamanchi, N.R., Vendrov, A., and Runge, M.S. (2005). Oxidative stress and vascular disease. Arterioscler. Thromb. Vasc. Biol. 25(1): 29–38.

Marathe, S.A., Ray, S., and Chakravortty, D. (2010). Curcumin increases the pathogenicity of *Salmonella enterica* serovar Typhimurium in a murine model. PLoS one 5(7): e11511.

Martínez-Romero, E., Rodríguez-Medina, N., Beltrán-Rojel, M., Silva-Sánchez, J., Barrios-Camacho, H., Pérez-Rueda, E., and Garza-Ramos, U. (2018). Genome misclassification of *Klebsiella variicola* and *Klebsiella quasipneumoniae* and isolated from plants, animals and humans. Salud Publica De Mexico. 60(1): 56–62.

Mauro, C.S.I., Guergoletto, K.B., and Garcia, S. (2016). Development of blueberry and carrot juice blend fermented by *Lactobacillus reuteri* LR92. Beverages 2(4): 37–48.

Mohamed, S.A., Saleh, R.M., Kabli, S.A., and Al-Garni, S.M. (2016). Influence of solid-state fermentation by *Trichoderma* spp. on solubility, phenolic content, antioxidant, and antimicrobial activities of commercial turmeric. Biosci. Biotechnol Biochem. 80(5): 920–928.

Mun, S.-H., Kim, S.-B., Kong, R., Choi, J.-G., Kim, Y.-C., Shin, D.-W., Kang, O.-H., and Kwon, D.-Y. (2014). Curcumin reverse methicillin resistance in *Staphylococcus aureus*. Molecules 19(11): 18283–18295.

Ng, C.C., Wang, C.Y., Wang, Y.P., Tzeng, W.S., and Shyu, Y.T. (2011). Lactic acid bacterial fermentation on the production of functional antioxidant herbal *Anoectochilus formosanus* Hayata. J. Biosci. Bioeng. 111(3): 289–293.

Panche, A.N., Diwan, A.D., and Chandra, S.R. (2016). Flavonoids: an overview. J. Nutr. Sci. 5: e47.

Peram, M.R., Jalalpure, S.S., Palkar, M.B., and Diwan, P.V. (2017). Stability studies of pure and mixture form of curcuminoids by reverse phase-HPLC method under various experimental stress conditions. Food Sci. Biotechnol. 26(3): 591–602.

Prasad, S., and Aggarwal, B.B. (2011). Turmeric, the golden spice. In: Benzie, I.F.F., and Wachtel-Galor, S. (Ed.). Herbal Medicine: Biomolecular and Clinical Aspects. 2nd edition. Boca Raton Publisher, CRC Press/ Taylor & Francis.

Priyadarsini, K.I. (2013). Chemical and structural features influencing the biological activity of curcumin. Curr. Pharm. Des. 19(11): 2093–2100.

Rosenthal, A., Pyle, D.L., and Niranjan, K. (1996). Aqueous and enzymatic processes for edible oil extraction. Enzyme Microb. Technol. 19(6): 402–420.

Shabana, M.H., Shahy, E.M., Taha, M.M., Mahdy, G.M., and Mahmoud, M.H. (2015). Phytoconstituents from *Curcuma longa* L. aqueous ethanol extract and its immunomodulatory effect on diabetic infected rats. Egypt. Pharm. J. 14(1): 36–43.

Sharifi-Rad, J., El Rayess, Y., Rizk, A.A., Sadaka, C., Zgheib, R., Zam, W., Sestito, S., Rapposelli, S., Neffe-Skocinska, K., Zielinska, D., Salehi, B., Setzer, W.N., Dosoky, N.S., Taheri, Y., El Beyrouthy, M., Martorell, M., Ostrander, E.A., Suleria, H.A.R., Cho, W.C., Maroyi, A., and Martins, N. (2020). Turmeric and its major compound curcumin on health: bioactive effects and safety profiles for food, pharmaceutical, biotechnological and medicinal applications. Front. Pharmacol. 11: 1021–1044.

Sharma, P., Kashyap, P., and Dhakane, A. (2022). Exploring the antioxidant potential of fermented turmeric pulp: effect of extraction methods and microencapsulation. Prep. Biochem. Biotechnol. 53(8): 968–977.

Sharma, R., Garg, P., Kumar, P., Bhatia, S.K., and Kulshrestha, S. (2020). Microbial fermentation and its role in quality improvement of fermented foods. Fermentation. 6(4): 106–126.

Suresh, D., Gurudutt, K.N., and Srinivasan, K. (2009). Degradation of bioactive spice compound: curcumin during domestic cooking. Eur. Food Res. Technol. 228(5): 807–812.

Surono, I.S., and Hosono, A. (2011). Fermented milk: types and standards of identity. (2nd ed). Elsevier, Amsterdam, pp. 470–476.

Yang, L., Guo, H., Li, Y., Meng, X., Yan, L., Zhang, D., Wu, S., Zhou, H., Peng, L., and Xie, Q. (2016). Oleoylethanolamide exerts anti-inflammatory effects on LPS-induced THP-1 cells by enhancing PPARα signaling and inhibiting the NF-κB and ERK1/2/AP-1/STAT3 pathways. Sci. Rep. 6(1): 34611–34623.

Yong, C.C., Yoon, Y., Yoo, H.S., and Oh, S. (2019). Effect of *lactobacillus fermentation* on the anti-inflammatory potential of turmeric. J. Microbiol. Biotechnol. 29(10): 1561–1569.

Journal of Food Bioactives
International Society for Nutraceuticals and Functional Foods
Original Research
J. Food Bioact. 2024;25:25–41

A comprehensive characterization of phenolics, amino acids and other minor bioactives of selected honeys and identification of botanical origin markers

Yan Zhu[a], Ronghua Liu[a], Lili Mats[a], Honghui Zhu[a], Joy Roasa[a,b], Tauseef Khan[c,d,e], Amna Ahmed[c,d,e], Yolanda Brummer[a], Steve Cui[a], John Sievenpiper[c,d,e,f,g], D. Dan Ramdath[a] and Rong Tsao*[a]

[a]Guelph Research and Development Centre, Agriculture and Agri-Food Canada, 93 Stone Road West, Guelph, Ontario N1G 5C9, Canada
[b]Department of Food Science, University of Guelph, Guelph, Ontario N1G 2W1, Canada
[c]Department of Nutritional Sciences, Temerty Faculty of Medicine, University of Toronto, Toronto, Canada
[d]Toronto 3D Knowledge Synthesis and Clinical Trials Unit, Clinical Nutrition, St Michael's Hospital, Toronto, Ontario, Canada.
[e]Clinical Nutrition and Risk Factor Modification Centre, St Michael's Hospital, Toronto, Ontario, Canada
[f]Division of Endocrinology and Metabolism, St Michael's Hospital, Toronto, Ontario, Canada
[g]Li Ka Shing Knowledge Institute, St Michael's Hospital, Toronto, Ontario, Canada
*Corresponding author: Rong Tsao, Guelph Research and Development Centre, Agriculture and Agri-Food Canada, 93 Stone Road West, Guelph, Ontario N1G 5C9, Canada. E-mail: rong.cao@agr.gc.ca
DOI: 10.31665/JFB.2024.18369
Received: January 04, 2024; **Revised received & accepted:** February 05, 2024
Citation: Zhu, Y., Liu, R., Mats, L., Zhu, H., Roasa, J., Khan, T., Ahmed, A., Brummer, Y., Cui, S., Sievenpiper, J., Ramdath, D.D., and Tsao, R. (2024). A comprehensive characterization of phenolics, amino acids and other minor bioactives of selected honeys and identification of botanical origin markers. J. Food Bioact. 25: 25–41.

Abstract

Phenolic and amino acid profiles along with organic acid, vitamin and mineral contents, major and minor sugars and enzyme activities of selected honey samples collected in North America were analyzed using different methods and potential markers of their botanical origin were identified. A total of 29 phenolic compounds were detected, of which some were found to be a good chemical markers to distinguish a genuine honey given its propolis origin. Quantitative data and principal component analysis showed that hesperidin, caffeic acid/isoferulic acid, and *p*-hydroxybenzoic acid/*p*-coumaric acid have the most positive relationship to the orange, alfalfa, and buckwheat honey, respectively, indicating their potential roles as chemical markers of these floral honeys. Free amino acid profiles were similar in all honeys except buckwheat which not only had significantly higher branched-chain amino acids but was the only floral honey that contained L-norvaline that was identified for the first time. The enzyme activities and the major and rare sugar composition helped explain the presence of the various organic acids in the honeys. Compositional data of these bioactives and other nutrients will not only serve as database information for honey derived from North America but also provide insightful knowledge for the underlining potential health benefits.

Keywords: Honey composition; Botanical origin; Phenolic compounds; Amino acids; L-norvaline; Rare sugar.

1. Introduction

Honey is a natural sweetener produced from honeydew or flower nectar by bees (Olas, 2020). In addition to sugars, mainly glucose and fructose, honey contains a variety of other nutrients and bioactive compounds, including phenolics, proteins/amino acids, organic acids, vitamins, minerals and enzymes (da Silva et al., 2016; Machado De-Melo et al., 2018). Honey is a nutritious food that of-

fers numerous health benefits (Battino et al., 2021; Zammit Young and Blundell, 2023). Its unique composition, particularly that of phenolic compounds and amino acids, makes it a valuable addition to a balanced diet.

Phenolic compounds are a class of naturally occurring compounds found in many plant-based foods. They are produced as secondary metabolites by plants and act as strong antioxidants to suppress oxidative stress, which has been linked to many adverse effects and chronic diseases such as obesity, metabolic disorders, type 2 diabetes, cardiovascular disease, and cancers (Battino et al., 2021; Cianciosi et al., 2018; Zammit Young and Blundell, 2023). In addition to their direct antioxidant function, phenolics have been shown to enhance antioxidant enzyme activities, inhibit production of pro-inflammatory cytokines, and directly attenuate oxidative stress-induced inflammatory signalling pathways, thereby reducing the risk of chronic diseases (Zhang and Tsao, 2016). Although relatively low in concentration, amino acids are another class of compounds found in honey with bioactive functions, mainly acting as precursors of protein synthesis and intermediates of various metabolic processes (Janiszewska et al., 2012).

Among honey products, floral honeys have garnered particular attention due to their specific composition and unique bioactivities. The documented health-promoting properties of such honeys have led to increased demand and high market value (Sultana et al., 2022). To determine the plant origin and differentiate adulterated products from natural honey, a melissopalynological strategy has been commonly used, using methods such as microscopic techniques to study the pollen contained in the honey. However, recent advances in analytical techniques capable of profiling honey constituents, such as carbohydrates, phenolic compounds, amino acids, volatile compounds, organic acids, proteins and nucleic acids, have immensely helped in providing insights on the nutrient and/or therapeutic characters of specific honey varieties, and identifying markers for discriminating the botanical origins of floral honeys (Wang et al., 2022). As a main source of phytochemicals, nectar-derived phenolic acids and flavonoids have therefore become good candidates for chemical markers of floral honeys. Previous studies have proposed hesperetin, kaempferol, and quercetin as botanical markers of citrus, rosemary, and sunflower honey, respectively (Tomás-Barberán et al., 2001). *p*-Coumaric acid and *p*-hydroxybenzoic acids were also reported to be unique in buckwheat honey (Sergiel et al., 2014; Shen et al., 2019). Free amino acids in honey originate from both plants and honeybees. Except for the predominant proline which originates from the hypopharyngeal glands in the worker honeybee (Davies, 1978), some other free amino acids were identified as botanical markers. For examples, leucine, isoleucine, and tyrosine are major amino acids in buckwheat honey (Dimins et al., 2022), and asparagine is enriched in ilex honey (Paramás et al., 2006). A non-proteinogenic amino acid, γ-aminobutyric acid, was unique to chestnut-tree honey (Paramás et al., 2006).

Even when honeys shares the same botanical origin, their compositions could be influenced by a number of factors including geographic location, environmental condition, processing method, and storage condition (Hermosín et al., 2003), which add challenges in identifying the right chemical markers. High-resolution instrumental analysis in combination with multivariable statistical analysis can offer a unique solution to this problem. Moreover, use of multiple markers from different groups of honey constituents could improve the confidence level in discriminating different honeys.

Meanwhile, although chemical profiling of phenolics and in some cases, free amino acids of honeys of many countries has been studied, such data and other compositional information including total protein, vitamins, mineral and amino acid compositions, organic acids, rare sugars and enzyme activities is lacking for North American honey varieties. Contribution of these components to health benefits and usefulness of them as markers for honey's plant origin have not been studied for North American honeys. This study therefore aims to carry out a comprehensive analysis of the composition of four selected floral honeys, alfalfa (*Medicago sativa*), buckwheat (*Fagopyrum esculentum*), clover (*Trifolium* spp.), orange (*Citrus sinensis*), and one multifloral honey (wildflower honey) purchased in North America, to identify chemical markers for their botanical origins, and to provide a nutritional and bioactives database for further studies on the potential health benefits of honey.

2. Materials and methods

2.1. Samples, chemicals and reagents

Honey samples were provided by the US National Honey Board. Fifteen honey samples with five varieties including alfalfa (n = 3), buckwheat (n = 3), clover (n = 4), orange (n = 3), and wildflower (n = 2) were produced and collected between 2020 and 2022. Details on honey samples are in Table S1. All samples were stored at −20°C before analysis.

Phenolic standards, including gallic acid, protocatechuic acid, neochlorogenic acid, *p*-hydroxybenzoic acid, vanillic acid, caffeic acid, chlorogenic acid, syringic acid, *p*-coumaric acid, trans-ferulic acid, isoferulic acid, *o*-coumaric acid, ellagic acid, hesperidin, myricetin, kaempferol-rutinoside, pinobanksin-5-methyl ether (P5ME), pinobanksin, quercetin, naringenin, luteolin, hesperetin, kaempferol, apigenin, isohamnetin, pinocembrin, chrysin, galangin, acacetin, 5-hydroxymethylfurfural (5-HMF), furfural, abscisic acid, 20 proteinogenic L-amino acids and L-norvaline, organic acid standards including acetic acid, citric acid, formic acid, gluconic acid, glutaric acid, glycolic acid, lactic acid, maleic acid, malic acid, malonic acid, oxalic acid, propionic acid, succinic acid, vitamin standards including ascorbic acid, riboflavin (B2), nicotinic acid (B3), pantothenic acid (B5), pyridoxine (B6), 2-ethylbutyric acid, glucose, fructose, sucrose, trehalose, kojibiose, maltose, isomaltose, turanose, palatinose, nigerose, melezitose. isomaltotriose and maltotriose, and other solvents and reagents including acetonitrile, formic acid, ammonium formate were obtained from Sigma-Aldrich (Oakville, ON, Canada). LC-MS grade methanol was obtained from Fisher Scientific (Ottawa, ON, Canada). Distilled and deionized water was purified in-house using a Milli-Q system (Bedford, MA, USA).

2.2. Extraction of 5-HMF, furfural, abscisic acid, and phenolic compounds

Phenolic extracts of honey were prepared using acidified aqueous methanol as previously described with modification (Zhang et al., 2017a). Briefly, honey samples were weighed and diluted to 30 % (w/v) solution with water and were acidified by formic acid to the final concentration of 1 % (v/v). 2-Hydroxy-4-methoxybenzoic acid was spiked in samples as an internal standard (IS) for evaluating the recovery efficiency of the extraction method. Twenty-five mL of acidified honey solution was then purified using OASIS HLB polymeric solid phase extraction cartridges (150 mg, Waters, Mississauga, ON, Canada) and eluted with 2 mL of 1 % (v/v) formic acid in methanol. The eluent was stored in −20°C freezer before LC-MS analysis.

2.3. Analysis of 5-HMF, furfural, abscisic acid, and phenolic compounds by LC-MS/MS

LC-MS/MS analysis was performed using a Thermo® Scientific Q-Exactive™ Orbitrap mass spectrometer coupled to a Vanquish™ Flex Binary UPLC System with a diode array detector (DAD) (Waltham, MA, USA). A Kinetex XB-C18 100A column (100 × 4.6 mm, 2.6 µm, Phenomenex Inc., Torrance, CA, USA) was used. The binary mobile phase consisted of solvent A (99.9% H_2O / 0.1% formic acid) and solvent B (94.9% methanol / 5% acetonitrile / 0.1% formic acid). The phenolic compounds and abscisic acid ($[M-H]^-$ = m/z 263.1289) were analyzed by using negative ionization mode and 5-HMF ($[M+H]^+$ = m/z 127.0390) and furfural ($[M+H]^+$ = m/z 97.0286) were detected in positive ionization mode. The negative mode solvent gradient was: 0–5 min, 0% to 12% B; 5–15 min, 12% to 23% B; 15–30 min, 23% to 50% B; 30 - 40 min, 50% to 80% B; 40–42 min, 80% to 100% B; 42–45 min, 100% B; 45–46 min, 100% to 0% B; 46–52 min, 0% B. The positive mode solvent gradient was: 0–10 min 2% B; 10–11 min, 2% to 100% B; 11–14 min, 100% B; 14–15 min, 100% to 2% B; 15–21 min, 2% B. The column temperature was set at 40°C, the flow rate was 0.700 mL/min, and the injection volume was 2 µL. UV peaks were monitored at 280 nm, 320 nm, 360 nm and 520 nm for the phenolic compounds. The spray voltages for both negative and positive modes were set at 4.5 kV. Mass spectrometry data were collected using DDMS2 method (TopN = 10, NCE = 30, intensity threshold was set at 1.0e5 counts) for compound identification, and with Full-MS mode for quantification. Data were visualized and analysed using Thermo FreeStyle™ 1.7PS2 software. Quantification was achieved using standard curves generated from the molecular ions of individual compounds in serial dilutions (0.005–10 mg/L; $r^2 > 0.995$).

2.4. Total protein content and analysis of free and hydrolyzed amino acids by HPLC

2.4.1. Total protein content

Honey samples were diluted to 30 % (w/v) solution by distilled water. The solution was filtered through a 0.22 µm PVDF syringe filter to remove any insoluble materials. Protein in honey was separated by centrifuging at 5,000 × g using an Amicon ultra centrifugal filter device with a molecular weight cut-off of 3,000 (Merck KGaA, Darmstadt, Germany) twice. The concentrated protein was collected and dissolved up to 2 mL in PBS buffer which was equivalent to 7.5 % (w/v) honey solution. Total protein was measured using a colorimetric assay kit (Bio-Rad, Mississauga, ON, Canada) according to the manufacturer's instructions. Briefly, 5 µL of sample or bovine serum albumin (BSA) standards were mixed with 25 µL of alkaline copper tartrate solution and 200 µL of diluted Folin reagent in a 96-well plate. The color developed by the reduction of Folin reagent by the copper-treated protein was measured at 750 nm. The total protein concentration was expressed as mg /100 g honey by using the BSA calibration curve.

2.4.2. Free amino acids

Honey samples were diluted to 5 % (w/v) solution with water. L-Norvaline was spiked in samples as an IS for recovery of amino acids after the derivatization. Diluted honey samples were filtered through a 0.22 µm syringe filter before derivatization. A mixed solution containing 20 proteinogenic amino acids and L-norvaline (IS) was prepared by dissolving the amino acids in 0.1 M hydrogen chloride (final concentration was each at 200 µM). Further dilutions were made for generating standard curves for amino acid quantification. Samples and standards were treated with the AccQ·Tag Ultra Derivatization Kit (Waters Limited, Mississauga, ON, Canada) according to the product manual.

Derivatized samples and standards were analyzed by an Agilent 1260 series HPLC system consisting of an autosampler, a degasser, a quaternary pump, a thermostatted column compartment and a DAD. Amino acids were separated on a Phenomenex Kinetex XB-C18 column (100 × 4.6 mm, 2.6 µm) (Phenomenex Inc., Torrance, CA, USA). A binary mobile phase consisting of 0.2 % formic acid in water (v/v, solvent A) and 95 % methanol mixed with 5 % acetonitrile (v/v, solvent B) was used. The solvent gradient was 0−8 min, 0−6 % B; 8−12 min, 6 % B; 12−24 min, 6−36% B; 24−26 min, 36−42% B, 26–28 min, 42–44 %, and 28−29 min, 44−100% B. An extra 9 min of a post-run was added to allow for column restoration. The flow rate was 0.7 mL/min and peaks were monitored at 360 nm. Quantification of amino acids was performed using linear curves ($R^2 > 0.999$) generated from standards with predefined concentrations between 0.5 and 200 µM. The recoveries were 99.0% to 103.7% as determined using the IS, L-norvaline. The limit of detection (LOD) and limit of quantification (LOQ) of individual amino acids ranged from 0.17 to 0.71 and 0.57 to 2.35 µg/g honey, respectively. Data analysis was conducted using Agilent Chem-Station software.

2.4.3. Hydrolyzed amino acids

Honey samples were diluted to 10 % (w/v) solution with distilled water. *L*-Norvaline was spiked in samples as an IS for evaluating the recovery efficiency of amino acids after the derivatization. The samples were further diluted by the same volume of 12 M HCl in glass tubes. The oxygen in tubes was removed by nitrogen flushing for 1 min in order to avoid oxidation during the heat treatment. A Fisherbrand™ heating block (Fisher Chemicals, Ottawa, ON, Canada) was set at 110°C and the samples were heated for 24 h. Samples were neutralized with 6 M sodium hydroxide and were finally adjusted to 2.5% (w/v) solution with distilled water, filtered through a 0.22 µm syringe filter before derivatization and HPLC analysis following the same aforementioned protocols for the free amino acids.

2.5. Identification of L-norvaline by LC-MS/MS

The same LC-MS system as described in Section 2.3 was used. Separation of L-norvaline in honey samples was done on an InfinityLab Poroshell 120 HILIC-Z column (2.1 × 100 mm, 2.7 µm, Agilent Technologies, Santa Clara, California, USA). The binary mobile phase consisted of solvent A (10 mM ammonium formate in 100% H_2O) and solvent B (10 mM ammonium formate in 90% acetonitrile / 10% H_2O). The solvent gradient was: 0–5 min, 100% to 80% B; 5–6 min, 80% to 70% B; 6–7 min, 70% to 50% B; 7 - 9 min, 50% to 20% B; 9–10 min, 20% B; 10–10.5 min, 20% to 100% B; 10.5–17 min, 100% B. The column temperature was set at 25°C, the flow rate was set at 0.3 mL/min, and the injection volume was 2 µL. The positive mode was used for ionization and the spray voltage was set at 4.5 kV. Mass spectrometry data were collected using a parallel reaction monitoring (PRM) method with nominal collision energy (NCE) set at 20. Data were visualized and analyzed using Thermo FreeStyle™ 1.7PS2 software.

2.6. Mineral contents

The minerals of calcium, iron, magnesium, phosphorus, potassium, sodium, and zinc in honey samples (50 g) were analyzed by SGS Crop Science Canada (Guelph, ON, Canada) according to the AOAC 965.09 - atomic absorption spectrophotometric method.

2.7. Vitamins

Honey samples were diluted to 5% (w/v) solution by distilled water before subject to analysis of vitamin C and B2, B3, B5 and B6. The solution was filtered through a 0.22 μm filter before analysis. LC-MS/MS analysis was performed using the same instrumentation as stated above. A Kinetex 2.6μ F5 100A column (150 × 4.6 mm, Phenomenex Inc., Torrance, CA, USA) was used. The binary mobile phase consisted of solvent A (99.9% H_2O / 0.1% formic acid) and solvent B (99.9% AcN / 0.1% formic acid). The solvent gradient was: 0–8 min, 3% B; 8–13 min, 3% to 100% B; 13–17 min, 100% B; 17–18 min, 100% to 3% B; 18–24 min, 3% B. The column temperature was set at 23°C, the flow rate was set at 0.3 mL/min, and the injection volume was 5 μL. The positive ionization mode was used with spray voltage set at 3.75 kV. Mass spectrometry data were collected using either Full-MS/DDMS2 method (TopN = 10, NCE =30) for qualitative study, or PRM method (NCE = 30) for quantification. Data were visualized and analyzed using Thermo FreeStyle™ 1.7PS2 and Xcalibur software.

2.7. Organic acids

2.7.1. Analysis of organic acids by LC-MS

Honey samples were diluted to 1% (w/v) solution by distilled water. The solution was filtered through a 0.22 μm filter to remove any insoluble materials. The same LC-MS system as described in Section 2.3 was used. Separation was done on a Phenomenex Rezex™ ROA-Organic Acid H^+ (8 %) column (150 × 4.6 mm, Phenomenex Inc., Torrance, CA, USA). The mobile phase was 0.5 % formic acid in water and the flow rate was set at 0.3 mL/min. The column temperature was set at 55°C and the injection volume was 0.5 μL. Mass spectrometry data were collected using Full MS method in negative ionization mode. The spray voltage was set at 4.0 kV. Data were visualized using Thermo FreeStyle™ 1.7PS2 software. Quantification of citric acid, formic acid, gluconic acid, glutaric acid, glycolic acid, lactic acid, maleic acid, malic acid, malonic acid, oxalic acid, succinic acid was achieved using standard curves generated from individual compounds in serial dilutions (0.05–20 mg/L; $r^2 > 0.980$).

2.7.2. Analysis of organic acids by GC

Honey samples were diluted to 2.5% (w/v) solution by 1 M formic acid and were spiked with the IS 2-ethylbutyric acid dissolved in 100% ethanol (final concentration was each at 100 μM). Samples were placed at room temperature for 2 h and vortexed vigorously for 15 s every 30 min. The samples were filtered into 2 mL GC vials using 0.2 μm nylon filters. The GC analysis was carried out using Agilent 6890A equipped with autosampler and FID detector. Acetic acid and propionic acid were analyzed using a Supelco Nukol fused-silica capillary column (30m × 0.25mm × 0.25μm). The oven temperature was programmed as follows: held at 70°C for 1 min, ramped at 7.5°C /min to 140°C and held for 3 min, and then ramped at 10°C /min to 200°C and held for 1 min. The inlet was set at 200°C and 1 μL of sample was injected at 5:1 splitting ratio. The FID detector temperatures were set at 250°C with gas flow rates as follows: 30 mL/min H_2, 350 mL/min Air, and 26.3 mL/min Makeup flow (N_2). The flow rate of He_2 carrier gas was 1.7 mL/min. Calibration curves were made in the range of 0.78–200 μM for both acetic and propionic acid. The LOD for acetic acid and propionic acid was 0.120 mg/100g and 0.296 mg/100 g honey, respectively.

2.7.3. Analysis of oxalic acid by colorimetric assay kit

Honey samples were diluted to 10% (w/v) solution by distilled water. The solution was filtered through a 0.22 μm filter to remove any insoluble materials. Oxalic acid was measured using a colorimetric assay kit (Abcam, Waltham, MA, USA) according to the manufacturer's instructions. Briefly, 25 μL of sample was mixed with the assay buffer up to 50 μL in wells of a 96-well plate. Two μL of oxalate converter was added to wells of each sample, oxalate standard, and blank (assay buffer). The conversion was done in 1 h at 37°C, then 50 μL of reaction mix (oxalate enzyme mix and probe) was added to each well. The color was developed at 37°C in 1 h with protection from light and was measured at 450 nm. The oxalic acid in honey sample was expressed as mg /100 g honey by using the oxalate calibration curve.

2.7.4. Analysis of formic acid by colorimetric assay kit

Honey samples were diluted to 30% (w/v) solution by distilled water. The solution was filtered through a 0.22 μm filter to remove any insoluble materials. Formic acid was measured using a colorimetric assay kit (Neogen Megazyme, Lansing, MI, USA) according to the manufacturer's instructions. Briefly, 10 μL of sample or formate standard was mixed with 200 μL of distilled water in wells of a 96-well plate, then 20 μL of assay buffer and NAD^+ were added to each sample, formate standard, and blank (distilled water) well. The reaction was initiated by adding 5 μL of formate dehydrogenase (FDH) at 25°C and lasted for 30 min. The absorbance change due to the production of NADH was measured at 340 nm before and after FDH reaction. The formic acid in honey sample was expressed as mg /100 g honey by calculation from the standard curve of formate.

2.8. Enzyme activity

2.8.1. Amylase activity assay

Honey samples were diluted to 30% (w/v) solution by distilled water. The solution was filtered through a 0.22 μm filter to remove any insoluble materials. Amylase activities were measured using a colorimetric assay kit (Abcam, Waltham, MA, USA) according to the manufacturer's instructions. Briefly, 50 μL of diluted honey samples or nitrophenol standard (0–20 nmol/well) was mixed with 100 μL of amylase reaction mix (ethylidene-pNP-G7 and α-glucosidase) in wells of a 96-well plate. Absorbance was measured immediately at 405 nm in a kinetic mode for 60 min at 25°C in dark. α-Amylase in honey cleaves the substrate ethylidene-pNP-G7 to produce smaller fragments that are eventually modified by α-glucosidase, causing the release of a chromophore that can be measured at 405 nm. The amylase activity was expressed as U/100

g honey by using the nitrophenol calibration curve. One U was defined as the amount of amylase that cleaves ethylidene-pNP-G7 to generate 1.0 µmol of nitrophenol per min at pH 7.2 at 25°C.

2.8.2. Diastase activity assay

Honey samples were diluted to 1% (w/v) solution by 0.1 M acetate buffer (pH = 5.2). The solution was filtered through a 0.22 µm filter to remove any insoluble materials. Diastase activities were measured using a colorimetric assay kit (Phadebas, Cambridge, MA, USA) according to the manufacturer's instructions. Briefly, 5.0 mL of diluted honey samples or 0.1M acetate buffer used as a blank control were mixed with one Phadebas® tablet at 40°C for 30 min. The Phadebas® tablet contained 45 mg of water-insoluble, cross-linked starch polymer carrying blue dye, which upon hydrolysis by diastase can generate a blue water-soluble product. The reaction was stopped by adding 1 mL of 0.5M sodium hydroxide solution. The absorbance of the supernatant after centrifugation at 1500 × *g* for 5 min was measured in 1 cm cuvette at 620 nm. The diastase activity was expressed as diastase number (DN) according to the formula provided by the manufacturer based on the difference of absorption at 620 nm between the sample and the blank.

2.8.3. Glucose oxidase activity assay

Honey samples were diluted to 30% (w/v) solution by distilled water. The solution was filtered through a 0.22 µm filter to remove any insoluble materials. Glucose oxidase activities were measured using a colorimetric assay kit (Abcam, Waltham, MA, USA) according to the manufacturer's instructions. Briefly, 50 µL of diluted honey samples or glucose oxidase standard was mixed with 50 µL of glucose oxidase reaction mix (glucose, AbRed indicator, and horseradish peroxidase) in wells of a 96-well plate. Absorbance was measured immediately at 570 nm in a kinetic mode for 30 min at 37°C. Glucose oxidase in samples catalyzed the oxidation of β-D-glucose into hydrogen peroxide and D-glucono-1,5-lactone. The produced hydrogen peroxide reacted with AbRed indicator when catalyzed by horseradish peroxidase to generate the compound which can be measured at 570 nm. The glucose oxidase activity was expressed as U /100 g honey by using the calibration curve. One U was defined as amount of glucose oxidase that reacts with 1.0 µmol of glucose per min at 37°C.

2.8.4. Catalase activity assay

Honey samples were diluted to 3% (w/v) solution by distilled water. The solution was filtered through a 0.22 µm filter to remove any insoluble materials. Catalase activities were measured using a colorimetric assay kit (Cayman Chemical, Ann Arbor, MI, USA) according to the manufacturer's instructions. Briefly, 20 µL of diluted honey samples or formaldehyde standard was mixed with 100 µL of assay buffer, 30 µL of methanol, and 20 µL of 35.3 mM hydrogen peroxide in wells of a 96-well plate. Catalase in samples catalyzes the peroxidation of methanol to produce formaldehyde after 20 min incubation at room temperature. The formaldehyde was measured calorimetrically at 540 nm with 4-amino-3-hydrazino-5-mercapto-1,2,4-triazole (purpald) and potassium periodate. The catalase activity was expressed as U/100 g honey by using the formaldehyde calibration curve. One U was defined as the amount of catalase that oxidizes methanol to generate 1.0 µmol of formaldehyde per min at room temperature.

2.8.5. Invertase activity assay

Honey samples were diluted to 30% (w/v) solution by distilled water. The solution was filtered through a 0.22 µm filter to remove any insoluble materials. Glucose in honey was removed by centrifuging at 5,000 × *g* using an Amicon ultra centrifugal filter device with a molecular weight cut-off of 10,000 Da (Merck KGaA, Darmstadt, Germany) for at least seven times. The concentrated protein was collected and dissolved up to 500 µL in PBS buffer. Invertase activities were measured using a colorimetric assay kit (Abcam, Waltham, MA, USA) according to the manufacturer's instructions. Briefly, 25 µL of concentrated protein solution was mixed with 15 µL of assay buffer and 10 µL of sucrose (i.e. invertase substrate) in microplate wells. The same volume of sample without adding sucrose was prepared simultaneously as a background control. Invertase in honey catalyzes the hydrolysis of sucrose by cleaving its glycosidic bond to form glucose and fructose. After 20 min of reaction, samples, background controls, and sucrose standards were mixed with provided enzyme mix and probe to generate a chromogen that can be measured at 570 nm. The absorption of background control was subtracted from the sample in order to eliminate the influence of residual glucose in a sample. The invertase activity was expressed as mU/100 g honey by using the glucose calibration curve. One mU was defined as the amount of invertase that cleaves sucrose to generate 1.0 mmol of glucose per min at 37°C.

2.8.6. Acid phosphatase activity assay

Honey samples were diluted to 30% (w/v) solution by distilled water. The solution was filtered through a 0.22 µm filter to remove any insoluble materials. Acid phosphatase activities were measured using a colorimetric assay kit (Abcam, Waltham, MA, USA) according to the manufacturer's instructions. Briefly, 20 µL of diluted honey samples were mixed with 60 µL of assay buffer in wells of a 96-well plate. Standard dilutions were prepared by mixing *p*-nitrophenyl phosphate (pNPP) and the assay buffer up to 120 µL to obtain the final concentrations of 0–20 nmol/well. Reaction was initiated by adding 50 µL of pNPP in samples and 10 µL of acid phosphatase in standards simultaneously. The same volume of sample was mixed with 50 µL of pNPP and 20 µL of stop solution as a background control. Acid phosphatase converts pNPP substrate to an equal amount of colored p-nitrophenol (pNP). The reaction was stopped by adding 20 µL of stop solution after incubation for 60 min at 25°C in dark. The produced pNP was measured at 405 nm. The absorption of background control was subtracted from the sample in order to eliminate the influence of the natural color in the sample. The acid phosphatase activity was expressed as mg P/100 g honey/24 h by using the pNPP calibration curve.

2.9. Total phenolic content (TPC)

TPC in honey was determined by the Folin-Ciocalteu method as described previously with slight modifications (Li et al., 2012). Briefly, honey samples were diluted to 30 % (w/v) solution by distilled water. Twenty-five µL of diluted sample or standard was mixed with 125 µL 0.2 M Folin-Ciocalteu reagent in wells of a 96-well microplate and allowed to react for 10 min at room temperature. Then 125 µL 7.5% (w/v) Na_2CO_3 was added and incubated for 60 min at room temperature. The absorbance was measured at 765 nm using a UV-visible microplate kinetic reader (EL 340, Bio-Tek Instruments, Inc., Winooski, VT, USA). TPC was expressed as

μg gallic acid equivalents per g honey (μg GAE/g honey) by using the gallic acid calibration curve.

2.10. Sugar analysis

Common and rare sugars of honey were analyzed using high performance anion exchange chromatography with pulsed amperometric detection (HPAEC-PAD, Dionex ICS-5000, Thermo-Fisher, USA). in conjunction with Dionex™ CarboPac™ PA1 analytical (250 mm × 4 mm) and guard (4 mm × 50 mm) columns. Glucose, fructose and sucrose were eluted at 25°C with 10 mM NaOH for 15 min, followed by 100 mM NaOH for 30 min at a flow rate of 1 mL/min. Separation of maltose, isomaltose, turanose, palatinose and nigerose was done under the same conditions as above-stated, except elution with 100 mM NaOH was 45 min. Honey samples were diluted in deionized water and filtered through a 0.45 μm nylon filter prior to injection. Quantification of all sugars was achieved by using calibration curves of standards. Concentrations were expressed as g/100 g honey. The moisture percentage was calculated using a digital refractometer with a pea sized honey sample (5 g) while taking temperature into account.

The total sugars were measured using the phenol-sulfuric acid method. Quantification was done using serial dilutions of glucose/fructose standards at concentrations ranging from 0–0.1 mg/mL. Standard or honey samples (0.1 mg/mL, 0.5 mL) were transferred into separate test tubes, to which phenol solution (5% in water, 0.5 mL) and sulfuric acid concentrate (2.5 mL) were added. The test tubes were vortexed and then cooled in a water bath for 15 min. Samples were transferred to cuvettes and the absorbance was measured at 490 nm using a spectrophotometer. Total sugar concentration of the honey samples was calculated using the standard curve generated from the standards and expressed as g/100 g.

Ash (mineral content) was measured according to the methods of (AOAC, 1999). Five g of honey was placed in a combustion pot, which was preheated to darkness with a gas flame to prevent honey foaming. Then, the darkened samples were incinerated at high temperature (400°C) in a burning muffle for 5 h (overnight). After cooling to room temperature, the obtained ash was weighed. Percentage of ash was determined by dividing the weight of the ash content by the original weight of the honey sample.

The colour of honey samples was measured using Pfund classifier. Homogenous honey samples devoid of air bubbles were transferred into a cuvette with a 10 mm light path until the cuvette was approximately half full. Deionized water was used as a blank. The cuvette was then placed in a spectrophotometer (GENESYS 50 UV-Visible Spectrophotometer, Thermo Fisher Scientific,), and the absorbance of the samples was measured at 560 nm. Measurements were performed in triplicate for each sample. The Pfund value (in mm) was a result of the mean absorbance value multiplied by the Pfund factor 3.15, and the colour was determined using the approved colour standards of the United States Department of Agriculture (USDA, 1985).

2.11. Statistical analysis

All honey samples were extracted and analyzed in triplicates, and the results were expressed as mean ± standard deviation. A one-way analysis of variance (ANOVA) followed by Tukey's Honest Significant Difference (HSD) test was performed using SigmaPlot 15.0 (Palo Alto, CA, USA) to analyze the difference of mean values of phenolics, free/hydrolyzed amino acids, TPC, and total protein in honeys of different botanical origins. Significant differences were considered at $p < 0.05$. Principal component analyses (PCA) were performed using original concentration units to gain an overview of the relationships between individual phenolics and free amino acids in various honeys. The PCA analysis was performed and visualized using biplot generated by R Studio Software (Boston, MA, USA). All raw data are tabulated in Table S2a-l.

3. Results and discussion

3.1. Characterization of phenolic compounds in honey varieties

TPC in honeys ranged from 379–1269 μg GAE/g, with buckwheat honey having the highest and significantly higher content than the rest of the honeys in the study (Table 1) .

A total of 29 phenolic compounds including phenolic acids, flavonoids, and flavonoid glycosides were identified based on congruent retention time, UVmax, exact mass of molecular ion $[M-H]^-$ and major fragment ions with the standards, and quantified by LC-MS/MS (Tables 2 and 3, Figure 1). Pinobanksin (1.012 - 7.481 μg/g), pinocembrin (0.985 - 7.514 μg/g), chrysin (0.229 - 2.159 μg/g) and galangin (0.194 - 2.005 μg/g) were the main phenolic compounds in all honeys. These are categorized as propolis-derived flavonoids since they are abundant in bud exudates of poplars which are collected by bees to produce propolis (Ferreres et al., 1996). P5ME was originally detected in propolis (Greenaway et al., 1990) but rarely reported in honey (Tomás-Barberán et al., 2001). Our present work identified the P5ME based on its $[M-H]^-$ at m/z 285.0768 and the major fragment ions of $[M-H-H_2O]^-$ at m/z 267.0663 and $[M-H-H_2O-CH_3]^-$ at m/z 252.0430, which was later confirmed with the authentic P5ME standard. Our study presents the first quantitative data of P5ME in honey (0.337 to 2.497 μg/g) (Table 3). Most nectar-derived flavonoids were detected in all floral and multifloral honeys, but the concentrations varied significantly. Clover honey possessed the greatest amount of kaempferol (4.784 ± 0.801 μg/g), quercetin (0.929 ± 0.170 μg/g), isorhamnetin (0.765 ± 0.100 μg/g), and naringenin (0.111 ± 0.079 μg/g), whereas alfalfa honey had the highest level of apigenin (0.876 ± 0.340 μg/g). Compared with flavonoids, phenolic acids were more honey-specific. For instance, caffeic acid and isoferulic acid were identified as the dominant phenolic acids in alfalfa honey. *P*-Hydroxybenzoic acid and *p*-coumaric acid, on the other hand, were uniquely abundant in buckwheat honey. These honey-specific phenolic acids and some unique flavonoids, such as hesperidin and hesperetin, are discussed below.

The PCA results of the main phenolic compounds (>2 μg/g) in the studied honey samples are shown in Figure 2A. Since the first two components (61.0 % and 23.9 %) accounted for most of the variance in the observations, the score plot was used to assess the observations for their clusters, outliers, and trends. The loading plot (Figure 2A) showed that flavonoids greatly influenced the first principal component, whereas phenolic acids mainly contributed to the second one. The correlations among pinobanksin, pinocembrin, chrysin, galangin and P5ME ranged from 0.738 to 0.994 (Table S3). Although the flavonoid profile can be helpful in differentiating adulterated honey from natural honey, the presence of these five flavonoids in all studied honey samples make them unsuitable candidates as molecular markers to distinguish specific botanical origin (Mao, Schuler, and Berenbaum (2013). Interestingly, hesperidin was in an opposite direction of all other flavonoids in the loading plot, suggesting a very unique compound in honey samples. By grouping these observations by honey variety, it was clear that three orange honey samples loaded the most posi-

Table 1. Total phenolic and protein contents of honeys

	Mean ± SD				
	Alfalfa	**Buckwheat**	**Clover**	**Orange**	**Wildflower**
TPC (μg GAE/g)	379.4 ± 42.2a	1269.1 ± 275.3b	425.4 ± 89.1a	414.6 ± 34.8a	507.0 ± 120.5a
Protein (μg/g)	3807.9 ± 420.0a	8830.7 ± 537.3b	4172.3 ± 357.3a	4346.6 ± 804.7a	5158.6 ± 252.1a

Means followed by a common letter within the same row are not significantly different by the Tukey's HSD test at the 5% level of significance.

Table 2. Identification of phenolic compounds, abscisic acid, furfural, and 5-HMF in honey by LC-MS

Peak	t_R (min)	λ_{max} (nm)	Formula	$[M-H]^-$ m/z	Major fragment ions
Gallic acid	4.63	270	$C_7H_6O_5$	169.0141	125.0245
Protocatechuic acid	7.00	260	$C_7H_6O_4$	153.0194	109.0296
5-HMF	7.49	285	$C_6H_6O_3$	127.0390*	109.0286, 81.0340
Furfural	8.24	275	$C_5H_4O_2$	97.0286*	69.0342
Neochlorogenic acid	8.65	325	$C_{16}H_{18}O_9$	353.0878	191.0564, 179.0353, 135.0452
p-Hydroxybenzoic acid	9.70	255	$C_7H_6O_3$	137.0242	93.0348
Vanillic acid	12.66	260	$C_8H_8O_4$	167.0348	152.0118, 123.0452, 108.0220
Caffeic acid	13.00	320	$C_9H_8O_4$	179.0352	135.0452
Chlorogenic acid	13.10	325	$C_{16}H_{18}O_9$	353.0878	191.0563
Syringic acid	15.09	270	$C_9H_{10}O_5$	197.0452	182.0223
p-Coumaric_acid	17.81	310	$C_9H_8O_3$	163.0401	119.0502
trans-Ferulic acid	19.79	320	$C_{10}H_{10}O_4$	193.0505	178.0274, 149.0611, 134.0374
Isoferulic acid	21.34	320	$C_{10}H_{10}O_4$	193.0506	178.0274, 134.0374
o-Coumaric acid	22.83	275	$C_9H_8O_3$	163.0401	119.0502
Ellagic acid	25.59	250	$C_{14}H_6O_8$	300.9990	155.1080
Hesperidin	25.66	280	$C_{28}H_{34}O_{15}$	609.1825	301.0723
Myricetin	26.35	250, 370	$C_{15}H_{10}O_8$	317.0305	178.9989, 151.0039, 137.0245
Kaempferol-rutinoside	27.47	265, 345	$C_{27}H_{30}O_{15}$	593.1512	285.0407, 284.0328
Abscisic acid	27.75	260	$C_{15}H_{20}O_4$	263.1289	219.1394, 204.1159, 151.0768
Pinobanksin-5-methyl ether	28.80	285	$C_{16}H_{14}O_5$	285.0768	267.0663, 252.0430
Pinobanksin	29.56	290	$C_{15}H_{10}O_7$	301.0354	253.0507
Quercetin	29.73	250, 370	$C_{15}H_{12}O_5$	271.0612	178.9989, 151.0039
Naringenin	29.97	290	$C_{15}H_{12}O_5$	271.0612	151.0039, 119.0502
Luteolin	31.18	250, 350	$C_{15}H_{10}O_6$	285.0406	133.0293
Hesperetin	31.34	285	$C_{16}H_{14}O_6$	301.0718	286.0485, 151.0039
Kaempferol	32.59	265, 365	$C_{15}H_{10}O_6$	285.0406	151.0039
Apigenin	33.23	265, 340	$C_{15}H_{10}O_5$	269.0455	151.0038
Isohamnetin	33.51	250, 370	$C_{16}H_{12}O_7$	315.0512	300.0282
Pinocembrin	35.31	285	$C_{15}H_{12}O_4$	255.0663	213.0560, 151.0039
Chrysin	36.73	265	$C_{15}H_{10}O_4$	253.0507	209.0611
Galangin	36.91	265, 360	$C_{15}H_{10}O_5$	269.0453	-
Acacetin	37.25	265, 330	$C_{16}H_{12}O_5$	283.0613	268.0377

*Positive ionization mode was used ($[M+H]^+$).

Table 3. Quantification of phenolic compounds, abscisic acid, furfural, and 5-HMF in honey by LC-MS

	Concentration (μg/g Honey), Mean ± SD				
	Alfalfa	**Buckwheat**	**Clover**	**Orange**	**Wildflower**
Phenolic compounds					
Gallic acid	0.049 ± 0.028^{a}	0.034 ± 0.001^{a}	0.038 ± 0.040^{a}	0.046 ± 0.021^{a}	0.017 ± 0.004^{a}
Protocatechuic acid	0.297 ± 0.076^{ab}	0.400 ± 0.021^{ab}	0.266 ± 0.112^{a}	0.695 ± 0.288^{b}	0.338 ± 0.056^{ab}
Neochlorogenic acid	0.025 ± 0.003^{a}	0.128 ± 0.083^{a}	0.037 ± 0.014^{a}	0.100 ± 0.078^{a}	0.321 ± 0.339^{a}
p-Hydroxybenzoic acid	1.734 ± 0.494^{a}	12.483 ± 4.230^{b}	2.562 ± 0.394^{a}	1.166 ± 0.625^{a}	3.139 ± 1.415^{a}
Vanillic acid	0.148 ± 0.028^{a}	0.232 ± 0.025^{a}	0.583 ± 0.071^{b}	0.266 ± 0.080^{ac}	0.507 ± 0.190^{bc}
Caffeic acid	6.884 ± 0.320^{a}	1.092 ± 0.082^{b}	1.945 ± 1.259^{b}	0.384 ± 0.232^{b}	1.185 ± 0.603^{b}
Chlorogenic acid	0.084 ± 0.006^{a}	0.336 ± 0.208^{a}	0.093 ± 0.028^{a}	0.104 ± 0.032^{a}	0.811 ± 0.728^{a}
Syringic acid	0.179 ± 0.066^{a}	0.221 ± 0.120^{a}	0.283 ± 0.058^{a}	0.157 ± 0.094^{a}	0.283 ± 0.029^{a}
p-Coumaric acid	1.673 ± 0.313^{ab}	4.910 ± 1.224^{c}	3.230 ± 0.714^{ac}	0.847 ± 0.672^{b}	1.993 ± 0.447^{ab}
Trans-Ferulic acid	0.360 ± 0.017^{a}	0.346 ± 0.048^{a}	0.731 ± 0.170^{b}	0.222 ± 0.163^{a}	0.493 ± 0.135^{ab}
Isoferulic acid	3.262 ± 0.228^{a}	0.179 ± 0.080^{b}	0.615 ± 0.677^{b}	n.d.	0.214 ± 0.174^{b}
o-Coumaric acid	0.019 ± 0.008^{a}	0.029 ± 0.006^{a}	0.118 ± 0.046^{b}	0.003 ± 0.002^{a}	0.063 ± 0.029^{ab}
Ellagic acid	0.040 ± 0.008^{a}	0.089 ± 0.066^{a}	0.098 ± 0.086^{a}	0.122 ± 0.034^{a}	0.157 ± 0.153^{a}
Hesperidin	0.063 ± 0.109^{a}	n.d.	0.011 ± 0.013^{a}	1.981 ± 0.234^{b}	n.d.
Myricetin	0.089 ± 0.093^{a}	0.129 ± 0.095^{a}	0.058 ± 0.024^{a}	0.016 ± 0.018^{a}	0.126 ± 0.073^{a}
Kaempferol-rutinoside	0.020 ± 0.019^{ab}	0.008 ± 0.014^{a}	0.035 ± 0.012^{ab}	0.049 ± 0.014^{b}	0.038 ± 0.016^{ab}
P5ME	1.448 ± 0.482^{ab}	1.997 ± 0.421^{a}	2.497 ± 0.804^{a}	0.337 ± 0.419^{b}	0.979 ± 0.111^{ab}
Pinobanksin	7.259 ± 1.003^{a}	5.155 ± 1.694^{ac}	7.481 ± 1.527^{a}	1.012 ± 1.298^{b}	2.539 ± 0.333^{bc}
Quercetin	0.625 ± 0.148^{a}	0.950 ± 0.211^{a}	0.929 ± 0.170^{a}	0.496 ± 0.284^{a}	1.076 ± 0.181^{a}
Naringenin	0.037 ± 0.064^{a}	0.033 ± 0.056^{a}	0.111 ± 0.079^{a}	0.023 ± 0.039^{a}	0.055 ± 0.077^{a}
Luteolin	0.143 ± 0.013^{a}	0.118 ± 0.024^{a}	0.150 ± 0.048^{a}	0.185 ± 0.099^{ab}	0.348 ± 0.130^{a}
Hesperetin	0.037 ± 0.011^{a}	0.007 ± 0.000^{a}	0.012 ± 0.006^{a}	0.218 ± 0.075^{b}	0.009 ± 0.001^{a}
Kaempferol	3.444 ± 1.052^{ab}	4.380 ± 0.343^{a}	4.784 ± 0.801^{a}	0.906 ± 0.338^{b}	4.369 ± 2.180^{a}
Apigenin	0.876 ± 0.340^{a}	0.531 ± 0.157^{ab}	0.653 ± 0.042^{a}	0.123 ± 0.103^{b}	0.589 ± 0.023^{ab}
Isorhamnetin	0.469 ± 0.076^{ab}	0.590 ± 0.075^{a}	0.765 ± 0.100^{a}	0.209 ± 0.187^{b}	0.464 ± 0.035^{ab}
Pinocembrin	6.468 ± 1.570^{ab}	5.618 ± 1.309^{ab}	7.514 ± 1.503^{a}	0.985 ± 1.322^{c}	2.794 ± 0.028^{bc}
Chrysin	2.052 ± 0.269^{ab}	1.883 ± 0.295^{ab}	2.159 ± 0.455^{a}	0.229 ± 0.215^{c}	1.116 ± 0.096^{bc}
Galangin	1.932 ± 0.227^{a}	1.656 ± 0.206^{ab}	2.005 ± 0.431^{a}	0.194 ± 0.199^{c}	0.875 ± 0.057^{bc}
Acacetin	0.263 ± 0.439^{a}	0.287 ± 0.209^{a}	0.024 ± 0.008^{a}	0.006 ± 0.004^{a}	0.008 ± 0.001^{a}
Sub-total	39.982 ± 4.252^{ab}	43.820 ± 8.674^{a}	39.786 ± 4.316^{ab}	11.080 ± 6.862^{c}	24.903 ± 2.246^{bc}
Non-phenolics					
5-HMF	10.059 ± 5.582^{a}	4.407 ± 4.744^{a}	6.317 ± 4.609^{a}	9.658 ± 1.285^{a}	4.131 ± 2.466^{a}
Furfural	0.956 ± 0.331^{a}	8.124 ± 2.575^{b}	0.858 ± 0.419^{a}	0.873 ± 0.324^{a}	0.977 ± 0.078^{a}
Abscisic acid	1.147 ± 0.595^{a}	1.080 ± 0.774^{a}	1.354 ± 0.945^{a}	7.634 ± 2.400^{b}	0.849 ± 0.172^{a}

n.d. = not detected. Means followed by a common letter within the same row are not significantly different by the Tukey's HSD test at the 5% level of significance.

tive direction of the vector of hesperidin, which indicated an exclusively high hesperidin level in orange honey. In fact, hesperidin was only quantifiable in orange honey with an average concentration of 1.981 μg/g in our study (Table 3). Hesperetin, an aglycone of hesperidin, has been considered a chemical marker for citrus honey (*Citrus* sp.) because it was found in the nectar of citrus blossoms (Ferreres et al., 1994; Mao et al., 2013). Our results showed that the concentration of hesperidin and hesperetin are in a ratio of 9.1 to 1.0, which is in agreement with a recent report (Maldonado et al., 2021). Based on data obtained in the present study,

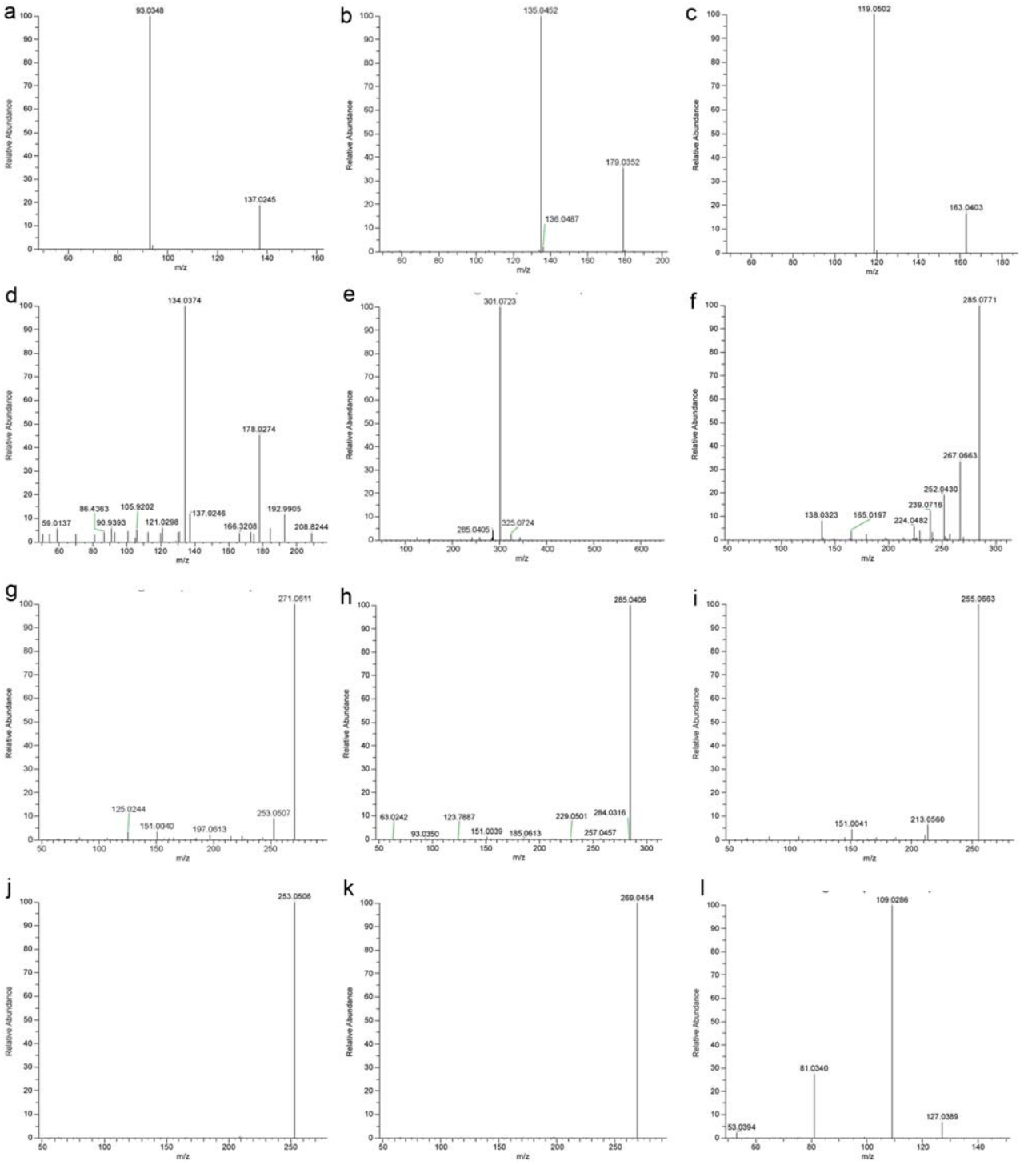

Figure 1. MS/MS spectra of selected phenolic compounds and 5-HMF. (a) *p*-Hydroxybenzoic acid; (b) Caffeic acid; (c) *p*-Coumaric acid; (d) Isoferulic acid; (e) Hesperidin; (f) Pinobanksin-5-methyl ether; (g) Pinobanksin; (h) Kaempferol; (i) Pinocembrin; (j) Chrysin; (k) Galangin; (l) 5-HMF.

we believe that hesperidin, a diglycoside of hesperetin, serves as a better chemical marker than hesperetin for orange honey. The second principal component mostly represents phenolic acids, among which the loadings of caffeic acid and isoferulic acid accumulated closely with a correlation of 0.996 (Table S3). These two phenolic acids in alfalfa honey samples were 6.884 ± 0.320 and 3.262 ± 0.228 μg/g, respectively, which were at least 3-fold higher than in other honeys (Table 3). The chemical markers of alfalfa honey

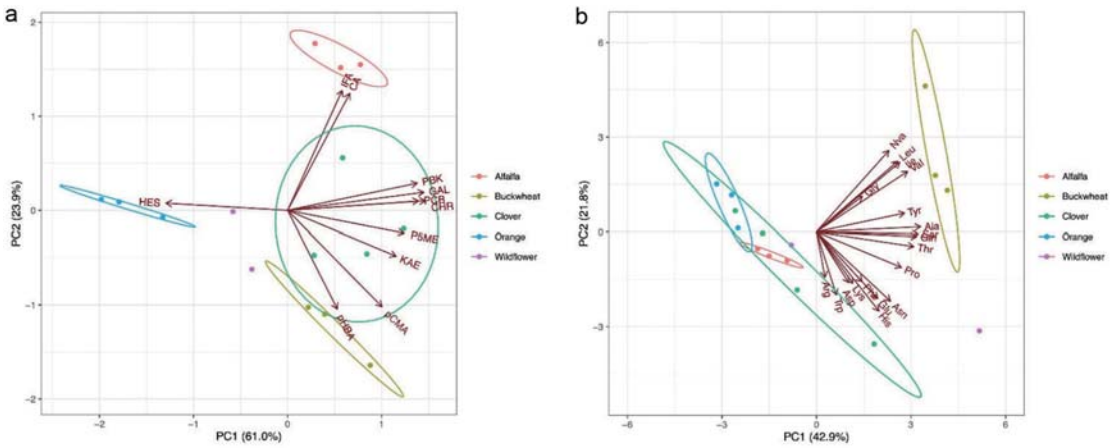

Figure 2. Principal component analysis biplots of phenolics (a) and free amino acids (b) contents in honey varieties. CA: caffeic acid, CHR: Chrysin, GAL: Galangin, HES: hesperidin, IFA: isoferulic acid, KAE: Kaempferol, pCMA: p-coumaric acid, pHBA: p-hydroxybenzoic acid, P5ME: pinobanksin-5-methyl ether, PBK: Pinobanksin, PCB: Pinocembrin. Ala: alanine, Arg: arginine, Asn: asparagine, Asp: aspartic acid, Cys: cysteine, Gln: glutamine, Glu: glutamic acid, Gly: glycine, His: histidine, Ile: isoleucine, Leu: leucine, Lys: lysine, Met: methionine, Nva: norvaline, Phe: phenylalanine, Pro: proline, Ser: serine, Thr: threonine, Trp: tryptophan, Tyr: tyrosine, Val: valine.

have not been clearly identified although several works made good attempts (Akbari et al., 2020; Ciappini, 2019). In the present study, isoferulic acid was identified and quantified for the first time in alfalfa honey. *p*-Hydroxybenzoic acid and *p*-coumaric acid, with a correlation of 0.858 (Table S3), was plotted in an opposite direction to the caffeic acid and isoferulic acid (Figure 2A). Buckwheat honey loaded the most positive direction of the vectors of *p*-hydroxybenzoic acid and *p*-coumaric acid with concentrations of 12.483 ± 4.230 and 4.910 ± 1.224 μg/g, respectively (Table 3). These two phenolic acids have been reported for buckwheat honey (Jiang et al., 2020; Sergiel et al., 2014; Shen et al., 2019) and shown to be representative compounds for buckwheat honey. Our result confirmed that *p*-hydroxybenzoic acid and *p*-coumaric acid can be employed collectively as good chemical markers for buckwheat honey.

3.2. Characterization of 5-HMF, furfural, and abscisic acid in honey varieties

5-HMF, furfural, and abscisic acid are three major non-phenolic compounds detected in each of tested honey samples. The concentrations were 4.131–10.059, 0.858–8.124, and 0.849–7.634 μg/g , respectively. 5-HMF is a dehydration product of reducing sugars such as glucose and fructose mostly via Maillard reaction, and has been found in honey and many food. Even though minor negative health effects have been reported for 5-HMF, it also contributes to many health benefits including antioxidant, anti-allergic, and anti-hypoxic effects (Chen et al., 2014; Suri and Chhabra, 2020). Although the safe level is not well clarified, the maximum limit of 5-HMF was established at 40 mg/kg honey in order to avoid extensive thermal processing (WHO, 1981). Furfural, produced by dehydration of pentose such as xylose, was also quantified in all honey samples. Except for the buckwheat honey which had a similar level of furfural to 5-HMF, furfural concentrations in all other honeys were significantly lower compared with 5-HMF (Table 3). Since both 5-HMF and furfural in honey are mainly produced during thermal processing and long storage, they are therefore not suitable for serving as chemical markers of the honey's botanical source.

Abscisic acid could be used as a botanical marker because of its differentiable contents in floral nectars. It has been reported as a marker of heather honey based on its high concentration of 4–18 μg/g (Tomás-Barberán et al., 2001). Our data showed a high concentration of abscisic acid in orange honey (7.634 ± 2.400 μg/g), which is 5.6–9.0 folds of that of other honeys (Table 3). Abscisic acid could be used as a secondary marker in combination with other primary chemical markers for discriminating between honeys of different botanic origins.

3.3. Total protein content and characterization of amino acids profiles in honey varieties

The total protein contents of different honeys were between 3808–8831 μg/g, with buckwheat honey having significantly higher concentration (ca. 2-fold) than the rest four honey varieties (Table 1). The intrinsic free amino acids and those produced by hydrolysis of the protein fraction of different honeys were also analyzed and the results are presented in Table 4.

The HPLC chromatograms of derivatized amino acids in a standard mix and different honey varieties are shown in Figure 3. All 21 L-amino acids including the IS were well baseline separated. Total free amino acids (sum of all quantified amino acids) ranged from 549.8 ± 72.7 to 1421.9 ± 53.5 μg/g for all honeys. Proline was the prevalent amino acid in all honey samples, ranging from 286.9 ± 33.6 μg/g in orange honey to 547.1 ± 162.4 μg/g in wildflower honey (Table 4). Proline in honey mostly originates from both nectar and hemolymph of honeybees (Łozowicka et al., 2021). A significant decrease in proline concentration in honey was reported when honeybee was fed with sucrose rather than pollens (Nisbet et al., 2018). The prevalence and the pollen origin make proline an important criterion for detecting honey adulteration (Dimins et al., 2022). Buckwheat honey contained the highest total free amino acid content, and total branched-chain amino acids (BCAA), including leucine, isoleucine and valine. The total BCAA in buckwheat honey was 276.6 μg/g, which was 6.7 to 16.5 folds of the BCAA concentrations found in other floral honeys (Table 4). Our result was highly comparable with the BCAA contents in buckwheat honey collected in Latvia (Dimins et al.,

Table 4. Intrinsic free amino acid and hydrolyzed amino acid concentrations in honey by HPLC

	Alfalfa	Buckwheat	Clover	Orange	Wildflower
Intrinsic free amino acids (μg/g Honey), Mean ± SD					
Ala	13.37 ± 2.54^{ab}	31.67 ± 6.70^{c}	12.52 ± 2.30^{ab}	10.21 ± 0.64^{b}	29.48 ± 15.52^{ac}
Arg	14.76 ± 5.02^{a}	15.05 ± 4.29^{a}	17.00 ± 3.62^{a}	16.81 ± 4.62^{a}	14.53 ± 2.77^{a}
Asn	40.76 ± 11.78^{a}	49.29 ± 12.67^{a}	52.98 ± 36.76^{a}	34.18 ± 7.05^{a}	71.59 ± 44.39^{a}
Asp	37.65 ± 2.13^{a}	24.49 ± 4.43^{a}	21.86 ± 4.45^{a}	16.86 ± 0.66^{a}	30.27 ± 8.29^{a}
Cys	n.d.	0.50 ± 0.87	n.d.	n.d.	n.d.
Gln	7.51 ± 0.96^{a}	72.00 ± 31.07^{a}	20.69 ± 6.44^{a}	12.01 ± 1.81^{a}	69.52 ± 64.61^{a}
Glu	26.11 ± 5.20^{a}	22.21 ± 3.25^{ab}	23.92 ± 5.48^{a}	10.04 ± 3.73^{b}	28.51 ± 9.67^{a}
Gly	18.90 ± 12.41^{a}	30.78 ± 11.53^{a}	12.70 ± 0.52^{a}	18.08 ± 11.15^{a}	14.14 ± 1.06^{a}
His	16.46 ± 2.26^{a}	15.89 ± 2.06^{a}	18.20 ± 5.59^{a}	14.73 ± 2.31^{a}	23.64 ± 9.17^{a}
Ile	4.70 ± 0.94^{a}	98.26 ± 36.83^{b}	11.70 ± 6.12^{a}	3.88 ± 0.57^{a}	20.39 ± 13.14^{a}
Leu	5.89 ± 0.99^{a}	115.26 ± 47.07^{b}	15.58 ± 8.15^{a}	5.90 ± 0.75^{a}	22.59 ± 12.45^{a}
Lys	12.83 ± 0.50^{ab}	14.04 ± 2.43^{ab}	17.34 ± 2.90^{a}	8.50 ± 1.89^{b}	15.13 ± 1.43^{a}
Met	n.d.	0.47 ± 0.81	n.d.	n.d.	n.d.
Nva	n.d.	38.98 ± 13.21	n.d.	n.d.	n.d.
Phe	32.17 ± 15.22^{a}	147.10 ± 7.10^{a}	252.65 ± 272.37^{a}	60.82 ± 31.64^{a}	152.04 ± 26.32^{a}
Pro	449.26 ± 117.20^{ab}	473.33 ± 18.42^{ab}	367.73 ± 68.07^{ab}	286.94 ± 33.57^{a}	547.05 ± 162.43^{b}
Ser	17.48 ± 3.52^{a}	34.82 ± 4.65^{a}	19.87 ± 2.50^{a}	18.28 ± 1.74^{a}	35.82 ± 19.83^{a}
Thr	8.25 ± 0.23^{a}	21.52 ± 1.46^{a}	8.41 ± 1.74^{a}	5.84 ± 0.22^{a}	28.10 ± 25.85^{a}
Trp	n.d.	n.d.	9.88 ± 14.69^{a}	0.28 ± 0.48^{a}	2.37 ± 0.00^{a}
Tyr	13.32 ± 2.86^{a}	153.26 ± 35.56^{b}	77.82 ± 77.82^{ab}	19.48 ± 10.27^{a}	63.83 ± 21.18^{ab}
Val	8.27 ± 0.87^{a}	63.03 ± 12.36^{b}	14.15 ± 6.98^{a}	6.98 ± 0.69^{a}	19.86 ± 7.26^{a}
Total	727.68 ± 133.58^{ab}	1421.93 ± 53.53^{a}	975.01 ± 496.75^{ab}	549.82 ± 72.71^{b}	1188.86 ± 442.49^{ab}
Amino acids after hydrolysis (μg/g Honey), Mean ± SD					
Ala	55.44 ± 13.80^{a}	177.78 ± 38.20^{b}	60.77 ± 7.57^{a}	46.26 ± 11.83^{a}	103.33 ± 34.11^{a}
Arg	40.82 ± 23.44^{a}	115.89 ± 8.45^{b}	46.80 ± 12.29^{a}	41.25 ± 3.94^{a}	68.80 ± 8.31^{a}
Asn	n.d.	n.d.	n.d.	n.d.	n.d.
Asp	214.19 ± 28.04^{a}	517.61 ± 135.17^{b}	218.58 ± 43.49^{a}	149.42 ± 31.30^{a}	340.40 ± 144.19^{ab}
Cys	18.06 ± 3.72^{a}	25.81 ± 1.40^{a}	20.84 ± 2.13^{a}	25.15 ± 5.87^{a}	28.80 ± 4.62^{a}
Gln	n.d.	n.d.	n.d.	n.d.	n.d.
Glu	182.59 ± 29.73^{ab}	510.71 ± 58.82^{c}	175.50 ± 19.44^{ab}	130.85 ± 24.62^{a}	396.76 ± 249.22^{bc}
Gly	74.69 ± 33.20^{a}	223.50 ± 7.03^{b}	58.32 ± 7.88^{a}	75.41 ± 37.57^{a}	78.72 ± 25.83^{a}
His	21.45 ± 1.60^{a}	66.00 ± 5.04^{b}	28.57 ± 7.98^{a}	25.22 ± 4.29^{a}	52.33 ± 28.65^{ab}
Ile	47.46 ± 9.29^{a}	290.31 ± 121.12^{b}	59.80 ± 11.22^{a}	37.20 ± 7.42^{a}	109.21 ± 15.21^{a}
Leu	72.55 ± 11.86^{a}	440.89 ± 166.35^{b}	88.96 ± 15.60^{a}	58.02 ± 10.82^{a}	138.27 ± 41.57^{a}
Lys	62.43 ± 11.01^{a}	135.83 ± 1.66^{b}	71.85 ± 14.99^{a}	55.50 ± 3.66^{a}	91.57 ± 28.20^{a}
Met	21.59 ± 4.40^{a}	68.44 ± 28.82^{b}	24.64 ± 5.93^{a}	25.20 ± 9.15^{a}	39.07 ± 0.62^{ab}
Nva	n.d.	40.08 ± 13.63	n.d.	n.d.	n.d.
Phe	95.33 ± 38.46^{a}	421.42 ± 56.81^{a}	325.09 ± 276.17^{a}	132.04 ± 48.79^{a}	300.36 ± 81.98^{a}
Pro	450.57 ± 106.69^{ab}	624.57 ± 63.12^{a}	400.83 ± 76.80^{ab}	313.10 ± 45.34^{b}	614.20 ± 237.51^{ab}
Ser	75.63 ± 12.49^{a}	243.24 ± 36.73^{b}	77.29 ± 9.98^{a}	59.12 ± 5.17^{a}	126.10 ± 47.49^{a}
Thr	50.64 ± 9.38^{a}	208.31 ± 45.25^{b}	52.45 ± 7.17^{a}	39.80 ± 4.42^{a}	101.53 ± 51.10^{a}
Trp	n.d.	n.d.	n.d.	n.d.	n.d.
Tyr	37.72 ± 15.45^{a}	221.64 ± 82.85^{b}	90.91 ± 38.34^{a}	51.27 ± 25.95^{a}	109.82 ± 16.94^{ab}
Val	58.00 ± 9.68^{a}	296.08 ± 86.44^{b}	68.71 ± 13.77^{a}	52.10 ± 3.56^{a}	107.82 ± 35.99^{a}
Total	1579.16 ± 299.20^{a}	4628.11 ± 918.98^{b}	1869.91 ± 451.09^{a}	1316.89 ± 186.77^{a}	2807.10 ± 1041.06^{a}

n.d. = not detected. Means followed by a common letter within the same row are not significantly different by the Tukey's HSD test at the 5% level of significance.

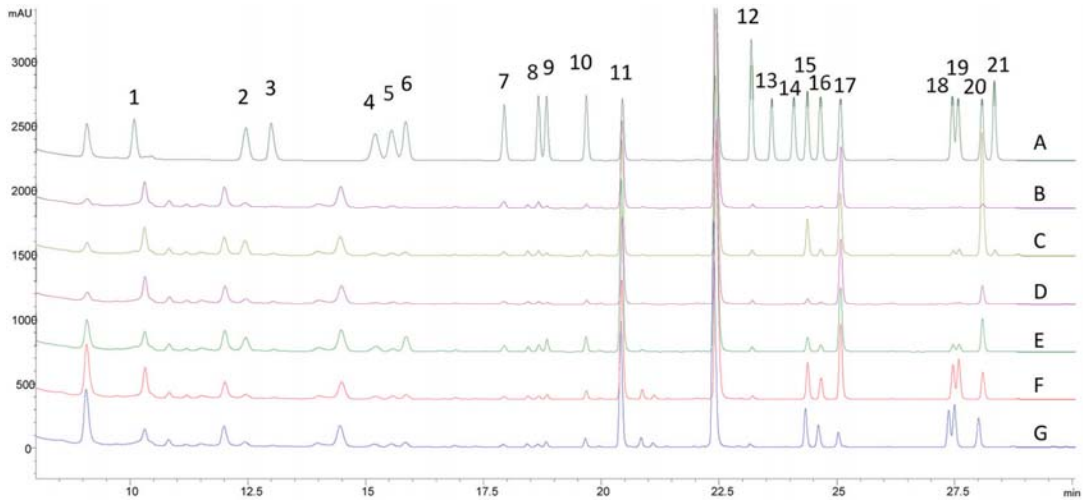

Figure 3. HPLC chromatograms of amino acid standards (A) and free amino acids with spiked internal standard of L-norvaline in honey varieties of alfalfa (B), clover (C), orange (D), wildflower (E), and buckwheat (F), as well as buckwheat honey without internal standard of norvaline (G). The HPLC peaks represent L-amino acid of histidine (1), asparagine (2), arginine (3), serine (4), glycine (5), glutamine (6), aspartic acid (7), glutamic acid (8), threonine (9), alanine (10), proline (11), lysine (12), cysteine (13), methionine (14), tyrosine (15), valine (16), norvaline (17), isoleucine (18), leucine (19), phenylalanine (20), and tryptophan (21).

2022). BCAA are essential amino acids and must be obtained from the diet. Their major health benefits, both acting as materials to build muscle tissues and to increase protein synthesis through the activation of mTOR signaling pathway, have been widely reported and understood (Zhang et al., 2017b). The high content of BCAA could make buckwheat honey a natural supplement of these essential nutrients. Phenylalanine is the most abundant essential amino acid in all studied honeys, at 252.7, 152.0, 147.1, 60.8, and 32.2 µg/g in clover, wildflower, buckwheat, orange, and alfalfa honey, respectively (Table 4). In addition to being a precursor of tyrosine, a recent study showed that phenylalanine may increase brain-derived neurotrophic factor in honey-treated rats and reduce the depressive-like behavior (Mustafa et al., 2019). As a conditionally essential amino acid, tyrosine was quantifiable mostly in buckwheat honey, followed by clover and wildflower honeys (Table 4).

The total amino acid contents after acid hydrolysis were generally 2–3 folds higher than the total free amino acids (Table 4). Again, buckwheat honey had the highest total concentration at 4,628.11 µg/g which was significantly higher than the rest of the honeys. This can be explained by its significantly higher total protein content compared to other honeys (Table 1). It is worth noting that asparagine, glutamine and tryptophan are known to be prone to acid hydrolysis (Mustatea et al., 2019), therefore they were not detected in samples subjected to this method (Table 4).

L-Norvaline has never before been reported for honey, and it was serendipitously found only in buckwheat honey of the present study when the spiked L-norvaline, serving as IS, showed abnormally higher concentration than its actual amount. The buckwheat honey samples were reanalyzed without spiked L-norvaline and its intrinsic L-norvaline was identified by MS/MS based on its matching $[M+H]^+$ at m/z 118.0864 and the major fragment ion of $[M\text{-}COOH+H]^+$ at m/z 72.0815 with the L-norvaline standard. It should be noted that the relative intensity of the ion at m/z 118 in buckwheat honey sample was lower than that of L-norvaline standard (t_R = 4.9 min) (Figure 4A, 4B). The extra m/z 118 ions are present due to an abundant unknown compound eluted earlier (t_R = 4.5 min) than L-norvaline, which produces a high background at m/z 118 (Figure 4C). L-Norvaline averaged 39.0 µg/g, which was the ninth most abundant among all 21 free amino acids in buckwheat honey, and it seems to be all in free form as the concentra-

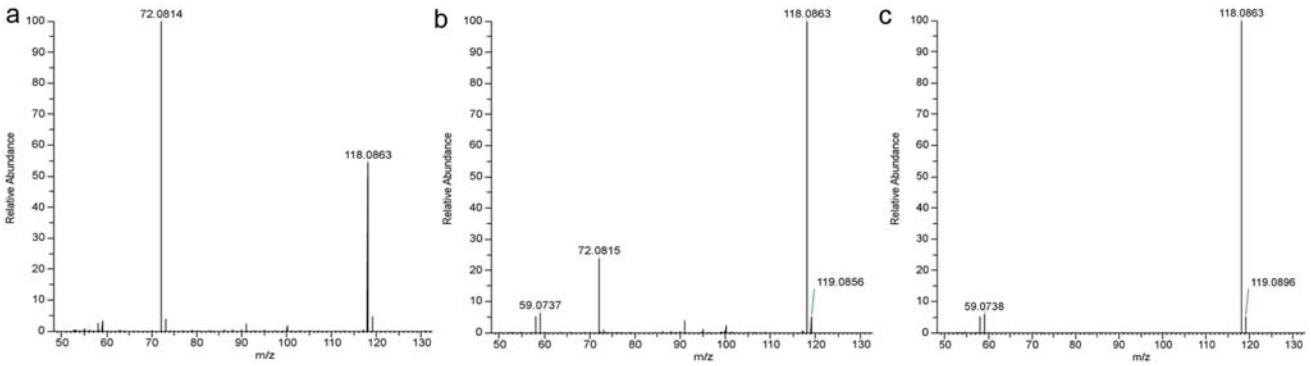

Figure 4. MS/MS spectra of diluted buckwheat honey samples (a), L-norvaline standard (b) and an unknown compound eluted earlier than L-norvaline but contributing a background at m/z 118.0864 (c).

tion was similar to that after the hydrolysis (Table 4). To the best of the authors' knowledge, the present finding is the first report of naturally occurring L-norvaline in buckwheat honey. Given its exclusive existence in the buckwheat honey, L-norvaline could mostly be originating from buckwheat flower, although further work on the amino acid profiling of buckwheat flower should be performed. As a potential inhibitor of arginase, L-norvaline raises the endogenous stock of L-arginine and consequently promotes the activity of nitric oxide synthase (NOS) which utilizes L-arginine as a substrate and produces nitric oxide. In contrast, substrate deficiency of NOS results in the production of superoxide anion rather than nitric oxide, which leads to the development of endothelial dysfunction due to the lack of nitric oxide. (Gilinsky et al., 2020; Pokrovskiy et al., 2011). This suggests the potential higher health benefits of buckwheat honey.

The contents of free amino acids were subjected to PCA to seek insights on the relationship between the amino acid composition and the honey varieties. We did not perform PCA analysis of amino acids resulted from acid hydrolysis because of the instability of certain amino acids and that in general all other amino acid concentrations followed similar trend as those for the intrinsic free amino acids. As shown in Figure 2B, the first two principal components explain about 64.70% of the total variance in all observations, thus were used to create the visualized biplot. The loading plot showed a cluster of vectors representing isoleucine, leucine, valine, tyrosine, and norvaline, resulting from their high correlation values between 0.717 and 0.995 (Table S4). By grouping the observations by honey variety, three buckwheat honey samples loaded the most positive direction of the vectors, which indicates that the BCAA, tyrosine, and norvaline level are most strongly correlated with buckwheat honey. While amino acids isoleucine, leucine, and tyrosine have been suggested as chemical markers for buckwheat honey (Dimins et al., 2022), the present study strongly points to L-norvaline, an non-proteinogenic amino acid, as a more appropriate marker or identifier for buckwheat honey.

3.4. Organic acid, vitamin and mineral compositions and enzymatic activities of honeys

The organic acid and mineral contents of selected honeys are shown in Table 5. A total of 7 minerals, i.e., calcium, iron, magnesium, phosphorus, potassium, sodium and zinc were detected and quantified. No statistical analysis was performed for the mineral contents due to their relatively insignificant amounts in the honey.

Organic acids are metabolites from oxidation of sugars during aerobic and/anaerobic fermentation of honey. They not only contribute to the organoleptic and physicochemical properties, but also act as antimicrobial and antioxidant agents, and have been used as indicators of honey freshness (Ķeķe and Cinkmanis, 2019). The predominant organic acid was gluconic acid in all honey samples, ranging from 2,574.58 to 6,430.92 μg/g (Table 5), which is in agreement with existing reports. Gluconic acid formation is known to be catalyzed by glucose oxidase from honeybees (Ķeķe and Cinkmanis, 2019) whose activity was also detected in the present study along with other enzymes (Table 5). This oxidation reaction also produces hydrogen peroxide, which is responsible for the antimicrobial activities; but the extra hydrogen peroxide is reduced by catalase to water and oxygen. Catalase activity was detected in all honey samples (Table 5). Hydrolytic enzymes such as amylase, diastase, and invertase are secreted by honeybees for converting oligo- and polysaccharides to monosaccharides; for example, diastase converts nectar polysaccharides (amylose) to glucose, and invertase converts the sucrose into fructose and glucose (Alaerjani et al., 2022). Acid phosphatase is also a hydrolytic enzyme but it catalyzes the production of inorganic phosphate from organic phosphate. Enzymatic activities of different honeys are listed in Table 5. Enzyme activities of honey have been used as markers of honey quality and botanic origin (Alaerjani et al., 2022). Among the vitamins, only B vitamins were detected and quantified, and buckwheat honey had significantly higher concentrations than other honey samples (Table 5).

3.5. Major and rare sugars

Table 6 shows the concentrations of individual and total sugars and the moisture contents of the honey samples. Total sugar content ranged from 78.53 g/100 g to 81.87 g/100 g with predominant sugars being the monosaccharides, fructose and glucose, which is in line with other reports (da Silva et al., 2016). Rare sugars in the honey samples included turanose, isomaltulose, nigerose and kojibiose among others sugars (de la Fuente et al., 2011; Doner, 1977; Escuredo et al., 2013). While we only measured some key rare disaccharides and trisaccharides, more than 25 of such have been reported (de la Fuente et al., 2011; Doner, 1977; Escuredo et al., 2013), comprising 5–15% of honey sugars. Our results show a similar amount of rare sugars when we subtract major sugars from total sugars measured using the phenol-sulfuric acid method. Rare sugars have individually shown to have metabolic benefits with majority being non-cariogenic (Ooshima et al., 1983) and exerting prebiotic (Chung et al., 2017; Hodoniczky et al., 2012; Sanz et al., 2005), anti-glycemic (Lee et al., 2016), anti-inflammatory (Chung et al., 2017), and immune modulation (Mirosaki et al., 1999) effects in animal models. These rare sugars have also been found to reduce blood glucose, body weight (Ahmed et al., 2022), and acute metabolic hormones related to obesity like GIP and GLP-1 activities in human studies (Keyhani-Nejad et al., 2015), thus explaining some metabolic benefits of honey (Ahmed et al., 2023).

4. Conclusions

The present study characterized the composition of major bioactive components and nutrients of typical honeys available in North America. Qualitative and quantitative data of phenolic compounds, protein and amino acids, organic acids, minerals, vitamins, and other minor components, including abscisic acid and furans were collected. A total of 29 phenolic compounds, mostly phenolic acids and flavonoids were identified and quantified. P5ME, along with pinobanksin, pinocembrin, chrysin and galangin, were found commonly and abundantly in all tested honeys. The propolis origin of P5ME could help to differentiate a genuine honey from an adulterated one. The profile of nectar-derived phenolic compounds displayed significant differences among different honey varieties. Results of the present study not only confirmed the use of previously reported chemical markers (e.g. *p*-hydroxybenzoic acid and *p*-coumaric acid for buckwheat honey, and hesperidin for orange honey), but also showed the potential use of caffeic acid and isoferulic acid as markers for alfalfa honey. Conversely, unlike the phenolic compounds, the free amino acid profiles of the studied honeys showed less diversity in all but buckwheat honey. The buckwheat honey possessed significantly higher levels of BCAA than other honeys, and contained L-norvaline exclusively. The serendipitous new finding of L-norvaline in buckwheat honey not only adds a new marker for identifying its botanic origin, but the unique bioactivity of L-norvaline may also confer additional

Table 5. Concentrations of organic acids, minerals, vitamins and enzyme activities in honeys

	Organic acid concentration (µg/g Honey), Mean ± SD							
	Alfalfa1	**Clover1**	**Clover2**	**Clover3**	**Golden1**	**Orange1**	**Wildflower1**	**Wildflower2**
Acetic acid[1]	223.37 ± 13.08	94.03 ± 4.14	259.55 ± 2.81	243.85 ± 7.57	305.32 ± 3.74	245.37 ± 9.08	279.07 ± 15.06	256.49 ± 11.63
Citric acid[2]	56.01 ± 1.38	83.43 ± 0.80	79.61 ± 1.88	59.30 ± 0.41	131.51 ± 2.83	80.29 ± 0.29	253.27 ± 2.02	139.50 ± 0.13
Formic acid[3]	7.47 ± 2.65	7.70 ± 3.14	7.94 ± 2.89	8.88 ± 2.23	12.05 ± 3.55	8.23 ± 1.03	10.29 ± 2.55	7.82 ± 0.67
Gluconic acid[2]	3,171.56 ± 62.04	3,760.88 ± 19.96	3,163.84 ± 21.90	2,574.58 ± 34.40	3,810.69 ± 106.84	3,838.48 ± 83.97	6,430.92 ± 55.44	3,719.23 ± 82.36
Gluctaric acid[2]	n.d.	n.d.	n.d.	n.d.	n.d.	n.d.	n.d.	n.d.
Glycolic acid[2]	n.d.	n.d.	n.d.	n.d.	n.d.	n.d.	n.d.	n.d.
Lactic acid[2]	48.49 ± 4.10	45.38 ± 7.09	48.97 ± 4.95	22.35 ± 2.38	47.03 ± 2.55	82.14 ± 1.89	114.75 ± 5.74	47.91 ± 0.96
Maleic acid[2]	1.94 ± 0.20	2.36 ± 0.19	2.25 ± 0.09	1.52 ± 0.24	1.94 ± 0.28	2.16 ± 0.13	2.03 ± 0.19	1.48 ± 0.08
Malic acid[2]	54.90 ± 0.30	29.13 ± 0.71	78.44 ± 3.02	40.23 ± 1.37	69.14 ± 1.28	342.37 ± 6.50	75.75 ± 1.56	94.38 ± 1.61
Malonic acid[2]	46.56 ± 5.82	98.92 ± 6.64	69.53 ± 4.33	46.10 ± 8.96	63.09 ± 4.72	30.39 ± 3.43	74.64 ± 5.01	60.00 ± 3.65
Oxalic acid[3]	124.59 ± 0.83	155.32 ± 3.51	181.52 ± 0.63	193.70 ± 2.84	147.50 ± 0.32	149.69 ± 1.14	217.89 ± 1.67	152.23 ± 2.38
Propionic acid[1]	n.d.	n.d.	n.d.	n.d.	n.d.	n.d.	n.d.	n.d.
Succinic acid[2]	10.31 ± 0.67	10.15 ± 1.14	15.61 ± 0.68	9.12 ± 1.37	13.09 ± 0.38	35.81 ± 0.44	17.53 ± 1.89	16.98 ± 0.86

	Unit	**Alfalfa1**	**Clover1**	**Clover2**	**Clover3**	**Golden1**	**Orange1**	**Wildflower1**	**Wildflower2**
Mineral contents (Mean ± SD)									
Calcium	%	<0.03	<0.03	<0.03	<0.03	<0.03	<0.03	<0.03	<0.03
Iron	ppm	<7	<7	<7	<7	<7	<7	7.05 ± 0.07	<7
Magnesium	%	<0.012	<0.012	<0.012	<0.012	<0.012	<0.012	<0.012	<0.012
Phosphorus	%	<0.014	<0.014	<0.014	<0.014	<0.014	<0.014	<0.014	<0.014
Potassium	%	0.03 ± 0.00	<0.03	<0.03	0.03 ± 0.00	0.03 ± 0.00	<0.03	0.05 ± 0.00	0.04 ± 0.00
Sodium	%	<0.013	<0.013	<0.013	<0.013	<0.013	<0.013	<0.013	<0.013
Zinc	ppm	<7	7.84 ± 1.19	<7	<7	<7	<7	7.44 ± 0.39	<7
Enzyme activity (Mean ± SD)									
Amylase	U/100g	1.279 ± 0.000	1.525 ± 0.090	1.824 ± 0.104	2.825 ± 0.128	1.270 ± 0.052	1.215 ± 0.148	1.644 ± 0.130	2.616 ± 0.074
Diastase	Diastase unit	5.24 ± 0.20	7.07 ± 0.11	8.86 ± 0.32	7.75 ± 0.19	7.01 ± 0.09	4.79 ± 0.06	7.37 ± 0.06	6.82 ± 0.08
Glucose Oxidase	U/100	0.679 ± 0.013	0.685 ± 0.008	0.765 ± 0.008	0.965 ± 0.032	1.277 ± 0.008	1.174 ± 0.020	1.007 ± 0.022	0.918 ± 0.027
Catalase	U/100g	43.44 ± 1.59	171.9 ± 4.3	163.9 ± 13.2	53.80 ± 0.61	157.8 ± 1.7	39.59 ± 4.38	156.2 ±7.2	91.34 ± 2.05
Invertase	mU/100g	16.08 ± 0.50	28.20 ± 2.09	26.59 ± 0.42	19.50 ± 0.714	34.40 ± 1.83	25.37 ± 1.31	53.87 ± 4.11	24.64 ± 0.87
Acid Phosphatase	mg P/100g /24 h	52.13 ± 3.90	55.49 ± 1.64	58.78 ± 2.11	60.04 ± 1.55	57.96 ± 2.09	60.23 ± 0.44	50.93 ± 1.16	58.40 ± 2.20

	Vitamins (µg/g Honey), Mean ± SD				
	Alfalfa	**Buckwheat**	**Clover**	**Orange**	**Wildflower**
Riboflavin (B2)	0.054 ± 0.079^{ab}	0.187 ± 0.010^{a}	0.022 ± 0.025^{b}	0.031 ± 0.045^{b}	0.098 ± 0.092^{ab}
Nicotinic acid (B3)	0.228 ± 0.048^{a}	0.849 ± 0.108^{b}	0.381 ± 0.015^{cd}	0.250 ± 0.040^{ac}	0.437 ± 0.059^{d}
Pantothenic acid (B5)	0.045 ± 0.019^{a}	0.162 ± 0.069^{a}	0.154 ± 0.079^{a}	0.071 ± 0.041^{a}	0.183 ± 0.108^{a}
Pyridoxine (B6)	0.011 ± 0.003^{a}	0.037 ± 0.015^{ab}	0.064 ± 0.021^{b}	0.017 ± 0.005^{ab}	0.073 ± 0.044^{b}
Ascorbic acid	n.d.	n.d.	n.d.	n.d.	n.d.

n.d. = not detected. Organic acids were quantified by GC (1), LC-MS (2), or specific assay kit (3).

Table 6. Concentrations of individual carbohydrates and sugar contents of honeys

	Carbohydrate concentration (g/100g Honey), Mean ± SD					
	Clover 1	**Clover 2**	**Clover 3**	**Clover 4**	**Orange 1**	**Orange 2**
Fructose	38.48 ± 0.57	37.84 ± 1.55	40.36 ± 1.89	40.69 ± 1.60	38.25 ± 0.41	39.44 ± 1.15
Glucose	34.57 ± 0.25	32.8 ± 1.32	32.03 ± 0.95	36.94 ± 1.62	31.78 ± 0.34	33.50 ± 0.89
Sucrose	0.72 ± 0.01	1.1 ± 0.05	0.58 ± 0.02	0.13 ± 0.003	0.68 ± 0.02	0.16 ± 0.003
Trehalose	n.t.	0.06 ± 0	0.42 ± 0.03	n.t.	n.t.	n.t.
Kojibiose	n.t.	1.47 ± 0.02	1.68 ± 0.03	n.t.	n.t.	n.t.
Turanose	n.t.	1.42 ± 0.03	1.53 ± 0.03	1.57 ± 0.06	n.d.	2.36 ± 0.09
Maltose	n.t.	2.47 ± 0.03	2.2 ± 0.03	1.41 ± 0.06	n.d.	1.39 ± 0.04
Isomaltose	n.t.	0.51 ± 0.01	0.55 ± 0.01	0.56 ± 0.02	n.d.	0.79 ± 0.03
Palatinose (isomaltulose)	n.t.	0.15 ± 0.01	0.15 ± 0.01	0.24 ± 0.007	n.d.	0.43 ± 0.03
Nigerose	n.t.	0.28 ± 0.01	0.31 ± 0.01	0.31 ± 0.02	n.d.	0.39 ± 0.02
Melezitose	n.t.	2.35 ± 0.22	1.29 ± 0.1	n.d.	n.d.	n.d.
Isomaltotriose	n.t.	0.02 ± 0.01	0.01 ± 0	n.d.	n.d.	n.d.
Maltotriose	n.t.	0.32 ± 0.01	0.48 ± 0.01	n.d.	n.d.	n.d.
Total sugars	78.52 ± 2.28	81.22 ± 4.77	81.14 ± 2.98	79.30 ± 2.80	78.34 ± 2.27	80.57 ± 0.90
Moisture	17.73 ± 0.42	16.67 ± 1.39	15.53 ± 0.64	15.27 ± 0.47	17.93 ± 0.46	15.33 ± 0.05

	Carbohydrate concentration (g/100g Honey), Mean ± SD					
	Alfalfa 1	**Alfalfa 2**	**Wildflower 1**	**Wildflower 2**	**Golden**	**Buckwheat**
Fructose	36.60 ± 1.28	39.66 ± 1.70	40.2 ± 1.87	41.53 ± 1.90	37.51 ± 0.60	37.47 ± 1.53
Glucose	32.49 ± 0.90	36.08 ±2.35	34.37 ± 0.88	36.98 ± 0.82	33.62 ± 0.33	33.56 ± 1.04
Sucrose	0.42 ± 0.04	0.17 ± 0.002	0.26 ± 0.02	0.11 ± 0.01	0.61 ± 0.08	0.12 ± 0.01
Trehalose	n.t.	n.t.	0.15 ± 0.01	n.t.	0.1 ± 0	n.t.
Kojibiose	n.t.	n.t.	1.58 ± 0.02	n.t.	1.57 ± 0.02	n.t.
Turanose	n.d.	1.99 ± 0.04	1.46 ± 0.07	1.31 ± 0.07	1.46 ± 0.05	n.t.
Maltose	n.d.	1.12 ± 0.01	1.81 ± 0.07	1.31 ± 0.04	1.45 ± 0.04	n.t.
Isomaltose	n.d.	0.56 ± 0.01	0.54 ± 0.03	0.41 ± 0.02	0.53 ± 0.01	n.t.
Palatinose (isomaltulose)	n.d.	0.33 ± 0.01	0.23 ± 0.02	0.17 ± 0.02	0.22 ± 0.01	n.t.
Nigerose	n.d.	0.29 ± 0.01	0.30 ± 0.01	0.23 ± 0.01	0.25 ± 0.01	n.t.
Melezitose	n.d.	n.d.	1.81 ± 0.31	n.d.	1.29 ± 0.1	n.d.
Isomaltotriose	n.d.	n.d.	0.03 ± 0	n.d.	0.01 ± 0	n.d.
Maltotriose	n.d.	n.d.	0.37 ± 0.01	n.d.	0.48 ± 0.01	n.d.
Total sugars	79.30 ± 5.23	81.81 ± 2.21	81.78 ± 2.79	80.67 ± 1.67	81.87 ± 2.2	78.94 ± 2.52
Moisture	17 ± 0.001	15.57 ± 0.19	16.13 ± 1.43	15.76 ± 0.51	16.8 ± 0	19.2 ± 0.72

n.t. = not tested; n.d. = not detected.

health-promoting properties for buckwheat honey. It should be noted that the composition of floral honey may be affected by several factors including geographical origin, seasonal changes, processing, and storage conditions; therefore, single components, such as phenolics, alone may not be sufficient markers for identifying the botanical origin of honeys. Our results suggest that combining markers of different chemical categories, such as phenolics and amino acids, and other phytochemicals (e.g., abscisic acid) could enhance the confidence in discriminating origins between different floral honeys. The current study also provides important baseline data for all major bioactive components of honeys, and thus, will contribute significantly to the identification of honey components for various health benefits. Moreover, our study showed that in addition to major sugars (glucose and fructose), the studied honeys were also sources of minor and rare sugars, which may further contribute to the different bioactivities of honey. Future work will

focus on the uniquely identified phenolic compounds, free amino acids, and rare sugars or their combinations for their contribution to potential health benefits.

Acknowledgments

We thank the National Honey Board of the United States of America and Glycemia Consulting Inc. (Toronto, Ontario, Canada) for providing honey samples and financial support. This is Project #J-002712 of Agriculture & Agri-Food Canada.

Supplementary material

Table S1. Sample information of tested honeys.

Table S2. (a) Raw data of the concentrations of individual phenolic compounds detected in different honey samples; (b) Raw data of the concentrations of individual amino acids detected in different honey samples; (c) Raw data of the concentrations of individual organic acids detected in different honey samples; (d) Raw data of the concentrations of minerals detected in different honey samples; (e) Raw data of the total phenolic contents (TPC) of different honey samples; (f) Raw data of the total protein contents of different honey samples; (g) Raw data of the enzyme activities of different honey samples; (h) Raw data of sugar concentrations of different honey samples; (i) Raw data of total carbohydrate concentrations of different honey samples; (j) Raw data of moisture contents of different honey samples; (k) Raw data of USDA color (Pfund Scale, mm) of different honey samples; (l) Raw data of ash contents of different honey samples.

Table S3. Correlation matrix of phenolics in honey samples.

Table S4. Correlation matrix of free amino acids in honey samples.

References

Ahmed, A., Khan, T.A., Dan Ramdath, D., Kendall, C.W.C., and Sievenpiper, J.L. (2022). Rare sugars and their health effects in humans: a systematic review and narrative synthesis of the evidence from human trials. Nutr Rev 80(2): 255–270.

Ahmed, A., Tul-Noor, Z., Lee, D., Bajwah, S., Ahmed, Z., Zafar, S., Syeda, M., Jamil, F., Qureshi, F., Zia, F., Baig, R., Ahmed, S., Tayyiba, M., Ahmad, S., Ramdath, D., Tsao, R., Cui, S., Kendall, C.W.C., de Souza, R.J., Khan, T.A., and Sievenpiper, J.L. (2023). Effect of honey on cardiometabolic risk factors: a systematic review and meta-analysis. Nutr. Rev. 81: 758–774.

Akbari, E., Baigbabaei, A., and Shahidi, M. (2020). Determination of the floral origin of honey based on its phenolic profile and physicochemical properties coupled with chemometrics. Int. J. Food Prop. 23(1): 506–519.

Alaerjani, W.M.A., Abu-Melha, S., Alshareef, R.M.H., Al-Farhan, B.S., Ghramh, H.A., Al-Shehri, B.M.A., Bajaber, M.A., Khan, K.A., Alrooqi, M.M., Modawe, G.A., and Mohammed, M.E.A. (2022). Biochemical Reactions and Their Biological Contributions in Honey. Molecules 27: 4719.

Battino, M., Giampieri, F., Cianciosi, D., Ansary, J., Chen, X., Zhang, D., Gil, E., and Forbes-Hernández, T. (2021). The roles of strawberry and honey phytochemicals on human health: A possible clue on the molecular mechanisms involved in the prevention of oxidative stress and inflammation. Phytomedicine 86: 153170.

Chen, P.X., Tang, Y., Zhang, B., Liu, R., Marcone, M.F., Li, X., and Tsao, R. (2014). 5-hydroxymethyl-2-furfural and derivatives formed during acid hydrolysis of conjugated and bound phenolics in plant foods and the effects on phenolic content and antioxidant capacity. J. Agric. Food Chem. 62(20): 4754–4761.

Chung, J.-Y., Kim, Y.-S., Kim, Y., and Yoo, S.-H. (2017). Regulation of Inflammation by Sucrose Isomer, Turanose, in Raw 264.7 Cells. J. Cancer Prev. 22(3): 195–201.

Cianciosi, D., Forbes-Hernández, T.Y., Afrin, S., Gasparrini, M., Reboredo-Rodriguez, P., Manna, P.P., Zhang, J., Bravo Lamas, L., Martínez Flórez, S., Agudo Toyos, P., Quiles, J.L., Giampieri, F., and Battino, M. (2018). Phenolic Compounds in Honey and Their Associated Health Benefits: A Review. Molecules 23(9): 2322.

Ciappini, M.C. (2019). Polyphenolic profile of floral honeys in correlation with their pollen spectrum. J. Apic. Res. 58(5): 772–779.

da Silva, P.M., Gauche, C., Gonzaga, L.V., Costa, A.C., and Fett, R. (2016). Honey: Chemical composition, stability and authenticity. Food Chem. 196: 309–323.

da Silva, P.M., Gauche, C., Gonzaga, L.V., Costa, A.C.O., and Fett, R. (2016). Honey: Chemical composition, stability and authenticity. Food Chem. 196: 309–323.

Davies, A.M.C. (1978). Proline in Honey: An Osmoregulatory Hypothesis. J. Apic. Res. 17(4): 227–233.

de la Fuente, E., Ruiz-Matute, A.I., Valencia-Barrera, R.M., Sanz, J., and Martínez Castro, I. (2011). Carbohydrate composition of Spanish unifloral honeys. Food Chem. 129(4): 1483–1489.

Dimins, F., Cinkmanis, I., Radenkovs, V., Augspole, I., and Valdovska, A. (2022). Analysis of 18 Free Amino Acids in Honeybee and Bumblebee Honey from Eastern and Northern Europe and Central Asia Using HPLC-ESI-TQ-MS/MS Approach Bypassing Derivatization Step. Foods 11(18): 2744.

Doner, L.W. (1977). The sugars of honey--a review. J. Sci. Food Agric. 28(5): 443–456.

Escuredo, O., Míguez, M., Fernández-González, M., and Carmen Seijo, M. (2013). Nutritional value and antioxidant activity of honeys produced in a European Atlantic area. Food Chem. 138(2-3): 851–856.

Ferreres, F., Andrade, P., Gil, M.I., and Tomas-Barberan, F.A. (1996). Floral nectar phenolics as biochemical markers for the botanical origin of heather honey. Z. Lebensm. Untersuch. Forsch. 202: 40–44.

Ferreres, F., Giner, J.M., and Tomas-Barberan, F.A. (1994). A comparative study of hesperetin and methyl anthranilate as markers of the floral origin of citrus honey. J. Sci. Food Agric. 65: 371–372.

Gilinsky, M.A., Polityko, Y.K., Markel, A.L., Latysheva, T.V., Samson, A.O., Polis, B., and Naumenko, S.E. (2020). Norvaline Reduces Blood Pressure and Induces Diuresis in Rats with Inherited Stress-Induced Arterial Hypertension. Biomed. Res. Int. 2020: 4935386.

Greenaway, W., English, S., and Whatley, F.R. (1990). Phenolic Composition of Bud Exudates of Populus deltoides. Z. Naturforsch. 45c: 587–593.

Hermosín, I., Chicón, R.M., and Cabezudo, M.D. (2003). Free amino acid composition and botanical origin of honey. Food Chem. 83: 263–268.

Hodoniczky, J., Morris, C.A., and Rae, A.L. (2012). Oral and intestinal digestion of oligosaccharides as potential sweeteners: A systematic evaluation. Food Chem. 132(4): 1951–1958.

Janiszewska, K., Aniołowska, M., and Nowakowski, P. (2012). Free Amino Acids Content of Honeys from Poland. Pol. J. Food Nutr. Sci. 62(2): 85–89.

Jiang, L., Xie, M., Chen, G., Qiao, J., Zhang, H., and Zeng, X. (2020). Phenolics and Carbohydrates in Buckwheat Honey Regulate the Human Intestinal Microbiota. Evidence-Based Complementary Altern. Med. 2020: 6432942.

Ķeķe, A., and Cinkmanis, I. (2019). Determination of organic acids in honey samples from Latvian market by high-performance liquid chromatography. Res. Rural Dev. 1: 229–233.

Keyhani-Nejad, F., Kemper, M., Schueler, R., Pivovarova, O., Rudovich, N., and Pfeiffer, A.F.H. (2015). Effects of Palatinose and Sucrose Intake on Glucose Metabolism and Incretin Secretion in Subjects With Type 2 Diabetes. Diabetes Care 39(3): e38–e39.

Lee, B.-H., Rose, D.R., Lin, A.H.-M., Quezada-Calvillo, R., Nichols, B.L., and Hamaker, B.R. (2016). Contribution of the Individual Small Intestinal α-Glucosidases to Digestion of Unusual α-Linked Glycemic Disaccharides. J. Agric. Food Chem. 64(33): 6487–6494.

Łozowicka, B., Kaczyński, P., and Iwaniuk, P. (2021). Analysis of 22 free amino acids in honey from Eastern Europe and Central Asia using

LC-MS/MS technique without derivatization step. J. Food Compos. Anal. 98: 103837.

Machado De-Melo, A.A., Almeida-Muradian, L.B.d., Sancho, M.T., and Pascual-Maté, A. (2018). Composition and properties of Apis mellifera honey: A review. J. Apic. Res. 57(1): 5–37.

Maldonado, L.M., Marcinkevicius, K., Salomón, V., Sánchez, A.C., Álvarez, A., Lupo, L., and Bedascarrasbure, E. (2021). Physicochemical and melissopalynological profiles of Citrus limon honey from Tucumán- Argentina. Hesperidin as a suitable marker of floral origin. RIA 47(3): 315–324.

Mao, W., Schuler, M.A., and Berenbaum, M.R. (2013). Honey constituents up-regulate detoxification and immunity genes in the western honey bee Apis mellifera. Proc. Natl. Acad. Sci. U S A 110(22): 8842–8846.

Mirosaki, S., Muroyama, K., Yamamoto, Y., Kusaka, H., Liu, T., and Yoshikai, Y. (1999). Immunopotentiating Activity of Nigerooligosaccharides for the T Helper 1-Like Immune Response in Mice. Biosci. Biotechnol. Biochem. 63(2): 373–378.

Mustafa, M.Z., Zulkifli, F.N., Fernandez, I., Mariatulqabtiah, A.R., Sangu, M., Nor Azfa, J., Mohamed, M., and Roslan, N. (2019). Stingless Bee Honey Improves Spatial Memory in Mice, Probably Associated with Brain-Derived Neurotrophic Factor (BDNF) and Inositol 1,4,5-Triphosphate Receptor Type 1 (Itpr1) Genes. Evidence-Based Complementary Altern. Med. 2019: 8258307.

Mustatea, G., Ungureanu, E.L., and Iorga, E. (2019). Protein acidic hydrolysis for amino acids analysis in food progress over time: a short review. J. Hyg. Eng. Des. 26: 81–87.

Nisbet, C., Kazak, F., and Ardali, Y. (2018). Determination of Quality Criteria that Allow Differentiation Between Honey Adulterated with Sugar and Pure Honey. Biol. Trace. Elem. Res. 186(1): 288–293.

Olas, B. (2020). Honey and Its Phenolic Compounds as an Effective Natural Medicine for Cardiovascular Diseases in Humans? Nutrients 12(2): 283.

Ooshima, T., Izumitani, A., Sobue, S., Okahashi, N., and Hamada, S. (1983). Non-cariogenicity of the disaccharide palatinose in experimental dental caries of rats. Infect. Immun. 39(1): 43–49.

Paramás, A.M.G., Bárez, J.A.G., Marcos, C.C., García-Villanova, R.J., and Sánchez, J.S. (2006). HPLC-fluorimetric method for analysis of amino acids in products of the hive (honey and bee-pollen). Food Chem. 95: 148–156.

Pokrovskiy, M.V., Korokin, M.V., Tsepeleva, S.A., Pokrovskaya, T.G., Gureev, V.V., Konovalova, E.A., Gudyrev, O.S., Kochkarov, V.I., Korokina, L.V., Dudina, E.N., Babko, A.V., and Terehova, E.G. (2011). Arginase Inhibitor in the Pharmacological Correction of Endothelial Dysfunction. Int. J. Hypertens. 2011: 515047.

Sanz, M.L., Gibson, G.R., and Rastall, R.A. (2005). Influence of Disaccharide Structure on Prebiotic Selectivity in Vitro. J. Agric. Food Chem. 53(13): 5192–5199.

Sergiel, I., Pohl, P., and Biesaga, M. (2014). Characterisation of honeys according to their content of phenolic compounds using high performance liquid chromatography/tandem mass spectrometry. Food Chem. 145: 404–408.

Shen, S., Wang, J., Chen, X., Liu, T., Zhuo, Q., and Zhang, S.Q. (2019). Evaluation of cellular antioxidant components of honeys using UPLC-MS/MS and HPLC-FLD based on the quantitative composition-activity relationship. Food Chem. 293: 169–177.

Sultana, S., Foster, K., Lim, L.Y., Hammer, K., and Locher, C. (2022). A Review of the Phytochemistry and Bioactivity of Clover Honeys (*Trifolium* spp.). Foods 11(13): 1901.

Suri, P.S., and Chhabra, P. (2020). A Review Presence of 5-Hydroxymethylfurfural (HMF) in Food Products: Positive and Negative Impacts on Human Health. Int. J. Forens. Sci. 5(2): 000194.

Tomás-Barberán, F.A., Martos, I., Ferreres, F., Radovic, B.S., and Anklam, E. (2001). HPLC flavonoid profiles as markers for the botanical origin of European unifloral honeys. J. Sci. Food Agric. 81: 485–496.

Wang, X., Chen, Y., Hu, Y., Zhou, J., Chen, L., and Lu, X. (2022). Systematic Review of the Characteristic Markers in Honey of Various Botanical, Geographic, and Entomological Origins. ACS Food Sci. Technol. 2: 206–220.

WHO. (1981). Standard for honey. Codex Alimentarius International food standards, CXS12.

Zammit Young, G.W., and Blundell, R. (2023). A review on the phytochemical composition and health applications of honey. Heliyon 9(2): e12507.

Zhang, H., and Tsao, R. (2016). Dietary polyphenols, oxidative stress and antioxidant and anti-inflammatory effects. Curr. Opin. Food Sci. 8: 33–42.

Zhang, H., Hassan, Y.I., Renaud, J., Liu, R., Yang, C., Sun, Y., and Tsao, R. (2017a). Bioaccessibility, bioavailability, and anti-inflammatory effects of anthocyanins from purple root vegetables using mono- and co-culture cell models. Mol. Nutr. Food Res. 61(10): 1600928.

Zhang, S., Zeng, X., Ren, M., Mao, X., and Qiao, S. (2017b). Novel metabolic and physiological functions of branched chain amino acids: a review. J. Anim. Sci. Biotechnol. 8: 10.

Journal of Food Bioactives
International Society for Nutraceuticals and Functional Foods
Original Research
J. Food Bioact. 2024;25:42–51

Sesamolin has the ability to induce longevity effects on the *Caenorhabditis elegans*, and the mechanism depends on the SIR-2.1 and AAK-2 proteins

Chia-Yu Chin[a], Pei-Jing Lee[a] and Nae-Cherng Yang[a,b*]

[a]Department of Nutrition, Chung Shan Medical University, Taichung 402, Taiwan
[b]Department of Nutrition, Chung Shan Medical University Hospital, Taichung 402, Taiwan
[*]**Corresponding author:** Nae-Cherng Yang, Department of Nutrition, Chung Shan Medical University, Taichung 402, Taiwan. Tel: +886-4-3609-7673; Fax: +886-4-2324-8175; E-mail: naeman@csmu.edu.tw
DOI: 10.31665/JFB.2024.18370
Received: December 26, 2023; **Revised received & accepted:** February 04, 2024
Citation: Chin, C.-Y., Lee, P.-J., and Yang, N.-C. (2024). Sesamolin has the ability to induce longevity effects on the *Caenorhabditis elegans*, and the mechanism depends on the SIR-2.1 and AAK-2 proteins. J. Food Bioact. 25: 42–51.

Abstract

Sesamolin, one of the prominent lignans in sesame seeds, offers diverse physiological benefits. However, the longevity effects and mechanisms of sesamolin remain unclear. We hypothesized that sesamolin can exert the longevity effects in the *Caenorhabditis* (*C.*) *elegans* when prepared with the γ-cyclodextrin to form an inclusion complex (named γCD-SM). In this study, the γCD-SM was prepared, and the lifespan assays, health indexes, and loss-of-function assays in the *C. elegans* or mutants were conducted. The results demonstrated that the γCD-SM significantly extended the *C. elegans'* lifespan and improved the health indexes, such as the pharyngeal pumping and body bends. The longevity effects of the γCD-SM were found to depend on the signaling of the SIR-2.1 and AAK-2. In conclusion, the γ-CD inclusion is a crucial step for assessing the sesamolin's longevity effects in the *C. elegans*. This study confirms that sesamolin exhibits the longevity effects, and its mechanism relies on the signaling of the SIR-2.1 and the AAK-2 proteins, suggesting its potential as a health-promoting ingredient.

Keywords: Sesamolin; Sesamin; Longevity effects; γ-cyclodextrin; *Caenorhabditis elegans*.

1. Introduction

Sesame (*Sesamum indicum L.*) is one of the earliest oil crops cultivated and consumed by humans within the *Pedaliaceae* family (Wei et al., 2022). In addition to its rich nutritional content, sesame contains various lignans such as sesamin, sesamolin, and sesamol (Pathak et al., 2014; Wei et al., 2022). Sesamolin, therefore, is a lignan present in sesame second only to sesamin in abundance (Wei et al., 2022), and its structure is similar to that of sesamin (Michailidis et al., 2019). Researches have confirmed that sesamolin has several beneficial effects on human health, including neuroprotection, inhibition of lipid peroxidation in the liver and kidneys, suppression of proliferation, and the induction of apoptosis in colorectal cancer cells, regulation of lipid metabolism, inhibition of melanin production, and the enhancement of the NK cell lytic activity (Kushiro et al., 2002; Michailidis et al., 2019; Rosalina and Weerapreeyakul, 2021; Wu et al., 2019). Previous studies have demonstrated the ability of sesamin to extend the lifespan of the *C. elegans* (Nakatani et al., 2018; Yaguchi et al., 2014); however, it is currently unclear as to whether sesamolin possesses the similar longevity effects so as to extend the lifespan and to improve the health in the *C. elegans*.

Although there have been studies investigating the ability of sesamolin to extend the lifespan of the nematodes, they have reached negative conclusions (Kashima et al., 2012). Compounds suitable for testing in the nematode models typically require a water solubility, as the test components must dissolve in the nematode growth medium (NGM) or the Luria Bertani (LB) broth used to spray the testing agent on the top surface of the NGM plates. Previous research has indicated that the liposoluble components

are not miscible with the water-soluble environment of the *C. elegans*' model (Avery and Thomas, 1997). To address this issue, some studies have proposed using the γ-cyclodextrin (γ-CD) to resolve the insolubility of the liposoluble components in a water-soluble environment (Kashima et al., 2012). The γ-CD is a cyclic molecule composed of glucopyranose monomers, featuring a hydrophilic surface and a lipophilic central cavity (Saokham and Loftsson, 2017). It includes the liposoluble components within its central cavity, thereby enhancing the solubility in a water-soluble environment (Echezarreta-Lopez et al., 2002; Uekama et al., 1982; Vianna et al., 1998). Research results have demonstrated that the γ-CD is suitable when used in the model of the *C. elegans* (Kashima et al., 2012). In the two previously mentioned reports exploring the longevity effects and mechanisms of the sesamin, researchers used the γ-CD to include sesamin, which was then applied onto the NGM plates for the *C. elegans* (Nakatani et al., 2018; Yaguchi et al., 2014). Given that sesamolin also exhibits a high liposolubility, it theoretically cannot dissolve in a liquid medium or broth, and be applied in or onto the NGM plates. Therefore, we are interested in the possibility that the lack of the longevity effects observed in the previous studies on sesamolin (Keowkase et al., 2018) may be attributed to the absence usage of the γ-CD as a carrier.

Additionally, past research has proposed that, for the lifespan assay in the *C. elegans*, using dead bacteria as a food source is more suitable so as to avoid the potential effects of the live bacteria on the test substance (Collins et al., 2006; Garigan et al., 2002); for instance, live *E. coli* can be pathogenic to the older nematodes; hence, a substance that reduces the pathogenicity of *E. coli* might extend the lifespan of the *C. elegans*. Furthermore, metabolites produced by the live bacteria could be detrimental to the *C. elegans* (Garigan et al., 2002). Moreover, the test substance itself might undergo metabolic transformations by the live bacteria, influencing the lifespan of the *C. elegans*; this could directly or indirectly influence the nematodes, leading to the distorted research results (Collins et al., 2006; Garigan et al., 2002; Liao et al., 2011). Indeed, the paper reporting the inability of sesamolin to induce the nematode longevity used live bacteria (Keowkase et al., 2018). Therefore, we are also interested in investigating as to whether interference in the results occurred due to the usage of the live bacteria.

In the mechanistic aspect, previous research has revealed that the ability of sesamin to extend the lifespan is lost in the mutants such as the SIR-2.1, AAK-2, and DAF-15 (note: these are all the loss-of-function mutants). This suggests that sesamin can extend the lifespan of the nematodes through the signal pathways related to the calorie restriction, including the SIR-2.1, AAK-2, and DAF-15 (Nakatani et al., 2018). The SIR-2.1, AAK-2, and the DAF-15 correspondingly represent the homologous proteins of the human Sirtuin 1 (SIRT1), AMP-activated protein kinase (AMPK), and the regulatory unit of the mTOR (raptor) in the *C. elegans*. Additionally, sesamin also has been demonstrated to extend the lifespan of the *C. elegans* by modulating the IIS pathway (Yaguchi et al., 2014). However, it remains unclear whether sesamolin can also extend the lifespan of the *C. elegans* through the similar signaling mechanisms.

Therefore, this study aims to investigate as to whether sesamolin, included in the γ-CD, has the ability to extend the lifespan and improve the health in the *C. elegans*. Initially, we prepared pure samples of sesamolin and sesamin using a preparative HPLC. Subsequently, we prepared the γ-CD-sesamolin inclusion complex (γCD-SM) and the γ-CD-sesamin inclusion complex (γCD-SA), and the preparation efficiency of both the inclusion complexes that were then analyzed using the analytical HPLC. We first examined the effects of the sesamin dosage on the lifespan assay to reveal the required dosage and extrapolate the dosage range for the sesamolin experiments. We then explored the effects of different dosages of the sesamolin on the lifespan of the *C. elegans*, and investigated the influence of using live or dead bacteria on the longevity capabilities by the administration with the γCD-SM and the γCD-SA as a positive control. Next, we assessed the effects of sesamolin on the health indexes, including the pharyngeal pumping and body bends. We also investigated the signal pathways using the loss-of-function mutants, including the SIR-2.1, AAK-2, DAF-15, and AKT-1 mutants. The SIR-2.1, AAK-2, and DAF-15 are crucial proteins in the signaling mechanisms of the calorie restriction longevity effects, while the AKT-1 is an important signaling protein in the IIS pathway (Sun et al., 2017). These pathways have been reported to be involved in the mechanisms underlying the effects of the sesamin on extending the lifespan of the *C. elegans*.

2. Materials and methods

2.1. Materials

All chemicals used were of the analytical grade. The NaCl, KCl, NaOH, Na_2HPO_4, and HCl were purchased from Merck (Darmstadt, Germany). Ampicillin sodium salt, fluorodeoxyuridine (FUdR), cholesterol, sodium dodecyl sulfate, and sodium azide were obtained from Sigma (St. Louis, MO, USA). The KH_2PO_4, $MgSO_4$, and $CaCl_2$ were purchased from J.T. Baker® (Phillipsburg, NJ, USA). The American bacteriological agar and yeast extract were obtained from Conda (Madrid, Spain). The vegetable peptone and tryptone were obtained from Fluka (Buchs, Switzerland). The γ-CD was purchased from Tokyo Chemical Industry (Tokyo, Japan). The wild-type *C. elegans* strain N2 was a gift from the *C. elegans* core facility (National Taiwan University, Taiwan). The AAK-2, AKT-1, DAF-15, SIR-2.1 mutants (note: all of these were loss-of-function mutants) obtained from the Caenorhabditis Genetics Center (University of Minnesota, USA). The sesame lignan samples were obtained from the Distinguished Professor Min-Hsiung Lee, Department of Agricultural Chemistry, National Taiwan University.

2.2. The preparation of sesamolin and sesamin samples

The obtained sesame lignan samples (prepared from waste sesame cakes by Professor Lee through processes such as grinding, extraction, and column chromatography) were subjected to purification through the preparative HPLC, as the system consisted of a Waters™ 600 controller and pump, a Reprosil C18 column (30 × 250 mm, 5 μm), a Varian Prostar 704 fraction collector, and a Water™ 486 tunable absorbance detector. The separation was achieved using a mobile phase of 40% methanol with isocratic elution for 150 minutes at a flow rate of 20 mL/min. UV signals were detected at a wavelength of 280 nm. The sample loop volume was 5 mL, and the column temperature was maintained at 25°C. The quality of the prepared sesamolin and sesamin were evaluated by the obtained chromatograms by following the analytic HPLC method.

2.3. Preparation of the γ-CD and sesamolin or sesamin inclusion complexes

According to the previous studies (Nakatani et al., 2018; Yaguchi et al., 2014), a saturated solution of the γ-CD (230 mg/mL) was

prepared and filtered under aseptic conditions so as to obtain a sterile saturated γ-CD solution. Moreover, a sterile solution of sesamolin or sesamin in ethanol (2.5 mg/mL) was prepared. Subsequently, the two solutions were mixed in a 10:1 ratio, stirred using a rotary mixer for 12–24 hours, and then subjected to high-speed centrifugation (4°C, 1,0000 rpm, 20 min) to obtain the solid inclusion complex to be weighed. To evaluate the efficiency of the inclusion, 5 mL of pure water containing a 0.5-mL sterile solution of sesamolin or sesamin in ethanol (equivalent to 3.4 μmol sesamolin or 3.5 μmol sesamin in the solutions, respectively), or the supernatant after the centrifugation of the γ-CD and sesamolin or sesamin mixtures, was subjected to extraction using 5 mL of ethyl acetate (EA) three times. The collected extracts were combined, and 1 mL was evaporated using nitrogen gas. Subsequently, 100 μL of EA was added for the reconstitution, and the concentration of sesamolin or sesamin was analyzed by the HPLC. Five concentrations of purified sesamolin or sesamin were used to establish the calibration curves for the quantifications. The efficiency was determined using the equation: [the total amount of sesamolin or sesamin in the 15-mL EA extracts for the pure water sample] – (the amount of sesamolin or sesamin in the suspension)/[the total amount of sesamolin or sesamin in the 15-mL EA extracts for the pure water sample]*100%. It has been calculated that approximately 1 mg of the solid inclusion complex contains 9.0 μg of sesamolin and 8.9 μg of sesamin.

2.4. Analytical HPLC method

The sesamolin and sesamin were analyzed by using an analytical HPLC system that included a Shimadzu system controller (Osaka, Japan), Shimadzu LC-10AD pump, Athena C18 column (4.6 × 250 mm, 5 μm), and Shimadzu SPD-10A UV-VIS detector. The analysis conditions involved a mobile phase of 60% methanol solution with isocratic elution for 40 minutes at a flow rate of 1 mL/min. UV signals were detected at a wavelength of 280 nm. The sample loop volume was 20 μL, and the column temperature was maintained at 25°C.

2.5. Assay of the lifespan of C. elegans

The nematodes' lifespan was assessed by following the previous methods with slight modifications (Sutphin and Kaeberlein, 2009). Synchronized larvae at the L2-3 stages were gently transferred onto a 5-cm Amp/FUdR plate (30 worms/plate; three plates per treatment, n = 90) with dead bacteria with the γCD-SM or γCD-SA at varying doses of sesamolin or sesamin on the surface, and cultured at 20°C. Plates were replaced every four days, and survival was assessed every two days. Nematodes were considered deceased if unresponsive to a platinum wire touch or lacking pharyngeal pumping. Survival data, along with an average, median, and maximum lifespan values, were analyzed using the SPSS, and the survival percentage was plotted using the Sigma Plot 8.0. As we described in the previous report (Yang et al., 2023), we used the proper concentrations of the γCD-SM or γCD-SA in the LB medium, and spread 200 μL of the corresponding solutions onto the surface NGM. Because the LB medium would dry out after spreading onto the surface of the NGM, thus, the dosage unit of nmol/plate was used rather than the molar concentration of the tested samples. All of the other handling procedures for the *C. elegans* have been described in our previous paper including the NGM plates with the dead bacteria that was prepared by the exposed plates to the UV at two doses of 9,999 × 100 mJ/cm^2 to eliminate bacteria (Yang et al., 2023).

2.6. Assay of the pharyngeal pumping in C. elegans

Pharyngeal pumping was determined as previously described (Iwasa et al., 2010; Zhao et al., 2017). The 10 nematodes for each group were randomly chosen to record the pharyngeal pumping with a charge-coupled device (CCD) video camera under a microscope on the 6th, 8th, 10th, 12th and 14th day of life. The number of pharyngeal beats within 60 seconds was calculated based on the slow-motion playback.

2.7. Assay of the body bends in C. elegans

Body bend was determined by the swimming test as described previously (Iwasa et al., 2010). The 10 nematodes for each group were randomly picked up to determine the body bends on the 10th day of life. After crawling on an NGM plate without the OP50 for 30 seconds to remove the excess E. coli from the worms, each nematode was placed in a well of a 24-well plate containing 1 mL of M9 buffer. The motility of the nematodes was recorded with a CCD video camera under a microscope, and the number of body bends within 30 seconds was calculated based on the slow-motion playback. Body bends were defined as the number of repeated twists at the center point of the nematode.

2.8. The loss-of-function test

One of the powerful advantages of the *C. elegans* model is used for the loss-of-function mutants to reveal the signaling pathway of a certain tested molecule. If a certain function, such as the lifespan-extending effect disappears in a certain loss-of-function mutant, the result indicates that the signaling mechanism of the tested molecule is via the mutated protein. The SIR-2.1, AAK-2, DAF-15, AKT-1 mutants were used for the loss-of function test in this study. With the exception that the wild-type nematodes were replaced with the mutants, all the procedures performed were the same as the above assay of the lifespan, pharyngeal pumping, and the body bend of the *C. elegans*.

2.9. Statistical Analysis

Data were analyzed using the Student's t-test or analysis of variance (ANOVA), followed by the Duncan's test for group mean comparisons using the SPSS v.14.0 software (SPSS, Inc., Chicago, IL, USA). The differences in the lifespan of the nematodes between the groups were analyzed using the Cox regression. The pharyngeal pumping was analyzed using a simple regression analysis method. A difference with a $p < 0.05$ was considered statistically significant.

Results

3.1 Preparation of sesamolin and sesamin samples

Initially, the sesame lignan samples obtained from Prof. Lee were subjected to the HPLC analysis, revealing a composition of approximately 60% sesamolin and 40% sesamin (Figure 1a). Subsequently, a preparative HPLC was employed for further separation and purification of the sesamolin and sesamin, followed by an analytical HPLC to assess the purification results. From the

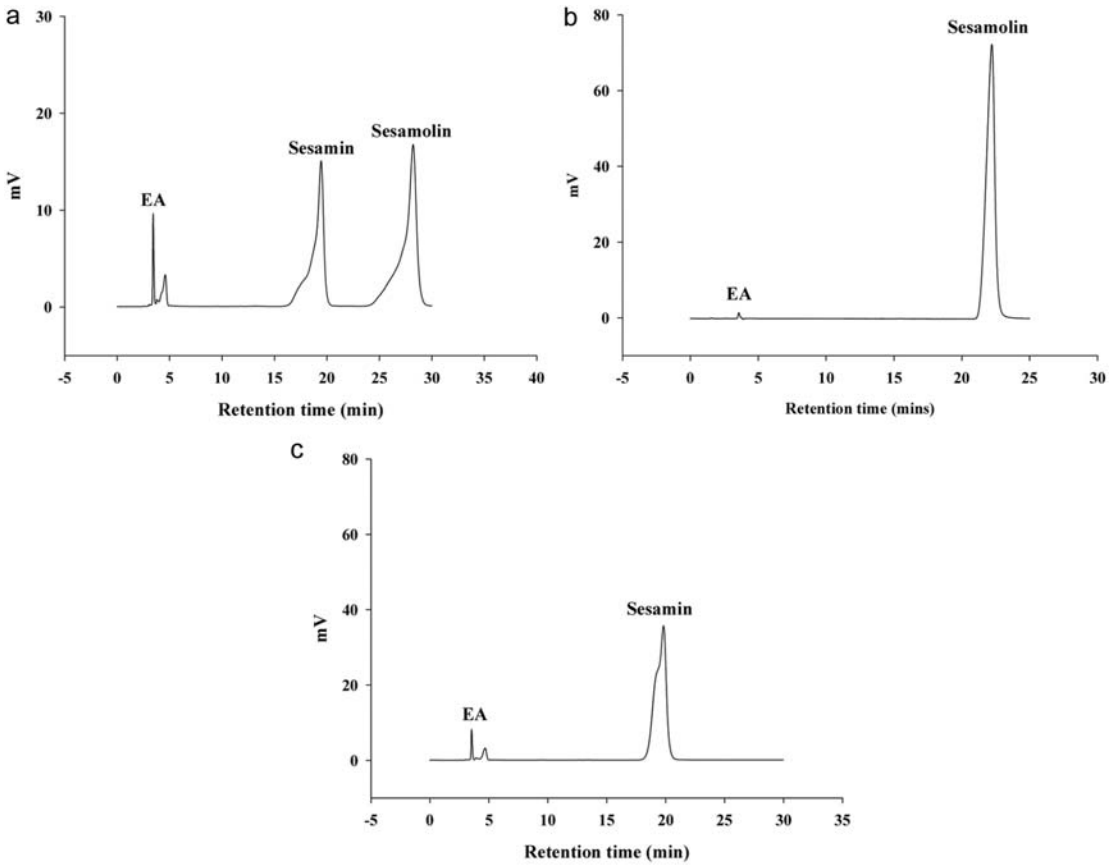

Figure 1. Preparation of sesamolin and sesamin samples. (a) The HPLC chromatogram for the initial obtained sesame lignan samples, which was prepared in ethyl acetate (EA) with a concentration of 0.35 mg/mL in the sample. (b) The HPLC chromatogram of the purified sesamolin sample by using the preparative HPLC, which was prepared in EA with a concentration of 1 mM sesamolin. (c) The HPLC chromatogram of the purified sesamin sample by using the preparative HPLC, which was prepared in EA with a concentration of 1 mM sesamolin.

chromatograms (Figures 1b and c), we confirmed that, aside from the solvent signals, only the signals corresponding to the sesamolin and sesamin were present. This indicates that the purified sesamolin and sesamin samples should be of sufficient quality and purity for use in this study.

3.2. Preparation efficiency of γ-CD and sesamin or sesamin inclusion complex

After confirming the quality of the samples, we utilized the γ-CD for the preparation of the sesamolin or sesamin inclusion complex. Using the analytical HPLC, we evaluated the efficiency of the γ-CD inclusion complexes by comparing the amounts of the sesamolin or sesamin in the EA extracts for the pure water sample or after the high-speed centrifugation. The more lignans included in the γ-CD, the lower the amount of the lignans in the supernatant after the centrifugation. The analysis results indicated that, for the γ-CD including sesamolin, the residual amount of not included lignans is only about 7.2% i.e., the concentration decreased by approximately 92.8% after the high-speed centrifugation (Figures 2a and b; Table 1). Similarly, for the γ-CD including the sesamin, the residual amount of not included lignans is only about 7.4% i.e., the analysis showed a concentration reduction of about 92.6% after the high-speed centrifugation (Figures 2c and d; Table 1). This suggests that, for both sesamolin and sesamin, after the inclusion and the high-speed centrifugation, the preparation efficiency of approximately 93% for both the sesamolin and sesamin in the solid inclusion complexes.

3.3. Effects of sesamolin and sesamin on the lifespan in wild-type C. elegans

Subsequently, we investigated as to whether the sesamolin has the ability to extend the lifespan of the *C. elegans* by the administrated nematodes with the γCD-SM that contained different doses of the sesamolin. The tested doses of the γCD-SM included 4, 16, 64, and 256 nmol/plate sesamolin. The results showed a significant extension of the nematode lifespan in the groups treated with the γCD-SM contained with 64 and 256 nmol/plate of sesamolin, with the mean lifespans extended by 15.7% and 18.7%, respectively (Figure 3b; Table 2). However, as the effects at 64 and 256 nmol/plate of sesamolin approached similarity, it suggests that the 256 nmol/plate of sesamolin is close to the dosage with the highest lifespan extension capacity. Additionally, we selected experimental doses for the γCD-SA based on a previous study reporting the optimal dosage for extending the nematode lifespan with the γCD-SA (Yaguchi et al., 2014). The report indicated that the optimal dosage for sesamin for extending the nematode lifespan was 6.3 μg/plate,

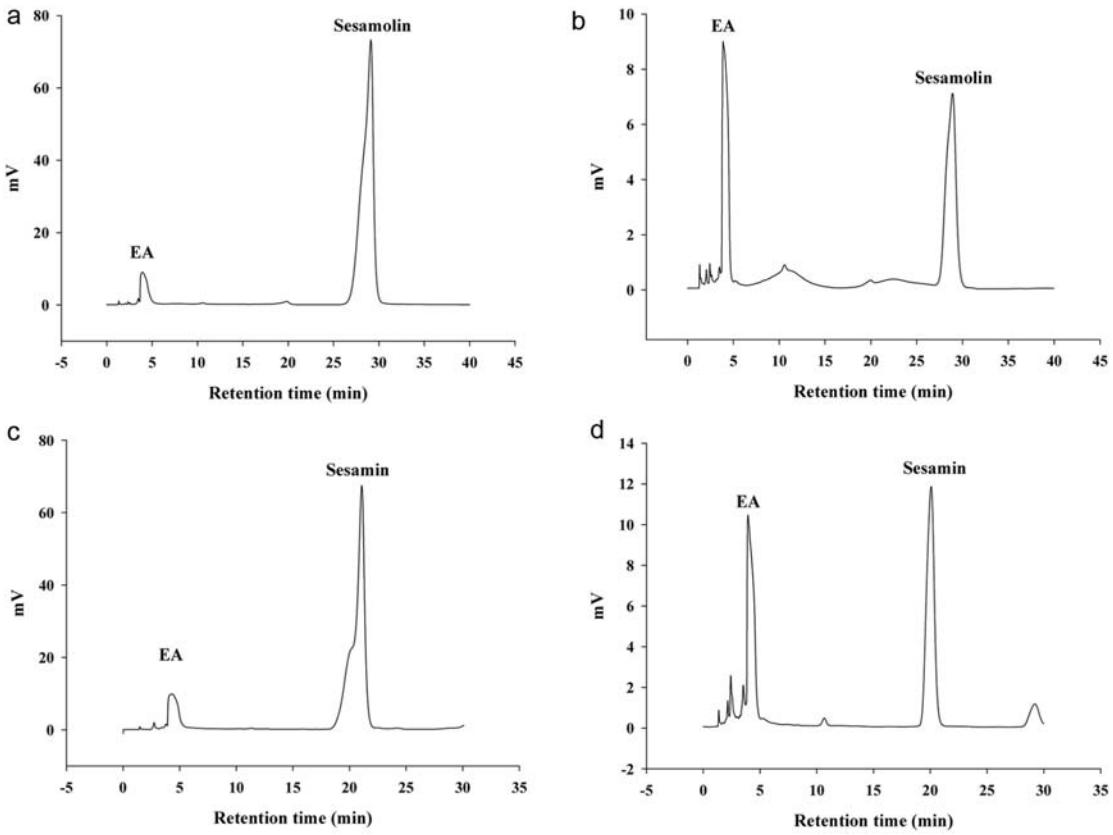

Figure 2. Efficiency evaluation of the preparation of the γ-cyclodextrin (γ-CD) and sesamolin or sesamin inclusion complexes. (a) The HPLC chromatogram of sesamolin in a pure water sample containing the original concentration of sesamolin, which was then extracted by ethyl acetate (EA). The extract (1 mL) was evaporated, reconstituted, and analyzed by HPLC, as described in the Methods. (b) The HPLC chromatogram of sesamolin after mixing with the γ-CD for 12-24 hours, followed by centrifugation and the same procedures as described in the Methods. (c) The original HPLC chromatogram of sesamin, as described in the Methods. (d) The HPLC chromatogram of sesamin after mixing and centrifugation, following the same procedures as described in the Methods.

which, when converted to the units used in this study, equals 16 nmol/plate. Thus, we initially used the γCD-SA contained 4, 16, and 64 nmol/plate of sesamin to perform the lifespan assay, and the results were similar to the previous report, showing that 16 nmol/plate of sesamin was the optimal dosage, extending the average lifespan by 11.5% ($p < 0.05$), while the 64 nmol/plate of sesamin only extended the mean lifespan by 2.6% ($p > 0.05$) (Figure 3a; Table 2). Therefore, for the subsequent study, we chose the γCD-SA contained with 16 nmol/plate of sesamin as the dosage for the positive control, and the γCD-SM were set at the dosages contained with 4, 16, 64, and 256 nmol/plate of sesamolin. When combining the results of these two lifespan assays, it demonstrates that sesamolin has a broader effective dosage range compared to sesamin, and the optimal dosage of sesamolin for extending the nematode lifespan is approximately 1.6 times higher than the optimal dosage for sesamin.

3.4. Effect of sesamolin and sesamin on the lifespan of wild-type C. elegans under dead or live bacterial culture

In previous studies on the lifespan assay of sesamolin, the cultivation was carried out using live bacteria (Keowkase et al., 2018). Whether this could potentially be a reason for the previous inabil-

Table 1. Analysis of the preparation efficiency of the γ-CD and sesamolin or sesamin inclusion complexes

	Samples	Lignan concentration in 100 µL EA, the reconstitutions (mM)	Lignan content in the EA extracts (%)[#]
Sesamolin	Original	2.22 ± 0.12	100 ± 5.55
	After centrifugation	0.16 ± 0.01	7.2 ± 0.51
Sesamin	Original	2.04 ± 0.11	100 ± 5.30
	After centrifugation	0.15 ± 0.02	7.4 ± 1.14

[#]The total amount of sesamolin or sesamin extracted by three rounds of 5 mL ethyl acetate (EA), expressed as a percentage, and the lignan content in the EA extracts after centrifugation, compared to the original.

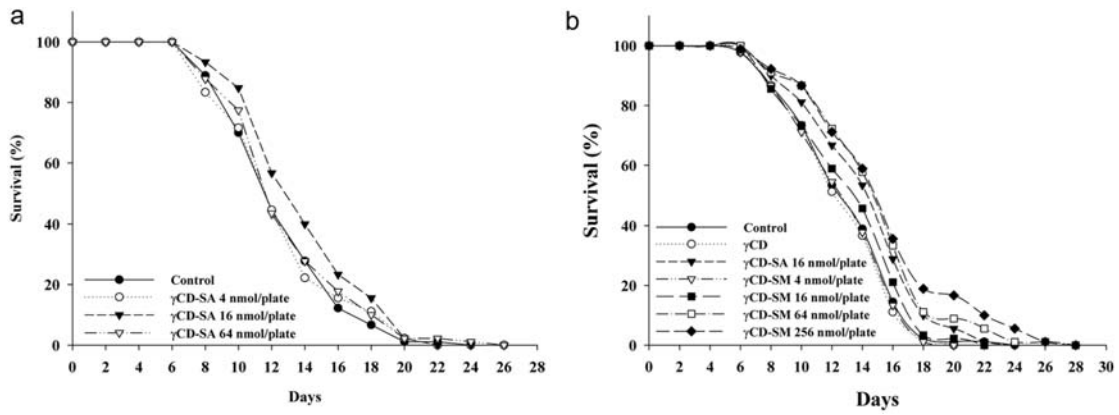

Figure 3. Effects of sesamolin and sesamin on the lifespan of the wild-type *C. elegans***.** The γ-CD and sesamolin or sesamin inclusion complexes (i.e., γCD-SM and γCD-SA) were prepared and the lifespan assay were conducted with (a) the γCD-SM contained the doses of sesamolin from 0, 4, 16, 64 nmol/plate, or (b) the γCD-SA contained the doses of sesamolin from 0, 4, 16, 64 to 256 nmol/plate. The method for the lifespan assay performed as described in Methods (n = 90).

ity of sesamolin to extend the lifespan of the *C. elegans*. Therefore, we further compared whether the γCD-SM and γCD-SA could also extend the lifespan of the *C. elegans* under live and dead bacterial culture conditions. Three independent lifespan assays were carried out for each of the bacterial culture conditions, and the resulting mean lifespans were subjected to a statistical analysis to assess the percentage increase in the mean lifespan. The results showed that, whether it was sesamolin or sesamin, there was no significant difference in the ability to extend the lifespan of the *C. elegans* under live or dead bacterial culture conditions (Figure 4; Figure S1).

3.5. Effect of sesamolin on the health indexes of wild-type C. elegans

Furthermore, we investigated whether the sesamolin has the ability to improve the health indexes in the *C. elegans*, including the pharyngeal pumping and body bends. Experiments were conducted using the most efficacious dosage of the γCD-SM, which contained a 256 nmol/plate of sesamolin. The results indicated that, compared to the control group, the γCD-SM significantly increased the frequency of the pharyngeal pumping and body bends in the *C. elegans* (Figure 5a, b). Taken together, these results demonstrated the ability of sesamolin to improve the health of the *C. elegans*.

3.6. Evaluation whether the longevity function of sesamolin disappears in the SIR-2.1, AAK-2, DAF-15, and AKT-1 mutants

We aimed to reveal the signaling pathways for sesamolin to extend the lifespan of the *C. elegans*. The mutants including the SIR-2.1, AAK-2, DAF-15 and AKT-1 were used for the loss-of function

Table 2. Effects of sesamin and sesamolin on the lifespan of wild-type *C. elegans*.

	Mean lifespan (Day)	Median lifespan (Day)	Maximum lifespan (Day)	*P* value##
Sesamin				
Control	13.0 ± 3.4	12	24	
γCD-SA 4 nmol/plate#	13.0 ± 3.7	12	22	0.896
γCD-SA 16 nmol/plate	14.7 ± 3.7	14	22	0.022*
γCD-SA 64 nmol/plate	13.8 ± 3.3	12	26	0.278
Sesamolin				
Control	13.4 ± 3.5	14	24	
γCD	13.2 ± 3.3	14	20	0.636
γCD-SA 16 nmol/plate	14.7 ± 3.8	16	24	0.043*
γCD-SM 4 nmol/plate	13.2 ± 3.4	14	20	0.764
γCD-SM 16 nmol/plate	13.8 ± 3.7	14	22	0.444
γCD-SM 64 nmol/plate	15.4 ± 4.1	16	28	0.003*
γCD-SM 256 nmol/plate	15.9 ± 4.8	16	28	<0.001*

#Sesamolin or sesamin was included in the γ-clodextrin to prepare the γCD-SM or γCD-SA. In the table, the γCD-SA 4 nmol/plate means that the inclusion complex contained 4 nmol of sesamin, and administrated for the *C. elegans,* vis versa. ##*P* values were obtained when compared to the control group by the Cox regression model. Values of the mean lifespan (n = 90 for each group) are expressed as mean ± SD.

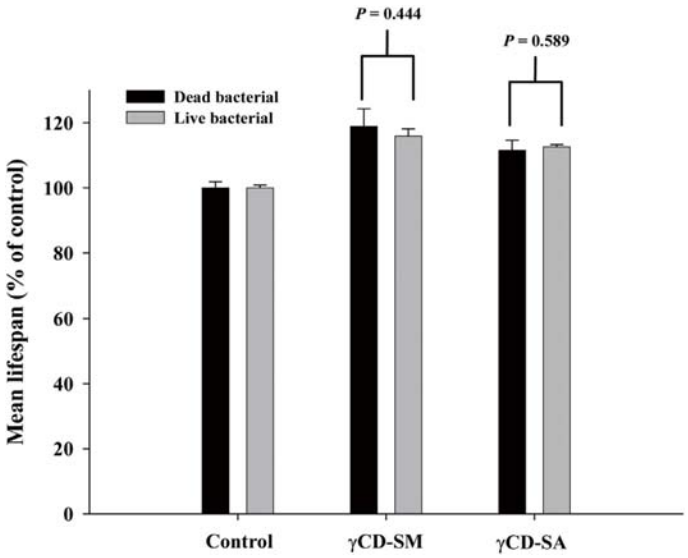

Figure 4. Effects of sesamolin and sesamin on the lifespan of the wild-type *C. elegans* under the dead bacterial or live bacterial culture. The γ-CD and sesamolin or sesamin inclusion complexes (i.e., γCD-SM and γCD-SA) were prepared. The obtained mean lifespan presented as a percentage increase in the mean lifespan as compared to the control from the lifespan assay under the dead bacterial and live bacterial culture. The data are from three independent lifespan assays, with n = 90 in each group. P values are indicated in the figures.

test. The results revealed that the longevity-extending and health-improving capabilities of the γCD-SM disappeared in the SIR-2.1 and the AAK-2 mutants (Figures 6a, b; Table S1). However, the longevity-extending and health-improving capabilities of the γCD-SM were still observed in the DAF-15 mutant (Figure 6c; Table S1) and in the AKT-1 mutant (Figure 6d; Table S1). Since the longevity effects of sesamolin do not depend on the AKT-1 in the IIS pathway and the downstream protein DAF-15, mutually confirming that the IIS pathway was not involved in the mechanism of the sesamolin's longevity effects. In summary, the longevity effects of sesamolin required the signaling mechanisms of the SIR-2.1 and AAK-2.

4. Discussion

The amount of sesamin and sesamolin in the sesame seeds is 200–500 mg/100 g and 200–300 mg/100 g, respectively (Hadipour et al., 2023). Previous studies have confirmed the longevity-enhancing ability of the sesamin. However, the sesamolin, structurally similar to the sesamin, does not exhibit a lifespan-extending effect in the *C. elegans*. Therefore, this study aims to explore as to whether the previous experiments did not use the γ-CD to include the sesamolin so as to increase the solubility in the medium or broth. The results indicate that the γCD-SM has a longevity effect in the *C. elegans*, significantly extending the lifespan of the *C. elegans*, with 256 nmol/plate of sesamolin showing the highest efficacy. The γCD-SM also significantly improves the health indexes, including the pharyngeal pumping and body bends. Furthermore, we found that whether using live or dead bacteria, there is no significant difference in the lifespan-extending effects of the γCD-SM or γCD-SA, indicating that the bacterial does not significantly interfere with the results. Additionally, through the loss-of-function tests with the mutants, we further explored the possible pathways

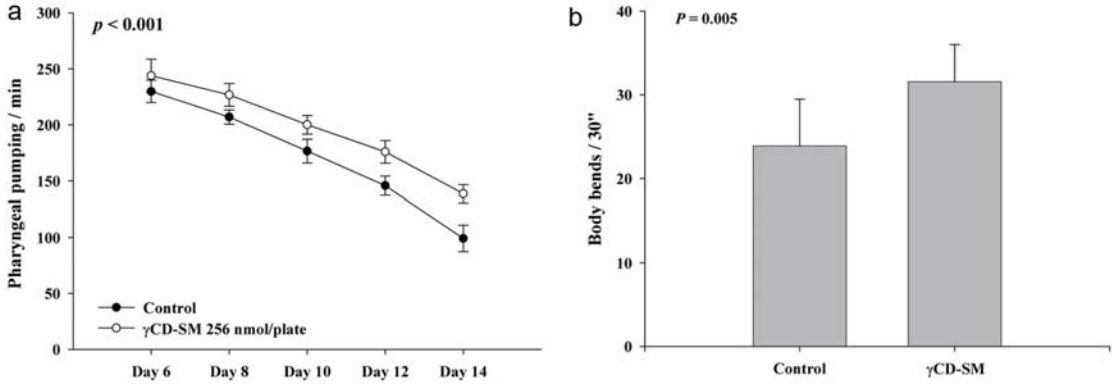

Figure 5. Effects of sesamolin on the health indexes of the wild-type *C. elegans*. For health indexes analysis, the nematodes were grown on plates containing with or without 256 nmol/plate of sesamolin administrated by the prepared γCD-SM. (a) The pharyngeal pumping and (b) the body bends were determined (n = 10) as described in Methods. P values are as shown in the figures.

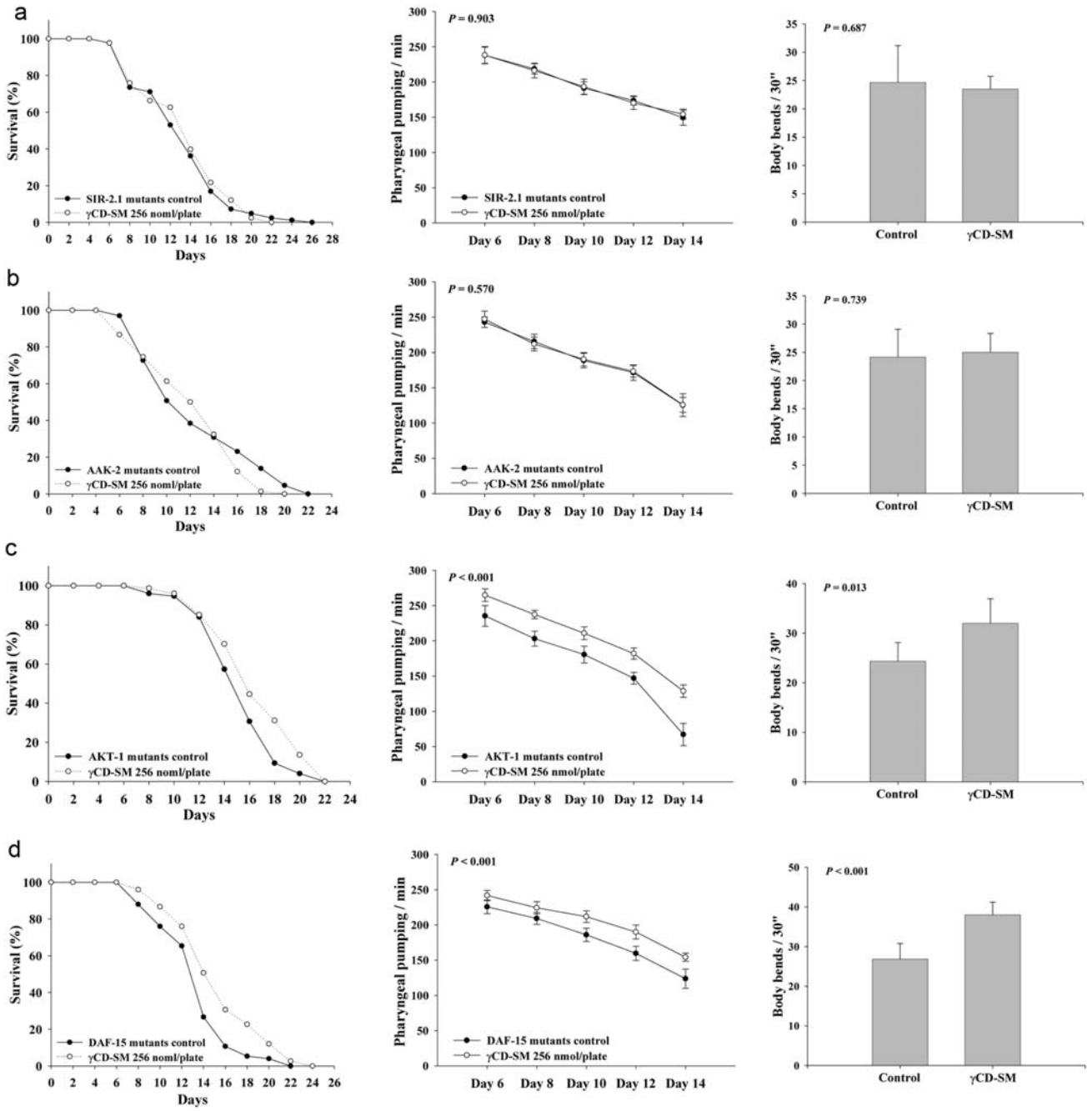

Figure 6. Effects of the sesamolin on the lifespan and health indexes of the SIR-2.1, AAK-2, AKT-1 and DAF-15 mutants. For the loss-of-function tests in the lifespan assay, the (a) SIR-2.1, (b) AAK-2, (c)AKT-1, and (d) DAF-15 mutants were grown on plates with or without 256 nmol/plate of sesamolin administrated by the prepared γCD-SM (n = 90) as described in Methods. For the loss-of-function tests in the health indexes analysis, the nematodes were grown on plates containing with or without 256 nmol/plate of sesamolin administrated by the prepared γCD-SM. The pharyngeal pumping and the body bends were determined (n = 10) as described in Methods. P values are as shown in the figures.

for the longevity effect of the sesamolin. The results showed that under supplementation with the γCD-M, the ability of the sesamolin to extend the lifespan and improve the health indicators disappears in the SIR-2.1 and AAK-2 mutants. This suggests that the longevity effect of the sesamolin in the *C. elegans* relies on the signaling pathways of the SIR-2.1 and AAK-2. To the best of our knowledge, this study is the first to demonstrate that sesamolin, a lignan in sesame, has the potential to extend the lifespan and improve the health indexes, suggesting its potential as a health-promoting substance for slowing the aging process.

Previous studies have shown that under the conditions of the inclusion of sesamin with the γ-CD and culturing nematodes with

live *E. coli* OP50, there is a significant extension of the lifespan of the *C. elegans* (Yaguchi et al., 2014). However, past research has indicated that in the lifespan experiments, using dead bacteria as a food source is more appropriate so as to avoid interference with the test substance, being mainly due to the effects of the live bacteria, either directly or indirectly affecting the nematodes (Collins et al., 2006; Garigan et al., 2002; Liao et al., 2011). Nevertheless, the results of this study demonstrate that using live or dead bacteria does not affect the ability of sesamin to extend the lifespan of the *C. elegans*. Additionally, previous research showed that sesamolin, when cultured with nematodes without the γ-CD inclusion and live *E. coli* OP50, did not significantly extend the lifespan of the *C. elegans* (Keowkase et al., 2018). This study also confirms that using live or dead bacteria as a food source has little impact on the ability of sesamolin to extend the lifespan of the *C. elegans*. However, the results indicated that the primary alteration in this study, using the γ-CD to include sesamolin, is sufficient to demonstrate the longevity effect of the sesamolin. This highlights the critical step of ensuring the solubility of the lipophilic components, such as sesamolin, in aqueous solutions. Although the effect of applying live or dead bacteria on the lifespan extension of sesamin and sesamolin is not significant, it is still recommended to use dead bacteria when evaluating other nutrients using the model of the *C. elegans*.

However, previous studies have demonstrated that the mechanism underlying the lifespan extension by sesamin relies on the IIS signaling and proteins such as the SIR-2.1, AAK-2, and DAF-15. It has also been shown that sesamin's ability to extend the lifespan of the *C. elegans* disappears under the conditions of caloric restriction (Vianna et al.), suggesting sesamin's potential as a CR mimetic. The CR involves reducing the calorie intake by approximately 25–30% without depriving the essential nutrients (Pignatti et al., 2020) and has been demonstrated to extend the healthspan and the lifespan in rodent and primate models (Acosta-Rodriguez et al., 2022; Mattison et al., 2017). The CR generally achieves its effects by (1) downregulating the IIS pathway, (2) reducing the mTOR signaling, (3) activating the sirtuin 1 pathway, and (4) modulating the AMPK pathway (Green et al., 2022). Increasing evidence indicates that the mTOR is a downstream molecule in the IIS pathway (Testa et al., 2014). Thus, the downregulation of the IIS pathway and the reduction of mTOR signaling under the CR likely represents the coordinated effects within the same signaling pathway. In this study, we found that the sesamolin's longevity effect on the nematodes relies on the assistance of the SIR-2.1 and AAK-2, indicating that the sesamolin may achieve its longevity effect through the SIR-2.1 and AAK-2 pathways. However, unlike sesamin, sesamolin's mechanism does not depend on the IIS pathway or its downstream TOR protein, suggesting that sesamolin may not completely act in the same manner as sesamin. Interestingly, the results of this study indicate that sesamolin's longevity effect seems to be superior to sesamin. For instance, the optimal dosage of sesamolin can extend the nematode lifespan by approximately 18.7% under conditions of dead bacteria cultivation, while the optimal dosage of sesamin only extends the nematode lifespan by 11.5%. Furthermore, this study also demonstrates that sesamolin has a broader effective dosage range when compared to sesamin. Therefore, the health-promoting longevity effect of sesamolin appears to be better than that of sesamin. This suggests that the longevity effect of the sesame extract may at least be the sum of the effects of various lignans, including sesamin and sesamolin. Future research will further evaluate the longevity effects of the sesame extract, including assessing the effects of other sesame lignans and the potential synergistic effects of the different lignans.

5. Conclusion

In conclusion, this study confirms that sesamolin, when included in the γ-cyclodextrin, possesses the ability to extend the lifespan and improve the health in the *C. elegans*, demonstrating the longevity effect of sesamolin. Moreover, sesamolin's capacity to extend the lifespan of the *C. elegans* appears to be more significant than that of the sesamin, and it exhibits a broader effective dosage range as compared to sesamin. Mechanistically, sesamolin's longevity effect on the *C. elegans* relies on the signaling mechanisms of the SIR-2.1 and AAK-2. However, the usage of live or dead bacteria as a food source does not significantly affect the ability of the sesamolin and sesamin to extend the lifespan of the *C. elegans*. In summary, sesamolin shows potential for development as a functional ingredient for the longevity.

Acknowledgments

This work was supported by grants from the National Science Foundation (MOST 109-2813-C-040-022-B), Taiwan. We thank distinguished professor Min-Hsiung Lee from the Department of Agricultural Chemistry, National Taiwan University for the gift of sesame lignan samples. The AAK-2, SIR-2.1, DAF-15 and AKT-1 mutants were provided by the Caenorhabditis Genetics Center (CGC), which is funded by the National Institutes of Health (NIH) Office of Research Infrastructure Programs (P40OD010440). The *C. elegans* strain N2 was a gift from the *C. elegans* core facility of Taiwan (National Tsing Hua University, Taiwan).

Conflict of interest

The authors declare no conflict of interest.

Author contributions

Conceptualization, N.C.Y.; methodology, N.C.Y. and C.Y.C.; formal analysis, N.C.Y., C.Y.C. and P.J.L.; investigation, N.C.Y., C.Y.C. and P.J.L.; resources, N.C.Y.; writing—original draft preparation, N.C.Y., C.Y.C. and P.J.L.; writing—review and editing, N.C.Y.; supervision, N.C.Y.; funding acquisition, N.C.Y. All authors have read and agreed to the published version of the manuscript.

Supplementary material

Figure S1. Effects of sesamolin and sesamin on the lifespan of wild-type *C. elegans* under dead bacterial or live bacterial culture.

Table S1. Effects of sesamolin on the lifespan of mutants.

References

Acosta-Rodriguez, V., Rijo-Ferreira, F., Izumo, M., Xu, P., Wight-Carter, M., Green, C.B., and Takahashi, J.S. (2022). Circadian alignment of early onset caloric restriction promotes longevity in male C57BL/6J mice. Science 376(6598): 1192–1202.

Avery, L., and Thomas, J.H. (1997). Feeding and Defecation. In: Riddle, D.L., Blumenthal, T., Meyer, B.J., and Priess, J.R. (Ed.). C. elegans II (2nd

ed).
Collins, J.J., Evason, K., and Kornfeld, K. (2006). Pharmacology of delayed aging and extended lifespan of Caenorhabditis elegans. Exp. Gerontol. 41(10): 1032–1039.
Echezarreta-Lopez, M.M., Perdomo-Lopez, I., Estrada, E., Vila-Jato, J.L., and Torres-Labandeira, J.J. (2002). Utility of nuclear magnetic resonance spectroscopy to characterize the structure of dexamethasone sodium phosphate inclusion complexes with cyclodextrins in solution and to analyze potential competitive effects. J. Pharm. Sci. 91(6): 1536–1547.
Garigan, D., Hsu, A.L., Fraser, A.G., Kamath, R.S., Ahringer, J., and Kenyon, C. (2002). Genetic analysis of tissue aging in Caenorhabditis elegans: a role for heat-shock factor and bacterial proliferation. Genetics 161(3): 1101–1112.
Green, C.L., Lamming, D.W., and Fontana, L. (2022). Molecular mechanisms of dietary restriction promoting health and longevity. Nat. Rev. Mol. Cell. Biol. 23(1): 56–73.
Hadipour, E., Emami, S.A., Tayarani-Najaran, N., and Tayarani-Najaran, Z. (2023). Effects of sesame (Sesamum indicum L.) and bioactive compounds (sesamin and sesamolin) on inflammation and atherosclerosis: A review. Food Sci. Nutr. 11(7): 3729–3757.
Iwasa, H., Yu, S., Xue, J., and Driscoll, M. (2010). Novel EGF pathway regulators modulate C. elegans healthspan and lifespan via EGF receptor, PLC-gamma, and IP3R activation. Aging Cell 9(4): 490–505.
Kashima, N., Fujikura, Y., Komura, T., Fujiwara, S., Sakamoto, M., Terao, K., and Nishikawa, Y. (2012). Development of a method for oral administration of hydrophobic substances to Caenorhabditis elegans: pro-longevity effects of oral supplementation with lipid-soluble antioxidants. Biogerontology 13(3): 337–344.
Keowkase, R., Shoomarom, N., Bunargin, W., Sitthithaworn, W., and Weerapreeyakul, N. (2018). Sesamin and sesamolin reduce amyloid-beta toxicity in a transgenic Caenorhabditis elegans. Biomed. Pharmacother. 107: 656–664.
Kushiro, M., Masaoka, T., Hageshita, S., Takahashi, Y., Ide, T., and Sugano, M. (2002). Comparative effect of sesamin and episesamin on the activity and gene expression of enzymes in fatty acid oxidation and synthesis in rat liver. J. Nutr. Biochem. 13(5): 289–295.
Liao, V.H., Yu, C.W., Chu, Y.J., Li, W.H., Hsieh, Y.C., and Wang, T.T. (2011). Curcumin-mediated lifespan extension in Caenorhabditis elegans. Mech. Ageing Dev. 132(10): 480–487.
Mattison, J.A., Colman, R.J., Beasley, T.M., Allison, D.B., Kemnitz, J.W., Roth, G.S., Ingram, D.K., Weindruch, R., de Cabo, R., and Anderson, R.M. (2017). Caloric restriction improves health and survival of rhesus monkeys. Nat. Commun. 8: 14063.
Michailidis, D., Angelis, A., Aligiannis, N., Mitakou, S., and Skaltsounis, L. (2019). Recovery of Sesamin, Sesamolin, and Minor Lignans From Sesame Oil Using Solid Support-Free Liquid-Liquid Extraction and Chromatography Techniques and Evaluation of Their Enzymatic Inhibition Properties. Front. Pharmacol. 10: 723.
Nakatani, Y., Yaguchi, Y., Komura, T., Nakadai, M., Terao, K., Kage-Nakadai, E., and Nishikawa, Y. (2018). Sesamin extends lifespan through pathways related to dietary restriction in Caenorhabditis elegans. Eur. J. Nutr. 57(3): 1137–1146.
Pathak, N., Rai, A.K., Kumari, R., and Bhat, K.V. (2014). Value addition in sesame: A perspective on bioactive components for enhancing utility and profitability. Pharmacogn. Rev. 8(16): 147–155.
Pignatti, C., D'Adamo, S., Stefanelli, C., Flamigni, F., and Cetrullo, S. (2020). Nutrients and Pathways that Regulate Health Span and Life Span. Geriatrics (Basel) 5(4): 95.
Rosalina, R., and Weerapreeyakul, N. (2021). An Insight into Sesamolin: Physicochemical Properties, Pharmacological Activities, and Future Research Prospects. Molecules 26(19): 5849.
Saokham, P., and Loftsson, T. (2017). gamma-Cyclodextrin. Int. J. Pharm. 516(1-2): 278–292.
Sun, X., Chen, W.D., and Wang, Y.D. (2017). DAF-16/FOXO Transcription Factor in Aging and Longevity. Front. Pharmacol. 8: 548.
Sutphin, G.L., and Kaeberlein, M. (2009). Measuring Caenorhabditis elegans life span on solid media. J. Vis. Exp. (27): 1152.
Testa, G., Biasi, F., Poli, G., and Chiarpotto, E. (2014). Calorie restriction and dietary restriction mimetics: a strategy for improving healthy aging and longevity. Curr. Pharm. Des. 20(18): 2950–2977.
Uekama, K., Fujinaga, T., Hirayama, F., Otagiri, M., and Yamasaki, M. (1982). Inclusi on complexations of steroid hormones with cyclodextrins in water and in solid phase. Int. J. Pharm 10(1): 1–15.
Vianna, R.F., Bentley, M.V.L., Ribeiro, G., Carvalho, F.S., Neto, A.F., de Oliveira, D.C., and Collett, J.H. (1998). Formation of cyclodextrin inclusion complexes with corticosteroids: their characterization and stability. Int. J. Pharm 167(1-2): 205–213.
Wei, P., Zhao, F., Wang, Z., Wang, Q., Chai, X., Hou, G., and Meng, Q. (2022). Sesame (*Sesamum indicum* L.): A Comprehensive Review of Nutritional Value, Phytochemical Composition, Health Benefits, Development of Food, and Industrial Applications. Nutrients 14(19): 4079.
Wu, D., Wang, X.P., and Zhang, W. (2019). Sesamolin exerts anti-proliferative and apoptotic effect on human colorectal cancer cells via inhibition of JAK2/STAT3 signaling pathway. Cell. Mol. Biol. (Noisy-le-grand) 65(6): 96–100.
Yaguchi, Y., Komura, T., Kashima, N., Tamura, M., Kage-Nakadai, E., Saeki, S., Terao, K., and Nishikawa, Y. (2014). Influence of oral supplementation with sesamin on longevity of Caenorhabditis elegans and the host defense. Eur. J. Nutr. 53(8): 1659–1668.
Yang, N.C., Chin, C.Y., Zheng, Y.X., and Lee, I. (2023). The Attenuation of Insulin/IGF-1 Signaling Pathway Plays a Crucial Role in the Myo-Inositol-Alleviated Aging in *Caenorhabditis elegans*. Int. J. Mol. Sci. 24(7): 6194.
Zhao, Y., Gilliat, A.F., Ziehm, M., Turmaine, M., Wang, H., Ezcurra, M., Yang, C., Phillips, G., McBay, D., Zhang, W.B., Partridge, L., Pincus, Z., and Gems, D. (2017). Two forms of death in ageing Caenorhabditis elegans. Nat. Commun. 8: 15458.

Journal of Food Bioactives
International Society for Nutraceuticals and Functional Foods
Original Research
J. Food Bioact. 2024;25:52–61

Fuji apple (*Malus domestica* Borkh. cv. Red Fuji) pomace extracts as a source of antimicrobial and antioxidant polyphenols

Jiankang Wang*, Zhengchun Liu, Lina Wei, Changyan Shao, Jing Wang, Yanan Zhu* and Yujiao Sun

School of Food Science and Engineering, Shaanxi University of Science & Technology, Xi'an 710021, China
*Corresponding author: Jiankang Wang and Yanan Zhu, School of Food Science and Engineering, Shaanxi University of Science & Technology, Xi'an 710021, China. E-mail: rjiankangwang@outlook.com (JW), yanan.zhu@sust.edu.cn (YZ)
DOI: 10.31665/JFB.2024.18371
Received: January 29, 2024; **Revised received & accepted:** February 27, 2024
Citation: Wang, J., Liu, Z., Wei, L., Shao, C., Wang, J., Zhu, Y., and Sun, Y. (2024). Fuji apple (*Malus domestica* Borkh. cv. Red Fuji) pomace extracts as a source of antimicrobial and antioxidant polyphenols. J. Food Bioact. 25: 52–61.

Abstract

This study aimed to assess the antibacterial and antioxidant properties of both crude polyphenol extract (CPE) and purified polyphenol extract (PPE) obtained from Fuji apple pomace. The antibacterial capacity of both extracts against *Staphylococcus aureus* was investigated by evaluating the inhibition zones, minimum bactericidal concentrations (MBC), growth curves and bacterial morphology of *S. aureus* treated with CPE or PPE, as well as the performance in simulated food systems. The antioxidant activity of CPE or PPE was assessed using the ABTS radical scavenging and ferric reducing antioxidant power (FRAP) assays. The results showed that PPE exhibited potent antibacterial activity against *S. aureus*, which was further confirmed by the bacterial morphology. It was revealed that PPE only exerted strong antibacterial effect in starch-based food system while CEP did not show such effect in all systems. The results of the ABTS and FRAP assays indicated that both PPE and CPE possess strong antioxidant activity, from which PPE showed much higher capacity than that of CPE. Therefore, PPE from Fuji apple pomace can be used as a novel antibacterial agent for food preservation and natural antioxidant for functional food and nutraceutical products.

Keywords: Fuji apple pomace; Crude polyphenol extract; Purified polyphenol extract; Antibacterial activity; *Staphylococcus aureus*; Antioxidant activity.

1. Introduction

There has been a growing awareness about harmful effects of chemical preservatives in food, which has led to an increase in research on extracts from natural botanical sources, especially those possessing the antimicrobial and antioxidant properties (Shahidi and Santhiravel, 2022; Gupta and Yadav, 2021). Polyphenols have been known for their abundant sources and antibacterial effects, which primarily exert such effects by modifying the permeability of cell membrane, disrupting cell wall rigidity and integrity, and inhibiting the synthesis of biomolecules in bacterial cells (Bouarab Chibane et al., 2019; Fei et al., 2018). Moreover, their hydroxyl structure renders antioxidant properties, which was mainly achieved by scavenging radicals and chelating redox-active metals (Fraga, 2007). Apple is one of the most broadly distributed and consumed fruit all over the world (Gulzar, 2023). Apple polyphenols, which are secondary metabolites in apples, are a collective term for the polyphenolic compounds found in different parts of the fruit, primarily including phenolic acid derivatives and flavonoids. They have been reported to have various physiological functions, such as the prevention of cancer, diabetes, liver dysfunction and hypertension (Wang et al., 2023; Clemens and Shahidi, 2022). Apple pomace, a by-product from apple processing, is a rich source of high value-added bioactive compounds such as polyphenols. Millions of tons of apples are processed to produce apple cider, juices, or concentrates every year worldwide, which

yield huge amounts of pomace (Fernandes et al., 2019), and apple pomace can be used for the extraction of polyphenols. Therefore, a complete understanding of functions of polyphenol extracts obtained from apple pomace can enhance the utilization of by-products from apple processing.

Staphylococcus aureus, a gram-positive bacterium, is among the prevalent foodborne pathogens. Chambers (2001) reported that only about 20□30 % of the global population has never been a carrier of *S. aureus*, while about 20 % are persistent carriers. *S. aureus* is highly pathogenic, which can cause a spectrum of infections on the skin and soft tissues (Chmielowiec-Korzeniowska et al., 2020). The heat and salt resistance of *S. aureus* facilitate its growth and multiplication in food products (Yehia et al., 2020), and it affects human body mainly by secreting staphylococcal enterotoxins, causing pathological reactions such as vomiting, diarrhea and cramps in the host (Wattinger et al., 2012). The serious threat posed by *S. aureus* to human health necessitates the identification of effective and safe strategies for inhibiting its reproduction in food. The antibacterial effect of *Golden Delicious* apple pomace polyphenols on *Escherichia coli* was evaluated using the diameter of inhibition zone and the minimum inhibitory concentration as the indexes, confirming its robust antibacterial activity (Zhang et al., 2016). Thus, it is important to extend the evaluation of the inhibitory effect of apple polyphenol to other commonly found foodborne bacteria, such as *S. aureus*. Antioxidant capacity of polyphenols can be evaluated using a variety of methods, from which the most used ones are free radical scavenging and ferric reducing power (FRAP) assays (Bai et al., 2013). The antioxidant capacities measured by ABTS assay are strongly correlated with the phenolics and flavonoids from antioxidant-rich foods, and ABTS assay is superior to other free radical scavenging assays when used on a range of plant foods (Floegel et al., 2011). Therefore, ABTS radical scavenging assay is suitable for evaluating the antioxidant activity of polyphenol extracts from apple pomace. The FRAP assay has demonstrated features of high reproducibility and easy operation, and thus it is widely used to understand the antioxidant capacity of polyphenol extracts (Thaipong et al., 2006).

In this study, crude polyphenol extract (CPE) and purified polyphenol extract (PPE) derived from Fuji apple (*Malus domestica* Borkh. cv. Red Fuji) pomace were selected to evaluate their bactericidal and antioxidant activities in various systems, respectively. Antibacterial effects of these polyphenol extracts were assessed by investigating the inhibition zones, minimum bactericidal concentrations (MBC), growth curves and bacterial morphology of *S. aureus* treated with CPE or PPE, as well as the bacteriostatic activity of both two extracts in simulated food matrices. The antioxidant activities of CPE or PPE were assessed according to their ferric reduction capacity using the FRAP method.

2. Materials and methods

2.1. Reagents and materials

Crude polyphenol extract (CPE) and purified polyphenol extract (PPE) from Fuji apple (*Malus domestica* Borkh. cv. Red Fuji) pomace were prepared in our laboratory. *Staphylococcus aureus* 25923 were purchased from ATCC. Phosphate buffered saline (1×, pH 7.4), acetic acid buffer (pH 3.6), 2,2′-azino-bis (3-ethylbenzothiazoline-6-sulfonic acid) (ABTS), 2,4,6-tris-(2-pyridyl)-*s*-triazine (TPTZ), ethanol (ACS grade), $K_2S_2O_8$ (AR grade), NaOH (AR grade), NaCl (AR grade), HCl (AR grade), $FeCl_3$ (AR grade), $FeSO_4$ (AR grade), L-ascorbic acid (AR grade), and Tween-80 (CR grade) was purchased from Merck (Shanghai, China). Isoamyl acetate (AR grade) was purchased from FUCHEN (Tianjin, China). Other reagents were purchased from OXOID (UK) unless otherwise specified.

2.2. Antibacterial activity determination

2.2.1. Preparation of bacterial strains inoculum

S. aureus was cultured for 40 h in tryptone soya broth (TSB) at 37°C accompanying a passage at the 24 h. The cultured bacteria were centrifuged at 1,700 r/min for 5 min and the supernatant was removed. The bacterial pellet was re-suspended in PBS buffer at an optical density (OD) at 600 nm of 1 followed by twice dilutions to get a final concentration of 6 log CFU/mL.

2.2.2. Inhibition zones measurement

The growth inhibition of *S. aureus* by CPE or PPE was determined using a modified agar diffusion method by measuring the diameters of inhibition zones (Singh et al., 2005). The assay involved coating 100 μL of the bacterial suspension uniformly on the surface of Luria-Bertani (LB) agar plates followed by attaching four sterile filter papers with a diameter of 6 mm. Ten μL of PBS buffer containing PPE (100 mg/mL) or CPE (100 mg/mL) was added onto each of three filter papers. In the negative control, the PBS buffer without PPE or CPE was added to the remaining filter paper. All tests were performed in triplicate. After incubating at 37°C for 24 h, the inhibition zones were measured accurately using a vernier caliper. When diameters of inhibitory zones were greater than 7 mm, inhibitory effects were considered. The larger the diameter of the inhibitory zone, the stronger the inhibitory effect is. On the other hand, when the diameter was 7 mm or less, it was considered ineffective.

2.2.3. Minimum bactericidal concentration

The minimum bactericidal concentrations (MBC) of polyphenol extracts against *S. aureus* were determined following the method described by Obroh et al. (2021) with minor modifications. CPE and PPE were diluted using the two-fold serial dilution method (Chandrasekaran and Venkatesalu, 2004) to concentrations of 25, 12.50, 6.25, 3.13, and 1.56 mg/mL. Four hundred microliter of polyphenol solution was mixed with the same volume of TSB medium containing 100 μL of bacterial suspension. Additionally, PBS buffer and penicillin-streptomycin mixture (1%) were used as negative and positive controls, respectively. The assay was conducted in triplicate. Following an incubation at 37°C for 24 h, 200 μL of the mixture was coated onto LB agar plate and further incubated at 37°C for 24 h. The MBC was determined as the lowest concentration of the polyphenol extracts applied that did not permit the presence of any visible bacterial colonies on the agar plate after the incubation.

2.2.4. Growth curves

The growth curves of *S. aureus* under treatments of CPE or PPE with different concentrations were established following the method of Pagliarulo et al. (2016) with minor modifications. Bacterial suspensions were prepared as described in section 2.2.1. Subse-

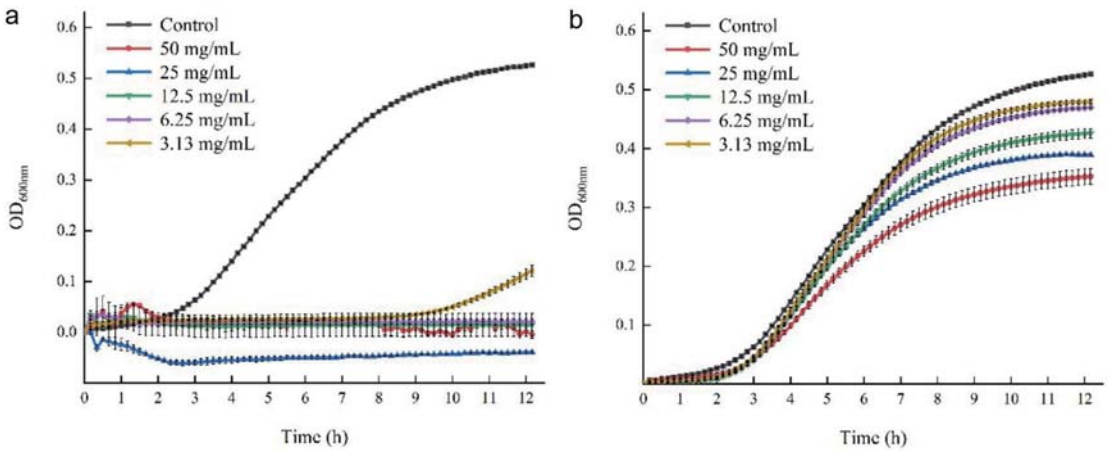

Figure 1. The Effect of PPE and CPE on the growth curves of *S. aureus* during 12 h of incubation. (a) *S. aureus* was treated with PPE; (b) *S. aureus* was treated with CPE.

quently, PBS buffer containing either CPE or PPE were added to the bacterial-containing TSB culture to achieve final polyphenol concentrations of 50, 25, 12.50, 6.25 and 3.13 mg/mL. The aforementioned polyphenol concentrations were selected based on the results of the MBC assay. Moreover, the CPE was tested using the same concentration as PPE, although its MBC was not obtained. PBS buffer was included as the negative control, and sterile TSB medium only containing equal concentration of CPE or PPE was used as the blank control. All samples were set in triplicate. Two-hundred microliter of tested samples were incubated in a 96-well plate covered by a film at 37°C for 12h at OD_{600} nm, with 10-min intervals to determine growths of bacteria in a microplate reader. The absorbance value of bacteria in the results was calculated by the formula: $OD_{600} = A - A_0$, where "OD_{600}" was the ordinate in Figure 1, "a" was the absorbance value of *S. aureus* treated with CPE or PPE at 600 nm, and "A_0" was the absorbance value of blank control at 600 nm.

2.2.5. Observation by scanning electron microscopy (SEM)

Scanning electron microscopy (SEM) was employed to examine the morphological changes of *S. aureus* cells treated with CPE or PPE with minor modifications (El-Maati et al., 2016). The cultured bacteria were diluted to an OD (600 nm) of 0.6 before use in subsequent assay. CPE or PPE was added to the bacterial suspension to achieve final concentrations of 0, 12.50 and 25 mg/mL. The cells were centrifuged at 8,000 r/min for 10 min at room temperature after an incubation at 37°C for 4 h. After twice re-suspensions in PBS buffer and centrifugations followed by a 10 min static standing for intermissions, the cells were fixed with 2.5% glutaraldehyde-PBS (v/v) solution and incubated at 4°C for 12 h. The cells were fixed with 2.5% glutaraldehyde-PBS (v/v) solution and allowed to stand at 4°C for 12 h. After washes with PBS buffer and sterile water, respectively, the cells were dehydrated using ethanol solutions with graded concentrations (30%, 50%, 70%, 80%, 90%, 100%) and left undisturbed for 10 min before centrifugation. Subsequently, the cells were resuspended in isoamyl acetate and were set to stand for 30 min before being centrifuged at 8,000 r/min for 10 min. The samples were finally dried at 40°C for 2 h, freeze-dried for 2 h to dryness, then loaded onto a carrier stage and sprayed with platinum before being visualized using a SEM.

2.2.6. Evaluation of the bacteriostatic effects of CPE and PPE in simulated food systems

The bacteriostatic activities of polyphenol extracts were further analyzed in simulated food systems containing starch, lipid or protein, respectively. The samples were prepared using the method described by Li et al. (2022) with minor modifications as a lower concentration of bacterial suspension was used.

2.2.6.1. Simulated starch-based food system

Different weights of corn starch (CS) were dissolved in 5 mL of 0.5% NaCl (w/v) solution and stirred evenly, and their concentrations of 0%, 1%, 2%, 3%, 4% and 5% (w/v) were obtained. The pH of the solutions was adjusted to 8.0 with 0.1 mol/L NaOH, and then the solutions were boiled for 2 min until the simulated system was formed with a high clarity. The test solution was prepared by adding CPE or PPE into the above simulated starch-based food matrices until the final concentration of 50 mg/mL (2 × MBC) was achieved. The solutions were left undisturbed for 60 min following mixing, and then they were centrifuged at 5,000 r/min for 2 min, which was followed by the collection of the supernatant.

Four sterilized Oxford cups (stainless cylinders with an outside diameter of 8.0 mm, inner diameter of 6.0 mm, and height of 10.0 mm) were placed on each LB agar plate previously coated by 0.1 mL bacterial suspension followed by filling each cup with 200 μL of test solution. Additionally, the PBS buffer was used instead of the test solution as a control in one of the Oxford cups.

2.2.6.2. Simulated lipid-based food system

Different volumes of canola oil (CO) were pipetted to a 50-mL volumetric flask with the addition of 1% (v/v) Tween-80 and diluted to volume with sterile water, which was shaken vigorously for preliminary mixing. The above solution was transferred to the beaker, they were then emulsified at 10,000 r/min three times with 1min intervals and 30 seconds each time to form the lipid-based food system, and the final concentrations of the canola oil were 0%, 1%, 2%, 3%, 4% and 5% (v/v). Further steps are described in Section 2.2.6.1.

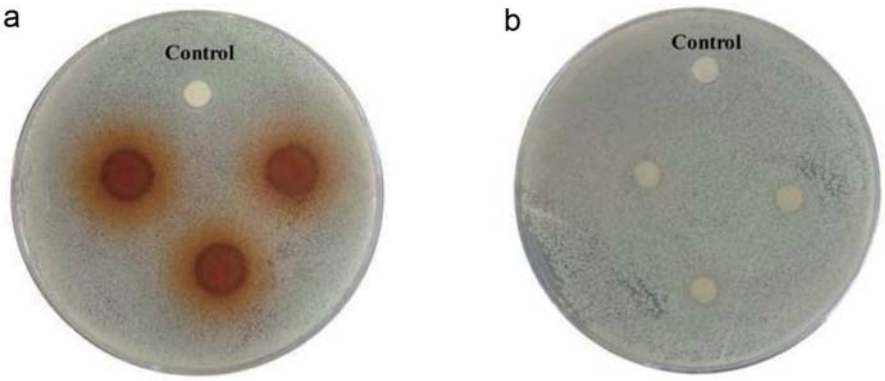

Figure 2. Halos (clear zones) of inhibition of growth of *S. aureus* formed around colonies of PPE and CPE on LB agar. (a) circle filter papers treated with PPE; (b) circle filter papers treated with CPE; Control: the control group.

2.2.6.3. Simulated protein-based food system

Different weights of soybean protein isolate (SPI) were added into 5mL of sterile water, and then the solutions were stirred magnetically at 500 r/min for 1 h at room temperature to form the protein-based food system, and the final concentrations of SPI were 0%, 1%, 2%, 3%, 4% and 5% (w/v). Further steps are described in Section 2.2.6.1.

2.3. Antioxidant potential determination

2.3.1. ABTS radical scavenging assay

The ABTS radical scavenging capacity of CPE or PPE was determined according to the method by Nguyen et al. (2020) with minor modifications. The ABTS stock solution (7 mmol/L) was evenly mixed with $K_2S_2O_8$ (7.35 mmol/L) solution at the ratio of 1:1 (v/v), and kept in the dark at room temperature for 12 h to became ABTS radical solution. Further, the absorbance of the ABTS radical solution at 734 nm was adjusted to 0.7 ± 0.02 by dilution with ethanol, and the ABTS working solution was obtained. An aliquot of 200 μL of CPE or PPE with different concentrations (12.50, 25, 50, 100, 200 μg/mL) was added to 1 mL of ABTS working solution, and they were placed under the condition of avoiding lights before the measurement of their absorbance. Additionally, distilled water and L-ascorbic were used as negative and positive controls, respectively. Distilled water mixed with CPE or PPE solution was used as a blank control. The absorbance of all samples was measured at 734 nm after incubating at 30°C for 6 min, and the results were calculated by the following formula:

$$\text{Scavenging ability of free radicals (100\%)} = \frac{A_0 - (A_1 - A_2)}{A_0} \times 100$$

where "A_0" was the absorbance of the negative control at 734 nm, "A_1" was the absorbance of ABTS working solution treated with L-ascorbic, CPE or PPE at 734 nm, and "A_2" was the absorbance of the blank control at 734 nm.

2.3.2. Ferric reducing antioxidant power (FRAP) assay

The ferric reducing antioxidant power (FRAP) was used to determine the antioxidant capacity of CPE or PPE (Stojiljković et al., 2016). An aliquot of 2.5 mL of 0.01 mol/L TPTZ (0.04 mol/L HCl) solution and 2.5 mL of 0.02 mol/L $FeCl_3$ were added to 25 mL of 0.3 mol/L acetic acid buffer (pH = 3.6) to create the FRAP reagent. Then, 120 μL of $FeS0_4$ solutions with various concentrations (0.2, 0.4, 0.6, 0.8, and 1.0 mmol/L) were added to 3.6 mL of FRAP reagent to prepare standard curve samples. After standing at 37°C for 10 min, the absorbance of all the samples were measured at 593 nm with a microplate reader, and a standard curve was created based on the absorbance. An aliquot of 120 μL of CPE or PPE with different concentrations (200, 400, 600, 800, 1,000 μg/mL) was added to 3.6 mL of FRAP reagent, which was placed under the condition of avoiding lights before the measurement of their absorbance. Additionally, the samples with L-ascorbic acid instead of CPE or PPE were used as a control. The absorbance of samples was measured at 593 nm after incubating at 37°C for 10 min. The results were expressed as mmol/g $FeS0_4$ equivalent.

2.4. Statistical analysis

Each assay was carried out in triplicate, and the results were recorded as means ± standard deviation (SD). The data were analyzed using SPSS 26.0.

3. Results and discussion

3.1. Antibacterial activity

3.1.1. Inhibition zone measurement

The agar diffusion assay was based on the formation of inhibition zones, due to the diffusion of the antimicrobial agent in the solid agar culture medium inhibiting the growth of microorganisms (Galvão et al., 2016). Zhu et al. (2019) reported that the inhibitory zone of purified polyphenol extract constituents from *Sanguisorba offcinalis* L. against *S. aureus* was twice that of crude polyphenol extract. In this study, the results of the antibacterial activities of PPE and CPE against *S. aureus* based on the diameter of inhibition zones are shown in Figure 2 and Table 1. It was observed that colonies formed on LB agar showed a transparent "halo" around the filter paper with the addition of PPE compared to the control group, while the filter paper treated CPE did not exhibit this effect. The diameter of the inhibition zone recorded in Table 1 further

Table 1. The diameters of Inhibition zone of PPE and CPE against *S. aureus* on LB agar

Groups	Diameter of inhibition zone (mm)	Assessment of inhibitory effect
Control	ND	–
PPE	11.15 ± 0.39	+
CPE	6.20 ± 0.14	–

ND: not detected; –: no inhibitory effect (diameter of inhibition zone ≤7 mm); +: positive inhibition inhibitory effect (diameter of inhibition zone >7 mm).

reflects the antibacterial capacities of PPE and CPE. PPE exhibited robust bacteriostatic activity with a diameter up to 11.15 ± 0.39 mm, while CPE had no inhibitory effect against *S. aureus* as a limited small zone diameter (≤7 mm) was formed. The results could be attributed to the higher content of polyphenols of PPE, which mainly include epicatechin acid, ferulic acid and chlorogenic acid, the key polyphenol species in Fuji apple pomace (Jakobek et al., 2020; Liu et al., 2021), which was confirmed to have strong antibacterial activity against gram-positive bacteria (Martinengo et al., 2021; Motallebi et al., 2020). It was reported that the purification process effectively increased the total phenolic content by 3.35 folds, from 13.83 to 46.45 mg of gallic acid equivalents per g of CPE/PPE (Mohammadi et al., 2024).

3.1.2. Minimum bactericidal concentration

It had been reported that some of the bactericidal agents can act as both bacteriostatic and bactericidal depending on their concentration (Chikezie, 2017). The lowest concentrations of PPE or CPE required to kill bacteria were identified as the minimum bactericidal concentrations (MBCs). Table 2 showed the MBC of PPE and CPE against *S. aureus*, which provided the basis for the selection of concentration of PPE or CPE in the subsequent bacteriostatic assay. PPE exhibited a strong bactericidal effect even at relatively low concentrations with an MBC of 25 mg/mL. The MBC of PPE was lower than the reported MBC of polyphenol extract from pomegranate against *S. aureus* (Lima et al., 2019), which could be explained by variations in their phenol content, strains sensitivity as well as antibacterial procedures employed in the test (Gullon et al., 2016). On the contrary, no apparent bactericidal activity was observed for CPE within the tested concentration range (1.56–50 mg/mL). Additional assays with high concentrations of CPE (100–400 mg/mL) were carried out (data not shown) to identify its MBC, and even though the number of bacteria decreased with increasing concentrations, colonies still did not completely disappear from the growing medium, and thus the MBC of CPE was not identified. As no specific MBC value was identified for CPE, the three subsequent antibacterial assays including growth curves, observation by scanning electron microscopy as well as antibacterial effect in simulated food systems were used the same concentration as PPE where the concentration selection was based on MBC.

3.1.3. Growth curves

The growth curves of *S. aureus* with the treatment of PPE (3.13–50 mg/mL) or CPE (3.13–50 mg/mL) over 12 h of incubation period were plotted to monitor the impact of these polyphenol extracts on the growth of *S. aureus*, which was depicted in Figure 1. The growth and life cycle of bacteria are divided into four periods: adaptation period, logarithmic period, stationary period, and decline period, and these stages are determined based on the number of surviving organisms at various intervals (Chesney, 1916). In this study, the growth curve of *S. aureus* in the control group showed the first three stages aforementioned, which indicated a normal growth of *S. aureus* cells. However, when PPE with concentrations from 6.25 to 50 mg/mL were added, the growth of *S. aureus* was completely inhibited, but when the concentration of PPE decreased to 3.13 mg/mL, the growth of *S. aureus* was inhibited at the initial stage. The growth curve showed different fluctuations when the concentration of PPE increased to 25 or 50 mg/mL. Higher concentrations of PPE may react with casein in tryptone soya broth (TSB), thereby impacting the absorbance (El-Messery et al., 2020). However, the trend of growth curves of *S. aureus* treated with CPE showed limited changes compared to the control group, the growth rate of the *S. aureus* decreased slightly, but the effect on the growth curve were stronger when higher concentrations of CPE were applied. Thus, both PPE and CPE demonstrated inhibitory effect on the growth of *S. aureus*, with PPE being more potent, which could be due to the higher polyphenol content of PPE and lower interference from the impurities, and the inhibitory effect improved as the concentrations of PPE or CPE increased.

3.1.4. Effect on the morphology of S. aureus

The morphological damage of *S. aureus* was observed by scanning electron microscope (SEM) in order to further reveal the antibacterial activity of PPE or CPE against *S. aureus* and its mechanism. The results are shown using photomicrographs at 30.0 K × and 50.0 K × magnification in Figure 3. It can be clearly seen that the majority cells of *S. aureus* in the control group were in uniform, full, and spherical shape with relatively smooth surfaces, and they displayed normal cell morphology without extracellular spillage or apparent damage. In spite of this, there were still a few cells with

Table 2. The minimum bactericidal concentrations (mg/mL) of PPE and CPE against *S. aureus*

Bacterium	Polyphenol extracts	Growth of bacteria				
		The concentration of the polyphenols (mg/mL)				
		1.56	3.13	6.25	12.50	25
S. aureus	PPE	++	+	+	+	–
	CPE	++	++	++	++	++

Note: –: aseptic growth; +: small amounts of bacteria growth (colony number ≤5); ++: mass bacterial growth (colony number >5).

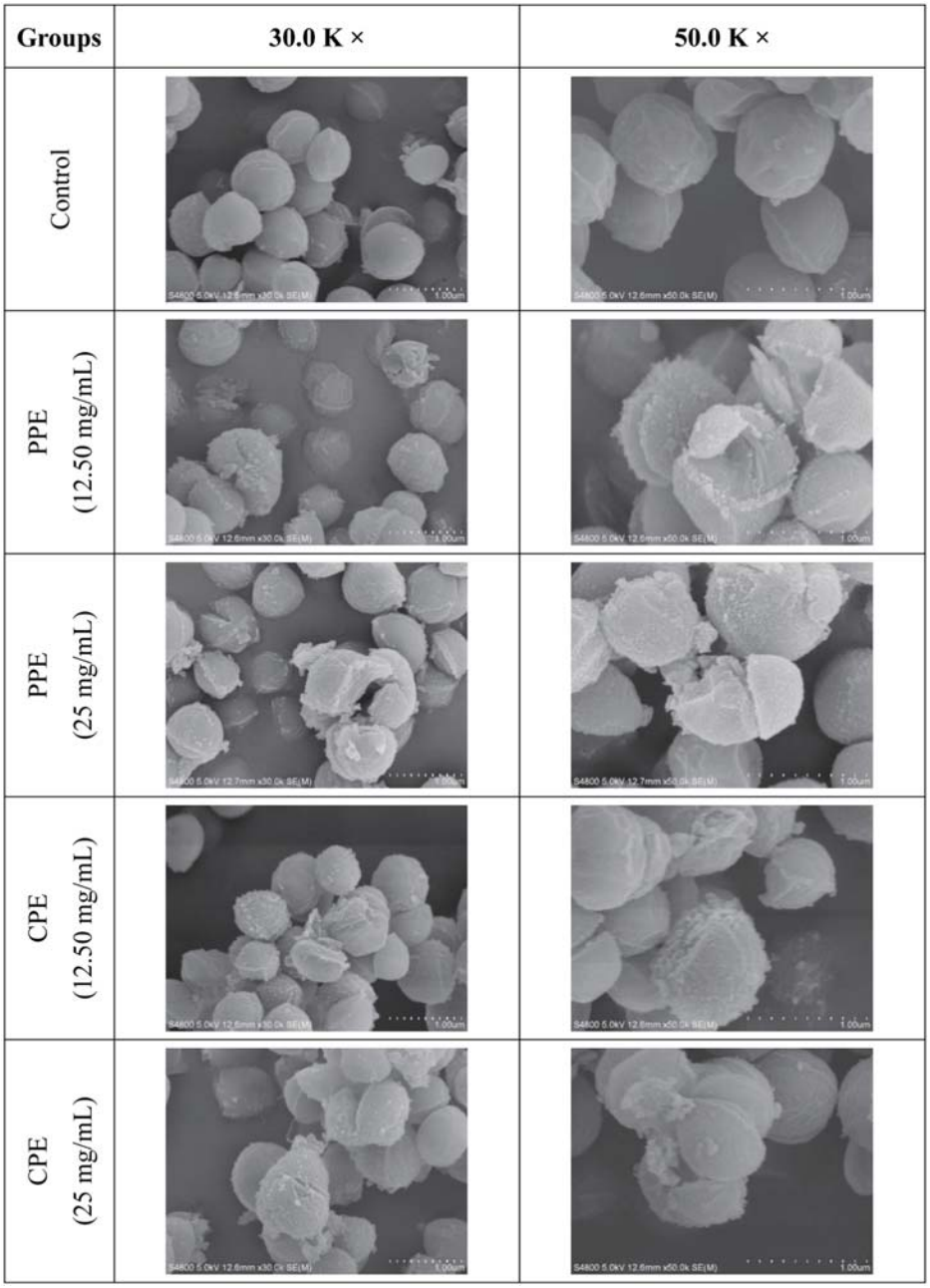

Figure 3. Scanning electron microscope (SEM) images at 30.0 K × and 50.0 K × magnification showing morphological changes of *S. aureus* treated with PPE or CPE.

a small degree of invagination, which could be due to the long drying time of cells before being loaded onto a carrier stage. In contrast to the control group, the surface of *S. aureus* cells treated with PPE or CPE showed wrinkles and cracks with some particulate matters, and these particulate matters might consist of cellular debris or leakage of cellular contents (Shen et al., 2015). These observations were similar to the morphological changes of *S. aureus* after being treated with punicalagin, a phenolic compound present in leaves of pomegranate peel, which was reported by Xu et al. (2017). In summary, PPE and CPE exhibited strong antibacterial activity against *S. aureus* at different degrees. The antibacterial activity of polyphenol extracts derived from Fuji apple pomace was primarily due to their ability to damage the cell membrane and cell wall of *S. aureus*. This may be because polyphenols can alter the fatty acid composition in the cell membrane, and inhibit the synthesis of ergosterol, thereby changing the cell membrane's permeability (Di Pasqua et al., 2006). Additionally, polyphenols can bind with the bivalent cations of the bacterial outer membrane (Nohynek et al., 2006). The destruction of the bacterial cell membrane and cell wall can lead to the leakage of intracellular compo-

Table 3. Bacteriostatic effects of PPE and CPE against *S. aureus* in simulated starch-based food matrices

Groups	Diameter of inhibition zone (mm)					
	Concentration of corn starch (w/v)					
	0%	1%	2%	3%	4%	5%
PPE	11.06 ± 0.60[a]	11.28 ± 0.24[a]	11.24 ± 0.34[a]	11.86 ± 0.26[a]	11.88 ± 0.28[a]	11.74 ± 0.16[a]
CPE	–	–	–	–	–	–
Control	–	–	–	–	–	–

Note: –: no inhibition (diameter of inhibition zone ≤9 mm); same letters indicate no significant difference ($p > 0.05$).

nents, which affected its normal growth and could even cause cell death (Zhong et al., 2023).

3.1.5. Evaluation of the bacteriostatic effects of PPE and CPE in simulated food systems

Natural preservatives' antimicrobial efficacy would be hampered by the intricate, multi-scale structure of food, which may consist of starch, lipid or protein (Wang et al., 2023). Thus, corn starch (CS), canola oil (CO) and soy protein isolate (SPI) were used to form simulated starch-based, lipid-based and protein-based food systems with their varying concentrations in order to evaluate the antibacterial activity of PPE or CPE in food matrices with different macronutrients. It was observed that PPE has strong antibacterial activity in simulated starch-based food matrices against *S. aureus*, which is supported by the presence of inhibition zones, but there was no significant difference ($p > 0.05$) among the effects of all concentrations employed. However, the antibacterial activity was not demonstrated in the simulated lipid-based and protein-based food matrices (data not shown), which were proved by the absence of the inhibition zone. Limited miscibility of PPE in lipid-based food systems may lead to its limited contact time with bacteria present in the emulsion (Pastene et al., 2009), and thus improving the solubility of polyphenol extracts can be one of the means to improve its antibacterial activity in the lipid-based food systems. On the other hand, polyphenols from the PPE could interact with proteins or lipids, which is leading to the formation of complexes that restrict their antimicrobial activity (Mandalari et al., 2016). CPE did not show any antibacterial activity in the three simulated food matrices, which could be due to its lower content of polyphenols as well as the interference from its impurities (Table 3).

3.2. Antioxidant activity

3.2.1. ABTS radical scavenging capacity

The ABTS radical scavenging assay is one of the commonly used methods to evaluate the antioxidant capacity of polyphenol extracts (Floegel et al., 2011). The principle of this method is that $K_2S_2O_8$ solution reacts with ABTS solution to oxidize ABTS into blue-green ABTS radicals, and after the addition of antioxidant substances such as L-ascorbic and polyphenols, ABTS radicals will be reduced into ABTS, and the color of the solution will change. Therefore, the ABTS radical scavenging capacity of L-ascorbic acid, polyphenols and other substances can be evaluated by detecting the absorbance of the sample at 734 nm. The ABTS radical scavenging ability of PPE and CPE were shown in Figure 4. The

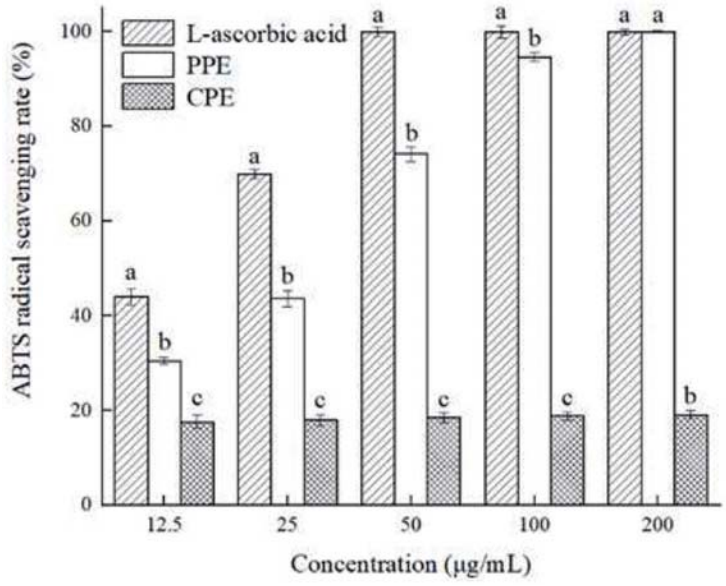

Figure 4. Antioxidant activity of PPE and CPE in ABTS radical scavenging test as compared with L-ascorbic acid. Different letters marked in the same concentration indicate significant differences ($p < 0.05$) between any two groups.

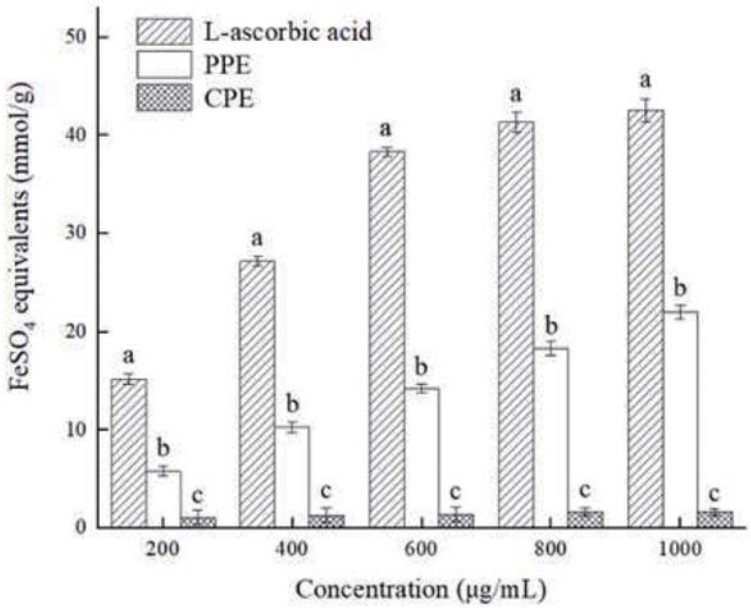

Figure 5. Antioxidant activity of PPE and CPE in FRAP test as compared with L-ascorbic acid. Different letters marked in the same concentration indicate significant differences ($p < 0.05$) between any two groups.

results indicated that the ABTS radical scavenging capacity of PPE increased when concentrations increased, and was significantly stronger ($p < 0.05$) than that of CPE with all concentrations tested. When the concentration is 12.5–100 μg/mL, the ABTS radical scavenging capacity of tested materials was as follows: L-ascorbic acid > PPE > CPE. However, when the concentration increased to 200 μg/mL, the ABTS radical scavenging rates of both PPE and L-ascorbic acid were about 99.99%, which were five times of that of CPE, from which demonstrated the strong antioxidant activity of PPE. In conclusion, both PPE and CPE showed strong ABTS radical scavenging capacity, from which PPE being more potent, which could be due to its higher content of polyphenols, mainly including chlorogenic acid, epicatechin and catechin (Qing et al., 2023; Serra et al., 2021).

3.2.2. Ferric reducing antioxidant power (FRAP)

The ferric reducing antioxidant power (FRAP) assay demonstrated features of high reproducibility, easy operation, and thus it is widely used to evaluate the antioxidant capacity of polyphenol extracts (Thaipong et al., 2006). The principle of this assay is to determine the reduction of Fe^{3+} to Fe^{2+} by measuring the absorbance of the Perl's Prussian blue complex (El-Maati et al., 2016), and a higher absorbance indicates a higher Fe^{3+} reducing capacity. Figure 5 illustrated the ferric reducing antioxidant power of PPE and CPE. The results indicated that PPE had a potent reducing capacity for Fe^{3+}, and its capacity increased when concentrations increased. However, CPE exhibited limited Fe^{3+} reducing activity at the concentration range selected. Both PPE and CPE showed significantly lower ($p < 0.05$) reducing power with all concentrations tested compared to that of L-ascorbic acid; meanwhile, PPE exhibited a significantly higher ($p < 0.05$) reducing power than that of CPE with all concentrations tested. In summary, the reducing capacity of tested materials to Fe^{3+} in this assay was as follows: L-ascorbic acid > PPE > CPE, and it demonstrated that PPE had stronger antioxidant activity than that of CPE, which could be due to its higher content of polyphenols (Guo et al., 2018).

4. Conclusion

Purified polyphenol extract (PPE) from Fuji apple pomace showed strong antibacterial activities in various systems tested, mainly by damaging the cell wall and membrane of bacteria, while it also demonstrated potent antioxidant activity in ABTS radical scavenging and FRAP assays due to its strong quenching capacity of ABTS radicals and reducing effect of Fe^{3+} to Fe^{2+}. The crude polyphenol extract exhibited limited antimicrobial and antioxidant properties in tested systems comparing to that of PPE, which may be due to its lower polyphenol content and the interference from the impurities. Therefore, polyphenol extract, especially its purified forms from Fuji apple pomace, can be used as a novel antibacterial agent for food preservation as well as natural antioxidant for functional food and nutraceutical products.

Acknowledgments

This work was supported by the National Foreign Expert Project Funded by the Ministry of Science and Technology of the People's Republic of China (G2022041012L), the Shaanxi Province Key Research and Development Program (Project No. 2017TSCXL-NY-02-03), the Department of Science and Technology of Shaanxi Province, P. R. China (No. 2023-YBNY-108), and Xian Science and Technology Bureau (22NYYF048).

Conflict of interest

The authors declare that there is no conflict of interest.

References

Bai, X.L., Zhang, H.W., and Ren, S. (2013). Antioxidant activity and HPLC analysis of polyphenol-enriched extracts from industrial apple pomace. J. Sci. Food Agric. 93(10): 2502–2506.

Bouarab Chibane, L., Degraeve, P., Ferhout, H., Bouajila, J., and Oulahal, N. (2019). Plant antimicrobial polyphenols as potential natural food preservatives. J. Sci. Food Agric. 99(4): 1457–1474.

Chambers, H. (2001). The changing epidemiology of *Staphylococcus aureus*? Emerging Infect. Dis. 7(2): 178–182.

Chandrasekaran, M., and Venkatesalu, V. (2004). Antibacterial and antifungal activity of *Syzygium jambolanum* seeds. J. Ethnopharmacol. 91(1): 105–108.

Chesney, A.M. (1916). The latent period in the growth of bacteria. J. Exp. Med. 24(4): 387–418.

Chikezie, I.O. (2017). Determination of minimum inhibitory concentration (MIC) and minimum bactericidal concentration (MBC) using a novel dilution tube method. Afr. J. Microbiol. Res. 11(23): 977–980.

Chmielowiec-Korzeniowska, A., Tymczyna, L., Wlazło, Ł., Nowakowicz-Dębek, B., and Trawińska, B. (2020). *Staphylococcus aureus* carriage state in healthy adult population and phenotypic and genotypic properties of isolated strains. Adv. Dermatol. Allergol. 37(2): 184–189.

Clemens, R.A., and Shahidi, F. (2022). Upregulation of immune system against COVID-19: The role of food science, nutrition and bioactive compounds. J. Food Bioact. 17: 1.

Di Pasqua, R., Hoskins, N., Betts, G., and Mauriello, G. (2006). Changes in membrane fatty acids composition of microbial cells induced by addiction of thymol, carvacrol, limonene, cinnamaldehyde, and eugenol in the growing media. J. Agric. Food Chem. 54(7): 2745–2749.

El-Messery, T.M., Mwafy, E.A., Mostafa, A.M., El-Din, H.M.F., Mwafy, A., Amarowicz, R., and Ozçelik, B. (2020). Spectroscopic studies of the interaction between isolated polyphenols from coffee and the milk proteins. Surf. Interfaces 20: 100558.

Fei, P., Ali, M.A., Gong, S.Y., Sun, Q., Bi, X., Liu, S.F., and Guo, L. (2018). Antimicrobial activity and mechanism of action of olive oil polyphenols extract against *Cronobacter sakazakii*. Food Control 94: 289–294.

Fernandes, P.A.R., Ferreira, S.S., Bastos, R., Ferreira, I., Cruz, M.T., Pinto, A., Coelho, E., Passos, C.P., Coimbra, M.A., Cardoso, S.M., and Wessel, D.F. (2019). Apple pomace extract as a sustainable food ingredient. Antioxidants 8(6): 189.

Fraga, C.G. (2007). Plant polyphenols: How to translate their in vitro antioxidant actions to in vivo conditions. IUBMB Life 59(4–5): 308–315.

Floegel, A., Kim, D.-O., Chung, S.-J., Koo, S.I., and Chun, O.K. (2011). Comparison of ABTS/DPPH assays to measure antioxidant capacity in popular antioxidant-rich US foods. J. Food Compos. Anal. 24(7): 1043–1048.

Galvão, G.V., Saviano, A.M., and Lourenço, F.R. (2016). Reduced incubation time for inhibition zone formation based on diffusion and growth mechanism elucidation. Anal. Methods 8(19): 3885–3891.

Gullon, B., Pintado, M.E., Pérez-Álvarez, J.A., and Viuda-Martos, M. (2016). Assessment of polyphenolic profile and antibacterial activity of pomegranate peel (*Punica granatum*) flour obtained from co-product of juice extraction. Food Control 59: 94–98.

Gulzar, Y. (2023). Fruit image classification model based on mobileNetV2 with deep transfer learning technique. Sustainability 15(3): 1906.

Guo, C.X., Qiao, J.P., Zhang, S.W., Ren, X.T., and Li, M.P. (2018). Purification of polyphenols from kiwi fruit peel extracts using macroporous resins and high-performance liquid chromatography analysis. Int. J. Food Sci. Technol. 53(6): 1486–1493.

Gupta, R., and Yadav, D.R.K. (2021). Impact of chemical food preservatives on human health. PalArch's Journal of Archaeology of Egypt/ Egyptology 18(15): 811–818.

Jakobek, L., Ištuk, J., Buljeta, I., Voća, S., Žlabur, J.Š., and Babojelić, M.S. (2020). Traditional, indigenous apple varieties, a fruit with potential for beneficial effects: Their quality traits and bioactive polyphenol contents. Foods 9(1): 52.

Lima, M.C., Paiva De Sousa, C., Fernandez-Prada, C., Harel, J., Dubreuil, J.D., and De Souza, E.L. (2019). A review of the current evidence of fruit phenolic compounds as potential antimicrobials against pathogenic bacteria. Microb. Pathog. 130: 259–270.

Liu, L., Zhang, C., Zhang, H., Qu, G., Li, C., and Liu, L. (2021). Biotransformation of polyphenols in apple pomace fermented by β-Glucosidase-Producing lactobacillus rhamnosus L08. Foods 10(6): 1343.

Li, Y.Z., Xiao, H.Q., Cao, D., Wang, L., Zeng, M.Q., Lin, Q.L., and Zhao, M.M. (2022). Antimicrobial stability of metal antimicrobial peptide SIF_4 in simulated single or multiple component food systems. Food Ferment. Ind. 48(12): 131–137.

Mandalari, G., Vardakou, M., Faulks, R., Bisignano, C., Martorana, M., Smeriglio, A., and Trombetta, D. (2016). Food matrix effects of polyphenol bioaccessibility from almond skin during simulated human digestion. Nutrients 8(9): 568.

Martinengo, P., Arunachalam, K., and Shi, C. (2021). Polyphenolic antibacterials for food preservation: Review, challenges, and current applications. Foods 10(10): 2469.

Mohammadi, N., Guo, Y.Y., Wang, K., and Granato, D. (2024). Macroporous resin purification of phenolics from Irish apple pomace: Chemical characterization, and cellular antioxidant and anti-inflammatory activities. Food Chem. 437: 137815–137823.

Motallebi, M., Khorsandi, K., Sepahy, A.A., Chamani, E., and Hosseinzadeh, R. (2020). Effect of rutin as flavonoid compound on photodynamic inactivation against *P. aeruginosa* and *S. aureus*. Photodiagn. Photodyn. Ther. 32: 102074.

Nguyen, N.Q., Nguyen, M.T., Nguyen, V.T., Le, V.M., Trieu, L.H., Le, X.T., Khang, T.V., Giang, N.T.L., Thach, N.Q., and Hung, T.T. (2020). The effects of different extraction conditions on the polyphenol, flavonoids components and antioxidant activity of Polyscias fruticosa roots. IOP Conf. Ser.: Mater. Sci. Eng. 736: 022067.

Nohynek, L.J., Alakomi, H.-L., Kähkönen, M.P., Heinonen, M., Helander, I.M., Oksman-Caldentey, K.-M., and Puupponen-Pimiä, R.H. (2006). Berry phenolics: Antimicrobial properties and mechanisms of action against severe human pathogens. Nutr. Cancer 54(1): 18–32.

Obroh, A.A., Oshim, I.O., Odeyemi, O., Urama, E.U., and Olise, N.A. (2021). Demonstration of the minimum inhibitory concentration (MIC) and minimal bactericidal concentration (MBC) of both *moringa oleifera* and *gongronema latifolium* extracts mixture against *Staphylococcus aureus*, *Salmonella typhi* and *Escherichia coli*. J. Adv. Med. Pharm. Sci. 23(1): 46–52.

Pagliarulo, C., De Vito, V., Picariello, G., Colicchio, R., Pastore, G., Salvatore, P., and Volpe, M.G. (2016). Inhibitory effect of pomegranate (*Punica granatum L.*) polyphenol extracts on the bacterial growth and survival of clinical isolates of pathogenic *Staphylococcus aureus* and *Escherichia coli*. Food Chem. 190: 824–831.

Pastene, E., Speisky, H., Troncoso, M., Alarcón, J., and Figueroa, G. (2009). In Vitro Inhibitory Effect of apple peel extract on the growth of *Helicobacter pylori* and respiratory burst induced on human neutrophils. J. Agric. Food Chem. 57(17): 7743–7749.

Qing, Y.L., Xiang, X., Li, S., Wang, M., Liang, Z.Y., and Ren, J.Y. (2023). Integrated evaluation the antioxidant activity of epicatechin from cell dynamics. Biotechnol. Prog. 39(3): e3328.

Serra, S., Anthony, B., Boscolo Sesillo, F., Masia, A., and Musacchi, S. (2021). Determination of post-harvest biochemical composition, enzymatic activities, and oxidative browning in 14 apple cultivars. Foods 10(1): 186.

Shahidi, F., and Santhiravel, S. (2022). Novel marine bioactives: Application in functional foods, nutraceuticals, and pharmaceuticals. J. Food Bioact. 19: 4–96.

Shen, S.X., Zhang, T.H., Yuan, Y., Lin, S.Y., Xu, J.Y., and Ye, H.Q. (2015). Effects of cinnamaldehyde on *escherichia coli* and *staphylococcus aureus* membrane. Food Control 47: 196–202.

Singh, R., Jain, A., Panwar, S., Gupta, D., and Khare, S.K. (2005). Antimicrobial activity of some natural dyes. Dyes Pigm. 66(2): 99–102.

Stojiljković, D., Arsić, I., and Tadić, V. (2016). Extracts of wild apple fruit (*Malus sylvestris* (L.) Mill., Rosaceae) as a source of antioxidant substances for use in production of nutraceuticals and cosmeceuticals. Ind. Crops Prod. 80: 165–176.

Thaipong, K., Boonprakob, U., Crosby, K., Cisneros-Zevallos, L., and Hawkins Byrne, D. (2006). Comparison of ABTS, DPPH, FRAP, and ORAC assays for estimating antioxidant activity from guava fruit extracts. J. Food Compos. Anal. 19(6–7): 669–675.

Wang, L., Wang, H., Liu, D., Han, Z., and Fan, J. (2023). A review of the poly-

phenols purification from apple products. Crit. Rev. Food Sci. Nutr.

Wattinger, L., Stephan, R., Layer, F., and Johler, S. (2012). Comparison of *Staphylococcus aureus* isolates associated with food intoxication with isolates from human nasal carriers and human infections. Eur. J. Clin. Microbiol. Infect. Dis. 31(4): 455–464.

Xu, Y.F., Shi, C., Wu, Q., Zheng, Z.W., Liu, P.F., Li, G.H., Peng, X.L., and Xia, X.D. (2017). Antimicrobial activity of punicalagin against *Staphylococcus aureus* and its effect on biofilm formation. Foodborne Pathog. Dis. 14(5): 282–287.

Yehia, H.M., Al-Masoud, A.H., Alarjani, K.M., and Alamri, M.S. (2020). Prevalence of methicillin-resistant (*mecA* gene) and heat-resistant *Staphylococcus aureus* strains in pasteurized camel milk. J. Dairy Sci. 103(7): 5947–5963.

Zhang, T.J., Wei, X.Y., Miao, Z., Hassan, H., Song, Y.B., and Fan, M.T. (2016). Screening for antioxidant and antibacterial activities of phenolics from *Golden Delicious* apple pomace. Chem. Cent. J. 10(1): 47.

Zhong, W.W., Tang, M.S., Xie, Y., Huang, X.Q., and Liu, Y.A. (2023). Tea polyphenols inhibit the activity and toxicity of *Staphylococcus aureus* by destroying cell membranes and accumulating reactive oxygen species. Foodborne Pathog. Dis. 20(7): 294–302.

Zhu, H., Chen, G., Chen, S., Wang, Q., Wan, L., and Jian, S. (2019). Characterization of polyphenolic constituents from *Sanguisorba officinalis* L. and its antibacterial activity. Eur. Food Res. Technol. 245(7): 1487–1498.

Journal of Food Bioactives
International Society for Nutraceuticals and Functional Foods
Original Research
J. Food Bioact. 2024;25:62–71

A novel combination against skin aging via promoting the synthesis of biological collagen

Bei-Bei Dong[a,b], Peng-Fei Zhang[c], Wu-Yan Guo[d*], Heng-Yu Zheng[e], You-Nan Kou[a,b], Huan Zhang[f], Ying-Chao Ma[g] and Bo Zhang[h*]

[a]College of Pharmacy, Nankai University, Tianjin, 300350, China
[b]Tianjin Key Laboratory of Early Druggability Evaluation of Innovative Drugs, Tianjin International Joint Academy of Biomedicine, Tianjin, 300457, China
[c]Tianjin Pharmaceutical and Cosmetic Evaluation and Inspection Center, Tianjin, 300191, China
[d]Tianjin JiAnKang Bio&TCM-technology Development Co., Ltd. Tianjin, 300457, China
[e]Breast Disease Center, Peking University First Hospital, Beijing, 100032, China
[f]College of Bioengineering, Tianjin University of Science and Technology, Tianjin, 300457, China
[g]College of Marine and Environmental Science, Tianjin University of Science and Technology, Tianjin, 300457, China
[h]Tsinghua University Institute of TCM-X, Beijing, 100084, China
[*]**Corresponding author:** Bo Zhang, Tsinghua University Institute of TCM-X, Beijing, 100084, China. E-mail: zhangbo.2007@tsinghua.org.cn; Wu-Yan Guo, Tianjin JiAnKang Bio&TCM-technology Development Co., Ltd. Tianjin, 300457, China. E-mail: guowuyan213@126.com

DOI: 10.31665/JFB.2024.18372
Received: January 02, 2024; **Revised received & accepted:** March 06, 2024
Citation: Dong, B.-B., Zhang, P.-F., Guo, W.-Y., Zheng, H.-Y., Kou, Y.-N., Zhang, H., Ma, Y.-C., and Zhang, B. (2024). A novel combination against skin aging via promoting the synthesis of biological collagen. J. Food Bioact. 25: 62–71.

Abstract

Supplementing collagen is considered to contribute to delaying skin aging. In this work, we developed a novel combination for improving skin aging by stimulating the biosynthesis of collagen. By screening a library of Chinese herbal medicines (CHM), we found that *Angelicae Dahuricae Radix* (Baizhi), *Lilii bulbus* (Baihe), *Glycyrrhizae radix et rhizoma* (Gancao), and *Jujubae fructus* (Dazao) substantially increased the mRNA expression levels of type I collagen, suggesting their potential anti-skin-aging activity. To keep the structural integrity of collagen, prolyl 4-hydroxylase (P4H), a key enzyme in collagen synthesis, was recombinantly expressed in *Escherichia coli*. In addition, the transfersome with added P-4H was prepared to improve the transdermal absorption of combination. Vitamin C (VC), the substrate required for the activity of P4H, was also incorporated into the combination. Eventually, an optimal combination, consisting of Baizhi, Baihe, Gancao, P4H transfersome and VC, was obtained by a series of combination experiments. Based on traditional CHM and modern biological agents, we developed a novel combination against skin aging by promoting the synthesis of collagen. Collectively, the combination show the high potential of application to delay skin aging.

Keywords: Chinese herbal medicines; Collagen; Hydroxyprolin; Skin aging; Transfersome.

1. Introduction

The skin undergoes morphological and physiological changes with aging, such as discolorations and wrinkles. How to restore youthfulness of skin has attracted much attention. Skin aging is a spontaneous and complex process of skin degeneration. Both environmental and hormonal factors affect the skin aging (Schäfer et al., 2020). Collagen, the most abundant extracellular matrix protein, accounts for 70~80% of the dry weight of skin (Zhang et al., 2020). During the skin aging process, the collagen stability

decreases greatly. Besides, the ability to replenish collagen naturally decreases by about 1% per year, also causing accelerated senescence in human skin (Edgar et al., 2018). Therefore, strategies of supplementing collagen hold great potential in delaying skin aging.

At present, topical treatments have become one of the most common methods in supplementing collagen (Kwatra, 2022). However, macromolecular collagen barely penetrates the skin due to the resistance of cuticle, so it merely plays a moisturizing role in the epidermis (Jepps et al., 2013). Besides, the collagen absorbed by skin is easily degraded by collagenases (Lagarto et al., 2020). Most topical supplements face the challenge of unsatisfactory therapeutic effects. It is urgent to develop an efficient topical collagen supplement.

We focused on supplementing skin collagen by endogenously promoting the biosynthesis of collagen and increasing collagenous stability. Among the various collagens, type I and III collagen are the most abundant (Chen et al., 2021). Different collagens have a common triple-helix conformation that consists of three almost identical polypeptide chains (Ricard-Blum, 2011). Proline (Pro) - hydroxyproline (Hyp) - glycine (Gly) is usually the most common triplet in collagens (Chattopadhyay and Raines, 2014). The interchain H-bondings between the hydrogen atom of Gly and the hydroxyl group of Hyp exert a critical action in stabilitizing collagen structure (Huang et al., 2009). It is noteworthy that the formation of Hyp is catalyzed by prolyl 4-hydroxylases (P4H) that act on Pro residues in peptides (Eriksson et al., 1999). So, P4H is the rate-limiting enzyme in the synthesis of collagen (Zhang et al., 2018). Vitamin C (VC), as a cofactor, participates in the synthesis of collagen (Stephens and Grande-Allen, 2007). In addition, some studies have confirmed Chinese herbal medicines (CHM) has a promoting role in collagen synthesis, such as *Lycium chinense Mill.* and *Angelica dahurica* (Lin and Chen, 2007). Transfersome can effectively protect the drug against undesired absorption into cutaneous blood vessels and are capable of retaining the drug in the skin (Elsayed et al., 2007).

Taken together, wwe developed a novel combination consisting of Baizhi, Baihe, Gancao, P4H transfersome and VC for promoting collagen production and stabilizing the collagen structure in skin. We then evaluated whether the combination functions on D-galactose-induced aging mice to determine whether the combination could promote collagen synthesis and improve skin conditions.Taken together, we attempted to combine the advantages of P4H and CHM to design a novel anti-skin aging combination.

2. Materials and methods

2.1. Materials

NIH-3T3 fibroblasts were purchased from Beijing Beina Institute of Biotechnology. All Chinese medicinal materials were provided by Anguo Kanghua Traditional Chinese Medicine sales Co. Ltd. Dulbecco's modifed eagle medium (DMEM), fetal bovine serum (FBS), dNTPs, T4 DNA ligase, Pfu polymerase, and Gene ruler were obtained from Thermo Fisher Scientific. RNA extraction kits, RNA reverse transcription kits, plasmid DNA mini-extraction kits, and gel recovery kits were purchased from Tiangen Biochemical Technology Company. Isopropyl-bate-D-thiogalactopyranoside (IPTG), VC, and soy lecithin (purity > 95%) were obtained from Shanghai Sangon Biological Company. FastDigest NcoI, FastDigest XbaI, GeneRulerT 1 kb DNA ladder, protein marker, FastDigest BamHI, and FastDigest XhoI were purchased from Thermo Scientific. Commercially available kits bicinchoninic acid assay (BCA) and hydroxyproline were provided by Nanjing Jiancheng Bioengineering Institute.

Table 1. Primer list used in this study

Primer	Sequence
GAPDH	F: TTGCTGATCCACATCTGCTGGAAG
	R: GGCCACTGCCGCATCCTCTTC
Collagen-I	F: ATGTTCAGCTTTGTGGACCTCCGGC
	R: CTTAGGACCAGCAGGACCAGTATCT
Collagen-III	F: ATGATGAGCTTTGTGCAATGTGGGA
	R: CATGGGGCCAGGAGCTCCGTTGTCT
pET16b(+)	F: GCTCTAGAATGGAGGGGTTTGAAACCAGCGAT
	R: CATGCCATGGTTTAACAGCACGGATCCATC

2.2. Extraction of 82 Chinese herbal medicines

Firstly, 80 g of each herb was pulverized and passed through a 60-mesh sieve. The pretreated dried powder was reflux-extracted twice with purified water (1 : 8, w/v) at 100°C for 2 h each time. After 50 h lyophilization (lyophilizer VS-502FD,Wuxi Woxin Instrument Co., Ltd.,China) the extracts were concentrated under reduced pressure at 45°C using rotary evaporator (Heidolph Hei VAP Rotary Evaporator, Germany) and then freeze-dried. Finally, the lyophilizates were stored at −20°C for back-up purposes.

2.3. Cell culture

NIH-3T3 fibroblasts grown in DMEM medium supplemented with 10% FBS and 1% penicillin/streptomycin. Cells were incubated at 37°C in an atmosphere containing 5% CO_2/95%. The growth of the cells was observed using an inverted microscope (*Chongqing* Optec Instrument Co. Ltd., China).

2.4. Cell viability assay

In 96-well culture plates, 1×10^4 cells/well were seeded for 24 h and treated with CHM extracts (5 mg/mL). After 24 h of treatment, cell viability was determined using the 3-(4,5-Dimethylthiazol-2-yl)-2,5-diphenyltetrazolium bromide (MTT) assay (Schoeman et al., 2020). MTT reagent (20 µL) was added to each well and incubated for 4 h and then terminated by adding 100 µL dimethylsulfoxide (DMSO). Next, the 96-well plate was incubated for 15 min at room temperature. Cell proliferation was assessed by measuring the absorbance at 570 nm.

2.5. Quantitative real-time polymerase chain reaction (RT-PCR)

NIH-3T3 cells (2×10^5 cells/mL) plated for 24 h were exposed with concentrations of CHM extracts. After 24 h, total RNA was extracted from the NIH-3T3 fibroblasts using the TRIzol reagent. Then total RNA was used to synthesize cDNA by reverse transcription. We performed PCR on the resultant cDNA from each sample using specific primers (Table 1). The amplification was carried out on a Thermal Cycler (Applied Biosystems, Thermo

fisher scientific, Waltham, MA, USA). The 20 µL reaction mixture contained 5 µL of cDNA, 1 µL of sense and antisense primers, 200 µM of each deoxynucleotide (DTT), 2 µL of GoTaq polymerase, 2 µL of 10 × Taq polymerase buffer. The reaction was cycled 40 times for 50 s at 95°C, 60 s at 58°C, and 90 s at 72°C. Data was analyzed using the 2-ΔΔCT values method and normalized to the expression levels of GAPDH.

2.6. The expression and purification of P4H

P4H gene of eukaryotic algal virus, *Paramecium bursaria Chlorella virus-1* (PBCV-1) was selected for as the target gene. Because it is small in size and simple in structure, and can be recombinantly expressed in prokaryotic expression system *Escherichia coli* (*E coli*) (Eriksson et al., 1999). Firstly, we obtained the sequence of P4H gene from GeneBank database. Plasmid vector pET16b(+) was used for expression in *E coli*. The Primer 5.0 was used to design primers (Primer sequences are provided in Table 1). Then, PCR was used to amplify fragments of the target genes.

The PCR product was digested with BamHI and XhoI, and ligated with into the corresponding sites of the expression vector pET16b(+). Subsequently, the ligation product was transformed into DH5α competent cells by heat shock method (Froger and Hall, 2007). *E. coli* DH5α cells grown at 37°C in luria broth (LB) containing ampicillin. The monoclonal colony was picked and inoculated in LB medium for 6 h. The plasmid extraction followed the manual provided with the kit. The recombinant plasmids were identified by PCR, double restriction enzyme digestion and sequencing analysis, respectively.

Thereafter, the recombinant plasmid was transferred into BL-21 competent cells, and added IPTG (final concentration: 1 mM) to induce the expression of target protein. Then the bacterial solution was shaken at 28°C, 220 rpm for 4 h. After centrifuging the bacterial liquid culture, the supernatant was discarded and the sediment was resuspended. The suspension was centrifuged and the supernatant was removed. A Ni column was used for affinity purification of the His-tagged P4H. Briefly, the supernatant was collected and applied to a Ni-NTA affinity chromatography column. Then the Ni-NTA column was washed with the wash buffer (His-Trap buffer supplemented with 60 mM imidazole) and the protein was eluted with elution buffer (His-Trap buffer supplemented with 300 mM imidazole). Eluted protein was concentrated using a 10 KD centrifugal filter to 1 mL. Finally, the protein were further purified by Superdex-200 gel-filtration size column. Single peak fractions were collected, snap frozen and stored at −80°C in aliquots. The purity of protein was examined by 12% SDS-PAGE.

2.7. Activity assay of P4H

According to literature, the P4H activity was evaluated by monitoring the hydroxylation of (PAPK)3, a short proline-rich peptide substrate (Myllyharju, 2003; Eriksson et al., 1999). The P4H enzyme activity reaction system (1.0 mL) was established *in vitro*. The system comprised the following components: $Fe(NH_4)_2(SO_4)_2$, 50 µM; α-ketoglutaric acid, 300 mM; ascorbate, 4 mM; tris (hydroxymethyl) aminomethane (Tris)-HCl, 50 mM; substrate, 300 µg; bovine serum albumin, 2 mg; catalase, 200 ug; and nicotinamide-adenine dinucleotide (NADH), 200 µg. The reaction mixtures were incubated at 37°C for 4 h and then quenched by methanol. Finally, the molecular weight difference of sample was analyzed using MALDI-TOF MS.

Table 2. Factors and Levels

Level	A (w/w)	B (%)	C (mg/mL)
1	90 : 10	6	2
2	85 : 15	3	5
3	80 : 20	1	10

A, B and C are the ratio of soy lecithin and cholesterol, total lipid concentration, and enzyme concentration, respectively.

2.8. Stability studies of P4H

The effect of temperature on the stability of the P4H was studied. The protease solution was placed at −20, 4, 25, and 50°C for 8 days, respectively, and samples were drawn at 1, 2, 3, 4, 5, 6, 7, and 8 days. Separately, the protease solution was also placed in a 50°C constant temperature water bath for 1 h and samples were taken at 5, 10, 15, 20, 25, 30, 40, and 60 min. Variation in P4H stability was confirmed qualitatively by 12% SDS-PAGE.

2.9. Preparation of P4H transfersome

P4H transfersome was prepared by the thin-film hydration method followed by extrusion. First, 1 mg/mL P4H solution was prepared using PBS as solvent. The different proportions of soy lecithin and cholesterol were dissolved in 5 mL organic solvent (methanol:dichloromethane = 1:3), and the solvent was evaporated under reduced pressure to obtain a thin lipid film in bottle bottom. Next, 5 mL P4H solution was add it to the bottle. The lipid film was eluted to obtain emulsion, ultrasonicated for 30 s, and filtered through 0.22 µm microporous membranes to collect the P4H transfersome solution. After centrifugation, the P4H transfersome was obtained. The softening material (cholesterol) was replaced by an equal amount of distilled water to prepare the normal liposome.

Then, the P4H transfersome solution was centrifuged at high speed. We measured the free P4H content in the supernatant by the BCA method (Schoel et al., 1995). The factors affecting the encapsulation rate are mainly the ratio of soy lecithin and cholesterol (A), drug concentration (B), and lipid concentration in the aqueous phase (C). In this study, orthogonal experiment on above three factors was preformed (Table 2), and the optimal preparation process parameters were determined. Encapsulation efficiency was calculated by the following formula:

$$EE\% = 1 - \frac{\text{unencapsulated drug}}{\text{total drug}} \times 100\%.$$

The skin of nude mice was harvested and refrigerated at 4°C for later use. P4H transfersome solution, P4H liposome solution, and P4H solution each was smeared by 0.5 mL to the skin surfaces and recovered after 12 h. Then the free P4H content in each solution was measured, and the transdermal efficiency was compared. Additionally, the morphological characteristics of P4H transfersome were observed under the transmission electron microscope.

2.10. Determination of hydroxyproline content

According to the composition of the formula (Table 3), all the ingredients are weighed in equal proportion and mixed. We pretreated NIH-3T3 cells with different formulae. After a 24 h incubation, cells were collected to detect the content of hydroxyproline. Simi-

Table 3. The components of different combinations

Combination	Components
CHM-1-1	Dazao + P4H transfersome + VC
CHM-1-2	Gancao + P4H transfersome + VC
CHM-1-3	Baizhi+ P4H transfersome + VC
CHM-1-4	Baihe + P4H transfersome + VC
CHM-2-1	Dazao + Gancao + P4H transfersome + VC
CHM-2-2	Dazao + Baizhi + P4H transfersome + VC
CHM-2-3	Dazao + Baihe + P4H transfersome + VC
CHM-2-4	Gancao + Baizhi + P4H transfersome + VC
CHM-2-5	Gancao + Baihe + P4H transfersome + VC
CHM-2-6	Baihe + Baizhi + P4H transfersome + VC
CHM-3-1	Dazao + Gancao + Baizhi+ P4H transfersome + VC
CHM-3-2	Dazao + Gancao + Baihe P4H transfersome + VC
CHM-3-3	Dazao + Baizhi + Baihe+ P4H transfersome + VC
CHM-3-4	Baizhi + Baihe+ Gancao + P4H transfersome + VC
CHM-4-1	Dazao + Baizhi + Baihe+ Gancao + P4H transfersome + VC

larly, the mice skin were collected, rinsed with normal saline, and cut into pieces. Then skin pieces were grinded using a tissue grinde (Thermo, USA) and the homogenate was centrifuged at 4,000 rpm for 10 min to obtain the supernatant. Subsequently, the hydroxyproline content of supernatant was measured using the ELISA kit.

2.11. Animals and treatments

Kunming mice (female, 8 weeks old, 25~30 g) were obtained from Xuhe Pharmaceutical Technology Co., Ltd. (Tianjin, China) and randomly divided into 6 groups (10 per group). Mice were housed in a ventilated animal room where the temperature and humidity were maintained (temperature 25 ± 1°C and humidity control 60 ± 5%). All mice experiments were performed according to the animal experiment guidelines approved by the Institutional Animal Care Committee at Nankai University and Tianjin Institute of Pharmaceutical Research New Drug Evaluation Co. Ltd. (Tianjin, China; approval ID: IACUC 2017532268, validity period: 22 March 2017 to 22 March 2022).

Mice were provided with water and pelleted diet and libitum. Drug dosage was calculated according to the calculation formula: DM (dose per kg body weight) = DH × R × (WH/WM), as detailed in The Methodology of Pharmacological Experiment. DM and DH are doses for mice and humans, and WM and WH are body weights of mice and humans, respectively (Lin et al., 2007). According to the method of pharmacology, the dosage for mice is adjusted to 9 times of the human dosage. In the control group, 0.2 mL of 0.9% saline water was injected subcutaneously in the back neck every day. The remaining mice received subcutaneous injections of 10% D-galactose every day for 42 d to prepare the subacute mouse aging model. The mice of drug treatment group were subcutaneously injected with different concentrations of CHM-3-4, respectively. The specific grouping situation was as Table 4 follows:

2.12. HE staining

HE staining was performed to observe the changes of collagen fibers using a HE staining kit. Following sacrifice, the dorsal skin was excised from mice. Then the skin specimens (approximately 1 cm^2) were fixed in the buffered neutral formalin (4%, w/v) for 24 h. After deparaffinization and rehydration, tissue sections were stained with hematoxylin solution for 5 minutes and soaked in 1% acid ethanol (1% HCl in 75% ethanol) for 30 s and then rinsed in distilled water. Finally the sections were cleared by xylene and mounted. Pictures were taken with an inverted microscope (Nikon, Tokyo, Japan).

2.13. Statistical analysis

All statistical analyses were performed by GraphPad Prism 9.0 software. Significant differences were evaluated via the one-way analy-

Table 4. The experimental animial grouping

Grouping	0.9% saline water (mL/d)	10% D-gal injection (mL/d)	Dose of application (mL/d)
Control	0.2	0	0
Model	0	0.2	0
L (200 mg/mL CHM-3-4)	0	0.2	0.2
M (400 mg/mL CHM-3-4)	0	0.2	0.2
H (800 mg/mL CHM-3-4)	0	0.2	0.2

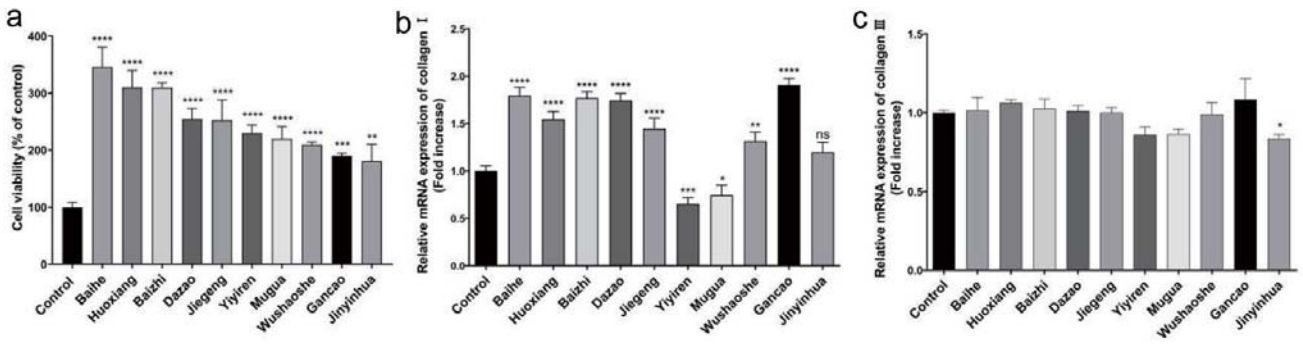

Figure 1. The effect of Gancao, Baizhi, Baihe, and Dazao extracts on cell viability and the mRNA levels of collagen. (a) Determination of cell viability in NIH-3T3 cells pretreated with ten CHM extracts. The mRNA levels of collagen I (b) and collagen III (c) in NIH-3T3 cells.

sis of variance (one-way ANOVA) were performed with GraphPad Prism. The experimental results are presented as the means ± standard deviation (SD), and P value< 0.05 was considered significant.

3. Results

3.1. *Glycyrrhizae radix et rhizoma (Gancao), Angelicae Dahuricae Radix (Baizhi), Lilii bulbus (Baihe), and Jujubae fructus (Dazao) increase the mRNA levels of type I collagen*

In order to obtain the CHM that could promote collagen expression, we measured the mRNA levels of collagen type I and III after drugs action. The effects of 82 CHM extracts on NIH-3T3 cells viability were studied through the MTT assay to to preliminarily screen drugs (Table S1, Figure S1). The top ten CHM extracts with an obvious effect on promoting cell proliferation were determined, including Baihe, *Pogostemincablin benth* (Huoxiang), Baizhi, Dazao, *Platycodonis radix* (Jiegeng), *Coicis semen* (Yiyiren), *Chaenomelis fructus* (Mugua), *Zaocys dhumnades* (Wushaoshe), Gancao, and *Lonicerae japonicae flos* (Jinyinhua) (Figure 1a). And the above CHM extracts at 5 mg/mL increased cell viability by 246.0%, 210.1%, 209.3%, 154.9%, 152.8%, 130.0%, 119.6%, 109.8%, 90.0%, and 80.8%, respectively.

Collagen type I and III are the main constituent structure of the skin (Tiganescu et al., 2018). We further evaluated the mRNA levels of collagen type I and III under the ten above CHM extracts treatment. The qRT-PCR results showed that the extracts of Gancao, Baizhi, Baihe and Dazao significantly increased the mRNA levels of collagen I by 82%, 69%, 63%, and 60%, respectively (Figure 1b). Mugua and Yiyiren both inhibited the transcript levels of type I collagen, and the other CHM extracts had no significant effect (Figure 1c). In addition, the results showed that treatment with the ten CHM extracts did not appear to significantly affect the expression of type III collagen. In this preliminary screen, four kinds of CHM had significantly promoting effects on the mRNA of collagen type I.

3.2. *Evaluation of the activity and stability of P4H*

The initial screen unveiled four CHM extracts that promoted the expression of collagen. Next, we intended to improve the stability of collagen. The P4H was recombinantly expressed and its activity and stability was examined. Viral P4H has been cloned from PBCV-1 and it can hydroxylate several synthetic peptides that corresponding to proline-rich repeats coded by the PBCV-1 genome, such as (Pro-Ala-Pro-Lys)n and $(Pro\text{-}Glu\text{-}Pro\text{-}Pro\text{-}Ala)_5$ (Myllyharju, 2003). Moreover, the proline in both positions in these repeats were hydroxylated by P4H (Eriksson et al., 1999). Mass spectrometry analysis indicated that the molecular weight of (PAPK)3 increased from 1,198.8 Da to 1,262.7 Da after incubation with P4H (Figure 2a). The result showed that the recombined P4H had the ability to selectively hydroxylate proline that located in the repeating position of (PAPK)3. Moreover, to study the stability of P4H, we measured the enzyme stability under different temperatures. We found the stability of P4H dropped as temperature increased. P4H is stable relatively when stored at 4 and 25°C (Figure 2b). In conclusion, P4H is active in proline hydroxylation and stable at room temperature.

3.3. *Preparation and characterization of P4H transfersome*

P4H has high molecular weight and is not easily absorbed by

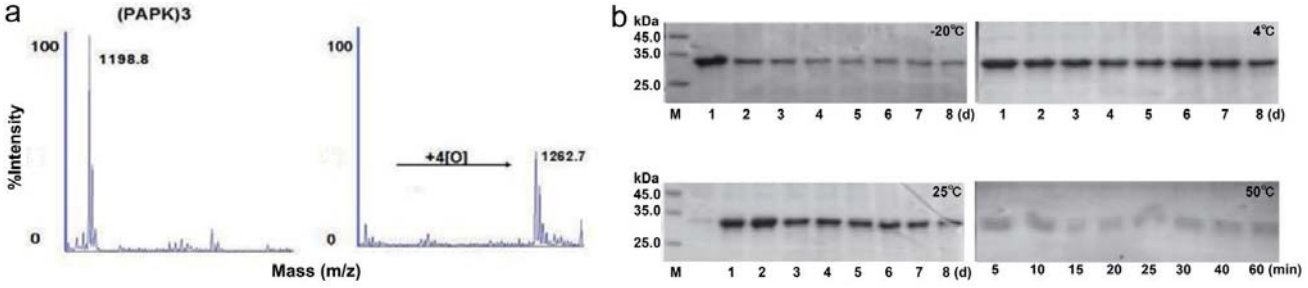

Figure 2. The activity and stability of P4H. (a) MALDI-TOF-TOF mass spectra of (PAGP)3 before and after application of P4H. (b) Effect of different temperatures on P4H stability.

Table 5. Encapsulation efficiency of P4H at different factor levels of the ratio of soy lecithin and cholesterol (A), total lipid concentration (B), and drug concentration (C), respectively

Number	A	B	C	Encapsulation efficiency(%)
1	1	2	1	22.0
2	1	1	2	36.9
3	1	3	3	18.5
4	2	2	2	15.6
5	2	1	3	26.4
6	2	3	1	13.6
7	3	2	3	24.5
8	3	1	1	20.9
9	3	3	2	22.1

the skin. So, transfersome was prepared to make P4H achieve a higher transdermal permeability. Transfersome is highly flexible vesicle and is widely used for skin delivery systems (Azimi et al., 2019). The stability of transfersome is involved with the types and the ratio of constituents used in their preparation (Hua et al., 2017). An orthogonal test was designed to study the optimum conditions for the preparation of P4H transfersome (Table 5). According to the value of range R (Table 6), the order of importance that influenced encapsulation rate of P4H transfersome was found to be (B) total lipid concentration > (A) ratio of soy lecithin and cholesterol > (C) enzyme concentration. The optimum combination of factors was A1B1C2, namely, ratio of soy lecithin to cholesterol of 9 : 1, total lipid concentration of 6%, and enzyme concentration of 5 mg/mL, while the encapsulation rate of P4H transfersome was 36.9%. In addition, as shown in the electron micrograph (Figure 3a), the newly prepared P4H transfersome was uniform in size and shape.

3.4. Transdermal rate of P4H transfersome

Next, the transdermal permeation efficiency of different P4H solutions was compared. Result showed that P4H transfersome solution had a better transdermal rate in a time- and concentration-dependent manner, reaching 13.05% at 10 h (Figure 3b). In contrast, P4H liposome solution and P4H solution had no permeation of P4H basically. The transfersome greatly overcome the insufficient skin penetration of P4H.

Table 6. Intuitive analysis of the test results

Index	A	B	C
K1	75.4	84.2	54.5
K2	55.6	60.1	74.6
K3	67.5	54.2	69.4
k1	25.1	28.1	18.2
k2	18.5	20.0	24.9
k3	22.5	18.1	23.1
R	6.6	10.0	6.7

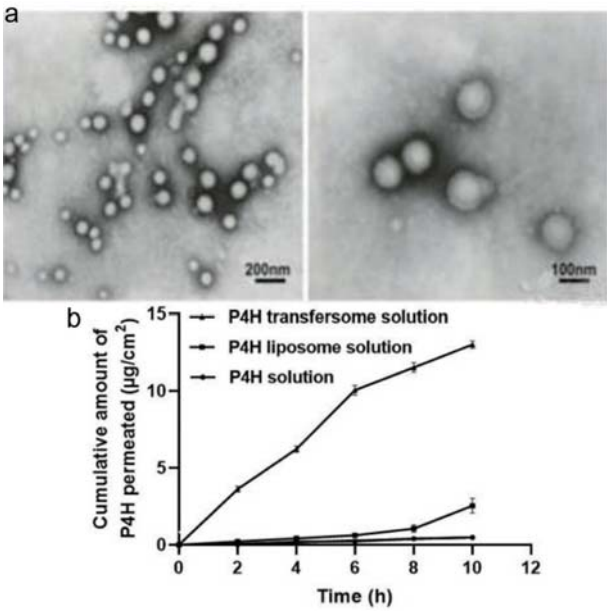

Figure 3. The P4H with homogeneous particle size and good transdermal rate was successfully prepared. (a) Transmission electron microscopy image of the P4H transfersome. (b) Cumulative P4H permeation of P4H transfersome solution, P4H liposome solution, and P4H solution, respectively.

3.5. The CHM-3-4 promotes collagen synthesis in NIH-3T3

The concept of the composition is to combine Chinese herbal medicines and P4H to explore a method of efficiently replenishing collagen in skin. To select the most efficient combination, a hydroxyproline assay was used to measure collagen content. The measurement of hydroxyproline levels can be used as an indicator of collagen content (Qiu et al., 2020). After 24 h of combination treatment, we assessed the levels of hydroxyproline in NIH-3T3 cells. Compared with the control group, the collagen content in combination treated groups was higher ($P < 0.05$), especially in CHM-3-4 treated group (Figure 4). Results suggested that CHM-3-4 treatment of NIH-3T3 fibroblasts could effectively promote collagen synthesis.

3.6. The CHM-3-4 promotes collagen synthesis in the skin of D-galactose-induced aging mice

Mouse chronically injected with D-galactose has been widely used as an aging animal model for anti-aging pharmacology research. Excessive D-galactose accumulated in the body will be converted into galactitol which can not be metabolized normally. The galactitol will further affect the osmotic pressure of cells, resulting in increased levels of reactive oxygen species, and damage to cells, and finally leading to aging (Palacios-Pedrero et al., 2021). HE staining illustrated the increased epidermal thickness of mice skin caused by D-galactose (Figure 5). In the control group, the epidermal thickness of mice was uniform and the collagen fibers in the dermis were wavy and arranged in order. Compared with the control group, D-galactose altered the epidermal and dermal morphology, which was characterized by epidermal thickening and a fracture of collagen fibers. Compared with the model group, the mice

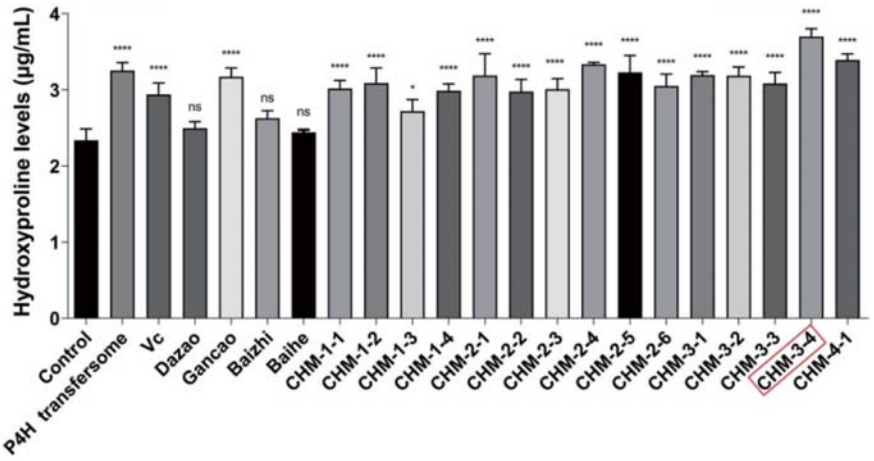

Figure 4. The combinations improve the content of hydroxyproline in NIH-3T3 cells.

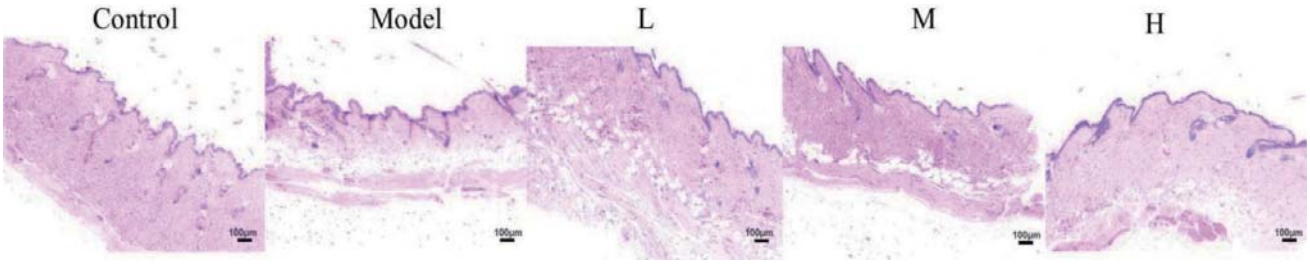

Figure 5. HE staining of cross-sectional slices from the dorsal skin of mice, magnification, ×100.

skin treated with CHM-3-4 had thinner epidermal thickness and more normal collagen fibers. The result confirmed that CHM-3-4 provided effective protection against D-galactose-induced damages to skin. It indicated that CHM-3-4 could alleviate collagen degradation in skin aging caused by D-galactose to some extent.

In addition, we examined whether the collagen content was increased in mice skin after combination treatment. Compared with the control group, the collagen content of mice skin in the model group was decreased by 25.4% ($P < 0.01$) (Figure 6). Compared with the model group, skin treated with high-dose combination had high collagen content. We have also seen an increase of collagen content in mice skin treated with the low-dose and middle-dose combination. It can be concluded that the CHM-3-4 could promote collagen synthesis in mice skin.

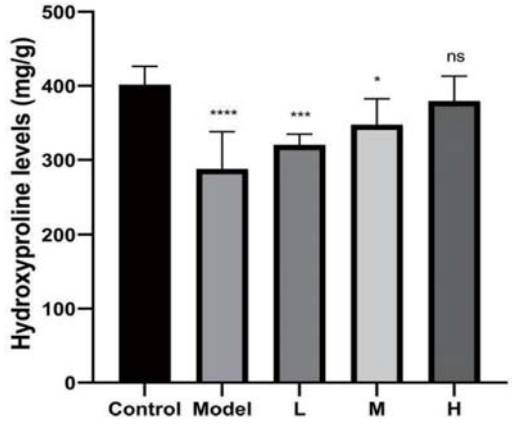

Figure 6. The hydroxyproline content in skin tissue of mice.

4. Discussion

In this study, we developed a novel combination consisting of Baizhi, Baihe, Gancao, P4H transfersome and VC for promoting collagen production and stabilizing the collagen structure in skin. We found that the combination showed an enhanced effect on the mRNA levels of type I collagen. Moreover, this combination also delayed the D-galactose-induced skin aging in mice. Thus, we suggested that this combination could be a potential candidate to be used as an anti-skin-aging product.

It has been reported that the therapeutic effect of reasonable combinations may be superior to single component (Ruan et al., 2006). Multicomponent interventions offer bright prospects for the control of complex diseases in a synergistic manner (Li et al., 2011). The concept of our study is to combine CHM with modern biotechnology to develop an anti-skin-aging agent. CHM, a kind of natural resources with abundant sources, has the characteristics of small side effects, simple and easy to use, and has been widely applied to skin maintenance (Li et al., 2022). Alternatively, mostly of topical collagen-containing products only focus on promoting collagen production and ignore to stabilize the structure of collagen. To compensate this defect, the recombinant P4H was successfully expressed in *E. coli*. At the same time, we added cofactors in the combination with P4H. In this study, the novel combination we prepared could play to the advantages of each component. It not only promoted col-

lagen synthesis but also stabilized the structure of collagen. Besides, we prepared transfersome which greatly improved the transdermal absorption of combination. In a word, this combination holds great promise for the resistance of skin aging due to its excellent ability in collagen biosynthesis and structural stability.

The choice of CHM to promoting collagen production for this study is because some traditional Chinese medicines could effectively delay skin aging and were expected to be developed as anti-skin-aging drugs in the future. And we selected 82 CHM extracts to determine whether could be used for skin benefit (Wang et al., 2021). Immediately afterward, we utilized the cell viability experiments to screen ten CHM extracts. Then in the in vitro studies, we found that four kinds of CHM (Baizhi, Baihe, Gancao, and Dazao) among ten above could promote the expression of type I collagen in NIH-3T3 cells. This indicated that these CHM extracts have beneficial action for the alleviation of skin aging. It has been reported that glycyrrhizin, a natural extract from the licorice roots, is generally considered to offer protection against cellular senescence (Zhang et al., 2022). Matrix metalloproteinases (MMPs) are known to contribute to the degradation of collagen during ultraviolet irradiation (Yamada et al., 2021). The flavonoid aicalein from Baihe protects cells from UVB irradiation–induced MMP-1 expression. Ursonic acid from Dazao downregulates the transcriptional expression of gelatinases (MMP-2 and MMP-9) by inhibiting of ERK and CREB signaling pathways in NSCLC cells (Maione-Silva et al., 2019). Moreover, ursonic acid suppresses the transcriptional levels of MMP-1 through reduced activation of ERK and c-Fos signaling pathways in HaCaT keratinocytes (Son and Lee, 2020). From the available literature, we speculated that the combination may play an important role in collagen synthesis by downregulating MAPK signaling. Future studies will further explore how the combination promotes the expression of collagen and the underlying mechanisms involved.

In this study, P4H was recombinantly expressed in *E. coli* to maintain the collagen structure. Prolyl hydroxylation is a post-translational modification that affects the structure, stability and function of collagen. P4H can catalyse hydroxylation of proline to hydroxyproline and plays a central role in the formation and stabilization of the triple helical domain of collagens (Zou et al., 2017). VC is a cofactor of P4H that modifies newly synthesized collagen on the route for secretion (Zhao et al., 2019). Stability tests at different temperatures showed that P4H was highly stable at room temperature. Additionally, the skin permeation of P4H is poor, due to its high molecular weight and hydrophilicity. Therefore, we prepared the P4H transfersome for the purposes of increasing permeability. Transfersome, also known as flexible liposome, has good biocompatibility and biodegradability (Gai et al., 2020). In addition, the transfersome is highly hydrophilic, which helps the drug to permeate through the hydrophilic layer of the skin, i.e., epidermis (Krenczkowska et al., 2020). Here, we prepared the P4H transfersome by thin film hydration method. On the basis of the orthogonal experiments, the optimal conditions were determined as following: ratio of soy lecithin to cholesterol of 9 : 1, total lipid concentration of 6%, and enzyme concentration of 5 mg/mL. The encapsulation rate of P4H transfersome was 36.9% under these conditions. Soy lecithin and cholesterol are used as liposome wall materials and are able to enhance the bioactivity by improving drug solubility and bioavailability. This might be explained by the fact that if the ratio was small, cholesterol content was relatively high, and the formed film is relatively flexible (Park et al., 2019). After screening various combinations of solvents, soy lecithin: cholesterol in ratio 9 : 1 was selected to prepare the P4H transfersome.

The current study established an in vitro cell model using NIH-3T3 to investigate the functions of CHM extracts in regulating collagen synthesis. The murine cell line NIH-3T3 has been used as a model system in a multitude of different studies since its first description in 1963 (Salih et al., 2017). In practice, NIH-3T3 fibroblasts are often used as adesirable cell models for evaluating collagen expression. During the biological progression of skin aging, the aberrant production of collagen plays a crucial role. Thus we assayed cell proliferation and collagen production of CHM extracts in NIH-3T3. The effect of combination on the skin of aging mice was assessed. We are aware that there is still room for improvement in our study. Our current study showed the beneficial effects of CHM with the use of simple NIH-3T3 cells and animal models. And in the future, more diverse cell lines and more advanced experimental models such as human 3D skin equivalents will be used to optimize our combination. Moreover, novel technologies such as network pharmacology will be used to explore the mechanism of action of the CHM combination in the present work (Wang et al., 2022; Zuo et al., 2018).

5. Conclusion

In this study, we designed a novel combination (Baizhi+Baihe+Gancao+P4H transfersome+VC), which effectively promoted the mRNA levels of collagen in NIH-3T3 cells. Moreover, this conclusion also verified in animal models. Taken together, we obtained a combination that could delay skin aging by promoting the generation of collagen.*These findings* suggest *the* combination to *be* a promising component for use in cosmetics or supplements that is being developed for anti-aging applications.

Acknowledgments

We would like to thanks to Jishou University for the fund support.

Statement of ethics

The study was conducted according to the standards of laboratory animals (GB14925-2001), and approved by the Institutional Review Board (or Ethics Committee) of Animal Ethics Committee of Tianjin International Joint Academy of Biomedicine.

Data availability statement

All data generated or analyzed during this study are included in this article. Further enquiries can be directed to the corresponding author.

Funding

This research was funded by China Postdoctoral Science Foundation (2020T130093ZX) and Open Project of Hunan Provincial Engineering Laboratory for Conservation and Comprehensive Utilization of Giant Salamander Resources (DNOC2101).

Conflict of interest

All authors reveal no conflict of interest in this study.

Supplementary material

Table S1. Chinese herbal medicines datebase.

Figure S1. Determination of cell viability in NIH-3T3 cells pretreated with CHM extracts.

References

Azimi, M., Khodabandeh, M., Deezagi, A., and Rahimi, F. (2019). Impact of the transfersome delivered human growth hormone on the dermal fibroblast cells. Curr. Pharm. Biotechnol. 20(14): 1194–1202.

Chen, Y., Yang, S., Lovisa, S., Ambrose, C.G., McAndrews, K.M., Sugimoto, H., and Kalluri, R. (2021). Type-I collagen produced by distinct fibroblast lineages reveals specific function during embryogenesis and osteogenesis imperfecta. Nat. Commun. 12(1): 7199.

Chattopadhyay, S., and Raines, R.T. (2014). Review collagen-based biomaterials for wound healing. Biopolymers 101(8): 821–833.

Edgar, S., Hopley, B., Genovese, L., Sibilla, S., Laight, D., and Shute, J. (2018). Effects of collagen-derived bioactive peptides and natural antioxidant compounds on proliferation and matrix protein synthesis by cultured normal human dermal fibroblasts. Sci. Rep. 8(1): 10474.

Elsayed, M.M., Abdallah, O.Y., Naggar, V.F., and Khalafallah, N.M. (2007). Deformable liposomes and ethosomes as carriers for skin delivery of ketotifen. Die Pharmazie 62(2): 133–137.

Eriksson, M., Myllyharju, J., Tu, H., Hellman, M., and Kivirikko, K.I. (1999). Evidence for 4-hydroxyproline in viral proteins. Characterization of a viral prolyl 4-hydroxylase and its peptide substrates. J. Biol. Chem. 274(32): 22131–4.

Froger, A., and Hall, J.E. (2007). Transformation of plasmid DNA into E. coli using the heat shock method. J. Visualized Exp. (6): e253.

Gai, X., Liu, C., Wang, G., Qin, Y., Fan, C., Liu, J., and Shi, Y. (2020). A novel method for evaluating the dynamic biocompatibility of degradable biomaterials based on real-time cell analysis. Regener. Biomater. 7(3): 321–329.

Hua, S., and Wu, S.Y. (2013). The use of lipid-based nanocarriers for targeted pain therapies. Front. Pharmacol. 4: 143.

Huang, L., Massa, L., and Karle, J. (2009). Kernel energy method applied to vesicular stomatitis virus nucleoprotein. Proc. Natl. Acad. Sci. 106(6): 1731–1736.

Jepps, O.G., Dancik, Y., Anissimov, Y.G., and Roberts, M.S. (2013). Modeling the human skin barrier-towards a better understanding of dermal absorption. Adv. Drug Delivery Rev. 65(2): 152–168.

Krenczkowska, D., Mojsiewicz-Pieńkowska, K., Wielgomas, B., Bazar, D., and Jankowski, Z. (2020). Ex vivo human skin is not a barrier for cyclic siloxanes (cyclic silicones): Evidence of diffusion, bioaccumulation, and risk of dermal absorption using a new validated GC-FID procedure. Pharmaceutics 12(6): 586.

Kwatra, B. (2022). Collagen supplementation: therapy for skin disorders: a review. World J. Pharm. Sci. 9(5): 2504–2518.

Lagarto, J.L., Nickdel, M.B., Kelly, D.J., Price, A., Nanchahal, J., Dunsby, C., French, P., and Itoh, Y. (2020). Autofluorescence lifetime reports cartilage damage in osteoarthritis. Sci. Rep. 10(1): 2154.

Li, S., Zhang, B., and Zhang, N. (2011). Network target for screening synergistic drug combinations with application to traditional Chinese medicine. BMC Syst. Biol. 5: 1–13.

Li, Z.Y., Li, X.K., Lin, Y., Feng, N., Zhang, X.Z., Li, Q.L., and Li, B.Q. (2022). A comparative study of three chemometrics methods combined with excitation-emission matrix fluorescence for quantification of the bioactive compounds aesculin and aesculetin in Cortex Fraxini. Front. Chem. 10: 984010.

Lin, Q.P., Guo, R.P., Xu, X.Y., and Liu, C.H. (2007). Preparation and quality evaluation of curcumin liposomes for injection. Chin. J. Nat. Med. 5(3): 207–210.

Lin, X.J., and Chen, C.Y. (2007). Advances on study of treatment of lumbar disk herniation by Chinese medicinal herbs. China J. Chin. Mater. Med. 32(3): 186–191.

Maione-Silva, L., De Castro, E.G., Nascimento, T.L., Cintra, E.R., Moreira, L.C., Cintra, B.A.S., Valadares, M.C., and Lima, E.M. (2019). Ascorbic acid encapsulated into negatively charged liposomes exhibits increased skin permeation, retention and enhances collagen synthesis by fibroblasts. Sci. Rep. 9(1): 522.

Myllyharju, J. (2003). Prolyl 4-hydroxylases, the key enzymes of collagen biosynthesis. Matrix Biol. 22(1): 15–24.

Palacios-Pedrero, M.Á., Osterhaus, A.D.M.E., Becker, T., Elbahesh, H., Rimmelzwaan, G.F., and Saletti, G. (2021). Aging and options to halt declining immunity to virus infections. Front. Immunol. 12: 681449.

Park, P., Franco, L.R., Chaimovich, H., Coutinho, K., Cuccovia, I.M., and Lima, F.S. (2019). Binding and flip as initial steps for BP-100 antimicrobial actions. Sci. Rep. 9(1): 8622.

Qiu, R., Murata, S., Oshiro, K., Hatada, Y., and Taniguchi, H. (2020). Transplantation of fetal liver tissue coated by ultra-purified alginate gel over liver improves hepatic function in the cirrhosis rat model. Sci. Rep. 10(1): 8231.

Ricard-Blum, S. (2011). The collagen family. Cold Spring Harbor Perspect. Biol. 3(1): a004978.

Ruan, W.J., Lai, M.D., and Zhou, J.G. (2006). Anticancer effects of Chinese herbal medicine, science or myth? J. Zhejiang Univ., Sci., B 7: 1006–1014.

Salih, A.M., Kakamad, F.H., Essa, R.A., Rauf, G.M., Masrur, S.A., Shvan, H.M., Rawezh, Q.S., Hunar, A.H., Dahat, A.H., and Othman, S. (2017). Porocarcinoma: A systematic review of literature with a single case report. Int. J. Surg. Case Rep. 30: 13–16.

Schäfer, L., Sorokowska, A., Sauter, J., Schmidt, A.H., and Croy, I. (2020). Body odours as a chemosignal in the mother–child relationship: new insights based on an human leucocyte antigen-genotyped family cohort. Philos. Trans. R. Soc., B 375(1800): 20190266.

Schoeman, R., Beukes, N., and Frost, C. (2020). Cannabinoid combination induces cytoplasmic vacuolation in MCF-7 breast cancer cells. Molecules 25(20): 4682.

Schoel, B., Welzel, M., and Kaufmann, S.H. (1995). Quantification of protein in dilute and complex samples: modification of the bicinchoninic acid assay. J. Biochem. Biophys. Methods 30(2-3): 199–206.

Son, J., and Lee, S.Y. (2020). Ursonic acid exerts inhibitory effects on matrix metalloproteinases via ERK signaling pathway. Chem.-Biol. Interact. 315: 108910.

Stephens, E.H., and Grande-Allen, K.J. (2007). Age-related changes in collagen synthesis and turnover in porcine heart valves. J. Heart Valve Dis. 16(6): 672–682.

Tiganescu, A., Hupe, M., Uchida, Y., Mauro, T., Elias, P.M., and Holleran, W.M. (2018). Topical 11 β-Hydroxysteroid dehydrogenase type 1 inhibition corrects cutaneous features of systemic glucocorticoid excess in female mice. Endocrinology 159(1): 547–556.

Wang, L., Zuo, X., Ouyang, Z., Qiao, P., and Wang, F. (2021). A systematic review of antiaging effects of 23 traditional Chinese medicines. Evidence-Based Complementary Altern. Med. 2021: 1–13.

Wang, X., Hu, Y., Zhou, X., and Li, S. (2022). Network pharmacology and traditional medicine: Setting the new standards by combining in silico and experimental work. Front. Pharmacol. 13: 1002537.

Yamada, C., Ho, A., Akkaoui, J., Garcia, C., Duarte, C., and Movila, A. (2021). Glycyrrhizin mitigates inflammatory bone loss and promotes expression of senescence-protective sirtuins in an aging mouse model of periprosthetic osteolysis. Biomed. Pharmacother. 138: 111503.

Zhang, H., Kang, J., Guo, W.Y., Wang, F., Guo, M., Feng, S., Zhou, W., Li, J., Tahir, A.T., Wang, S., Du, X., Zhao, H., Wang, W., Zhu, H., and Zhang, B. (2022). An optimal medicinal and edible Chinese herbal formula attenuates particulate matter-induced lung injury through its anti-oxidative, anti-inflammatory and anti-apoptosis activities. Chin. Herb. Med. 15(3): 407–420.

Zhang, Y., Lin, X., Zhang, L., Hong, W., and Zeng, K. (2018). MicroRNA-222 regulates the viability of fibroblasts in hypertrophic scars via matrix metalloproteinase 1. Exp. Ther. Med. 15(2): 1803–1808.

Zhang, Q., Zhou, D., Wang, H., and Tan, J. (2020). Heterotopic ossification of tendon and ligament. J. Cell. Mol. Med. 24(10): 5428–5437.

Zhao, B., Zhang, Y., Xiong, Y., and Xu, X. (2019). Rutin promotes the formation and osteogenic differentiation of human periodontal ligament stem cell sheets in vitro. Int. J. Mol. Med. 44(6): 2289–2297.

Zou, Y., Donkervoort, S., Salo, A.M., Foley, A.R., Barnes, A.M., Hu, Y., Ma-

kareeva, E., Leach, M.E., Mohassel, P., Dastgir, J., Deardorff, M.A., Cohn, R.D., DiNonno, W.O., Malfait, F., Lek, M., Leikin, S., Marini, J.C., Myllyharju, J., and Bönnemann, C.G. (2017). P4HA1 mutations cause a unique congenital disorder of connective tissue involving tendon, bone, muscle and the eye. Hum. Mol. Genet. 26(12): 2207–2217.

Zuo, J., Wang, X., Liu, Y., Ye, J., Liu, Q., Li, Y., and Li, S. (2018). Integrating network pharmacology and metabolomics study on anti-rheumatic mechanisms and antagonistic effects against methotrexate-induced toxicity of Qing-Luo-Yin. Front. Pharmacol. 9: 1472.

Journal of Food Bioactives
International Society for Nutraceuticals and Functional Foods
Original Research
J. Food Bioact. 2024;25:72–80

Exploring the anti-inflammatory effect of clove water extract in lipopolysaccharide-stimulated RAW264.7 cells and mouse peritoneal macrophages

Sellen Gurusmatika[a], Momoko Ishida[b,c], Kosuke Nishi[a,b,c] and Takuya Sugahara[a,b,c*]

[a]Department of Applied Bioresource Science, The United Graduate School of Agricultural Sciences, Ehime University, Matsuyama, Ehime 790-8566, Japan
[b]Department of Bioscience, Graduate School of Agriculture, Ehime University, Matsuyama, Ehime 790-8566, Japan
[c]Food and Health Function Research Center, Ehime University, Matsuyama, Ehime 790-8566, Japan
[*]**Corresponding author:** Takuya Sugahara, Department of Bioscience, Graduate School of Agriculture, Ehime University, Matsuyama, Ehime 790-8566, Japan. Tel: +81-89-946-9863; E-mail: sugahara.takuya.mz@ehime-u.ac.jp
DOI: 10.31665/JFB.2024.18373
Received: January 31, 2024; **Revised received & accepted:** March 06, 2024
Citation: Gurusmatika, S., Ishida, M., Nishi, K., and Sugahara, T. (2024). Exploring the anti-inflammatory effect of clove water extract in lipopolysaccharide-stimulated RAW264.7 cells and mouse peritoneal macrophages. J. Food Bioact. 25: 72–80.

Abstract

Clove (*Syzygium aromaticum* L) is a precious spice that has been extensively used by many countries over the centuries to add flavor and for medicinal purposes. Because of its abundance of phytochemical compounds, clove has been shown to have positive benefits on human health. Hence, we investigated the anti-inflammatory activity of clove water extract (CWE) in LPS-stimulated RAW264.7 cells and mouse peritoneal macrophages. The results showed that CWE significantly inhibited the production of IL-6 and TNF-α in a dose-dependent manner, as well as the production of nitric oxide (NO), without any cytotoxic effects at less than 20 mg/mL, through down-regulating IL-6, TNF-α, and iNOS gene expression. Moreover, CWE impeded the MAPKs and inhibited the translocation of NF-κB from the cytosol to the nucleus. These results suggest that CWE possesses anti-inflammatory properties by inhibiting the MAPKs and NF-κB pathways.

Keywords: anti-inflammation; cytokines; clove; macrophages; MAPK; NF-κB.

1. Introduction

Inflammation plays a key role in the body's immune defense mechanism (Venkatalakshmi et al., 2016) and thus has been of special concern to scientists around the world for a long time. It is an immune response that recognizes and neutralizes invasion by harmful microbes, prevents infection, and initiates the wound-healing process (Duque and Descoteaux, 2014; Oishi and Manabe, 2018). Inflammation can be either chronic or linked to disorders such as mental illness, cardiovascular diseases, cancer, autoimmune diseases, and diabetes (Netea et al., 2017; Hirano, 2021). Cell and tissue damage may arise from an unbalanced response between immune stimulation and resolution, which causes excessive inflammatory cytokine production (Leiherer et al., 2013; Duque and Descoteaux, 2014).

Macrophages, important components of the immune system, are capable of eliminating pathogens, destroying dead cells, and initiating inflammation through cytokine signaling regulation and growth factors (Sigola et al., 2016; Hamidzadeh et al., 2017). Suppressing production of inflammatory mediators is one effective therapeutic approach for treating inflammatory disorders and combating harmful chronic inflammation (Scull et al., 2010; Oishi and Manabe, 2018). Recently, healthy food choices and therapeutic compounds from herbal medicine have gained interest for treating and reducing the risk of inflammation diseases. Natural products also have several other characteristics such as being non-toxic, effective, and secure in applying pharmacologically due to their pleiotropic immunomodulatory properties (Ali et al., 2008; Jiang, 2019; Ugbogu et al., 2021).

Clove (*Syzygium aromaticum* L) is a dried flower bud from the

clove tree in the family Myrtaceae, and is commercially cultivated in Indonesia, Madagascar, India, and China. Since ancient times, clove has been largely used as a spice in cooking to improve flavor, as a cosmetic, and for medicinal purposes (Cortés-Rojas et al., 2014). This plant is abundant in phytochemical compounds such as eugenol, gallic acid, and eugenol acetate. The essential oil of clove has been reported to possess positive biological activities such as antioxidant, antimicrobial, antinociceptive, anti-depressant, and anticancer (El-Maati et al., 2016; Hu et al., 2018; Haro-González et al., 2023). However, there are only a limited number of studies on the potential of water extracts of clove. Hence, this study aimed to investigate the anti-inflammatory effect of clove water extract (CWE) in lipopolysaccharide (LPS)-stimulated RAW264.7 cells and mouse peritoneal macrophages (P-mac), and its mechanism of action involved in the iNOS, mitogen-activated protein kinase (MAPK), and NF-κB signaling pathways.

2. Materials and methods

2.1. Materials

Clove powder was purchased from S&B Foods Inc. (Tokyo, Japan). Roswell Park Memorial Institute 1640 (RPMI 1640) medium and WST-8 reagent were obtained from Nacalai Tesque (Kyoto, Japan). Fetal bovine serum (FBS), Dulbecco's modified Eagle's medium (DMEM), and LPS from *Escherichia coli* 026/B6 were purchased from Sigma-Aldrich (St. Louis, MO, USA). The enzyme-linked immunosorbent assay (ELISA) kits for IL-6 and TNF-α were purchased from BioLegend (San Diego, CA, USA) and Invitrogen (Carlsbad, CA, USA), respectively. Goat anti-rabbit IgG antibody and antibodies against ERK1/2, phosphorylated ERK1/2, JNK, phosphorylated JNK, p38, phosphorylated p38, histone H3, NF-κB p65, and glyceraldehyde-3-phosphate dehydrogenase (GAPDH) were purchased from Cell Signaling Technology (Danvers, MA, USA). The reagents and chemicals used were of analytical grade.

2.2. Sample preparation

Based on previous research (Pandey et al., 2024) which mentions several components contained in clove and following the method by Nishi et al. (2021), the water extraction of clove components was performed as followings. Clove powder was suspended in distilled water at 100 mg/mL and homogenized overnight at 12°C. The mixture was subsequently centrifuged at 70,000 ×g for 1 h at 4°C, filtrated using a 0.45 μm membrane, and freeze-dried. The freeze-dried clove extract was weighed and then dissolved in distilled water at 40 mg/mL. The clove extract was filtered using a 0.22 μm membrane for sterilization. This water extract was referred to as CWE and used for further experiments.

2.3. Cells and cell culture

The mouse macrophage-like cell line RAW264.7 cells were obtained from the European Collection of Authenticated Cell Cultures (ECACC, London, UK). The medium used to culture the cells was DMEM supplemented with 10% FBS and antibacterial compounds (100 U/mL of penicillin and 100 μg/mL of streptomycin). The cells were incubated at 37°C under humidified 5% CO_2 in air. Meanwhile, to collect P-mac, 8-week-old female BALB/c mice (Japan SLC, Hamamatsu, Japan) were injected into the peritoneum with 3 mL of sterile 3.0% thioglycolate and left for 3 days to deteriorate the peritoneum. Three days after injection, peritoneal exudate cells were collected through lavaging the peritoneal cavity by injection of 3 mL of phosphate-buffered saline (PBS, pH 7.4). Harvested cells were centrifuged at 200 ×g for 5 min at 4°C, and the cell pellet was washed with RPMI 1640 medium and centrifuged again. The cell pellet was then suspended in 10% FBS-RPMI 1640 medium and incubated for 2 h. After incubation for 2 h, adherent cells were used as P-mac. In the subsequent experiments, P-mac was detached by pipetting in cold PBS. All animal experiments described were conducted by protocols approved by the Ehime University Animal Care and Use Committee and were performed under applicable guidelines and regulations for the Care and Use of Laboratory Animals of Ehime University.

2.4. Cell viability

The cytotoxicity of CWE against RAW264.7 cells and P-mac was analyzed using WST-8 reagents according to a published method (Ishida et al., 2022). The RAW264.7 cells and P-mac were seeded in 96-well culture plates (Violamo, Osaka, Japan) at a concentration of 2.0×10^5 cells/well in 10% FBS-DMEM and 10% FBS-RPMI 1640 medium, respectively, and cultured for 18 h in a CO_2 incubator. After removing the medium, 200 μL of fresh 10% FBS-DMEM or 10% FBS-RPMI 1640 medium containing 1 μg/mL of LPS and serial concentrations of CWE were added to each well and cultured for 6 h. Subsequently, after washing the cells with fresh medium, 200 μL of fresh medium containing 5% WST-8 was added to each well, and the cells were incubated for 30 min at 37°C in the dark. Cell viability was measured at 450 nm with reference at 655 nm using an iMark microplate reader (Bio-Rad Laboratories, Hercules, CA, USA).

2.5. Cytokine production

The amounts of IL-6 and TNF-α produced by the LPS-stimulated RAW264.7 cells and P-mac were measured according to a previous study (Gurusmatika et al., 2023) by using the mouse IL-6 and mouse TNF-α ELISA kits, respectively. The RAW264.7 cells and P-mac at a density of 2.0×10^5 cells/well were seeded in 96-well culture plate in 10% FBS-DMEM for the RAW264.7 cells or 10% FBS-RPMI 1640 medium for the P-mac in a CO_2 incubator. After 18 h of incubation and the culture medium was discharged, the cells were treated with fresh 10% FBS-DMEM for the RAW264.7 cells or 10% FBS-RPMI 1640 medium for the P-mac. To stimulate the cells, 1 μg/mL LPS was added at the indicated periods in the presence or absence of CWE, then incubated for 6 h in a CO_2 incubator. After incubation, the culture media were collected, and the concentrations of IL-6 and TNF-α were then measured using the respective ELISA kits. The assays were done in triplicate.

2.6. Nitric oxide (NO) production

RAW264.7 cells were seeded into a 96-well culture plate (2.0×10^5 cells/well) in 10% FBS-DMEM and cultured for 28 h in a CO_2 incubator. After incubation, fresh medium containing 1 μg/mL of LPS, 20 ng/mL of IFN-γ, and serial concentrations of CWE were administered to change the medium, followed by incubation for 24 h in a CO_2 incubator. The NO concentration in the culture medium was analyzed by using a Griess Reagent System kit (Promega, Madison, WI, USA) according to the manufacturer's instructions.

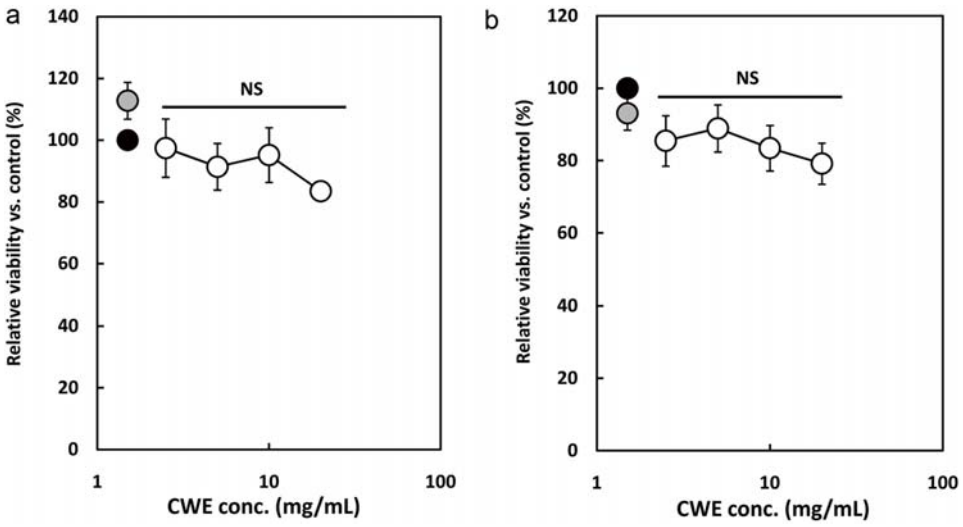

Figure 1. Effect of clove water extract (CWE) on the cell viability of lipopolysaccharide (LPS)-stimulated RAW264.7 cells and mouse peritoneal macrophages (P-mac). The RAW264.7 cells and P-mac were treated with 1 μg/mL of LPS and serial concentrations of CWE for 6 h. Relative viable cell number was then measured using a WST-8 reagent. Data are presented as the mean ± SD (n = 3). NS indicates no statistical significance against control (LPS) using the Tukey test. (a) RAW264.7 cells. (b) P-mac. Black circle: LPS without CWE (control); grey circle: distilled water without LPS (blank); open circles: LPS with CWE.

The absorbance of the mixture solution at 540 nm was measured using the iMark microplate reader.

2.7. Real-time RT-PCR

RAW264.7 cells were cultured in a 24-well culture plate at 3.0 × 10^5 cells/well in 10% FBS-DMEM for 18 h in a CO_2 incubator. After preculture, the cells were treated with 1 μg/mL of LPS and serial concentrations of CWE or distilled water as control in 10% FBS-DMEM, then incubated for 6 h in a CO_2 incubator. Total RNA was collected from the cells using Sepasol-RNA I super G (Nacalai Tesque) and used as a template for cDNA synthesis. As described by Ishida et al. (2019), real-time RT-PCR was performed with slight modifications. In brief, the reagents were prepared as follows: 10 μL of Thunderbird SYBR qPCR Mix (Toyobo, Osaka, Japan), 1 μM forward primer, 1 μM reverse primer, and 0.1 μg of a cDNA sample. The PCR amplification conditions were 3 s at 95°C and 30 s at 60°C. The PCR was performed using a StepOnePlus System (Applied Biosystems, Foster City, CA, USA). Relative gene expression was normalized to the β-actin gene expression level. Specific oligonucleotide sequences used for each gene are as follows: mouse β-actin, 5′-CATCCGTAAAGACCTCTATGCCAAC-3′ (forward) and 5′-ATGGAGCCACCGATCCACA-3′ (reverse); mouse TNF-α, 5′-CTACTCCCAGGTTCTCTTCAA-3′ (forward) and 5′-GCAGAGAGGAGGTTGACTTTC-3′ (reverse); mouse IL-6, 5′-AAGCCAGATCCTTCAGAGAGAT-3′ (forward) and 5′-TTGGATGGTCTTGGTCCTTAGC-3′ (reverse); mouse iNOS, 5′-CCAAGCCCTCACCTACTTCC-3′ (forward) and 5′-CTCTGAGGGCTGACACAAGG-3′ (reverse).

2.8. Western blotting

RAW264.7 cells were seeded in a 6-well culture plate at 5.0 × 10^5 cells/well in 10% FBS-DMEM and cultured in a CO_2 incubator for 18 h. After the cells were twice washed with sterilized PBS, the medium was changed to 10% FBS-DMEM containing 1 μg/mL LPS and serial concentrations of CWE or distilled water as control, then incubated for 15 min in a CO_2 incubator. The cells were lysed using a homogenizer and centrifuged at 12,000 rpm, 4°C for 1 min (cytosol) and 5 min (nucleus). The cytosolic and nuclear proteins were prepared using a CelLytic NuCLEAR Extraction kit (Sigma-Aldrich). After processing the protein separation using SDS-PAGE, the proteins were transferred to a polyvinylidene fluoride (PVDF) membrane (Hybond-P; GE Healthcare, Buckinghamshire, UK) using a transblotting instrument. Immunoblotting with various antibodies was performed as previously described (Gurusmatika et al., 2017). Specific protein and serial concentrations of CWE or distilled water as control bands were visualized using a ChemiDoc XRS Plus apparatus (Bio-Rad Laboratories), and the chemiluminescent intensity was quantified using Quantity One software (Bio-Rad Laboratories).

2.9. Statistical analysis

All experiments were repeated in triplicate. Data were shown as mean ± standard deviation (SD). Differences among groups were tested using the Tukey multiple comparison test. $^{*}p < 0.05$, $^{**}p < 0.01$, and $^{***}p < 0.001$ against control were considered statistically significant.

3. Results

3.1. Effect of CWE on cell viability of LPS-stimulated RAW264.7 cells and P-mac

The cytotoxic effect of CWE was evaluated using a WST-8 assay to determine the optimal concentration that is acceptable for subsequent experiments. A cell viability test was performed using a WST-8 kit after 6 h incubation of the RAW264.7 cells and P-mac with the addition of 1 μg/mL of LPS and serial concentrations of CWE. As shown in Figure 1a, the survival rate was from 83.5 to

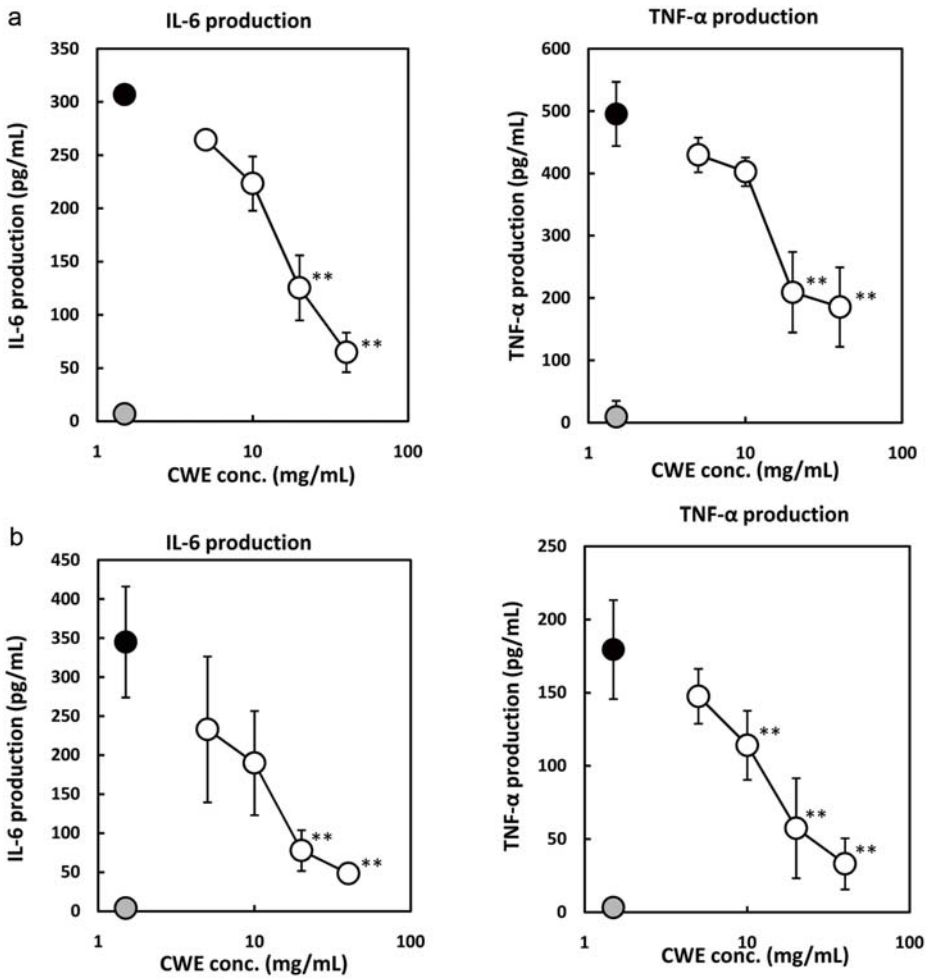

Figure 2. Effect of CWE on IL-6 and TNF-α production by LPS-stimulated RAW264.7 cells and mouse peritoneal macrophages (P-mac). The RAW264.7 cells and P-mac were treated with 1 μg/mL of LPS and serial concentrations of CWE for 6 h. The culture medium was subsequently used for measurement with the ELISA kits. Data are presented as the mean ± SD (n = 3). $^{**}p < 0.01$ against control (LPS) using the Tukey test. (a) RAW264.7 cells. (b) P-mac. Black circle: LPS without CWE (control); grey circle: distilled water without LPS (blank); open circle: LPS with CWE.

113%, showing that there was no significant cytotoxicity of CWE to the LPS-stimulated RAW264.7 cells at the tested concentrations. Similarly, Figure 1b shows that CL also did not affect the cell viability of P-mac. The WST-8 assay results indicated that the viability of the RAW264.7 cells and P-mac is not affected by CWE at the various concentrations tested. Therefore, the subsequent experiments were performed at less than 40 mg/mL of CWE.

3.2. Effect of CWE on cytokine production in LPS-stimulated RAW 264.7 cells and P-mac

Macrophages regulate inflammation and trigger the production of pro-inflammatory cytokines such as IL-6, IL-1β, and TNF-α through several inflammation signaling pathways when undergoing LPS stimulation (Scull et al., 2010; Duque and Descoteaux, 2014). Therefore, the effect of CWE on IL-6 and TNF-α production in the LPS-stimulated macrophages was analyzed. As shown in Figure 2a, LPS treatment stimulated the production of IL-6 and TNF-α by the RAW264.7 cells compared with control, as well as in the P-mac experiment (Figure 2b). CWE significantly suppressed the production of IL-6 and TNF-α by the RAW264.7 cells in a dose-dependent manner (Figure 2a). Similar results were also observed in P-mac (Figure 2b). According to these results, CWE has anti-inflammatory properties by inhibiting IL-6 and TNF-α production by not only the macrophage cell line but also the primary macrophages.

3.3. Effect of CWE on mRNA expression of the LPS-stimulated RAW264.7 cells

The mRNA gene expressions of IL-6 and TNF-α were analyzed using RT-PCR to determine the mechanism of the anti-inflammatory effect of CWE. Similarly to the previous result in the ELISA experiment, as shown in Figure 3, LPS treatment (control; black circle) markedly increased the gene expression levels of IL-6 and TNF-α compared with blank (distilled water without LPS; gray circle), while CWE treatment significantly downregulated their gene expression levels at 10 mg/mL ($p<0.01$) in the LPS-stimulated RAW264.7 cells (open circles). These results suggested that

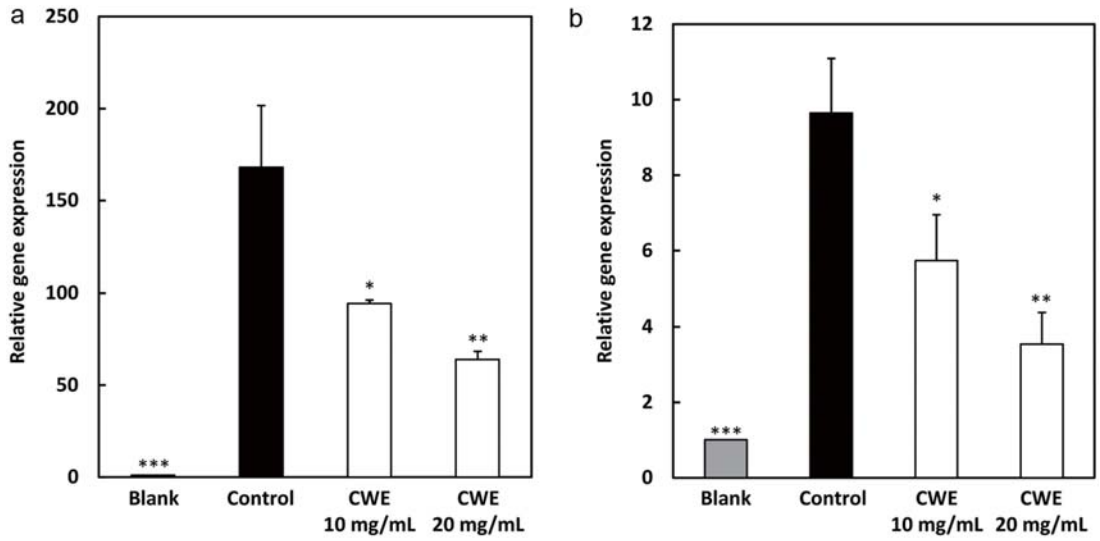

Figure 3. Effect of CWE on mRNA expression levels of IL-6 and TNF-α in LPS-stimulated RAW264.7 cells. The RAW264.7 cells were treated with 1 μg/mL of LPS and serial concentrations of CWE and incubated for 6 h. After incubation, the mRNA expression levels of IL-6 and TNF-α were evaluated using real-time RT-PCR. Data are presented as the mean ± SD (n = 3). $^{*}p < 0.05$, $^{**}p < 0.01$, $^{***}p < 0.001$ against control (LPS) using the Tukey test. Blank: distilled water without LPS; Control: distilled water with LPS.

the mode of action of the anti-inflammatory activity of CWE was related to the inhibition of inflammatory gene transcription.

3.4. Effect of CWE on nitric oxide production and iNOS expression in LPS-stimulated RAW264.7 cells and P-mac

Nitric oxide (NO), an inflammatory mediator, can stimulate the production of pro-inflammatory cytokines, which can also stimulate the production of NO, creating a positive feedback loop that intensifies inflammation (Baek et al., 2020; Park et al., 2020). Therefore, inhibiting NO production reduces inflammation. In this study, NO production was evaluated using a Griess kit by measuring NO released in a culture medium. After treating the LPS-stimulated RAW264.7 cells with serial concentrations of CWE for 24 h, the NO concentration in the culture medium was subsequently measured. The result showed that NO production was suppressed by CWE in the LPS-stimulated RAW264.7 cells in a dose-dependent manner (Figure 4a).

In addition, the mRNA of iNOS was examined to explore the possibility that CWE suppresses the synthesis of NO by inhibiting the gene expression of the corresponding synthase, iNOS. As shown in Figure 4b, CWE inhibited iNOS mRNA expression at 10 mg/mL in the LPS-stimulated RAW264.7 cells, which is similar to the suppression of NO production. In brief, these data revealed that CWE suppresses NO production by downregulating iNOS gene expression in the LPS-stimulated RAW264.7 cells.

3.5. Effect of CWE on iNOS expression and MAPK and NF-κB signaling pathways

Inflammatory signaling pathways such as MAPK and NF-κB are important transcription factors in the inflammation-regulating system (Nishi et al., 2021). Therefore, to investigate the potential mechanism of the anti-inflammatory effect of CWE, the effect of CWE on the essential intracellular signaling pathways such as MAPK and NF-κB, and the protein expression level of iNOS, were investigated using Western blot analysis. As shown in Figure 5a, the MAPK family such as JNK, p38, and ERK in the RAW264.7 cells induced by LPS were highly phosphorylated, while JNK and p38 phosphorylation was significantly inactivated by CWE at 10 mg/mL. In contrast, CWE treatment notably increased ERK phosphorylation at 10 mg/mL. Moreover, as depicted in Figure 4b, CWE treatment significantly suppressed the translocation of NF-κB from the cytosol to the nucleus in the LPS-treated RAW264.7 cells. Next, we further analyzed the inflammation-related iNOS expression. iNOS is another key signaling pathway that regulates the release and gene expression of pro-inflammatory mediators and the inflammatory cytokine response. As shown in Figure 4c, the iNOS protein expression level was attenuated by CWE treatment compared with control. The results suggested that CWE inhibits the production of inflammatory cytokines and the inflammatory mediator NO by LPS-induced inflammation in the RAW264.7 cells via suppressing phosphorylation of JNK and p38, NF-κB translocation, and iNOS expression.

4. Discussion

Clove is a high-priced spice due to its large range of applications in food and beverages, use in fragrances, and for pharmacological purposes. Several studies have revealed the biological activities of compounds contained in clove. Haro-González et al. (2021) reported that the main constituents of clove are eugenol, eugenol acetate, and caryophyllene. In addition, clove is one of the most abundant plant sources of phenolic compounds such as eugenol, eugenol acetate, and β-caryophyllene (Uddin et al., 2017; Gaspar et al., 2018). The essential oil of clove has been reported to possess many positive benefits through its antioxidant, antimicrobial, anticancer, and wound-healing activities (Bachiega et al., 2012; Percival et al., 2012; Cortés-Rojas et al., 2014; Zari et al., 2021). In this study, we investigated the anti-inflammatory activity and underlying mechanisms of CWE against LPS-stimulated RAW264.7

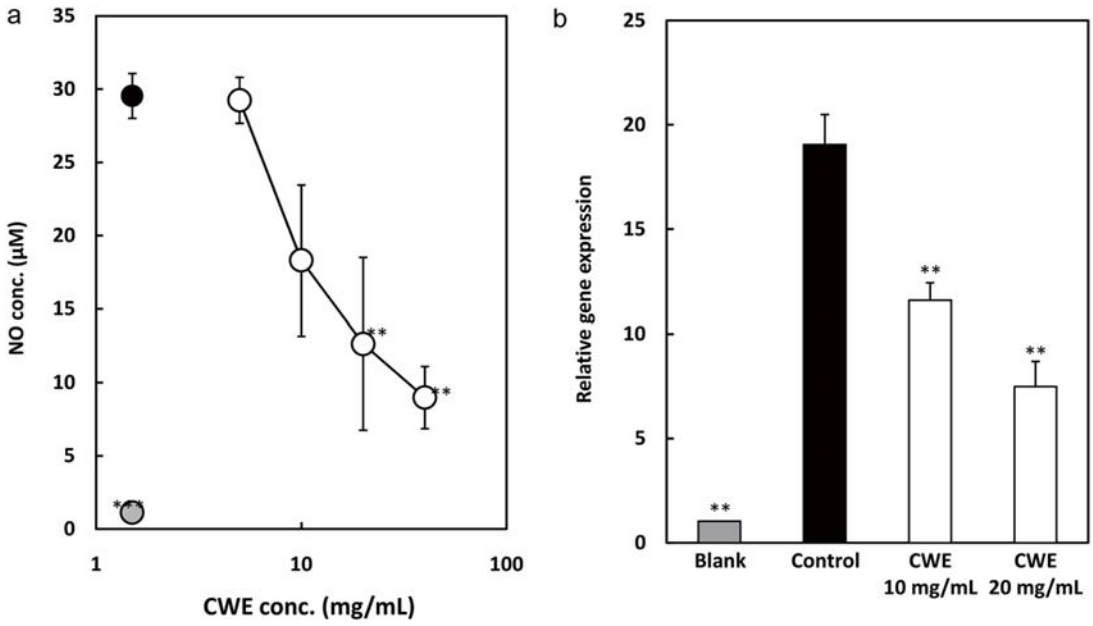

Figure 4. Effect of CWE on NO production and mRNA expression of iNOS in LPS-stimulated RAW264.7 cells. The RAW264.7 cells were treated with 1 μg/ml LPS and serial concentrations of CWE for 6 h. The culture medium was subsequently used to measure NO concentration. Data are presented as the mean ± SD (n = 3). $^{**}p < 0.01$, $^{***}p < 0.001$ against control (LPS) using the Tukey test. (a) NO production. Black circle: LPS without CWE (control); grey circle: distilled water without LPS (blank); open circle: LPS with CWE. (b) iNOS gene expression level.

cells and P-mac.

Macrophages are key immune cells that play an important role in the inflammation system. Various cells can change their primary transcriptional program to combat harmful molecules, such as LPS (Sigola et al., 2016). Macrophages are pivotal in the inflammatory response through their ability to release inflammatory cytokines (IL-6, TNF-α, IL-1β) and mediators (NO) in response to LPS exposure (Guha and Mackman, 2001; Duque and Descoteaux, 2014). Therefore, we used mouse macrophage cell line RAW264.7 cells and P-mac as a model for this study. The RAW264.7 cells and P-mac treated with LPS were cultured in 10% FBS-DMEM and 10% FBS-RPMI 1640 medium, respectively, with the addition of CWE. The concentration of inflammatory substances IL-6, TNF-α, and NO in the culture medium was measured. The synthesis of IL-6 and TNF-α in macrophages generally increases after LPS exposure (Figure 2a, b). Our result showed that CWE significantly suppressed the production of IL-6 and TNF-α in a dose-dependent manner without cytotoxicity (Figure 1a, b) in the LPS-stimulated RAW264.7 cells as well as in P-mac (Figure 2a, b). Pro-inflammatory cytokines such as IL-6 and TNF-α play an important role in the inflammation system. The synthesis of TNF-α in macrophages predominates and subsequently promotes the production of several other inflammatory cytokines, such as IL-6, IL-1β, and IFNs (Baek et al., 2020). Many human disorders, including cancer, severe depression, Alzheimer's disease, and inflammatory bowel disease, have been linked to the deregulation of TNF-α release (Susanto et al., 2018; Heloneida et al., 2019). Consequently, measurement of TNF-α attenuate activity is crucial for investigating potential anti-inflammatory agents as long as this cytokine contributes to the inflammation mediation system. Furthermore, to confirm the relationship between the inhibition of the mRNA level and the anti-inflammation effect of CWE, real-time RT-PCR analysis was conducted. CWE at 20 mg/mL and 10 mg/mL significantly inhibited the mRNA expression levels of IL-6 and TNF-α compared with control treated with LPS only (Figure 3). These findings indicated that the anti-inflammatory activity of CWE is mediated through transcriptional regulation of inflammatory cytokines.

Next, we also explored the potential role of CWE in the modulation of another inflammatory mediator, NO, and its gene expression of the corresponding synthase, iNOS. The result showed that CWE inhibited iNOS gene expression (Figure 4b) and iNOS production (Figure 5c). In the human immune system, NO formation is biosynthesized by iNOS in macrophages. In addition, LPS-exposed macrophages induce inflammatory mediators, such as COX-2, an essential enzyme in the production of PGE_2, and inflammatory cytokines such as IL-6 and TNF-α (Baek et al., 2020; Kang et al., 2022). Pathogenesis is the process in which an infection leads to disease from prolonged inflammatory responses modulated by inflammatory cytokines including IL-6 and TNF-α, and inflammatory mediators like NO and PGE_2. During the inflammatory process, iNOS and COX-2 gene expression is markedly up-regulated in the accelerated synthesis of NO and PGE_2, respectively. Furthermore, IL-6 is suspected to be involved in LPS-stimulated intracellular action, while TNF-α triggers a variety of inflammatory consequences, such as sepsis and cytotoxicity. These inflammatory cytokines promote overexpression of NO and iNOS, and excessive inflammatory mediators are linked to tissue damage and multiple organ failure. Hence, the efficacy of anti-inflammatory medication may be assessed by blocking the synthesis of pro-inflammatory mediators (Jeong et al., 2019; Lee et al., 2021).

Selective intracellular systems, such as the signaling cascade that initiates the activation of MAPKs and the nuclear factor NF-κB, are triggered by macrophages to recognize and react to extracellular stimuli. The family of serine-threonine kinases known as MAPKs has a vital role in transducing signals to control immune responses and inflammatory factors in response to an extensive range of extracellular stimuli, involving cytotoxic agents and oxidative stress (Zhang and Liu, 2002; Jeong et al., 2019).

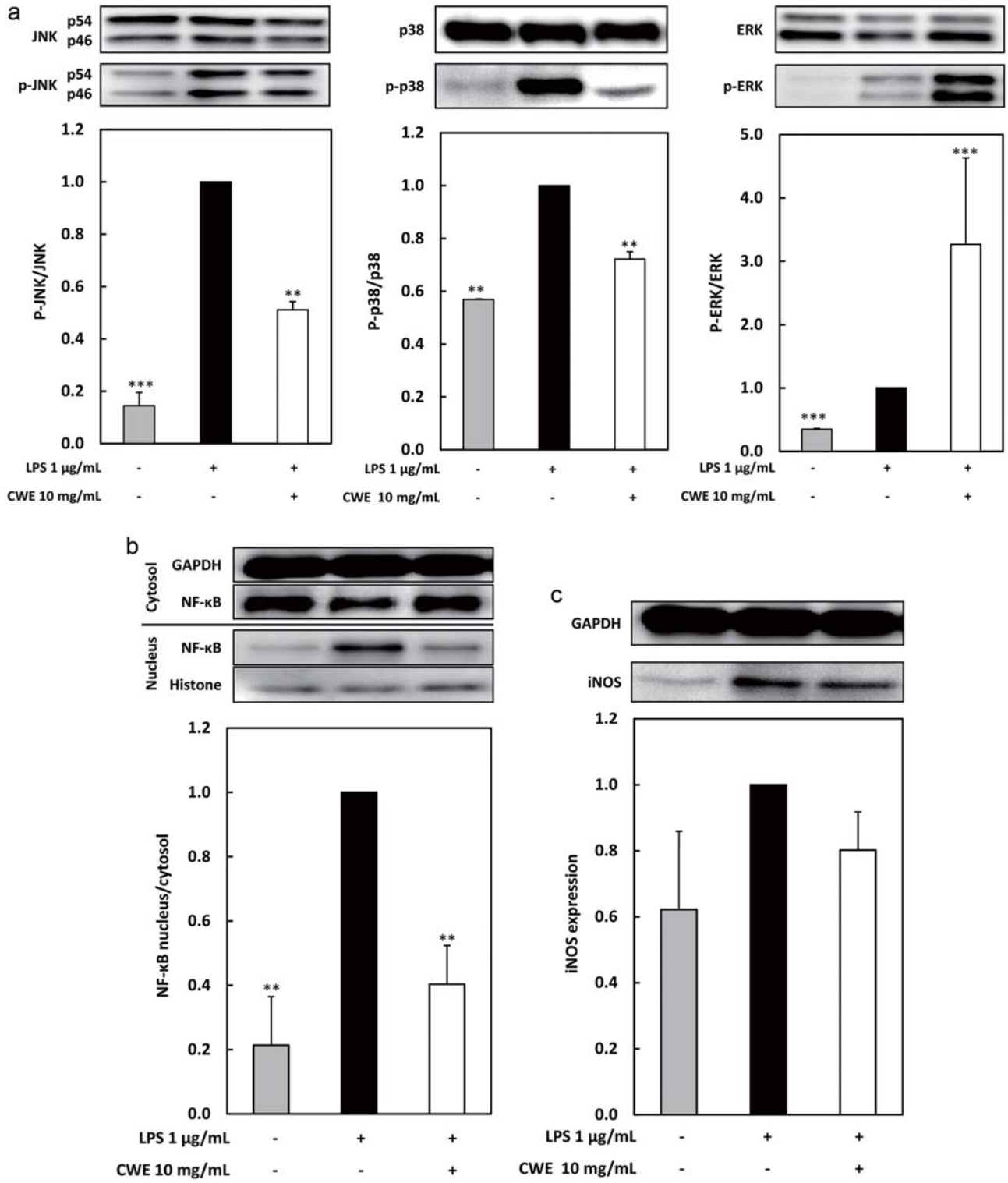

Figure 5. Effect of CWE on MAPK and NF-κB signaling pathways, and iNOS protein expression, in LPS-stimulated RAW264.7 cells. The RAW264.7 cells were treated with 1 µg/mL of LPS and serial concentrations of CWE and incubated for 15 min. (a) The phosphorylated protein levels of ERK, JNK, and p38 were evaluated using immunoblot analysis. p-ERK, p-JNK, and p-p38 represent phosphorylated ERK, JNK, and p38, respectively. (b) The protein amounts of cytosolic and nuclear NF-κB were evaluated using immunoblot analysis. (c) The protein amount of iNOS was evaluated using immunoblot analysis. Data are presented as the mean ± SD (n = 3). $^{**}p < 0.01$, $^{***}p < 0.001$ against control (LPS) using the Tukey test.

NF-κB signaling is a transcription factor that, when activated, can regulate pro-inflammatory cytokines and mediators in LPS-stimulated macrophages (Harbeoui et al., 2019; Gurusmatika et al., 2023). Hence, in this current research, we analyzed proteins related to MAPKs and NF-κB to elucidate the anti-inflammatory mechanism. Our finding showed that the phosphorylation level of JNK and p38 MAPK was attenuated by CWE, whereas the phosphorylation level of ERK was elevated (Figure 5a). In addition, as shown in Figure 5b, CWE inhibited the translocation level of NF-κB from the cytosol to the nucleus in the LPS-treated RAW264.7 cells. These results suggested that JNK and p38 MAPK signaling cascade, are involved in the anti-inflammatory effect of CWE, as well as NF-κB translocation. Several studies have revealed that MAPK regulates the secretion of various inflammatory mediators including NO and cytokines. As a result, p38 and JNK are molecules that have an anti-inflammatory effect (Ishida et al., 2013; Ishida et al., 2022; Gurusmatika et al., 2017).

GTP-binding proteins initiate the JNK cascade, similar to the ERK pathway. While Ras generates ERK, small GTPases that resemble Ras, such as Rac and Cdc42, generate signals that trigger JNK. On the other hand, the kinase p38 is described as a MAPK that is involved in regulating inflammation responses. In the cytoplasm, the binding process of NF-κB to its inhibitory protein IκB is inactivated under normal physiological circumstances, while the IKK complex is activated by pro-inflammatory cytokines, causing the phosphorylation of the IκB protein to auto-ubiquitination and proteasome destruction. Released NF-κB is subsequently translocated from the cytosol into the nucleus, where it binds to nucleotropic DNA to initiate expression factors to produce inflammation mediators and cytokines (Xu et al., 2021; Liu et al., 2022).

NO, resulting from iNOS protein expression, is a pro-inflammatory mediator that is released by macrophages. It initiates the inflammatory response, increases vascular permeability, and promotes the production of pro-inflammatory mediators and cytokines. Our findings indicated that CWE imparts anti-inflammatory activity by suppressing IL-6 and TNF-α production by in the LPS-stimulated RAW264.7 cells and P-mac. In addition, inhibition of iNOS gene and protein expression undoubtedly affects NO synthesis, thereby reducing NO production through down-regulation of iNOS gene expression by CWE treatment in the LPS-stimulated RAW264.7 cells. Furthermore, suppression is regulated by the inhibition of transcription factor NF-κB and iNOS in parallel with the attenuation of the p38 and JNK pathways. Clove consists of many natural compounds, such as phenolics, proteins, vitamins, and minerals. Although many studies have shown the anti-inflammatory activity of eugenol, the major component in clove, in the present study we conducted a sample extraction with water. Eugenol is optimally extracted in ethanol solvent but low water solubility (Pandey et al., 2024). In addition to some flavonoids like kaempferol and its derivatives, clove also contains the phenolic acids caffeic, elagic, and ferulic. Therefore, phenolic substances such as gallic acid, flavonolglucosides, phenolic volatile oils (eugenol, acetyl eugenol), and tannins are responsible for the health benefits of cloves (El-Maati et al., 2016; Chniguir et al., 2019; Zari et al., 2021). Active compounds in CWE have not yet been studied, and will be explored in future studies.

5. Conclusion

The current study provides evidence that clove water extract exerts anti-inflammatory activity in LPS-stimulated RAW264.7 cells and peritoneal macrophages. The extract significantly attenuated the production of IL-6, TNF-α, and NO by LPS-stimulated macrophages. The anti-inflammatory activity of the extract was attributed to inhibiting the gene expression of IL-6, TNF-α, and iNOS, which are interrupted through JNK and p38 MAPKs, the NF-κB signaling cascade, and iNOS protein. The results of this study show that clove water extract is a safe and better natural alternative candidate as a therapeutic agent for chronic inflammation and oxidative stress-related diseases.

Acknowledgments

The animal experiment was conducted at the Division of Genetic Research Support of the Advanced Research Support Center (ADRES), Ehime University.

Conflict of interest

The authors declare no conflict of interest.

Author contributions

Conceptualization, T.S.; Methodology, S.G.; Software, S.G.; Validation, S.G.; Formal Analysis, S.G., M.I., K.N. and T.S.; Investigation, S.G.; Data Curation, S.G.; Writing – Original Draft Preparation, S.G.; Writing – Review & Editing, M.I., K.N. and T.S.; Visualization, S.G.; Supervision, K.N. and T.S.

References

Ali, B.H., Blunden, G., Tanira, M.O., and Nemmar, A. (2008). Some phytochemical, pharmacological and toxicological properties of ginger (*Zingiber officinale* Roscoe): A review of recent research. Food Chem. Toxicol. 46(2): 409–420.

Bachiega, T.F., de Sousa, J.P., Bastos, J.K., and Sforcin, J.M. (2012). Clove and eugenol in noncytotoxic concentrations exert immunomodulatory/ anti-inflammatory action on cytokine production by murine macrophages. J. Pharm. Pharmacol. 64(4): 610–616.

Baek, S., Park, T., Kang, M., and Park, D. (2020). Anti-inflammatory activity and ROS regulation effect of sinapaldehyde in LPS-stimulated RAW264.7 macrophages. Molecules 25(18): 4089.

Chniguir, A., Zioud, F., Marzaioli, V., El-Benna, J., and Bachoual, R. (2019). Syzygium aromaticum aqueous extract inhibits human neutrophils myeloperoxidase and protects mice from LPS-induced lung inflammation. Pharm. Microbiol. 57(1): 56–64.

Cortés-Rojas, D.F., de Souza, C.R.F., and Oliveira, W.P. (2014). Clove (*Syzygium aromaticum*): Aprecious spice. Asian Pac. J. Trop. Biomed. 4(2): 90–96.

Duque, G.A., and Descoteaux, A. (2014). Macrophage cytokines: Involvement in immunity and infectious diseases. Front. Immunol. 5: 491.

El-Maati, M.F.A., Mahgoub, S.A., Labib, S.M., Al-Gaby, A.M.A., and Ramadan, M.F. (2016). Phenolic extracts of clove (*Syzygium aromaticum*) with novel antioxidant and antibacterial activities. Eur. J. Integr. Med. 8(4): 494–504.

Gaspar, E.M., Duarte, R., and Santana, J.C. (2018). Volatile composition and antioxidant properties of clove products. Biomed. J. Sci. Tech. Res. 9(4): 7270–7276.

Guha, M., and Mackman, N. (2001). LPS induction of gene expression in human monocytes. Cell Signal. 13(2): 85–94.

Gurusmatika, S., Nishi, K., Harmayani, E., Pranoto, Y., and Sugahara, T. (2017). Immunomodulatory activity of octenyl succinic anhydride modified porang (*Amorphophallus oncophyllus*) glucomannan on mouse macrophage-like J774.1 cells and mouse primary peritoneal

macrophages. Molecules 22(7): 1187.
Gurusmatika, S., Ishida, M., Nishi, K., and Sugahara, T. (2023). Anti-inflammatory potentials of rendang seasoning (Sumatran traditional food) water extract in RAW264.7 cells and mouse peritoneal macrophages. J. Funct. Food Nutraceutical 5(1): 1–12.
Hamidzadeh, K., Christensen, S.M., Dalby, E., Chandrasekaran, P., and Mosser, D.M. (2017). Macrophages and the recovery from acute and chronic inflammation. Annu. Rev. Physiol. 79: 567–592.
Harbeoui, H., Hichami, A., Aidi Wanners, W., Lemput, J., Saidani Tounsi, M., and Khan, N.A. (2019). Anti-inflammatory effect of grape (*Vitis vinifera* L.) seed extract through the downregulation of NF-κB and MAPK pathways in LPS-induced RAW264.7 macrophages. S. Afr. J. Bot. 125: 1–8.
Haro-González, J.N., Castillo-Herrera, G.A., Martínez-Velázquez, M., and Espinosa-Andrews, H. (2021). Clove essential oil (*Syzygium aromaticum* L. Myrtaceae): Extraction, chemical composition, food applications, and essential bioactivity for human health. Molecules 26(21): 6387.
Haro-González, J.N., de Alba, B.N.S., Martínez-Velázquez, M., Castillo-Herrera, G.A., and Espinosa-Andrews, H. (2023). Optimization of clove oil nanoemulsions: Evaluation of antioxidant, antimicrobial, and anticancer properties. Colloids Interfaces 7(4): 64.
Heloneida, A., Lima, M.S.R., Oliveira, V.C., Pluvezam, G., Morais, K.P., and Maciel, B.L.L. (2019). Mechanisms of action of molecules with anti-YNF-alpha activity on intestinal barrier inflammation (A systematic review protocol). Medicine 96: 39.
Hirano, T. (2021). IL-6 in inflammation, autoimmunity and cancer. Int. Immunol. 33(3): 127–148.
Hu, Q., Zhou, M., and Wei, S. (2018). Progress on the antimicrobial activity research of clove oil and eugenol in the food antisepsis field. J. Food Sci. 83(6): 1476–1483.
Ishida, M., Nishi, K., Watanabe, H., and Sugahara, T. (2013). Inhibitory effect of aqueous spinach extract on degranulation of RBL-2H3 cells. Food Chem. 136(2): 322–327.
Ishida, M., Takekuni, C., Nishi, K., and Sugahara, T. (2019). Anti-inflammatory effect of aqueous extract from Kawachi-bankan (*Citrus maxima*) peel *in vitro* and *in vivo*. Cytotechnology 71(4): 797–807.
Ishida, M., Takekuni, C., Nishi, K., and Sugahara, T. (2022). *p*-Synephrine suppresses inflammatory responses in lipopolysaccharide-stimulated RAW264.7 cells and alleviates systemic inflammatory response syndrome in mice. Food Funct. 13(9): 5229–5239.
Jeong, Y.H., Oh, Y.C., Cho, W.K., Yim, N.H., and Ma, J.Y. (2019). Hoveniae semen seu fructus ethanol extract exhibits anti-inflammatory activity via MAPK, AP-1, and STAT signaling pathways in LPS-stimulated RAW264.7 and mouse peritoneal macrophages. Mediators Inflammation 2019: 9184769.
Jiang, T.A. (2019). Health benefits of culinary herbs and spices. J. AOAC Int. 102(2): 395–411.
Kang, J.K., Kang, H.K., and Hyun, C.G. (2022). Anti-Inflammatory effects of spiramycin in LPS-activated RAW264.7 macrophages. Molecules 27(10): 3202.
Lee, N., Heo, Y.J., Choi, S.E., Jeon, J.Y., Han, S.J., Kim, D.J., Kang, Y., Lee, K.W., and Kim, H.J. (2021). Anti-inflammatory effects of empagliflozin and gemigliptin on LPS-stimulated macrophage via the IKK/NF-κB, MKK7/JNK, and JAK2/STAT1 signalling pathways. J. Immunol. Res. 2021: 9944880.
Leiherer, A., Mündlein, A., and Drexel, H. (2013). Phytochemicals and their impact on adipose tissue inflammation and diabetes. Vasc. Pharmacol. 58(1–2): 3–20.
Liu, W., Chen, X., Li, H., Zhang, J., An, J., and Liu, X. (2022). Anti-inflammatory function of plant-derived bioactive peptides: A review. Foods 11(15): 2361.
Netea, M.G., Balkwill, F., Chonchol, M., Cominelli, F., Donath, M.Y., Giamarellos-Bourboulis, E.J., Golenbock, D., Gresnigt, M.S., Heneka, M.T., Hoffman, H.M., Hotchkiss, R., Joosten, L.A., Kastner, D.L., Korte, M., Latz, E., Libby, P., Mandrup-Poulsen, T., Mantovani, A., Mills, K.H.G., Nowak, K.L., O'Neill, L.A., Pickkers, P., van der Poll, T., Ridker, P.M., Schalkwijk, J., Schwartz, D.A., Siegmund, B., Steer, C.J., Tilg, H., van der Meer, J.W.M., van de Veerdonk, F.L., and Dinarello, C.A. (2017). A guiding map for inflammation. Nat. Immunol. 18(8): 826–831.
Nishi, K., Ito, T., Kadota, A., Ishida, M., Nishiwaki, H., Fukuda, N., Kanamoto, N., Nagata, Y., and Sugahara, T. (2021). Aqueous extract from leaves of Citrus unshiu attenuates lipopolysaccharide-induced inflammatory responses in a mouse model of systemic inflammation. Plants (Basel) 10(8): 1708.
Oishi, Y., and Manabe, I. (2018). Macrophages in inflammation, repair and regeneration. Int. Immunol. 30(11): 511–528.
Park, Y.J., Cheon, S.Y., Lee, D.S., Cominguez, D.C., Zhang, Z., Lee, S., and An, H.J. (2020). Anti-inflammatory and antioxidant effects of Carpesium cernuum L. methanolic extract in LPS-stimulated RAW264.7 macrophages. Mediators Inflammation 2020: 3164239.
Pandey, V.K., Srivastava, S., Ashish, Dash, K.K., Singh, R., Dar, A.H., Singh, T., Faroqui, A., Shaikh, A.M., and Kovacs, B. (2024). Bioactive properties of clove (*Syzygium aromaticum*) essential oil nanoemulsion: A comprehensive review. Heliyon 10(1): e22437.
Percival, S.S., Vanden Heuvel, J.P., Nieves, C.J., Montero, C., Migliaccio, A.J., and Meadors, J. (2012). Bioavailability of herbs and spices in humans as determined by ex vivo inflammatory suppression and DNA strand breaks. J. Am. Coll. Nutr. 31(4): 288–294.
Scull, C.M., Hays, W.D., and Fischer, T.H. (2010). Macrophage pro-inflammatory cytokine secretion is enhanced following interaction with autologous platelets. J. Inflamm. (Lond.) 7: 53.
Sigola, L.B., Fuentes, A.L., Millis, L.M., Vapenik, J., and Murira, A. (2016). Effects of Toll-like receptor ligands on RAW264.7 macrophage morphology and zymosan phagocytosis. Tissue Cell 48(4): 389–396.
Susanto, S., Sumarpo, A., Parikesit, A.A., Putra, A.B., Ishida, E., Tabuch, K., and Sugahara, T. (2018). Short communication: Immunostimulatory effect of tempoyak (fermented durian) on inducing cytokine production (IL-6 and TNF-α) by RAW264.7 cells. Biodiversitas 19(1): 318–322.
Uddin, M.A., Shahinuzzaman, M., Rana, M.S., and Yaakob, Z. (2017). Study of chemical composition and medicinal properties of volatile oil from clove buds (Eugenia Caryophyllus). Int. J. Pharm. Sci. Res. 8(2): 895–899.
Ugbogu, O.C., Emmanuel, O., Agi, G.O., Ibe, C., Ekweogu, C.N., Ude, V.C., Uche, M.E., Nnanna, R.O., and Ugbogu, E.A. (2021). A review on the traditional uses, phytochemistry, and pharmacological activities of clove basil (*Ocimum gratissimum* L.). Heliyon 7(11): e08404.
Venkatalakshmi, P., Vadivel, V., and Brindha, P. (2016). Role of phytochemicals as immunomodulatory agents: A review. Int. J. Green Pharm. 10(1): 1–18.
Zhang, W., and Liu, H.T. (2002). RMAPK signal pathways in the regulation of cell proliferation in mammalian cells. Cell Res. 12(1): 9–18.
Xu, J., Xiao, C.M., Xu, H.S., Yang, S.X., Chen, Z.M., Wang, H.Z., Zheng, B.S., Mao, B.Z., and Wu, X.Q. (2021). Anti-inflammatory effects of Ganoderma lucidum sterols via attenuation of the p38 MAPK and NF-κB pathways in LPS-induced RAW264.7 macrophages. Food Chem. Toxicol. 150: 112073.
Zari, A.T., Zari, T.A., and Hakeem, K.R. (2021). Anticancer properties of eugenol: A review. Molecules 26(23): 7407.

Journal of Food Bioactives
International Society for Nutraceuticals and Functional Foods
Original Research
J. Food Bioact. 2024;25:81–94

In silico ADME and molecular simulation studies of pharmacological activities of phytoconstituents of *Annona muricata* (L.) Fruit

Iseoluwa Isaac Ajayi[a], Toluwase Hezekiah Fatoki[b*], Ayodele Sunday Alonge[a], Courage Dele Famusiwa[c], Ibrahim Olabayode Saliu[d], Olapade Samuel Akinlolu[e], Chinemelum Adaora Onodugo[c] and Rachel Temitope Ojo[a]

[a]Department of Biological Sciences, Bamidele Olumilua University of Education, Science and Technology Ikere-Ekiti, Ekiti State, Nigeria
[b]Applied Bioinformatics Laboratory, Department of Biochemistry, Federal University Oye-Ekiti, Ekiti State, Nigeria
[c]Phytomedicine and Molecular Toxicology Research Laboratory, Department of Biochemistry, Federal University Oye-Ekiti, Ekiti State, Nigeria
[d]Department of Neuroscience, Washington University School of Medicine, St. Louis, MO, United States
[e]Department of Chemistry, Federal University Oye-Ekiti, Ekiti State, Nigeria
[*]**Corresponding author:** Toluwase Hezekiah Fatoki, Applied Bioinformatics Laboratory, Department of Biochemistry, Federal University Oye-Ekiti, Ekiti State, Nigeria. E-mail: toluwase.fatoki@fuoye.edu.ng
DOI: 10.31665/JFB.2024.18374
Received: February 03, 2024; **Revised received & accepted:** February 27, 2024
Citation: Ajayi, I.I., Fatoki, T.H., Alonge, A.S., Famusiwa, C.D., Saliu, I.O., Akinlolu, O.S., Onodugo, C.A., and Ojo, R.T. (2024). *In Silico* ADME and molecular simulation studies of pharmacological activities of phytoconstituents of *Annona muricata* (L.) Fruit. J. Food Bioact. 25: 81–94.

Abstract

Annona muricata Lin is known for its ethnomedicinal uses as food, decoctions, or infusions to address various conditions like skin infections, fever, diabetes, insomnia, malaria, hypertension, nervous disorders, diarrhea, and cancer. The study aimed to analyze the phytochemicals such as acetogenins, alkaloids, cyclopeptides, and flavonoids, present in *A. muricata* fruit, evaluate their pharmacokinetics, and understand binding dynamics with key molecular targets relevant to human well-being. Results indicated a mix of high and low gastrointestinal absorption (GIA) among *A. muricata* phytochemicals, with some demonstrating blood-brain barrier (BBB) permeability. Molecular target prediction highlighted frequent interactions with Programmed cell death protein 4 (PDCD4). Protein-protein interaction analysis revealed central connectivity of tyrosinase (TYR), Tyrosine 3-monooxygenase (TH), interleukin 2 (IL2), and others. Molecular docking results identified Luteolin 3,7-di-O-glucoside with the highest binding affinity for PDCD4 (−7.65 kcal.mol^{-1}), followed by Annonaine (−7.294 kcal.mol^{-1}); meanwhile, Dexamethasone (standard compound) exhibited a binding affinity of −6.682 kcal.mol^{-1}. Molecular dynamic simulation indicated a stable binding energy ΔGbind (Total) for the Annonaine - PDCD4 complex (−35.851 kcal.mol^{-1}) and Dexamethasone - PDCD4 complex (−28.489 kcal.mol^{-1}). In conclusion, this study suggests potential anticancer properties of *A. muricata* based on modulation of PDCD4 protein, influencing the CDK/Akt/STAT3 pathway. Further *in vivo* investigations are necessary to validate these findings.

Keywords: *A. muricata*; Phytoconstituents; Muricatocin A; Muricatetrocin B; PDCD4; anticancer.

1. Introduction

Annona muricata Lin., commonly referred to as soursop, is a member of the Annonaceae plant family and is extensively cultivated in tropical and subtropical regions, including Southeast Asia, South America, and the rainforests of Africa (Mutakin et al., 2022). The various plant parts of *A. muricata* L, encompassing leaves, bark, fruit, and seeds, have been traditionally used for ethnomedicinal purposes to address a diverse range of health issues (Mutakin et al., 2022; Nwonuma et al., 2023).

A. muricata is known for containing compounds with pharmacological activity, such as flavonoids, terpenoids, saponins, coumarins, lactones, anthraquinones, glycosides, tannins, and phytosterols, as identified in its leaf extract (Gavamukulya et al., 2014). The plant harbors approximately 100 phytochemicals distributed across its various parts (Mutakin et al., 2022). Notably, all parts of *A. muricata*, including fruit, stem, leaf, seed, root, and twigs, exhibit specific anticancer properties. These properties are believed to involve the inhibition of matrix metallopeptidases (MMP-2 and MMP-9), induction of apoptosis by enhancing caspase-3 expression, and modulation of the Bax/Bcl-2 ratio with cell cycle arrest at G0/G1 phase (Pieme et al., 2014; Moghadamtousi et al., 2014; Yang et al., 2015; Abdullah et al., 2017; Indrawati et al., 2017; Kim et al., 2018; Drishya et al., 2020; Hadisaputri et al., 2021).

This study adopts a comprehensive computational approach to unveil the inherent pharmacological importance of *A. muricata*, offering insights that are challenging to obtain in wet labs. Computational methods play a crucial role in expanding the understanding of the plant's medicinal applications and its mechanism of action. Previous computational studies have explored *A. muricata's* potential in treating hypertension by targeting angiotensin I converting enzyme (Suhandi et al., 2022), and antimalarial effect by analyzing interaction with six *Plasmodium falciparum* proteins (Nwonuma et al., 2023). Computational study of anti-prostate cancer potential of showed binding affinities between - 9.854 and 8.179 kcal.mol^{-1} for Human steroid 5′-reductase 2 enzyme, and that the binding free energy was in a range of −83.14 to −100.06 kcal.mol^{-1} (Apeh et al., 2023). Molecular docking results of the study of hypoglycemic effect of phytochemicals in *A. muricata* ripe fruit pulp showed better binding affinity for aldose reductase, afterwards alpha-amylase and alpha-glucosidase, through the interaction of epoxymurin-A, montecristin, and dicaffeoylquinic acid (Akinlolu et al., 2023). Therefore, the objective of this study is to computationally investigate *A. muricata's* fruit phytochemicals (such as acetogenins, alkaloids, cyclopeptides, and flavonoids), assessing their pharmacokinetics and binding dynamics with key molecular targets, contributing to the overall promotion of human well-being.

2. Materials and methods

2.1. Ligand preparation

The primary phytochemical constituents of *A. muricata* (L.) fruit were identified based on literature findings (Coria-Tellez et al., 2018), and their structures were retrieved from the NCBI PubChem Compound database (https://pubchem.ncbi.nlm.nih.gov/) in SMILES formats.

2.2. In silico Pharmacokinetics prediction

The *in silico* ADME (absorption, distribution, metabolism, and excretion) screening of the compounds was conducted using the SwissADME server (www.swissadme.ch), employing default parameters and the SMILES format (Daina et al., 2017).

2.3. In silico target prediction

The SMILES representation of each ligand facilitated target prediction analysis on the SEA Search Server (http://www.sea.bkslab.org/) (Keiser et al., 2007), with Homo sapiens selected as the target organism.

2.4. Protein-protein interaction analysis

To establish relationships among the predicted targets of *A. muricata* phytochemicals, target proteins underwent protein-protein interaction (PPI) profiling on the STRING webserver (https://string-db.org/, Szklarczyk et al., 2021).

2.5. Target gene network analyses

Predicted target gene IDs were compiled for network analyses, including transcription factor enrichment analysis, protein-protein interaction network expansion, and kinase enrichment analysis. This comprehensive analysis utilized the eXpression2Kinases (X2K) Web server (https://maayanlab.cloud/X2K/), with the human organism selected as the background reference (Clarke et al., 2018).

2.6. Molecular docking

The SMILES of the ligands underwent 3D structure optimization using ACDLab/Chemsketch software, saved in .mol format, and further converted to .pdb format using PyMol software. The 3D structure of c-Myc was obtained as AlphFold pdb format from UniProt database (UniProt ID: P01106). Both ligand and c-Myc target protein structures were formatted to pdbqt using AutoDock Tools (ADT) v1.5.6 (Morris et al., 2009). Ligand-protein docking was executed with AutoDock Vina v1.2.3 (Trott and Olson, 2010; Eberhardt et al., 2021), following established protocols (Fatoki et al., 2023). The resulting binding affinity and ligand-target interactions were analyzed and visualized using ezLigPlot on the ezCADD webserver (http://dxulab.org/software) (Tao et al., 2019).

2.7. Molecular dynamics simulation

Molecular dynamics simulations lasting 100 nanoseconds were conducted using Desmond, a Schrödinger LLC package (Bowers et al., 2006; Schrödinger, 2018; Fatoki et al., 2024). Initial protein and ligand complexes from the docking studies underwent preprocessing with Maestro's protein preparation wizard, including optimization and minimization. The systems were prepared using the System Builder tool, employing an orthorhombic TIP3P solvent model. The OPLS-2005 force field governed the simulation, with neutralization achieved by adding 0.15 M NaCl counter ions to mimic physiological conditions (Fatoki, 2022). The NPT ensemble with 310 K temperature and 1 atm pressure was selected, and models were relaxed before simulation. Trajectories were saved every 100 ps, and post-simulation analysis assessed for root-mean-square deviation (RMSD), root-mean-square fluctua-

tion (RMSF), and protein-ligand interaction profiles. Additionally, prime molecular mechanics/generalized Born surface area (MMGBSA) was used to evaluate binding free energy (Zhang et al., 2017; Schrödinger, 2019; Fatoki et al., 2024).

3. Results

The investigation into the phytoconstituents of *A. muricata* (L) revealed diverse pharmacokinetic characteristics. Table 1 illustrates that certain phytoconstituents exhibit low gastrointestinal absorption (GIA) due to insolubility, except for Annonaine, Asimilobine, Cinnamic acid, Coumaric acid, Fisetin, Kaempferol, Morin, Nornuciferine, and Reticuline, which are soluble and demonstrate high GIA. Additionally, Annonaine, Asimilobine, Cinnamic acid, Coumaric acid, N-methylcoclaurine, Nornuciferine, and Reticuline permeate the blood-brain barrier (BBB), while some compounds can inhibit specific cytochromes (CYPs) and act as substrates for P-glycoprotein (P-gp).

Table 2 presents the results of molecular target prediction, highlighting that *A. muricata* phytocompounds frequently target Programmed cell death protein 4 (PDCD4), followed by nuclear receptor subfamily 0 group B member 2 (NR0B2), Cytochrome P450 1B1 (CYP1B1), and others. Rankings are based on p-value and Maximum Tanimoto Coefficient (MTC), indicating similarity between compounds from reference and query targets.

The protein-protein interaction network of *A. muricata* molecular targets identifies Cytochrome P450 1B1 (CYP1B1) as a central protein linking metabolism to functional activity pathways. This is illustrated by key proteins such as tyrosinase (TYR), Tyrosine 3-monooxygenase (TH), interleukin 2 (IL2), Testosterone 17-beta-dehydrogenase 3 (HSD17B3), and others, as shown in Figure 1. Furthermore, the molecular target genes network of *A. muricata* bioactive compounds reveals signaling pathways involving kinases (e.g., MAPK3, MAPK14, CDK1, CDK2, GSK3B, ERK1, ERK2, CSNK2A1, CLK2, CHEK2, PRKDC, BUB1B) and transcription factors (e.g., PPARG, STAT3, FOS, TRIM28, EZH2, TCF3, REST, ZBTB44, ZNF529, NANOG), as depicted in Figures 2 and 3.

Table 3 displays the molecular docking results of *A. muricata* phytochemicals with the highly targeted protein PDCD4. Luteolin 3,7-di-O-glucoside exhibited the highest binding affinity for PDCD4 (−7.65 kcal.mol^{-1}), followed by Annonaine (−7.294 kcal.mol^{-1}) and Dihydrokaempferol-hexoside (−7.012 kcal.mol^{-1}). In comparison, the standard compound Dexamethasone showed a binding affinity of −6.682 kcal.mol^{-1}. Figure 4 illustrates the binding pose of the complex with high binding affinity, highlighting the involved amino acid residues.

MDS was employed to assess the structural stability of both the protein and the binding status of the ligand in a physiologically relevant environment. The outcomes of the MDS studies, using the PDCD4-Annonaine and PDCD4-Dexamethasone binding complexes, are presented in Figure 5, providing valuable insights into the dynamic behavior and interactions of the protein-ligand complexes under realistic conditions.

For the Annonaine - PDCD4 complex, RMSD analysis indicated an RMSD of 18.0 Å for the protein and 16 Å for the ligand over the 0–100 ns period (Figure 5a). RMSF of PDCD4 showed maximal fluctuation at amino acid residues 100–150 and C-terminal (Figure 5b). Protein-ligand interactions revealed details about the involved amino acid residues in hydrophobic interactions, hydrogen bonds, water bridges, and ionic interactions, including GLU161, PHE164, GLU165, and LYS242 (Figure 5c). For the Dexamethasone - PDCD4 complex, RMSD analysis indicated an RMSD of 21 Å for the protein and 12.5 Å for the ligand over the 0–100 ns period (Figure 5d). RMSF of PDCD4 showed maximal fluctuation at amino acid residues 100–150 and N-terminal (Figure 5e). Protein-ligand interactions revealed details about the involved amino acid residues in hydrophobic interactions, hydrogen bonds, water bridges, and ionic interactions, including GLU165, GLU195, SER198, and LYS238 (Figure 5f).

A schematic of detailed ligand atom interactions with the protein residues is presented in Figure 6, validating the amino acid residues involved in the docking interactions. The computed binding free energies using MMGBSA are presented in Table 4, providing insights into the stability and energetics of the protein-ligand interactions throughout the simulation. Notably, the Annonaine - PDCD4 complex at 0ns and 100ns exhibited a binding energy of −35.851 kcal.mol^{-1} and −39.019 kcal.mol^{-1} respectively, while the Dexamethasone - PDCD4 complex at 0ns and 100ns displayed a binding energy of −28.489 and −28.284 kcal.mol^{-1} respectively. Thus, the stability of the two complexes were maintained during the simulation.

4. Discussion

A. muricata, a noteworthy member of the Annonaceae family, exhibits diverse pharmacological properties. This study computationally evaluated the phytoconstituents of *A. muricata* for pharmacokinetic properties, molecular targets, gene signaling pathway kinases, transcription factors, binding affinity, and stability with PDCD4.

According to Mutakin et al. (2022), the major compounds and secondary metabolites are present in the *A. muricata* plant are acetogenins, flavonoids, alkaloids, essential oils, carotenoids, vitamins, and cyclopeptides; and that its pharmacological properties included wound healing properties (4%), antihypertensive (6%), antiviral (8%), antibacterial (8%), antidiarrhea (8%), antiprotozoal (10%), antidiabetic (14%), antiulcer (17%), and anticancer (25%). Also, previous studies have reported cytotoxic effect of annonacin, annonacin-10-one cis-annoreticuin, and corossolone; whereas kaempferol, montecristin, luteolin 3,7-di-o-glucoside, kaempferol 3-o-rutinoside, and morin possessed antioxidant properties (Coria-Tellez et al., 2018; Akinlolu et al., 2023)

The pharmacokinetics assessment unveiled that most phytoconstituents possess moderate solubility and intestinal absorption, with some capable of permeating the blood-brain barrier (BBB). Moreover, insolubility of some phytochemicals especially phenolic compounds, could be modified by their interactions within the food product matrix to form soluble complexes and conjugates, that increase absorption rate, reduce first-pass metabolism and subsequent increase bioavailability. Notably, Annonaine demonstrated favorable gastrointestinal absorption (GIA), potentially attributed to its large molecular size without predicted inhibitory effects on cytochromes (CYPs). Conversely, quercetin displayed high GIA, likely due to its moderate molecular size and some inhibitory effects on specific CYPs. GIA plays a pivotal role in drug efficacy, influencing the bioavailability of administered doses. Alterations in CYP activity can impact drug metabolism, affecting bioavailability or efficacy (Martin et al., 2013). Molecular size, expressed in terms of molecular weight and volume, serves as crucial toxicity metrics influencing compound bioavailability and toxicity (Kostal, 2016). The toxicity of drug decreases as the lipophilicity (Log P value) decreases, because the higher the lipophilicity the lesser the solubility. Log P value around 2.2 are considered more suitable for

Table 1. Predicted pharmacokinetics properties of selected ligands

SN	Ligands	Predicted ADME Parameter from SWISSADME												
		MW	MR	TPSA (Å^2)	Log P	ESOL Log S	ESOL Class	GIA	BBB per-meant	P-gp	CYPs inhibitor	Lip	BS	SA
1	Annonacin	596.88	172.67	116.45	6.92	−7.13	Poorly soluble	Low	No	No	CYP3A4	1	0.55	7.36
2	Annonacin-10-one	594.86	171.71	113.29	6.83	−6.8	Poorly soluble	Low	No	Yes	CYP3A4	1	0.55	7.18
3	Annonaine	265.31	80.13	30.49	2.88	−3.71	Soluble	High	Yes	Yes	CYP1A2, CYP2D6, CYP3A4	0	0.55	3.36
4	Cis-Annoreticuin	596.88	172.67	116.45	6.94	−7.13	Poorly soluble	Low	No	No	CYP3A4	1	0.55	7.36
5	Asimilobine	267.32	82.59	41.49	2.65	−3.54	Soluble	High	Yes	Yes	CYP1A2, CYP2D6, CYP3A4	0	0.55	3.24
6	Cinnamic acid	148.16	43.11	37.3	1.79	−2.37	Soluble	High	Yes	No	NONE	0	0.85	1.67
7	Corossolone	578.86	170.55	93.06	7.75	−7.66	Poorly soluble	Low	No	Yes	NONE	2	0.17	6.9
8	Coumaric acid	164.16	45.13	57.53	1.26	−2.02	Soluble	High	Yes	No	NONE	0	0.85	1.61
9	Dicaffeoylquinic acid	516.45	126.9	211.28	0.91	−3.65	Soluble	Low	No	Yes	NONE	3	0.11	4.83
10	Dihydrokaempferol-hexoside	450.39	105.12	186.37	−0.5	−2.8	Soluble	Low	No	Yes	NONE	2	0.17	5.24
11	Epoxymurin-A	530.86	167.55	38.83		−10.03	Insoluble	Low	No	Yes	NONE	2	0.17	6.47
12	Epoxymurin-B	530.86	167.55	38.83		−10.03	Insoluble	Low	No	Yes	NONE	2	0.17	6.47
13	Epomusenin-A	558.92	177.17	38.83		−10.75	Insoluble	Low	No	Yes	NONE	2	0.17	6.73
14	Epomusenin-B	558.92	177.17	38.83		−10.75	Insoluble	Low	No	Yes	NONE	2	0.17	6.73
15	Fisetin	286.24	76.01	111.13	1.55	−3.35	Soluble	High	No	No	CYP1A2, CYP2D6, CYP3A4	0	0.55	3.16
16	Kaempferol	286.24	76.01	111.13	1.58	−3.31	Soluble	High	No	No	CYP1A2, CYP2D6, CYP3A4	0	0.55	3.14
17	Kaempferol 3-O-rutinoside	594.52	139.36	249.2		−3.42	Soluble	Low	No	Yes	NONE	3	0.17	6.48
18	Luteolin 3,7-di-O-glucoside	610.52	140.26	269.43		−3.22	Soluble	Low	No	Yes	NONE	3	0.17	6.39
19	Montecristin	574.92	180.05	66.76	9.92	−9.64	Poorly soluble	Low	No	Yes	NONE	2	0.17	6.82
20	Morin	302.24	78.03	131.36	1.2	−3.16	Soluble	High	No	No	CYP1A2, CYP2D6, CYP3A4	0	0.55	3.25
21	Muricatetrocin B	470.64	129.41	116.45	3.8	−4.1	Moderately soluble	High	No	No	CYP3A4	0	0.55	6.21
22	Muricatocin A	612.88	173.84	136.68	6.17	−6.61	Poorly soluble	Low	No	No	CYP3A4	1	0.55	7.5
23	Myricetin	318.24	80.06	151.59	0.79	−3.01	Soluble	Low	No	No	CYP1A2, CYP3A4	1	0.55	3.27
24	N-methylcoclaurine	299.36	90.52	52.93	2.59	−3.82	Soluble	High	Yes	Yes	CYP2D6	0	0.55	2.92
25	Nornuciferine	281.35	87.06	30.49	3.01	−3.74	Soluble	High	Yes	Yes	CYP1A2, CYP2D6, CYP3A4	0	0.55	3.35
26	Reticuline	329.39	97.01	62.16	2.6	−3.88	Soluble	High	Yes	Yes	CYP2D6	0	0.55	3.07
27	Sabadelin	530.86	167.55	38.83		−10.03	Insoluble	Low	No	Yes	NONE	2	0.17	6.47
28	Xylomatenin	622.92	181.81	116.45	7.47	−7.43	Poorly soluble	Low	No	No	CYP3A4	1	0.55	7.58

Physicochemical properties: Molecular weight (MW), Molar Refractivity (MR), Total polar surface area (TPSA). Lipophilicity: Consensus Log P. Water Solubility: ESOL Log S, ESOL Class. Pharmacokinetics: Gastrointestinal absorption (GIA), Blood-brain barrier (BBB), P-glycoprotein (P-gp) substrate, Inhibition of Cytochrome P450 (CYPs) type CYP1A2, CYP2C19, CYP2C9, CYP2D6, and CYP3A4. Druglikeness: Lipinski (Lip), Bioavailability Score (BS), Medicinal Chemistry: Synthetic accessibility (SA).

Table 2. Target prediction results

SN	Compound	Target gene code	Target description	p-value	MTC
1	Annonacin	PDCD4	Programmed cell death protein 4	4.236e-74	0.36
		PTGER2	Prostaglandin E2 receptor EP2 subtype	1.586e-06	0.32
2	Annonacin-10-one	PDCD4	Programmed cell death protein 4	6.804e-70	0.33
		IL6ST	Interleukin-6 receptor subunit beta	4.887e-23	0.30
		PPM1A	Protein phosphatase 1A	7.318e-23	0.28
		SLCO2A1	Solute carrier organic anion transporter family member 2A1	8.104e-18	0.28
3	Annonaine	TAS1R1	Taste receptor type 1 member 1	3.462e-06	0.29
4	Cis-Annoreticuin	PDCD4	Programmed cell death protein 4	4.236e-74	0.36
5	Asimilobine	TH	Tyrosine 3-monooxygenase	1.001e-39	0.32
		DRD1	D(1A) dopamine receptor	1.11e-16	0.39
		MMP26	Matrix metalloproteinase-26	1.384e-07	0.32
6	Cinnamic acid	HCAR2	Hydroxycarboxylic acid receptor 2	8.423e-10	1.00
		NR0B2	Nuclear receptor subfamily 0 group B member 2	9.432e-46	0.31
		GPR183	G-protein coupled receptor 183	2.941e-42	0.39
		SENP2	Sentrin-specific protease 2	3.568e-41	0.33
		CYP1B1	Cytochrome P450 1B1	6.792e-40	0.48
		RCOR3	REST corepressor 3	1.157e-39	0.31
		PAM	Peptidyl-glycine alpha-amidating monooxygenase	1.372e-38	0.52
		CHRNA10	Neuronal acetylcholine receptor subunit alpha-10	1.097e-35	0.28
7	Corossolone	PDCD4	Programmed cell death protein 4	3.7e-33	0.30
		PPM1A	Protein phosphatase 1A	2.063e-23	0.29
8	Coumaric acid	CA3	Carbonic anhydrase 3	1.966e-29	1.00
		CA6	Carbonic anhydrase 6	4.201e-29	1.00
		CA5B	Carbonic anhydrase 5B, mitochondrial	5.523e-27	1.00
		CA5A	Carbonic anhydrase 5A, mitochondrial	2.466e-26	1.00
		CA14	Carbonic anhydrase 14	7.845e-21	1.00
		CA7	Carbonic anhydrase 7	9.975e-20	1.00
		AKR1B1	Aldo-keto reductase family 1 member B1	5.551e-16	1.00
9	Dicaffeoylquinic acid	NSD2	Histone-lysine N-methyltransferase NSD2	0.0008982	1.00
		CXCL12	Stromal cell-derived factor 1	1.437e-76	0.38
		NR0B2	Nuclear receptor subfamily 0 group B member 2	3.814e-47	0.33
		MYOC	Myocilin	1.277e-31	0.39
10	Dihydrokaempferol-hexoside	TOP1	DNA topoisomerase 1	6.893e-61	0.36
		SLC5A2	Sodium/glucose cotransporter 2	8.932e-58	0.43
		SLC28A3	Solute carrier family 28 member 3	9.656e-53	0.42
		TYR	Tyrosinase	5.641e-36	0.42
		IL2	Interleukin-2	5.276e-30	0.40
		CBS	Cystathionine beta-synthase	2.038e-27	0.48
11	Epoxymurin-A	PDCD4	Programmed cell death protein 4	1.016e-45	0.36
		LYPLA2	Acyl-protein thioesterase 2	1.4e-22	0.29

Table 2. Target prediction results - *(continued)*

SN	Compound	Target gene code	Target description	p-value	MTC
12	Epoxymurin-B	PDCD4	Programmed cell death protein 4	1.016e-45	0.36
		LYPLA2	Acyl-protein thioesterase 2	1.4e-22	0.29
13	Epomusenin-A	PDCD4	Programmed cell death protein 4	1.016e-45	0.36
		LYPLA2	Acyl-protein thioesterase 2	1.4e-22	0.29
14	Epomusenin-B	PDCD4	Programmed cell death protein 4	1.016e-45	0.36
		LYPLA2	Acyl-protein thioesterase 2	1.4e-22	0.29
15	Fisetin	ELAVL3	ELAV-like protein 3	2.048e-65	0.66
		HSD17B3	Testosterone 17-beta-dehydrogenase 3	1.047e-52	0.43
		ALDH2	Aldehyde dehydrogenase, mitochondrial	4.45e-50	0.41
		CYP1B1	Cytochrome P450 1B1	6.994e-39	0.66
16	Kaempferol	ELAVL3	ELAV-like protein 3	1.407e-81	0.78
		PTPRS	Receptor-type tyrosine-protein phosphatase S	5.492e-59	0.75
		CBS	Cystathionine beta-synthase	9.017e-51	0.45
		CREB1	Cyclic AMP-responsive element-binding protein 1	5.513e-45	0.30
		P4HB	Protein disulfide-isomerase	6.101e-41	0.52
17	Kaempferol 3-O-rutinoside	P4HB	Protein disulfide-isomerase	3.535e-71	1.00
		SLC28A3	Solute carrier family 28 member 3	1.353e-43	0.35
		ELAVL3	ELAV-like protein 3	2.773e-43	0.39
		IL2	Interleukin-2	1.262e-31	0.42
		TYR	Tyrosinase	9.763e-30	0.34
		XDH	Xanthine dehydrogenase/oxidase	1.157e-25	0.65
18	Luteolin 3,7-di-O-glucoside	CREB1	Cyclic AMP-responsive element-binding protein 1	5.266e-69	0.35
		SLC5A2	Sodium/glucose cotransporter 2	3.962e-60	0.41
		SLC28A3	Solute carrier family 28 member 3	3.077e-50	0.40
		IL2	Interleukin-2	5.836e-40	0.89
19	Montecristin	PDCD4	Programmed cell death protein 4	1.128e-77	0.41
		SLCO2A1	Solute carrier organic anion transporter family member 2A1	2.172e-38	0.32
		POLH	DNA polymerase eta	3.331e-16	0.31
20	Morin	PTPRS	Receptor-type tyrosine-protein phosphatase S	6.131e-56	1.00
		MPG	DNA-3-methyladenine glycosylase	1.089e-50	1.00
		DAPK1	Death-associated protein kinase 1	1.344e-21	1.00
		ELAVL3	ELAV-like protein 3	8.402e-82	0.68
		P4HB	Protein disulfide-isomerase	3.742e-36	0.44
21	Muricatetrocin B	PDCD4	Programmed cell death protein 4	2.688e-59	0.33
22	Muricatocin A	PDCD4	Programmed cell death protein 4	1.009e-81	0.40
23	Myricetin	ELAVL3	ELAV-like protein 3	2.196e-101	1.00
		XDH	Xanthine dehydrogenase/oxidase	5.844e-36	1.00
24	N-methylcoclaurine	DRD1	D(1A) dopamine receptor	1.982e-95	0.58
		DHCR7	7-dehydrocholesterol reductase	2.187e-43	0.50
		TUBB1	Tubulin beta-1 chain	5.991e-26	0.35

Table 2. Target prediction results - *(continued)*

SN	Compound	Target gene code	Target description	p-value	MTC
		ABCB1	ATP-dependent translocase ABCB1	9.037e-26	0.45
		SLC18A2	Synaptic vesicular amine transporter	4.29e-24	0.35
25	Nornuciferine	TUBB	Tubulin beta chain	4.386e-25	0.31
26	Reticuline	DRD1	D(1A) dopamine receptor	9.256e-98	0.56
		DHCR7	7-dehydrocholesterol reductase	3.993e-44	0.51
		TUBB1	Tubulin beta-1 chain	1.432e-43	0.40
		FSHR	Follicle-stimulating hormone receptor	1.151e-29	0.30
		NDUFA1	NADH dehydrogenase [ubiquinone] 1 alpha subcomplex subunit 1	5.531e-17	0.32
27	Sabadelin	PDCD4	Programmed cell death protein 4	1.016e-45	0.36
		LYPLA2	Acyl-protein thioesterase 2	1.4e-22	0.29
28	Xylomatenin	PDCD4	Programmed cell death protein 4	9.378e-70	0.41
		SLCO2A1	Solute carrier organic anion transporter family member 2A1	1.494e-36	0.31

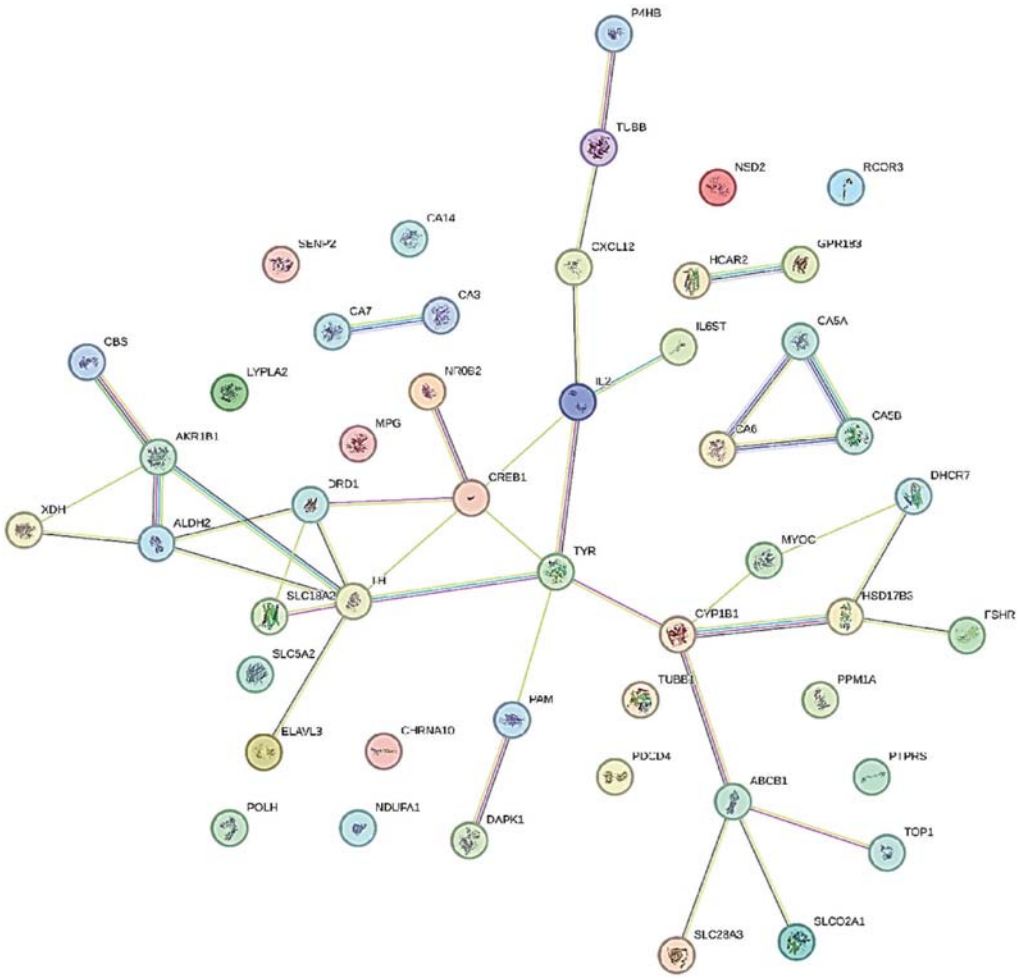

Figure 1. Protein-protein interaction of *A. muricata* molecular targets.

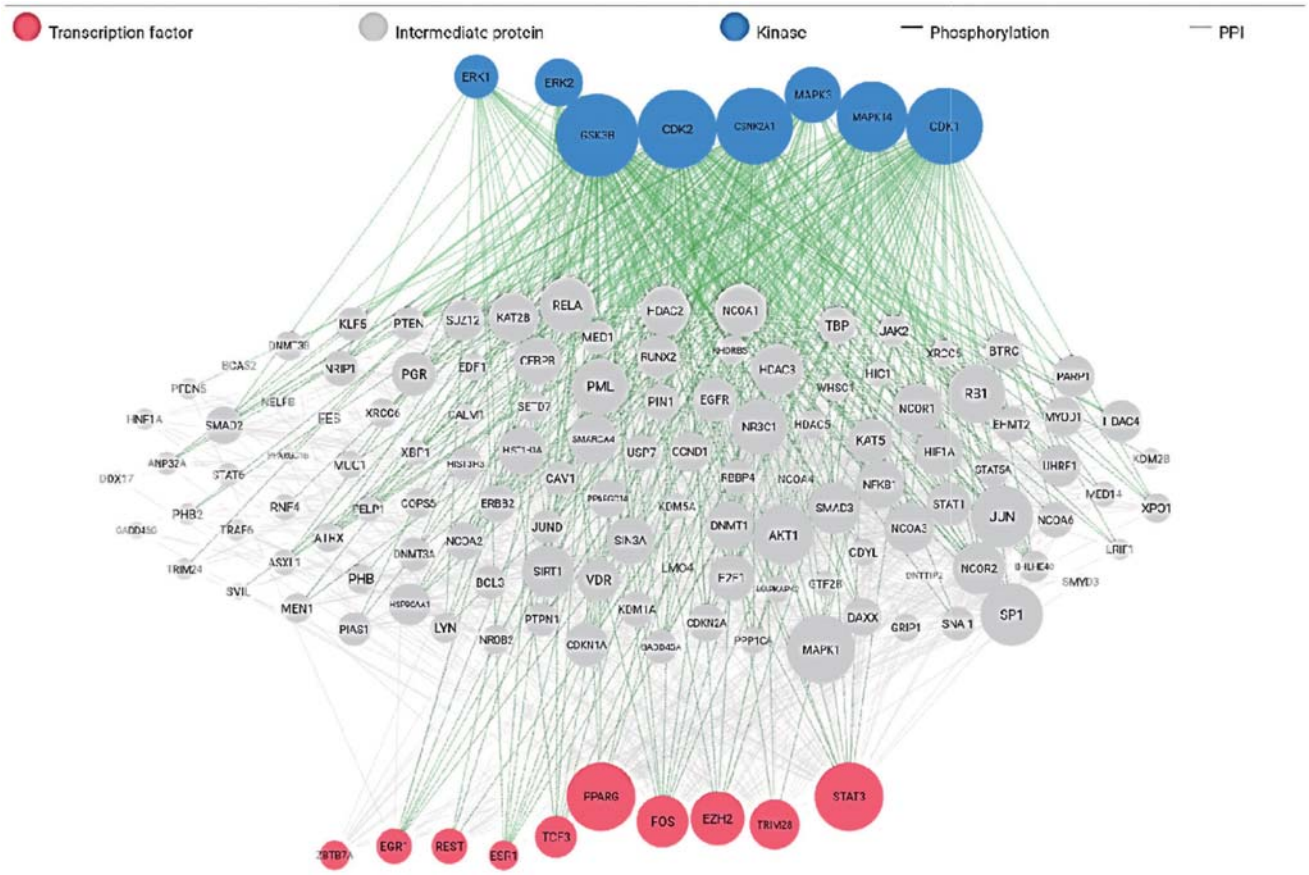

Figure 2. Overall molecular target genes network.

oral bioavailability (Arnott and Planey, 2012).

The number of hydrogen-bond donors and acceptors serves as fundamental molecular descriptors predicting the oral bioavailability of small drug candidates, while the number of heavy atoms, combined with binding affinity from docking, determines ligand efficiency (Ibraheem et al., 2019). Generally, hydrogen-bond donors and acceptors are presumed to impact passive diffusion across cell membranes, a critical event in drug absorption and distribu-

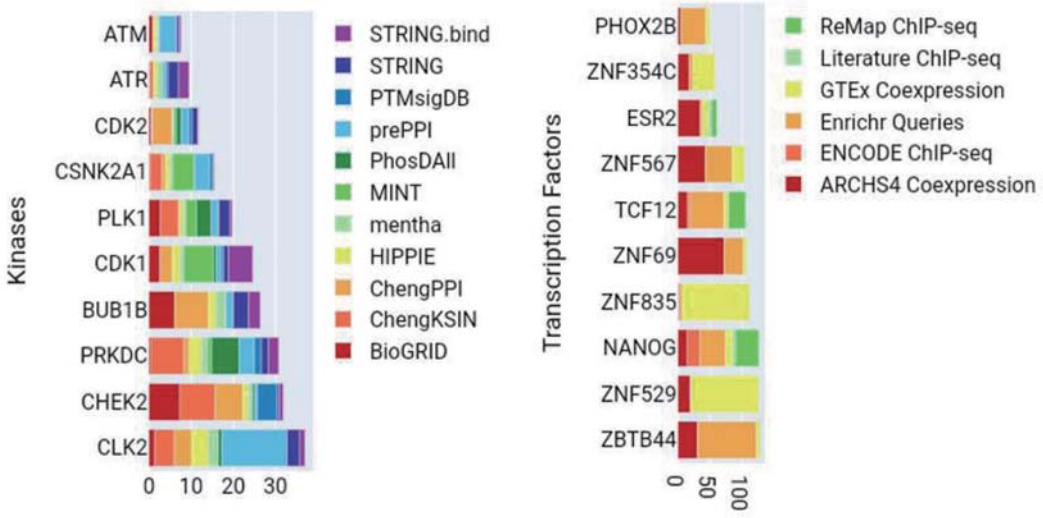

Figure 3. Average rank of kinases and transcription factors across all the library.

Table 3. Molecular docking results

S.N	Phytochemicals	PubChem CID	PDCD4 (AlphaFold ID: AF-Q53EL6) Binding Affinity ΔG (kcal.mol^{-1})
1	Annonacin	354398	−4.741
2	Annonacin-10-one	180161	−4.591
3	Annonaine	160597	−7.294
4	Cis-Annoreticuin	72778911	−4.869
5	Asimilobine	160875	−6.409
6	Cinnamic acid	444539	−3.96
7	Corossolone	4366126	−4.615
8	Coumaric acid	637542	−5.183
9	Dicaffeoylquinic acid	12358846	−6.775
10	Dihydrokaempferol-hexoside	10478918	−7.012
11	Epoxymurin-A	5281161	−4.416
12	Epoxymurin-B	131752983	−3.789
13	Epomusenin-A	10507050	−3.842
14	Epomusenin-B	10698082	−3.614
15	Fisetin	5281614	−6.979
16	Kaempferol	5280863	−6.749
17	Kaempferol 3-O-rutinoside	5318767	−6.629
18	Luteolin 3,7-di-O-glucoside	5490298	−7.65
19	Montecristin	102083640	−3.861
20	Morin	5281670	−6.884
21	Muricatetrocin B	393472	−5.362
22	Muricatocin A	133072	−5.191
23	Myricetin	5281672	−6.538
24	N-methylcoclaurine	440595	−5.946
25	Nornuciferine	41169	−6.226
26	Reticuline	439653	−5.907
27	Sabadelin	101006011	−3.426
28	Xylomatenin	10484035	−4.5
STD	Dexamethasone	5743	−6.682

Docking parameter: PDCD4 [spacing: 0.525, box size: 126 × 126 × 126, center: −9.248 × 0.161 × 1.314].

tion (Coimbra et al., 2021). P-glycoprotein (P-gp), a membrane transporter, actively pumps drugs out of cells, influencing drug bioavailability. The interplay of gastrointestinal absorption (GIA), blood-brain barrier (BBB) penetration, P-gp modulation, and cytochrome inhibition collectively shapes the pharmacokinetics and pharmacodynamics of phytochemicals or bioactive compounds.

Target prediction revealed that human programmed cell death 4 (PDCD4) is possibly the most frequent protein modulated by *A. muricata* phytochemicals. However, those targeting PDCD4 were found to be poorly soluble or insoluble, exhibit low GIA, and were not BBB permeants. PDCD4, an apoptosis-associated gene, is regulated by interleukins IL-2, IL-12, and IL-15, and functions as a tumor suppressor gene, playing essential roles in apoptosis, protein translation, signal transduction, and inflammation mediator stimulation (Zhang et al., 2014; Pin et al., 2020). Loss or downregulation of PDCD4 expression promotes tumor cell proliferation, invasion, and metastasis while reducing tumor cell apoptosis in various cancer types (Wang et al., 2019). PDCD4 downregulation is associated with chemoresistance, coinciding with a reduction in eukaryotic initiation factor-4A (eIF4A) interaction (González-Ortiz et al., 2022). Notably, cryptotanshinone, a natural terpene, has been reported to potentially upregulate eIF4A, suggesting a potential increase in PDCD4 expression (Galindo-Hernandez et al., 2019; González-Ortiz et al., 2022). Thus, *A. muricata* phytochemicals could be extrapolated with the same effect on PDCD4 directly or indirectly, because activation but not inhibition of PDCD4 expression could account for anticancer properties of *A. muricata*.

Numerous studies have demonstrated that PDCD4 overexpres-

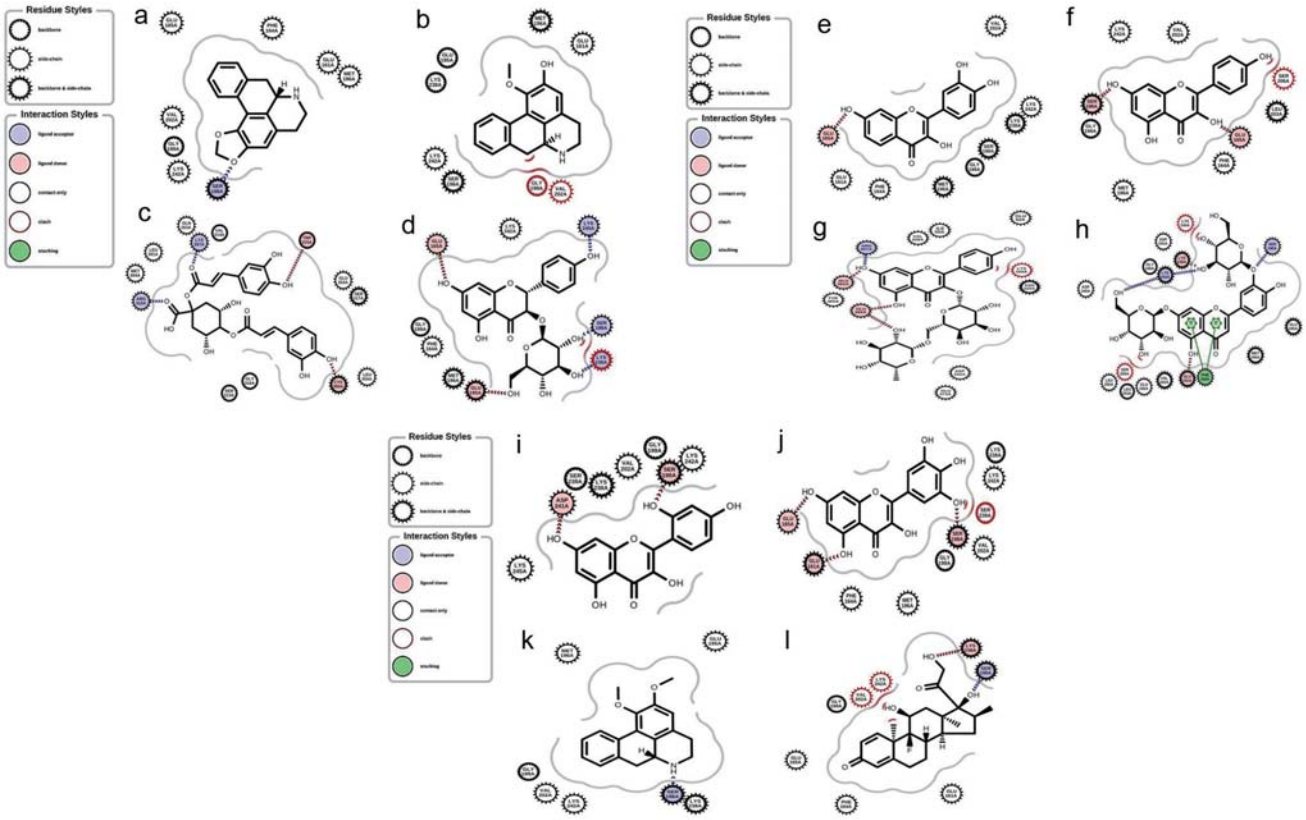

Figure 4. Interaction of the binding poses of PDCD4 with: (a) Annonaine; (b) Asimilobine; (c) Dicaffeoylquinic acid; (d) Dihydrokaempferol-hexoside; (e) fisetin; (f) Kaempferol; (g) Kaempferol-3-O-rutinoside; (h) Luteolin-3,7-di-O-glucoside; (i) Morin; (j) Myricetin; (k) Nornuciferine; (l) Dexamethasone.

sion significantly enhances the chemosensitivity of various cancer cells, including acute myeloid leukemia, breast cancer, ovarian cancer, non-small cell lung cancer (NSCLC), rectal cancer, and pancreatic cancer, to chemotherapy drugs like dexamethasone and taxol (Shibahara et al., 1995; Wang et al., 2019). PDCD4 overexpression in lung tumor cells has been linked to the suppression of the transcriptional activation of Nrf2 through its negative regulator, Keap1 (Hwang et al., 2020).

This study predicted several kinases involved in the mechanism of action of *A. muricata* phytochemicals. The implicated signaling pathways connecting many of these kinases and transcription factors include MAPK, PI3K/Akt, and JAK/STAT3 pathways, crucial for cell survival, proliferation, and apoptosis. These findings align with previous report that inhibition of STAT3 pathway led to the downregulation of MicroRNA-21 and upregulation of PDCD4 (Asangani et al., 2008; Singh et al., 2015). Additionally, AKT2, among the AKT isoforms, has been reported to interact with PDCD4, suppressing PDCD4 in glioma cells. PDCD4 regulates the expression of IL-5, CCL-5, VEGF, and CXCL10 via the NF-kB pathway. Depletion of PDCD4 levels promotes angiogenic activity of glioma cells through the VEGF-STAT3 pathway (Pin et al., 2020). PDCD4 inhibits NF-κB signaling to reduce NF-κB-dependent matrix metallopeptidase (MMP-9) expression in cancer cells, impacting tumor cell migration and apoptosis (Parks et al., 2004; Mao et al., 2017). A study by Drishya et al. (2020) reported that transcription factors RECK and TIMP-2 mediate the inhibition of MMP-2 and MMP-9 by *A. muricata*. Reduced PDCD4 expression promotes cell growth through the PI3K/Akt signaling pathway in NSCLC (Zhen et al., 2016). Furthermore, upregulation of PDCD4 suppresses the expression of the cell cycle regulatory molecule, cyclin-dependent kinase 4 (CDK4), while downregulation of PDCD4 enhances CDK4 expression (Jin et al., 2006; Hwang et al., 2010).

Molecular docking, a computational technique, predicts ligand binding sites and affinities on receptor surfaces. It involves generating numerous ligands poses on the receptor surface and scoring their predicted binding affinities (Rentzsch and Renard, 2015). The results of molecular docking studies revealed that only two compounds, Muricatetrocin B (−5.362 kcal.mol^{-1}) and Muricatocin A (−5.191 kcal.mol^{-1}), among the 13 compounds targeting PDCD4, exhibited good binding affinity. A binding affinity score of ≤−5.00 kcal.mol^{-1} indicates a strong affinity between the target protein and the ligand (Wong et al., 2022). Also, aromatic pi-pi interactions of the ligands with amino acid residues such as tryptophan, tyrosine, histidine, and phenylalanine within the target proteins, are very essential in drug design because it promotes molecular recognition and interactions, improve specificity and efficacy (Apeh et al., 2023).

Molecular dynamics simulation (MDS) was employed to assess atomic-level variations in the protein-ligand system and evaluate the stability of the protein-ligand complex in a dynamic environment (Fatoki, 2023). MD simulations track the evolution of cartesian coordinates for every atom in a system using a general physics model governing particle interaction (McCammon and Karplus, 2002). RMSD and Rg are utilized for assessing flexibility, compactness, and conformational divergence of protein struc-

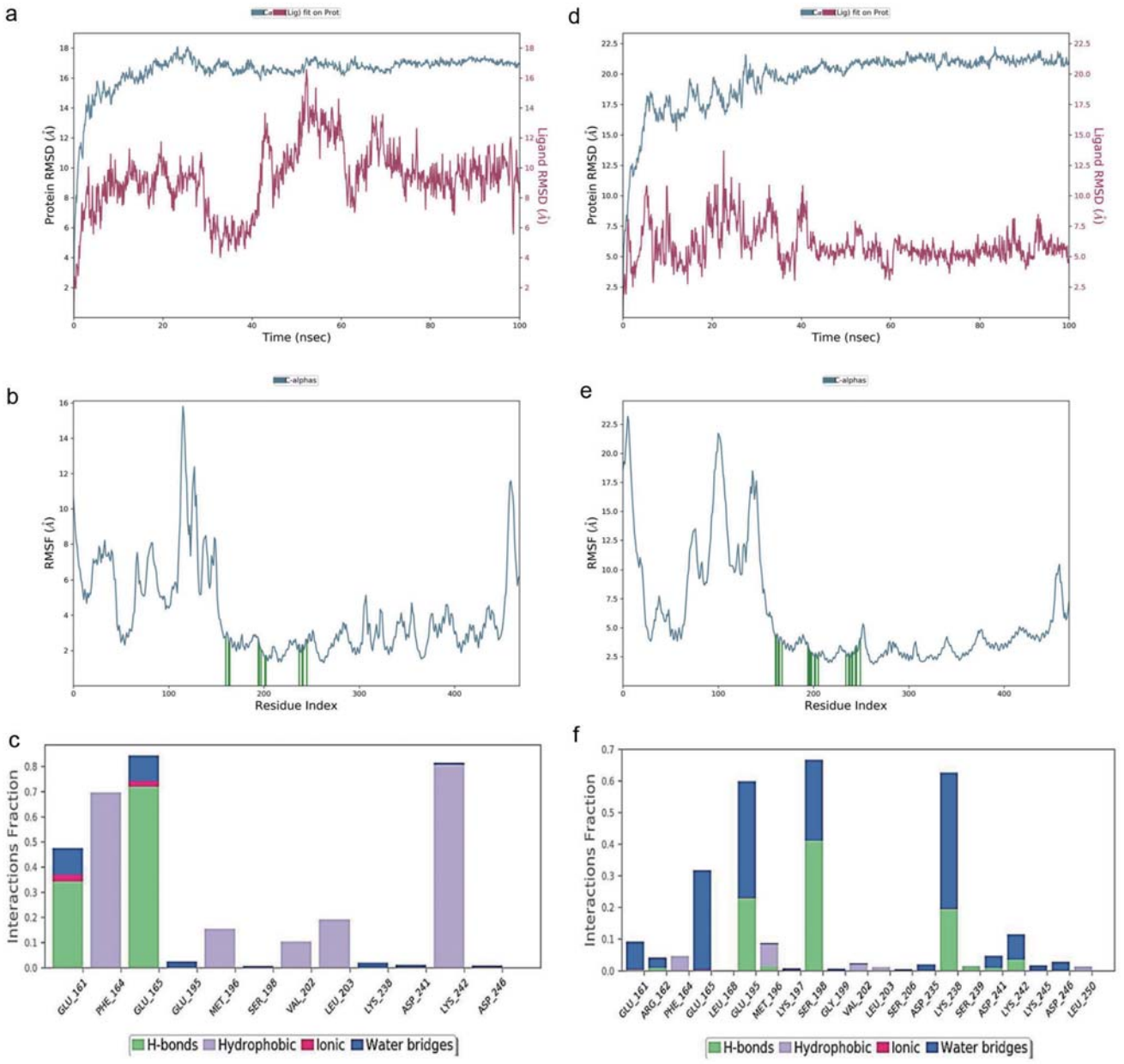

Figure 5. Protein-ligand complex simulation results (a) RMSD of Annonaine and PDCD4 (b) RMSF of PDCD4 on binding to Orientin. (c) Interaction profile of the contact between Annonaine and PDCD4 (d) RMSD of Dexamethasone and PDCD4. (e) RMSF of PDCD4 on binding to Quercetin; (f) Interaction profile of the contact between Dexamethasone and PDCD4.

tural ensembles. RMSD values less than 4 Å indicate relatively small conformational changes, suggesting stability during simulation (Fatoki et al., 2023). Protein-ligand interactions (or contacts) showed the contribution of amino acid residues in terms of hydrogen bonds, hydrophobic, ionic and water bridges, during the simulation, and could be used to elaborate the RMSF of the protein. The protein-ligand interactions stacked bar charts are normalized over the course of the trajectory; for instance, a value of 0.7 suggests that 70% of the simulation time the specific interaction was maintained. Prime MM-GBSA provides various energy properties, reporting energies for ligand, receptor, and complex structures, along with energy differences related to strain and binding (Fatoki, 2023). The total binding free energy confirms the stability of the complexes under physiological conditions.

5. Conclusion

Natural molecules emerge as promising candidates in drug development, offering numerous advantages and minimal side effects. The extract from *A. muricata* or its specific phytochemicals presents potential implications in drug discovery for conditions

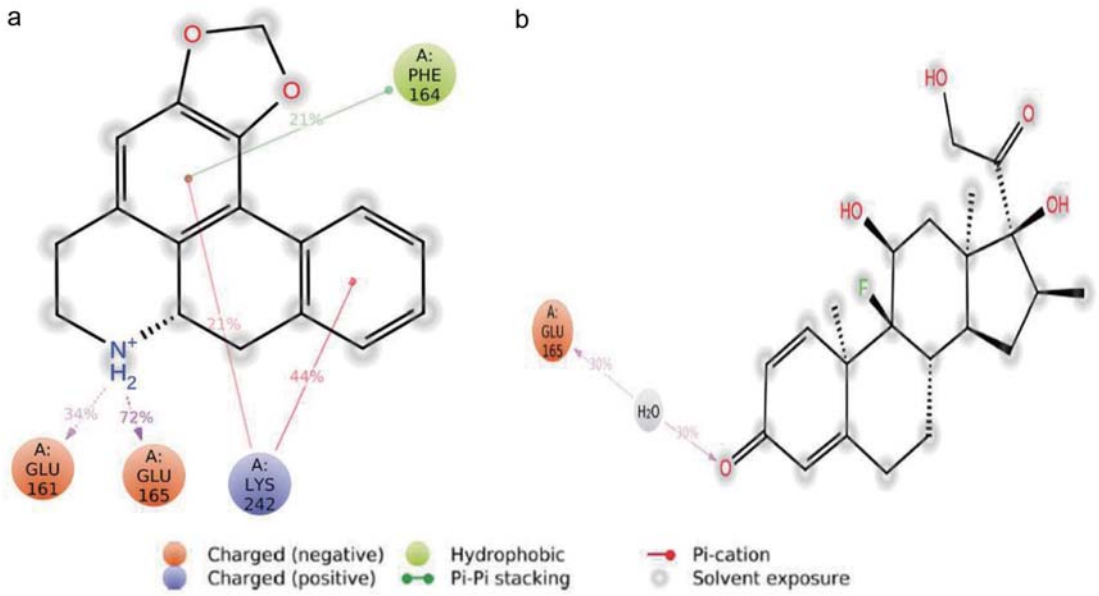

Figure 6. A schematic of detailed ligand-protein interactions (a) Annonaine and PDCD4 (b) Dexamethasone and PDCD4.

Table 4. Prime MMGBSA binding energy of interaction of PDCD4 with Annonaine and Dexamethasone respectively, before and after molecular dynamics simulation.

Complex	Simulation Time (ns)	MMGBSA ΔG^{bind} (kcal.mol^{-1})							
		Coulomb	Covalent	Hbond	Lipo	Packing	Solv_GB	vdW	G^{bind} (Total)
Annonaine and PDCD4	0	−64.428	2.791	−0.60	−14.323	−0.541	69.403	−28.149	−35.851
	100	−52.471	1.676	−0.797	−15.184	−1.519	52.998	−23.720	−39.019
Dexamethasone and PDCD4	0	0.913	0.092	−0.420	−7.605	0	11.380	−32.850	−28.489
	100	−4.693	−0.012	−0.027	−8.555	0	15.696	−30.694	−28.284

Covalent: Covalent binding energy; Coulomb: Coulomb energy; Lipo: Lipophilic energy; Hbond: Hydrogen bonding energy; Packing: Pi-pi packing correction; Solv GB: Generalized Born electrostatic solvation energy; vdW: Van der Waals energy; Total: Total energy (Prime energy).

like cancer and neurodegenerative diseases, operating through a mechanism of action that targets PDCD4. This study pioneers the notion that the anticancer properties of *A. muricata* may be attributed to PDCD4 overexpression, influencing the CDK/Akt/STAT3 pathway. Future research should delve into in vivo gene expression studies to evaluate the therapeutic efficacy of *A. muricata* extract or its specific phytochemicals, Muricatocin A and Muricatetrocin B, across various cancer types.

References

Abdullah, M., Syam, A.F., Meilany, S., Laksono, B., Prabu, O.G., Bekti, H.S., Indrawati, L., and Makmun, D. (2017). The Value of Caspase-3 after the Application of *Annona muricata* Leaf Extract in COLO-205 Colorectal Cancer Cell Line. Gastroenterol. Res. Pract. 2017: 165.

Ajiboye, B.O., Akinnusi, P.A., Fatoki, T.H., Adigun, D.K., Adewole, Z.O., Efekemo, E.O., Ayotunde, B.T., Julius, B.P., Falode, J.A., Ajuwon, O.R., and Oyinloye, B.E. (2023). *In silico* assessment of *Hibiscus sabdariffa* as a possible therapeutic agent for breast cancer management. Informatics Med. Unlocked 41: 101330.

Akinlolu, O.S., Fatoki, T.H., and Momodu, D.U. (2023). Hematological and Hypoglycemic Effects of Ethanolic Extract of *Annona muricata* Ripe Fruits Pulp on Streptozotocin-induced Diabetes in Rats: *In vivo* and *In silico* Studies. J. Complement. Altern. Med. Res. 21(2): 32–42.

Apeh, V.O., Adegboyega, A.E., Chukwuma, I.F., Ugwah-Oguejiofor, C.J., Aja, P.M., Ofeimun, J.O., Ale, B.A., Johnson, G.I., Ebenyi, L.N., Iwaloye, O., Ejembi, S.A., Ezugworie, F.N., and Johnson, T.O. (2023). An *insilico* study of bioactive compounds of Annona muricata in the design of ani-prostate cancer agent: MM/GBSA, pharmacophore modeling and ADMET parameters. Informatics Med. Unlocked 43: 101377.

Arnott, J.A., and Planey, S.L. (2012). The influence of lipophilicity in drug discovery and design. Expert Opinion on Drug Discovery 7(10): 863–875.

Asangani, I.A., Rasheed, S.A., Nikolova, D.A., Leupold, J.H., Colburn, N.H., Post, S., and Allgayer, H. (2008). MicroRNA-21 (miR-21) post-transcriptionally downregulates tumor suppressor Pdcd4 and stimulates invasion, intravasation and metastasis in colorectal cancer. Oncogene 27: 2128–2136.

Bowers, K.J., Chow, E., Xu, H., Dror, R.O., Eastwood, M.P., Gregersen, B.A., Klepeis, J.L., Kolossvary, I., Moraes, M.A., Sacerdoti, F.D., Salmon, J.K., Shan, Y., and Shaw, D.E. (2006). Scalable algorithms for molecular dynamics simulations on commodity clusters. In Proceedings of the 2006 ACM/IEEE conference on Supercomputing. Association for Computing Machinery, Tampa, Florida, p. 84.

Clarke, D.J.B., Kuleshov, M.V., Schilder, B.M., Torre, D., Duffy, M.E., Keenan, A.B., Lachmann, A., Feldmann, A.S., Gundersen, G.W., Silverstein, M.C., Wang, Z., and Ma'ayan, A. (2018). eXpression2Kinases (X2K) Web: linking expression signatures to upstream cell signaling net-

works. Nucleic Acids Res. 46(W1): 171–179.
Coimbra, J.T., Feghali, R., Ribeiro, R.P., Ramos, M.J., and Fernandes, P.A. (2021). The importance of intramolecular hydrogen bonds on the translocation of the small drug piracetam through a lipid bilayer. RSC Adv. 11(2): 899–908.
Coria-Tellez, A.V., Montalvo-Gonzalez, E., Yahia, E.M., and Obledo-Vazquez, E.N. (2018). *Annona muricata*: A comprehensive review on its traditional medicinal uses, phytochemicals, pharmacological activities, mechanisms of action and toxicity. Arabian J. Chem. 11: 662–691.
Daina, A., Michielin, O., and Zoete, V. (2017). SwissADME: a free web tool to evaluate pharmacokinetics, drug-likeness and medicinal chemistry friendliness of small molecules. Sci. Rep. 7(1): 42717.
Drishya, G., Nambiar, J., Shaji, S.K., Vanuopadath, M., Achuthan, A., Kumar, A., Alias, A., Sherif, A., Joseph, C., Divya, P., Kumar, D.S., Bose, C., Nair, S.V., Sudarslal, S., Kumar, G.B., Lakshmi, S., and Nair, B.G. (2020). RECK and TIMP-2 Mediate Inhibition of MMP-2 and MMP-9 by *Annona muricata*. J. Biosci. 45: 89.
Eberhardt, J., Santos-Martins, D., Tillack, A.F., and Forli, S. (2021). AutoDock Vina 1.2.0: New Docking Methods, Expanded Force Field, and Python Bindings, J. Chem. Inf. Model 61(8): 3891–3898.
Fatoki, T.H., Balogun, C.T., Oluwadare, O.T., Famusiwa, C.D., Oyebiyi, O.R., Ejimadu, B.A., Lawal, O.E., Amosun, B.E., Adeyeye, T.O., and Falode, J.A. (2023). *In Silico* Evaluation of Nutri-Pharmacological Potentials of Phytochemicals in Sorghum (Sorghum bicolor) Grains. J. Food Bioact. 23: 58–67.
Fatoki, T.H., Faleye, B.C., Nwagwe, O.R., Awofisayo, O.A., Adeseko, C.J., Jeje, T.O., Ayenero, M.E., Fatoki, J.M., Akinlolu, O.S., Momodu, D.U., Enibukun, J.S., and Omuekwu, N.F. (2024). Friedelin Could Moderately Modulate Human Carbonic Anhydrases: An in Silico Study. Biointerface Res. Appl. Chem. 14(2): 49.
Fatoki, T.H. (2023). Human adenovirus DNA polymerase is evolutionarily and functionally associated with human telomerase reverse transcriptase based on in silico molecular characterization that implicate abacavir and zidovudine. Front. Bioinform. 3: 1123307.
Fatoki, T.H. (2022). Effect of pH on structural dynamics of HMGCoA reductase and binding affinity to β-sitosterol. J. Biomol. Struct. Dyn. 41(10): 4398–4404.
Galindo-Hernandez, O., Cordova-Guerrero, I., Diaz-Rubio, L.J., Pulido-Capiz, A., Diaz-Villanueva, J.F., Castaneda-Sanchez, C.Y., Serafin-Higuera, N., and Garcia-Gonzalez, V. (2019). Protein translation associated to PERK arm is a new target for regulation of metainflammation: A connection with hepatocyte cholesterol. J. Cell Biochem. 120: 4158–4171.
Gavamukulya, Y., Abou-Elella, F., Wamunyokoli, F., and AEl-Shemy, H. (2014). Phytochemical Screening, Anti-Oxidant Activity and in Vitro Anticancer Potential of Ethanolic and Water Leaves Extracts of *Annona muricata* (Graviola). Asian Pac. J. Trop. Med. 7: S355–S363.
González-Ortiz, A., Pulido-Capiz, A., Castañeda-Sánchez, C.Y., Ibarra-López, E., Galindo-Hernández, O., Calderón-Fernández, M.A., López-Cossio, L.Y., Díaz-Molina, R., Chimal-Vega, B., Serafín-Higuera, N., Córdova-Guerrero, I., and García-González, V. (2022). eIF4A/PDCD4 Pathway, a Factor for Doxorubicin Chemoresistance in a Triple-Negative Breast Cancer Cell Model. Cells 11: 4069.
Hadisaputri, Y.E., Habibah, U., Abdullah, F.F., Halimah, E., Mutakin, M., and Abdulah, R. (2021). Antiproliferation Activity and Apoptotic Mechanism of Soursop (*Annona muricata* L.) Leaves Extract and Fractions on MCF7 Breast Cancer Cells. Breast Cancer Targets Ther. 13: 447–457.
Hwang, S.K., Minai-Tehrani, A., Lim, H.T., Shin, J.Y., An, G.H., Lee, K.H., Park, K.R., Kim, Y.S., Beck, G.R. Jr, Yang, H.S., and Cho, M.H. (2010). Decreased level of PDCD4 (programmed cell death 4) protein activated cell proliferation in the lung of A/J mouse. J. Aerosol. Med. Pulm. Drug Deliv. 23: 285–293.
Hwang, S.K., Jeong, Y.J., and Chang, Y.C. (2020). PDCD4 inhibits lung tumorigenesis by the suppressing p62-Nrf2 signaling pathway and upregulating Keap1 expression. Am. J. Cancer Res. 10: 424–439.
Ibraheem, O., Fatoki, T.H., Enibukun, J.M., Faleye, B.C., and Momodu, D.M. (2019). *In Silico* Toxicological Analyses of Selected Dumpsite Contaminants on Human Health. Nova Biotechnol. Chim. 18(2): 144–153.
Indrawati, L., Ascobat, P., Bela, B., Abdullah, M., and Surono, I.S. (2017). The Effect of an *Annona muricata* Leaf Extract on Nutritional Status and Cytotoxicity in Colorectal Cancer: A Randomized Controlled Trial. Asian Pac. J. Clin. Nutr. 26: 606–612.
Jin, H., Kim, T.H., Hwang, S.K., Chang, S.H., Kim, H.W., Anderson, H.K., Lee, H.W., Lee, K.H., Colburn, N.H., Yang, H.S., Cho, M.H., and Cho, C.S. (2006). Aerosol delivery of urocanic acid-modified chitosan/programmed cell death 4 complex regulated apoptosis, cell cycle, and angiogenesis in lungs of K-ras null mice. Mol. Cancer Ther. 5: 1041–1049.
Keiser, M.J., Roth, B.L., Armbruster, B.N., Ernsberger, P., Irwin, J.J., and Shoichet, B.K. (2007). Relating protein pharmacology by ligand chemistry. Nat. Biotech. 25(2): 197–206.
Kim, J.Y., Dao, T.T.P., Song, K., Park, S.B., Jang, H., Park, M.K., Gan, S.U., and Kim, Y.S. (2018). *Annona muricata* Leaf Extract Triggered Intrinsic Apoptotic Pathway to Attenuate Cancerous Features of Triple Negative Breast Cancer MDA-MB-231 Cells. Evid.-Based Complement. Altern. Med. 2018: 916.
Kostal, J. (2016). Computational chemistry in predictive toxicology: Status quo et quo vadis? In: Fishbein, J.C., and Heilman, J.M. (Ed.). Advances in Molecular Toxicology, Vol. 10. Elsevier, pp. 139–186.
Mao, X.H., Chen, M., Wang, Y., Cui, P.G., Liu, S.B., and Xu, Z.Y. (2017). MicroRNA-21 regulates the ERK/NF-kappaB signaling pathway to affect the proliferation, migration and apoptosis of human melanoma A375 cells by targeting SPRY1, PDCD4 and PTEN. Mol. Carcinog. 56: 886–894.
Martin, P., Giardiello, M., McDonald, T.O., Rannard SP, , and Owen, A. (2013). Mediation of in vitro cytochrome P450 activity by common pharmaceutical excipients. Mol. Pharm. 10: 2739–2748.
McCammon, J.A., and Karplus, M. (2002). Molecular dynamics simulations of biomolecules. Nat. Struct. Biol. 9(9): 646–652.
Moghadamtousi, S.Z., Kadir, H.A., Paydar, M., Rouhollahi, E., and Karimian, H. (2014). *Annona muricata* Leaves Induced Apoptosis in A549 Cells through Mitochondrial-Mediated Pathway and Involvement of NF-κB. BMC Complement. Altern. Med. 14: 1–13.
Morris, G.M., Huey, R., Lindstrom, W., Sanner, M.F., Belew, R.K., Goodsell, D.S., and Olson, A.J. (2009). AutoDock4 and AutoDockTools4: automated docking with selective receptor flexibility. J. Comput. Chem. 30(16): 2785–2791.
Mutakin, M., Fauziati, R., Fadhilah, F.N., Zuhrotun, A., Amalia, R., and Hadisaputri, Y.E. (2022). Pharmacological Activities of Soursop (*Annona muricata* Lin.). Molecules 27: 1201.
Nwonuma, C.O., Balogun, E.A., and Gyebi, G.A. (2023). Evaluation of Antimalarial Activity of Ethanolic Extract of *Annona muricata* L.: An *in vivo* and an *in silico* Approach. J. Evid.-Based Integr. Med. 28: 1–30.
Parks, W.C., Wilson, C.L., and Lopez-Boado, Y.S. (2004). Matrix metalloproteinases as modulators of inflammation and innate immunity. Nat. Rev. Immunol. 4: 617–629.
Pieme, A.A., Kumar, G.G., Dongmo, S.S., Moukette, M.M., Boyoum, F.F., Ngogang, Y.Y., and Saxena, K.K. (2014). Antiproliferative Activity and Induction of Apoptosis by *Annona muricata* (Annonaceae) Extract on Human Cancer Cells. BMC Complement. Altern. Med. 14: 1–10.
Pin, G., Huanting, L., Chengzhan, Z., Xinjuan, K., Yugong, F., Wei, L., Shifang, L., Zhaojian, L., Kun, H., Weicheng, Y., Yingying, L., Yongming, Q., and Yanan, Y. (2020). Down-Regulation of PDCD4 Promotes Proliferation, Angiogenesis and Tumorigenesis in Glioma Cells. Front. Cell Dev. Biol. 8: 593685.
Rentzsch, R., and Renard, B.Y. (2015). Docking small peptides remains a great challenge: an assessment using AutoDock Vina. Brief Bioinform. 16(6): 1045–1046.
Schrödinger. (2018). Schrödinger release 2018-3. Desmond molecular dynamics system, D.E. Shaw research, New York, NY, 2018. Maestro Desmond Interoperability Tools, Schrödinger, New York, NY, 2018.
Schrödinger. (2019). What do all the Prime MM-GBSA energy properties mean? www.schrodinger.com/kb/1875.
Shibahara, K., Asano, M., Ishida, Y., Aoki, T., Koike, T., and Honjo, T. (1995). Isolation of a novel mouse gene MA-3 that is induced upon programmed cell death. Gene. 166: 297–301.
Shivakumar, D., Williams, J., Wu, Y., Damm, W., Shelley, J., and Sherman, W. (2010). Prediction of Absolute Solvation Free Energies using Molecular Dynamics Free Energy Perturbation and the OPLS Force Field. J. Chem. Theory Comput. 6: 1509–1519.
Singh, M., Garg, N., Venugopal, C., Hallett, R., Tokar, T., McFarlane, N.,

Mahendram, S., Bakhshinyan, D., Manoranjan, B., Vora, P., Qazi, M., Arpin, C.C., Page, B., Haftchenary, S., Rosa, D.A., Lai, P.S., Gomez-Biagi, R.F., Ali, A.M., Lewis, A., Geletu, M., Murty, N.K., Hassell, J.A., Jurisica, I., Gunning, P.T., and Singh, S.K. (2015). STAT3 pathway regulates lung-derived brain metastasis initiating cell capacity through miR-21 activation. Oncotarget 6(29): 27461–27477.

Suhandi, C., Bagaskhara, P.P., Puspita, R.I.S., Amalia, S.H., Azzahra, A.B., and Citraloka, Z.G. (2022). In Silico Study of Compound Extract in Soursop Plant (Annona muricata) as ACE Inhibitor in Hypertension Disease. Indones. J. Comput. Biol 1(1): 7–15.

Szklarczyk, D., Gable, A.L., Nastou, K.C., Lyon, D., Kirsch, R., Pyysalo, S., Doncheva, N.T., Legeay, M., Fang, T., Bork, P., Jensen, L.J., and von Mering, C. (2021). The STRING database in 2021: Customizable protein#x2013;protein networks, and functional characterization of user-uploaded gene/measurement sets. Nucleic Acids Res. 49: D605–D612.

Tao, A., Huang, Y., Shinohara, Y., Caylor, M.L., Pashikanti, S., and Xu, D. (2019). ezCADD: A Rapid 2D/3D Visualization-Enabled Web Modeling Environment for Democratizing Computer-Aided Drug Design. J. Chem. Inf. Model 59: 18–24.

Trott, O., and Olson, A.J. (2010). AutoDock Vina: improving the speed and accuracy of docking with a new scoring function, efficient optimization, and multithreading. J. Comput. Chem. 31(2): 455–61.

Wang, D., Hou, Q., Zhao, L., Gao, J., Xiao, Y., and Wang, A. (2019). Programmed cell death factor 4 enhances the chemosensitivity of colorectal cancer cells to Taxol. Oncol. Lett. 18: 1402–1408.

Wong, F., Krishnan, A., Zheng, E.J., Stark, H., Manson, A.L., Earl, A.M., Jaakkola, T., and Collins, J.J. (2022). Benchmarking Al-phaFold-enabled molecular docking predictions for antibiotic discovery. Mol. Syst. Biol. 18: e11081.

Yang, C., Gundala, S.R., Mukkavilli, R., Vangala, S., Reid, M.D., and Aneja, R. (2015). Synergistic Interactions among Flavonoids and Acetogenins in Graviola (*Annona muricata*) Leaves Confer Protection against Prostate Cancer. Carcinogenesis 36: 656–665.

Zhang, D., Shi, Z., Li, M., and Mi, J. (2014). Hypoxia-induced miR-424 decreases tumor sensitivity to chemotherapy by inhibiting apoptosis. Cell Death Dis. 5: e1301.

Zhang, X., Perez-Sanchez, H., and Lightstone, F.C. (2017). A Comprehensive Docking and MM/GBSA Rescoring Study of Ligand Recognition upon Binding Antithrombin. Curr. Topics Med. Chem. 17: 1631–1639.

Zhen, Y., Li, D., Li, W., Yao, W., Wu, A., Huang, J., Gu, H., Huang, Y., Wang, Y., Wu, J., Chen, M., Wu, D., Lyu, Q., Fang, W., and Wu, B. (2016). Reduced PDCD4 expression promotes cell growth through PI3K/Akt signaling in non-small cell lung cancer. Oncol. Res. 23: 61–68.

Journal of Food Bioactives

The Journal of Food Bioactives (JFB), a publication of the International Society for Nutraceuticals and Functional Foods (ISNFF), aims to bring together the results of fundamental and applied research on food bioactives, functional food ingredients, nutraceuticals and natural health products that are known to possess or perceived to have health-promoting properties.

Preface

Review

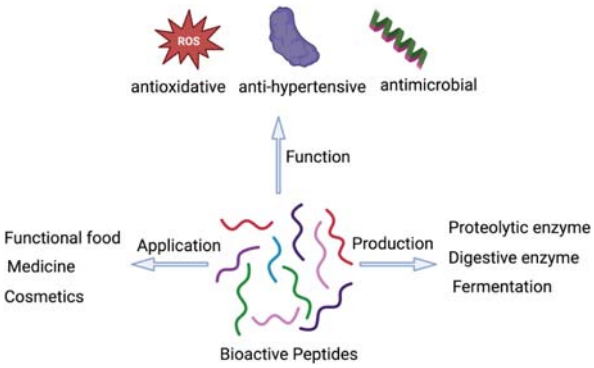

Original Research

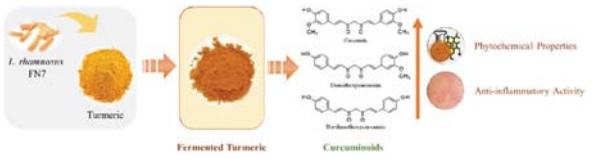

25

A comprehensive characterization of phenolics, amino acids and other minor bioactives of selected honeys and identification of botanical origin markers

Yan Zhu, Ronghua Liu, Lili Mats, Honghui Zhu, Joy Roasa, Tauseef Khan, Amna Ahmed, Yolanda Brummer, Steve Cui, John Sievenpiper, D. Dan Ramdath, Rong Tsao

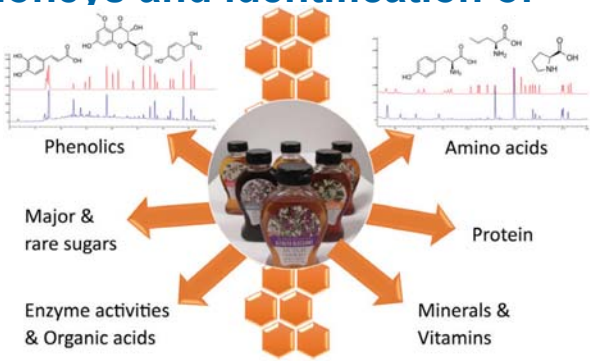

Phenolic and amino acid profiles along with organic acid, vitamin and mineral contents, major and minor sugars and enzyme activities of selected honey samples collected in North America were analyzed using different methods and potential markers of their botanical origin were identified.

42

Sesamolin has the ability to induce longevity effects on the *Caenorhabditis elegans*, and the mechanism depends on the SIR-2.1 and AAK-2 proteins

Chia-Yu Chin, Pei-Jing Lee, Nae-Cherng Yang

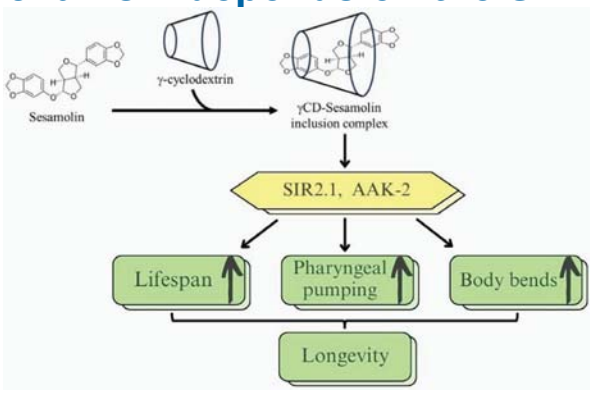

Sesamolin, one of the prominent lignans in sesame seeds, offers diverse physiological benefits.

52

Fuji apple (*Malus domestica* Borkh. cv. Red Fuji) pomace extracts as a source of antimicrobial and antioxidant polyphenols

Jiankang Wang, Zhengchun Liu, Lina Wei, Changyan Shao, Jing Wang, Yanan Zhu, Yujiao Sun

This study aimed to assess the antibacterial and antioxidant properties of both crude polyphenol extract (CPE) and purified polyphenol extract (PPE) obtained from Fuji apple pomace.

62

A novel combination against skin aging via promoting the synthesis of biological collagen

Bei-Bei Dong, Peng-Fei Zhang, Wu-Yan Guo, Heng-Yu Zheng, You-Nan Kou, Huan Zhang, Ying-Chao Ma, Bo Zhang

Supplementing collagen is considered to contribute to delaying skin aging.

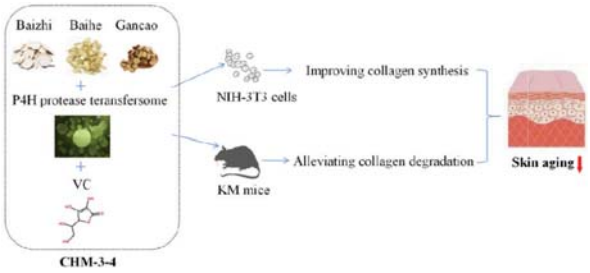

72

Exploring the anti-inflammatory effect of clove water extract in lipopolysaccharide-stimulated RAW264.7 cells and mouse peritoneal macrophages

Sellen Gurusmatika, Momoko Ishida, Kosuke Nishi, Takuya Sugahara

Clove (*Syzygium aromaticum* L) is a precious spice that has been extensively used by many countries over the centuries to add flavor and for medicinal purposes.

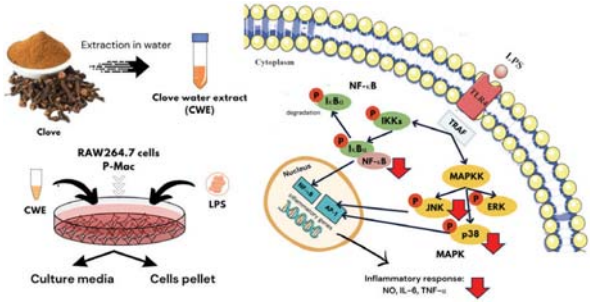

81

In silico ADME and molecular simulation studies of pharmacological activities of phytoconstituents of *Annona muricata* (L.) Fruit

Iseoluwa Isaac Ajayi, Toluwase Hezekiah Fatoki, Ayodele Sunday Alonge, Courage Dele Famusiwa, Ibrahim Olabayode Saliu, Olapade Samuel Akinlolu, Chinemelum Adaora Onodugo, Rachel Temitope Ojo

Annona muricata Lin is known for its ethnomedicinal uses as food, decoctions, or infusions to address various conditions like skin infections, fever, diabetes, insomnia, malaria, hypertension, nervous disorders, diarrhea, and cancer.

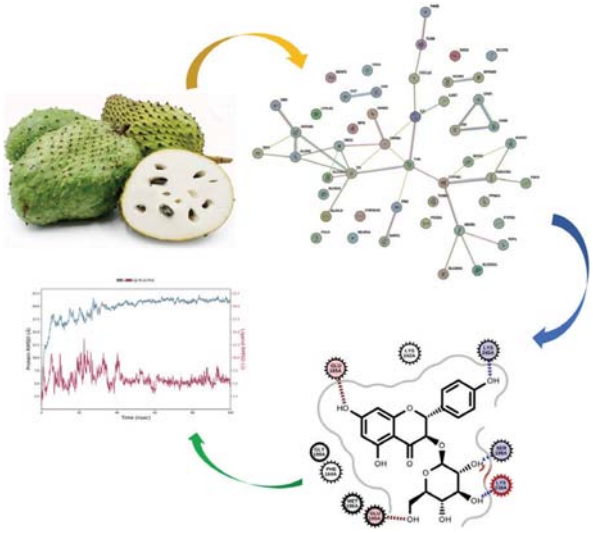

Journal of Food Bioactives

TABLE OF CONTENTS